UNIVERSITAT DE BARCELONA

Chemical tools for the study of sphingolipid metabolism in diseases

Mazen Aseeri

UNIVERSITY OF BARCELONA

FACULTY OF BIOLOGY

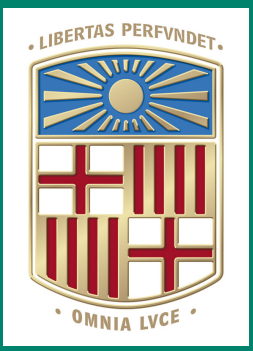

CHEMICAL TOOLS FOR THE STUDY OF SPHINGOLIPID METABOLISM IN DISEASES

DOCTORAL THESIS

MAZEN ALI ASEERI

2023

UNIVERSITY OF BARCELONA
FACULTY OF BIOLOGY
DOCTORATE PROGRAMM OF BIOMEDICNE

CHEMICAL TOOLS FOR THE STUDY OF SPHINGOLIPID METABOLISM IN DISEASES

Thesis presented by Mazen Aseeri to obtain the Doctorate degree
from the University of Barcelona

The thesis was performed at the Department of Biological Chemistry
Institute of Advanced Chemistry of Catalonia
Instituto de Química Avanzada de Cataluña (IQAC-CSIC)

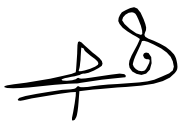

Mazen Ali Aseeri

Josefina Casas Brugulat	Gemma Triola Guillem	Marta Cascante Serratosa
Director	Director	Tutor

ACKNOWLEDGEMENTS

First and foremost I am extremely grateful to my supervisors, Dr. Josefina Casas and Dr. Gemma Triola and Dr. Marta Cascante for their invaluable advice, continuous support, and patience during my PhD study. Their immense knowledge and plentiful experience have encouraged me in all the time of my academic research and daily life.

I would also like to thank Dr. Gemma Fabrias and Dr. Mireia Casasampere for their technical support on my study. I would like to thank all the members of the Research unit of bioactive molecules (RUBAM). It is their kind help and support that have made my study and life, in Barcelona, a wonderful time.

Finally, I would like to express my gratitude to all members of my family, without which their tremendous encouragement in the past few years, this thesis would have not come into existence.

This work has been funded by the Ministry of Economy, Industry and Competitiveness (project CTQ2017-85378-R), and a fellowship from the Ministry of Higher Education of Saudi Arabia.

The following list includes the articles published in the duration of this thesis:

M. Aseeri, J.L. Abad, A. Delgado, G. Fabriàs, G. Triola, J. Casas. High-throughput discovery of novel small-molecule inhibitors of acid Ceramidase. *Journal of Enzyme Inhibition and Medicinal Chemistry (J Enzyme Inhib Med Chem)*. 2023 38(1):343-348. doi: 10.1080/14756366.2022.2150183. PMID: 36519337.

N. Bielsa, M. Casasampere, M. Aseeri, J. Casas, A. Delgado, J.L. Abad, G. Fabriàs. Discovery of deoxyceramide analogs as highly selective ACER3 inhibitors in live cells. *European Journal of Medicinal Chemistry (Eur J Med Chem).* 2021 Apr 15;216:113296. doi: 10.1016/j.ejmech.2021.113296. Epub 2021 Feb 24. PMID: 33677352.

Y.F. Ordóñez, J.L. Abad, M. Aseeri, J. Casas, V. Garcia, M. Casasampere, E.H. Schuchman, T. Levade, A. Delgado, G. Triola, G. Fabrias. Activity-Based Imaging of Acid Ceramidase in Living Cells. *Journal of the American Chemical Society (J Am Chem Soc)*. 2019 May 15;141(19):7736-7742. doi: 10.1021/jacs.8b11687. Epub 2019 May 2. PMID: 31030513.

ABBREVIATIONS

1-deoxySLs	1-deoxysphingolipids
ABP/s	Activity-based probe/s
AC	Acid ceramidase
ACER/s	Alkaline ceramidase/s
ACER1	Alkaline ceramidase 1
ACER2	Alkaline ceramidase 2
ACER3	Alkaline ceramidase 3
AMP	Adenosine monophosphate
AMPK	AMP-activated protein kinase
aSMase	Acid sphingomyelinase
C1P	Ceramide-1-phosphate
C1PP	Ceramide-1-phosphate phosphatase
CDase/s	Ceramidase/s
CDK/s	Cyclin-dependent kinase/s
Cdk2	Cyclin-dependent kinase 2
Cer/s	Ceramide/s
Cer1P	Ceramide-1-phosphate
CerK	Ceramide kinase
CerS	Ceramide synthase/s
CERT	Ceramide transfer protein
CPTP	Ceramide-1-phosphate transfer protein
DBCO-PEG$_4$5/6-TAMRA	Dibenzylcyclooctyne-PEG4-5/6-Tetramethylrhodamine
Des1	Dihydroceramide desaturase 1
ERAD	Endoplasmic reticulum-associated degradation
ERT	Enzyme replacement therapy
FD	Farber's disease
dhCer	Dihydroceramide
dhS1P	Dihydrosphingosine-1-phosphate
dhSo	Dihydrosphingosine
GBA	Glucocerebrosidase
GlcCer	Glucosylceramide
GlcCerS	Glucosylceramide synthase
HPLC	High-resolution liquid chromatography
HTS	High-throughput screening
IC_{50}	Half-maximal inhibitory concentration
KSa	3-ketosphingnanine
KSR	3-ketosphinganine reductase
LacCer	Lactosylceramide
LC-MS	Liquid chromatography–mass spectrometry

MAM	Mitochondrial-associated membranes
MAPK	Mitogen-activated protein kinase
MBCD	Methyl-β-cyclodextrin
MDR1	Multidrug resistance 1
NC	Neutral ceramidase
nSMase	Neutral sphingomyelinase
OH	Hydroxyl group
PEA	Phosphoryl ethanolamine
phCer	Phytoceramide
PHS	Phytosphingosine
PI3K	Phosphatidylinositol-3-kinase
ER	Endoplasmic reticulum
rhAC	Recombinant human acid ceramidase
rhNC	Recombinant human neutral ceramidase
S1P	Sphingosine-1-phosphate
S1PL	Sphingosine-1-phosphate lyase
S1PP	Sphingosine-1-phosphate phosphatase
S1PR/s	Sphingosine-1-phosphate receptor/s
Sa	Sphinganine
SK/s	Sphingosine kinase/s
SK1	Sphingosine kinase 1
SK2	Sphingosine kinase 2
SL/s	Sphingolipid/s
SM	Sphingomyelin
SMase	Sphingomyelinase
SMS	Sphingomyelin synthase/s
SMS1	Sphingomyelin synthase 1
SMS2	Sphingomyelin synthase 2
So	Sphingosine
SPAAC	Strain promoted alkyne−azide cyclo-addition
SPT	Serine palmitoyltransferase
WT	Wilde type

CHEMICAL STRUCTURES

Inhibitors of Alkaline Ceramidase 3 (ACER3)

20l

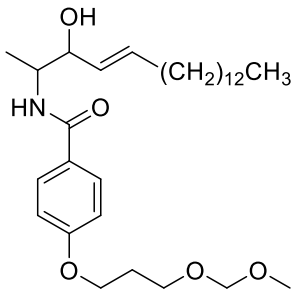

20m

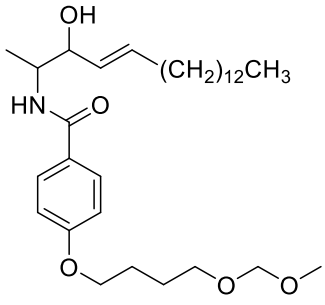

Activity-based Probes for Acid ceramidase (AC) labelling

SOBRAC: X=Br
SOCLAC: X=Cl

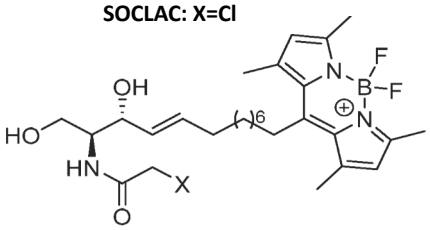

Inhibitors of AC

W000113402_C12

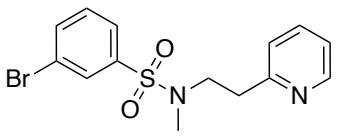

W000113414_H19

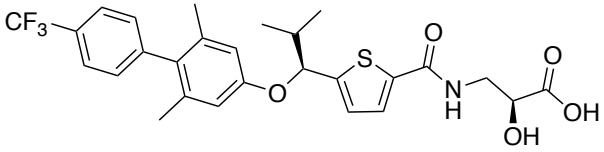

W000113402_O07

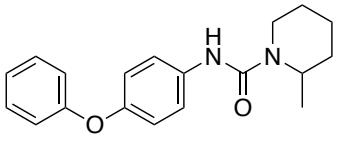

W000113403_I18

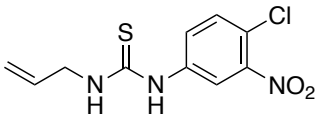

W000113414_D15

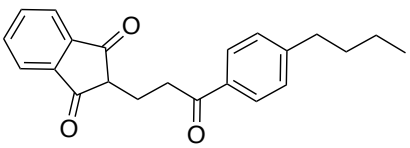

W000113414_I13

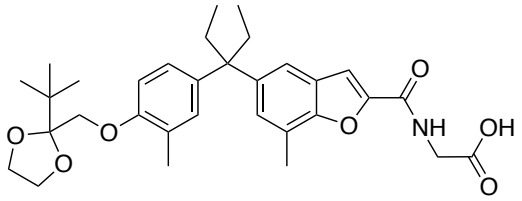

W000113407_J11

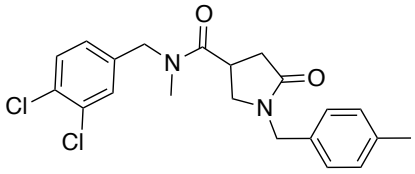

W000113400_H06

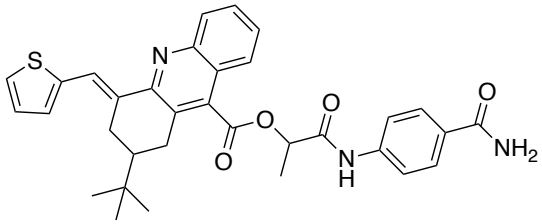

W000113414_C16

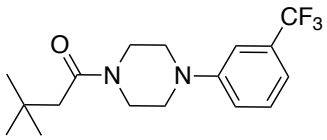

Summary of the chemical structures of the compounds used in this thesis.

INDEX

INTRODUCTION

1. Sphingolipids

The major classes of lipids which compose mammalian cellular membranes are glycerophospholipids, sterols and sphingolipids (SLs)[1,2], and they differ by the structure of their hydrophobic skeleton. SLs are derived from the amino-alcohol sphingosine and are present in all eukaryotic membranes[3]. In the 19th century, J. L. W. Thudichum[4] was the first to describe and isolate these lipids, which would later be known as sphingosines. Inspired by the mythological figure of the sphinx and its enigmatic nature, he assigned them the name "Sphingolipids"[5]. SLs comprise a vast family of lipids with a broad variety of functions. Besides their structural function as membrane lipids, SLs are involved in different cellular processes such as growth, death, senescence, adhesion, migration, inflammation, differentiation, and intracellular transport[6,7].

1.1 Structure of Sphingolipids

SLs are amphipathic molecules, similar in that to all other membrane lipids[8]. They are usually composed of a polar (hydrophilic) head and two non-polar (hydrophobic) tails[9]. One of the two tails is an amino-alcohol called sphingosine or sphingoid base, which in mammals is often made of 18 carbon atoms[10], and the other tail is a fatty acid of variable lengths. Both tails are joined together by an amide bond (Figure 1).

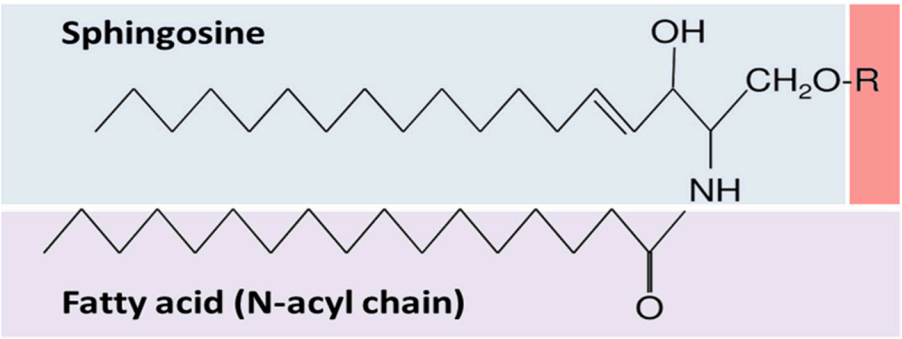

Figure 1. General structure of sphingolipids: SLs are made up of a sphingosine (Sphingoid base) bound to a fatty acid chain via an amide bond. R represents the different polar groups[11].

In mammals, the most commonly occurring sphingoid bases are sphingosine (So), sphinganine (Sa), also called dihydrosphingosine (dhSo), and phytosphingosine (PHS)[12]. These bases can exist in their free formula or amide-linked to a fatty acid chain of more complex sphingolipids[13]. SLs may be classified based on: the sphingoid base, the fatty acids attached to the sphingoid base, as well as their diverse polar groups. As shown in figure 2, N-acylated So, Sa and PHS become ceramide (Cer), dihydroceramide (dhCer), and phytoceramide (phCer), respectively.

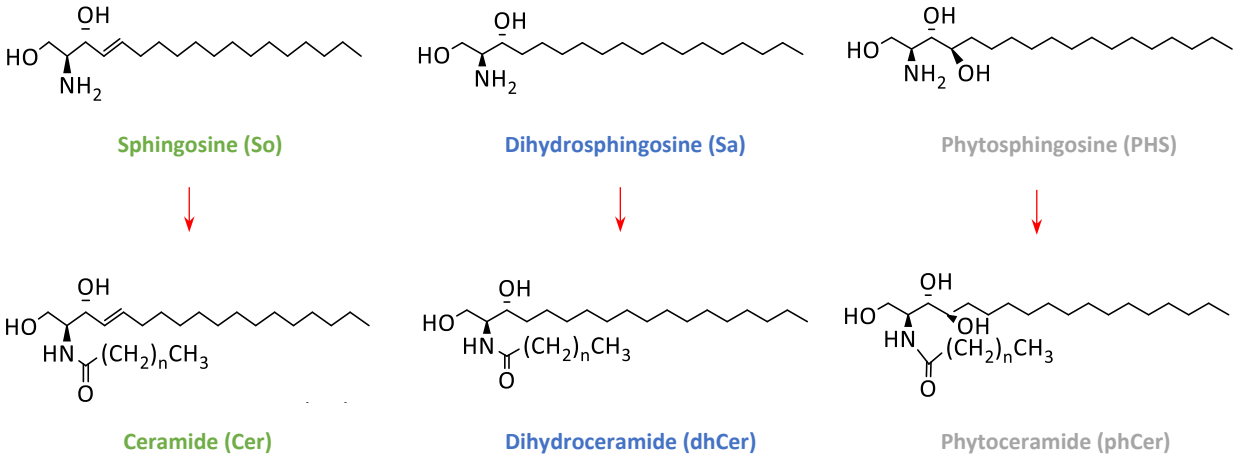

Figure 2. Structures of the mammalian most commonly found sphingoid bases and their N-acylation products.

Ceramide, among all other sphingolipids, contains the simplest polar head structure consisted of two hydroxyl groups[14,15]. Derivatives of ceramide are formed by the substitution of the hydroxyl group at the first carbon atom (C1) (Figure 3). For example, Glycosphingolipids are the products of ceramide glycosylation with a a wide range of carbohydrates of varying complexity[16,17], among which glucosylceramide representing the simplest structure[18]. Another derivative is Sphingomyelin (SM) which has a phosphorylcholine moiety. The addition of a phosphate group to the hydroxyl at C1 of the ceramide or Sphingosine, produces ceramide-1-phosphate (Cer1P) or sphingosine-1-phosphate (S1P), respectively. Thousands of SLs species have been identified over the years[19]. They differ in solubility, as well as in their biological properties depending on the degree of unsaturation, the polar head and the length of the fatty acid contained[20].

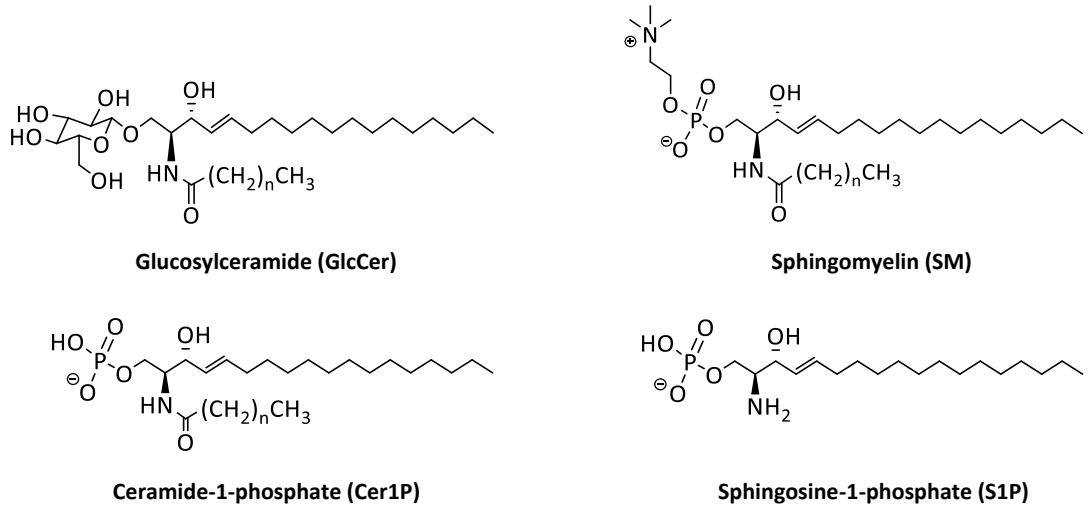

Figure 3. Ceramide and sphingosine derivatives formed by the substitution of the hydroxyl group at the first carbon atom (C1).

1.2 Sphingolipids Metabolism

Probably, the domain most explored in the field of sphingolipids is their metabolism, where most of the metabolic pathways and the enzymes by which they are synthesized and degraded have been well illustrated[21]. Cer, the central molecule of sphingolipid metabolism, is mostly synthesized from non-sphingolipid precursors via the de novo anabolic pathway. Yet, Cer can also be formed through two other alternative pathways: The catabolic pathway where hydrolysis of complex sphingolipids takes place, particularly SM, and the recycling pathway of sphingoid bases (Figure 4).

The equilibrium between biosynthesis and catabolism of different SLs will often ensure the metabolic homeostasis of the total mass of sphingolipids. This is achieved through a well-balanced de novo biosynthesis, catabolic and recycling pathways[20].

1.2.1 The de novo biosynthesis pathway

The de novo biosynthesis of ceramide is a multi-step process that occurs at the endoplasmic reticulum (ER)[22,23]. It commences with the conjugation of L-serine with palmitoyl-CoA to form 3-ketosphingnanine (KSa)[24]. The former reaction is catalyzed by the action of serine palmitoyltransferase (SPT), a heterodimeric enzyme possessing an N-terminal hydrophobic region in each monomer[25]. In mammals, SPT utilizes palmitoyl-CoA as a substrate to produce the most common sphingoid base of 18-carbon atoms. Thus, in eukaryotes, SLs are mostly consisting of an 18-carbon backbone[26]. However, in certain cases, 20-carbon atoms or 16-carbon atoms sphingolipids backbones can be generated when SPT uses other substrates such as stearoyl-CoA and myristoyl-CoA, respectively[27]. Mutations in SPT exhibit an increased preference for L-alanine as a substrate rather than L-serine, rendering an increased production of 1-deoxysphingolipids (1-deoxySLs)[28,29]. Moreover, in cases of low serine levels, SPT may use other amino acids as alternative substrates, such as glycine[30]. These atypical sphingolipids differ structurally from canonical SLs in that they lack the C1-hydroxyl group, which is essential in the synthesis of complex SLs and for their final degradation to phosphoethanolamine and hexadecenal[28]. As such 1-deoxySLs conversion to complex SLs and their degradation via the canonical catabolic pathway, are both not possible[28].

The de novo synthesis continues with the reduction of KSa to Sa catalyzed by 3-ketosphinganine reductase (KSR). Acylation of Sa, binding the corresponding fatty acid, yields dhCer. This reaction is catalyzed by various ceramide synthases (CerS) differing in their specificity for fatty acid chain lengths[31]. Next, desaturation of dhCer by adding a cis double bond at C4-C5 is catalyzed by dihydroceramide desaturase 1 (Des1) to ultimately generate Cer[20,32]. Later, Cer and, to a lesser extent, dhCer form more complex sphingolipids such as Sphingomyelin (SM) and dihydrosphingomyelin (dhSM) or glucosylceramide (GlcCer) and glucosyldihyroceramide (GlcdhCer). This takes place in the Golgi apparatus, after Cer translocation from the ER to it through vesicle-dependent or vesicle-independent pathways[33]. The addition of specific constituents at the C1-OH position of Cer yields different complex sphingolipids. Thus, the addition of a phosphorylcholine group to Cer by the action of Sphingomyelin synthases (SMS1 and SMS2)

generates SM[34], whereas under the action of glucosylceramide synthase (GlcCerS)[35] or ceramide kinase (CerK)[36] yields glycosphingolipids and ceramide-1-phosphate (C1P), respectively (Figure 3).

1.2.2 The catabolic pathway

An alternative pathway of Cer metabolism is its hydrolysis through different ceramidases (CDase) to produce So, which is a substrate of sphingosine kinases (SK1 and SK2) to generate sphingosine-1-phosphate (S1P)[37]. The final products of this pathway; phosphorylethanolamine (PEA) and hexadecenal are produced through the irreversible degradation of S1P by sphingosine-1-phospate lyase (S1PL)[38].

Complex sphingolipids are a source of Cer when degraded. The hydrolysis of SM by sphingomyelinases; acidic (aSMase) or neutral (nSMase), produces phosphorylcholine and Cer[39]. This pathway occurs in the lysosomes, mitochondria and plasma membrane, and is commonly known as the sphingomyelinase (SMase) pathway. Also, the hydrolysis of glycosphingolipids via specific lysosomal hydrolases generates Cer[40]. In addition, Cer can be generated from the hydrolysis of the phosphorylated sphingolipid C1P[41].

1.2.3 The recycling pathway

This pathway occurs in the lysosomes where S1P is hydrolyzed by sphingosine-1-phosphate phosphatase (S1PP) to generate So, which is then recycled back into ceramide under the action of ceramide synthase (CerS)[42].

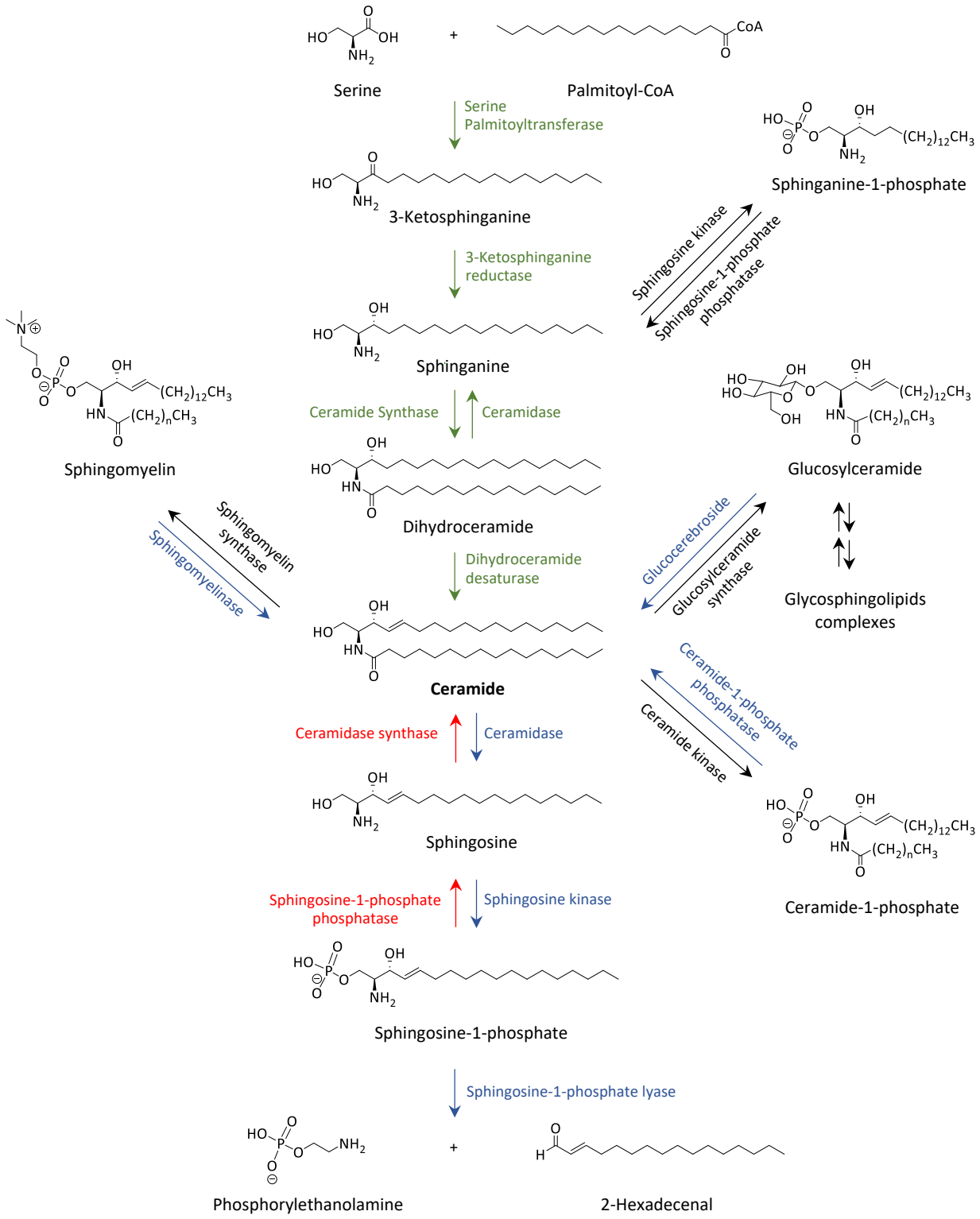

Figure 4. Sphingolipids metabolic pathways. Green arrows indicate de novo biosynthesis pathway, while blue and red arrows refer to catabolic and recycling pathways, respectively.

1.3 Compartmentalization of Sphingolipids

Biosynthesis of SLs is a highly conserved process comprising a series of enzymatic reactions that occur in various cellular compartments[43] (Figure 5). The initial stages of the de novo synthesis of Cer take place in the cytosolic face of the ER[44], as well as in other membranes such as the prenuclear membrane and mitochondrial-associated membranes (MAM), an ER-like membrane involved in cell signaling and closely associated with both mitochondria and ER[45]. The formation of SM and GluCer by the addition of a polar head to the Cer occurs in the Golgi apparatus. The translocation of Cer from the ER to the Golgi apparatus is not carried out via regular transport through the cytosol but rather by active mechanisms due to Cer hydrophobic properties[46].

These mechanisms of Cer transport to Golgi apparatus, with or without vesicles, were described by Fukasawa et al[47]. Ceramide transfer protein (CERT) is one of the proteins that was characterized as responsible for the non-vesicular transport of Cer[48,49]. SM synthesis is initiated on the luminal face of the Golgi apparatus, and it is dependent on CERT for Cer delivery[50]. GluCers, however, are synthesized in the cytosolic face of Golgi[51], where Cer is delivered to it via vesicles[52]. GluCer synthesis takes place in the cis-Golgi region and is subsequently translocated to the trans-Golgi compartment through FAPP2 protein (four-phosphate adaptor protein 2)[53]. It is at this region of Golgi where the enzymes responsible for lactosylceramide (LacCer) and glycosphingolipids synthesis exist[54]. And for these complex molecules to be formed, GluCer shall move from the cytosolic surface to the Golgi lumen[55], via P-glycoprotein or multidrug resistance 1 (MDR1) protein[56].

Once SM and GluCer are synthesized at the Golgi, they are generally transferred to the plasma membrane in a vesicular manner[57]. In the plasma membrane, SMase, CDase and SK catalytic actions over SM and GluCer, generate Cer, So and S1P respectively. Cer can be phosphorylated by CerK to form C1P[58] on the cytosolic face of the Golgi[59]. Unlike both SM and GluCer, C1P is not transported in vesicles, however it requires the specific ceramide-1-phosphate transfer protein (CPTP) for its trafficking to the plasma membrane or to other cellular compartments[60,61]. Interchangeably, complex sphingolipids in the plasma membrane are endocytosed and delivered to the lysosomes, where they are hydrolyzed into So, under the action of the acidic isoforms of SMase, glucocerebrosidase (GBA), and CDase[62]. This free So base is then capable of leaving the lysosome and being trafficked across membranes due to its solubility, until it reaches ER where it is recycled to form Cer.

SLs are also metabolized in the nucleus as the nuclear matrix contains SM[63–65]. By SMase and CDase, SM is hydrolyzed generating So. The synthesis of S1P is catalyzed by SK2, the nuclear isoform of SK, which could be involved in the transcription of certain genes[66]. Cer and several additional SLs are also found in the mitochondria[67]. Although Cer in the ER can be translocated to the mitochondria by the membrane contact of the two organelles, Cer is also generated within the mitochondria by the actions of CerS or a reverse isoform of neutral CDase[68].

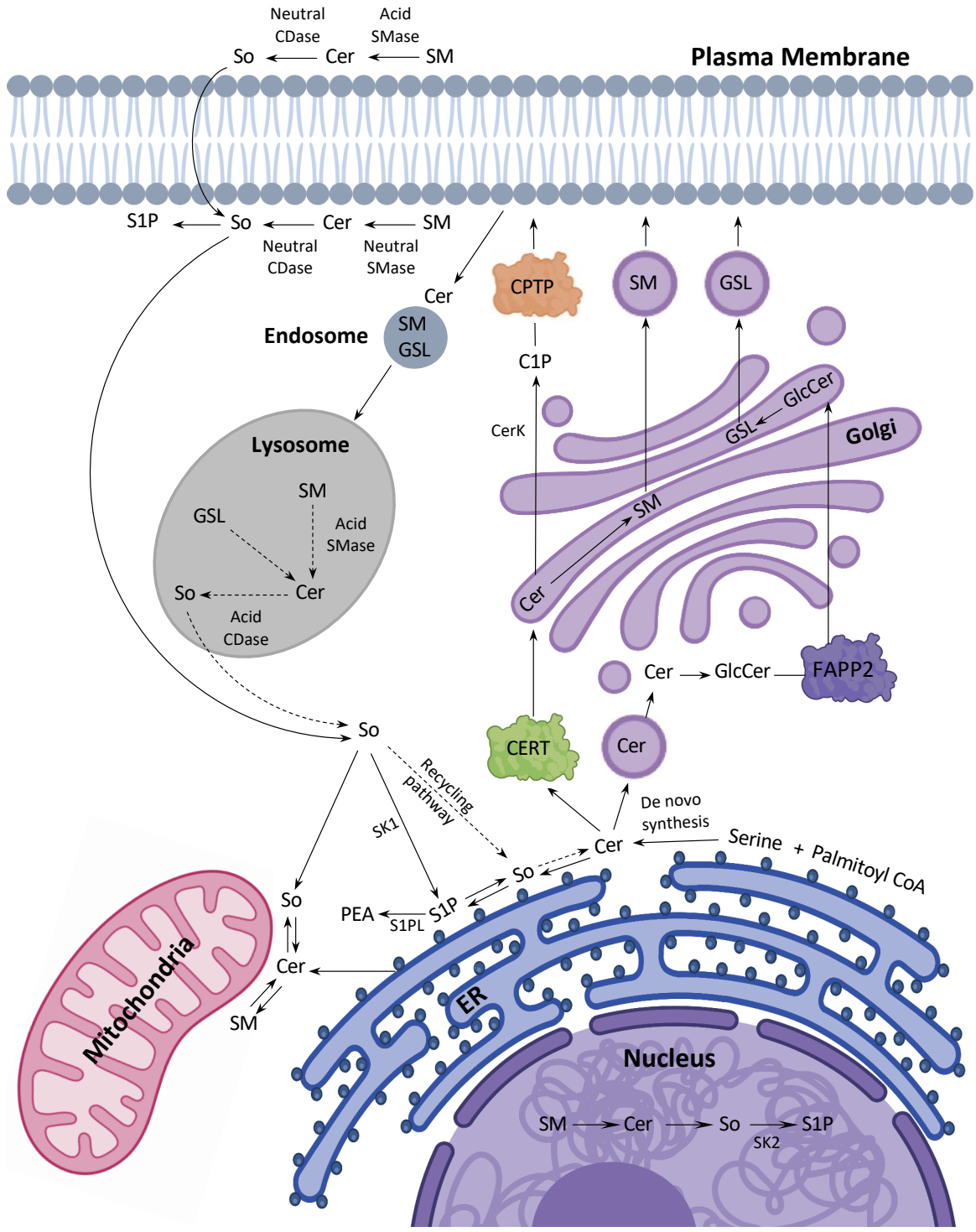

Figure 5. Compartmentalization of sphingolipid metabolism.

2. Sphingolipids in cell signaling

The metabolism of SLs can be regulated at various levels, ranging from controlling the expression of the enzymes involved in the pathways to allosteric mechanisms. Among the several SLs found, each one has its signaling and regulatory functions and this may in turn explain their vast structural diversity and the complexity of their metabolic pathways.

2.1 Bioactive sphingolipids

Besides their structural role as cell membrane lipids, Cer and its metabolic products take part in regulating signaling pathways involved in many physiological and pathophysiological processes such as proliferation, differentiation, migration, angiogenesis, apoptosis, senescence, autophagy and inflammatory responses[69]. Although SLs play an essential role in cellular homeostasis, their metabolic dysregulation and/or changes in their cellular localization can cause the onset and progression of diseases[70].

2.1.1 Ceramide

Cer is the key molecule of sphingolipids metabolism, and possibly the most investigated SL among all others. Cer role in various cellular processes has been illustrated, including their involvement in cell differentiation[71,72], apoptosis[73–75], senescence[76] and cell cycle arrest[77]. The study of the roles of the different Cer subspecies has been made possible through the analysis of the sphingolipidome using mass spectrometry[78]. The Cer subspecies are diverse owing to the heterogeneity of the fatty acid chain contained in each one, which its determination is subject to the activity of six different CerS[79]. Each CerS has a specific preference for fatty acids, and therefore generating certain subspecies of Cer[80]. According to the length and the unsaturation of the fatty acid attached to the sphingoid base, the physicochemical properties of Cer will be determined and therefore also its physiological properties[81].

The subcellular location of Cer also has its own role in determining its biological behavior[82]. In the plasma membrane, for instance, it has been noted that the Cer generated from the hydrolysis of SM initiates growth arrest and cell death by oxidative stress[83,84]. Whereas in the mitochondria, acting as a cellular messenger in apoptosis is Cer's most prominent function[85]. Particularly, the effects of Cer converge at the mitochondrial level, at which the anti-apoptotic proteins (Bcl-2 and Bcl-XL) are inhibited and the potential of the mitochondrial membrane is decreased, allowing pores to be created and the release of cytochrome C into the cytosol[86,87]. This triggers apoptosome formation followed by the activation of caspases, which in its turn leads to the initiation of the intrinsic apoptotic cell death[88,89]. In the lysosome, Cer can also be generated by the action of acid SMase, activating then cathepsin D[90,91], which cleaves the BID protein leading to the induction of apoptosis[92,93]. Since the membranous structures of ER and the nucleus are connected, the Cer generated in the ER can function in the nucleus by inhibiting the activity of telomerase, and thus

regulating senescence and aging[94,95]. The nuclear Cer can also activate phosphatase-1 which triggers the alternative splicing of the pro-apoptotic caspase-9[96].

Besides their apoptotic role, Cer's most characteristic signaling is its ability to induce cell cycle arrest, in the G0/G1 phase, via the activation of retinoblastoma protein (Rb)[97,98]. Moreover, it has been shown that Cer is also involved in cell cycle arrest through modulating cyclin-dependent kinases (CDKs), such as the cell division protein cyclin-dependent kinase 2 (cdk2)[99] and in the regulation of cell differentiation[71,82,100]. Finally, autophagy is affected by Cer involvement in the regulation of the autophagic protein Beclin 1[101,102].

2.1.2 Sphingosine-1-phosphate

Many essential physiological and pathological processes are influenced by S1P, working as a mediator molecule[103]. One of the most prominent effects of S1P is its resistance to apoptosis, which is a signaling opposite to that of Cer[104]. Besides that, S1P is involved in cell growth, survival, proliferation, migration, inflammation and angiogenesis[105–107]. Also, S1P has shown an ability to induce autophagy, as a way to protect the cell from apoptosis and to promote its survival[108].

In addition to its intracellular signaling, S1P can also act extracellularly as it is often released out of the cell binding cell surface receptors of high specificity to S1P, through which they signal in autocrine and/or paracrine manners[109]. These receptors are named S1P receptors (S1PRs) and are coupled to the G protein, therefore regulating multiple intracellular signaling pathways[110]. Five S1PRs (S1P1-5) have been identified, of which their expressions vary depending on tissue and cell type. S1P1-3 receptors are ubiquitously expressed, while the expressions of S1P4 is restricted to the lung and lymphatic tissues, and S1P5 is limited to the skin and the brain[111]. Once activated, these receptors trigger various signaling pathways including phosphatidylinositol-3-kinase (PI3K), mitogen-activated protein kinase (MAPK), AMP-activated protein kinase (AMPK), as well as other intracellular mediators[112]. Signaling of S1P through these receptors has effects on cell proliferation, invasion, migration, angiogenesis and rearrangement of cytoskeleton[113]. Although the extracellular signaling of S1P via S1PRs is very well known, its intracellular effects are not exactly determined. Though, it appears that the S1P which has no involvement in extracellular signaling, has effects on regulating cell growth and suppressing apoptosis[114].

The multiple and diverse actions of S1P have shed light on the importance of regulating its intracellular levels. S1P is a product of the phosphorylation of So by the SK enzyme, which is eventually degraded through the action of S1PL, as well as by phosphatases. Although S1P generation has been shown to be mainly dependent on the activities of SK1 and SK2, it is also restricted by the availability of So. It is this point at which sphingolipid rheostat is spoken of (Figure 6).

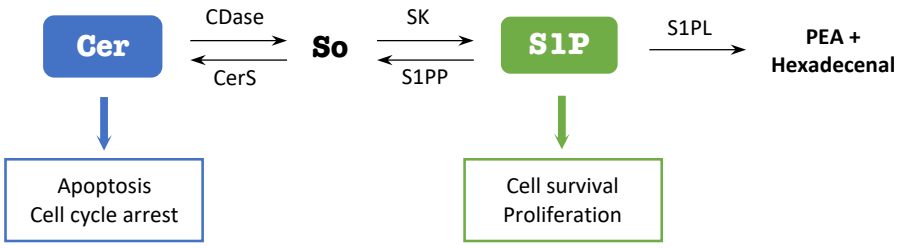

Figure 6: The interconvertible relationship between Cer and S1P. The balance between bioactive SLs with opposing signaling effects determines cell fate.

Reaching this rheostat confers homeostasis to cells, and this is achieved through the balance between Cer and S1P levels, which are understood to be metabolites of opposite roles. There is Cer on one side, which is associated with anti-proliferative processes such as apoptosis, senescence and cell cycle arrest. Similarly, and on the same side, there is So which is also related to cell cycle arrest and apoptosis[115]. On the other side, there is S1P which is involved in pro-survival processes such as proliferation, cell survival and growth, thus making it a lipid of an antagonistic function to that of Cer. As Cer and S1P are interconvertible metabolites, it is not their absolute amounts that determine cell fate, but rather their relative levels. Given that So generation is dependent on CDase activity, it is possible to say that the right balance between CDase and S1PL activities is the key determinant for a well-maintained cellular homeostasis.

2.2 Enzymes of sphingolipid metabolism

Disorders of sphingolipid metabolism are commonly known by sphingolipidoses[116]. Mutations in the genes that encode the enzymes responsible for metabolizing SLs, cause their inactivation or lack of activity, which in its turn lead to the accumulation of associated lipids in cell organelles and thus, the manifestation of diseases. For instance, Farber's disease (also called lipogranulomatosis) is a metabolic disorder which is caused due to mutations in *ASAH1* gene encoding lysosomal acid CDase[117]. Whereas, mutations in SMPD1 gene, which encodes aSMase, cause autosomal recessive Niemann-Pick types A and B diseases, result in severe lysosomal disorders often leading to death before completing three years of age[118]. Another sphingolipidosis is Gaucher disease which is caused due to point mutation in GBA1 gene, leading to the accumulation of glycosphingolipids in the lysosomes of immune cells (macrophages or monocytes)[119].

Although SLs constitute only a minor percentage of the total cellular lipids, changes in their levels or in the activity of their metabolic enzymes are strongly related to the onset and progression of several diseases[120]. Apart from the disorders mentioned earlier, abnormal sphingolipid metabolism has been observed in cardiovascular diseases, type 2 diabetes, cancer, chronic inflammation and neurodegenerative disease such as Alzheimer's disease. This involvement explains the reason why several enzymes of sphingolipid metabolism have been considered promising therapeutic targets.

2.2.1 Ceramidases

CDases hydrolyse Cer to produce So and a fatty acid chain. So can be later phosphorylated to generate the S1P by the action of SKs. As the only pathway for S1P generation is by the phosphorylation of So, S1P levels are totally dependent on the availability of So formed by the action of CDases. This indicates that CDases are key players not merely in Cer regulation but also in S1P generation, which therefore make them enzymes of significant role in cell fate determination[121–123]. According to their optimal pH of activity, CDases are classified into acid (AC), neutral (NC) and alkaline (ACER). There are five human CDases encoded by five distinct genes: AC encoded by *ASAH1* gene, NC encoded by *ASAH2* gene and the three alkaline CDases ACER1, ACER2 and ACER3 encoded by *ASAH3*, *ASAH3L* and *PHCA* genes, respectively (Table 1).

Enzyme	Gene	Optimal pH	Subcellular location
Acid ceramidase (AC)	*ASAH1*	4.5	Lysosome
Neutral ceramidase (NC)	*ASAH2*	7.6	Plasma membrane, mitochondria, Golgi apparatus and secreted
Alkaline ceramidase 1 (ACER1)	*ASAH3*	8.5	Endoplasmic reticulum
Alkaline ceramidase 2 (ACER2)	*ASAH3L*	7-9	Golgi apparatus
Alkaline ceramidase 3 (ACER3)	*PHCA*	9.5	Endoplasmic reticulum and Golgi apparatus

Table 1: Five types of human CDases encoded by five different genes can be found in cells and they are classified according to the optimal pH for their enzymatic activity and their subcellular location.

CDases vary in their subcellular location, tissue distribution and substrate specificity. AC is expressed in the lysosomes, while NC is found in the mitochondria[124,125], Golgi apparatus[126], plasma membrane or secreted into extracellular space[127]. In regards to alkaline ceramidases, ACER1 is solely expressed in the ER of epithelial skin cells[128,129], ACER2 is found in Golgi apparatus[130,131] and ACER3 is located in ER and Golgi[132]. Together ACER2 and ACER3 are expressed in all tissues. However, their expressions in the placenta are particularly high[133–135]. In addition to the hydrolysis of Cer, certain CDases have shown a reverse activity under the action of the same enzyme. In this context, Cer is generated from a sphingoid base by a CDase (in this case its reverse action) [136–138]. Unlike the activity expressed by CerS which utilizes acyl-CoA as a substrate, the reversed activity of CDase employs free fatty acids[139,140].

2.2.1.1 Acid ceramidase

In humans, AC (also known by *N*-acylsphingosine amidohydrolase 1) is encoded by *ASAH1* gene. AC is a heterodimeric glycoprotein made of two subunits, an α non-glycosylated subunit of 13 kDa and a β glycosylated subunit of 40 kDa[141]. It is initially synthesized as an inactive precursor in the ER, which is then processed in the lysosomes into the mature form of the enzyme, where the α and β subunits are attached via disulfide bonds[142]. This post modification of AC requires an acidic pH to be initiated, thus preventing premature activation of the enzyme prior to its arrival to the lysosome. After the cleavage of the precursor protein, the enzyme has an active site nucleophilic thiol contained in the cysteine residue (Cys 143), which is exposed at the N-terminus of the β subunit. Regarding substrates, Cers containing fatty acids with carbon chains of C12-C14 are considered AC best substrates, as compared to shorter chains (≤C6) or longer ones (≥C16)[143]. Moreover, unsaturated Cer (C18:1 or C18:2) are preferred substrates for AC over saturated Cer (C18)[144]. The hydrolytic action of AC functions optimally at a pH of 4.5 and its enzymatic activity does not require the binding of metal ions[145].

In human cells, AC is considered a central enzyme in the degradation of Cer, and deficiency in its activity causes Farber's disease, also known as lipogranulomatosis[117]. It is a congenital autosomal recessive disease, which is characterized by the accumulation of Cer in multiple tissues such as liver, lungs and spleen. AC also plays a role in other disorders such as type 2 diabetes, where it prevents it from happening by the modulation of the insulin signaling pathways[146]. In Alzheimer's disease, significantly high levels of AC controls neuronal apoptosis[147,148]. Aberrant AC expression have also been observed in several tumor cell lines such as prostate cancer[149,150], melanoma[151,152] and neck and head cancers[153]. Generally, AC overexpression promotes the survival of cancerous cells through the excessive conversion of Cer (pro-apoptotic) into S1P (anti-apoptotic). For example, knockout of AC in mice was found to cause death in the early stages of embryos, which reinforces the validity of the role AC plays in cell survival. Conversely, death was delayed in embryos after treatment with exogenous S1P, indicating that the deadly effect of AC silencing is partly due to the inability to generate S1P[154].

2.2.1.2 Neutral ceramidase

NC (also known as N-acylsphingosine amidohydrolase 2) is an integral protein of the plasma membrane, with a catalytic domain facing towards the extracellular space[155]. In regard to substrates, it seems that NC has preference for long-chain Cer (C16-C22) over very long ones (≥C24)[156], with an inability to hydrolyze dhCer[143]. However, its exact substrate specificity has not yet been determined. NC optimum pH of activity is in the range of 6.5 and 8.5, where metal ions are not required for its activity[124]. NC can be secreted when a proteolysis of its terminal region occurs, causing it to be loosely attached to the membrane and finally leaving it[157]. The presence of NC in mitochondria has also been described in HEK293105 and MCF-7 cell lines. Given that NC is found in the plasma membrane and extracellularly secreted, NC can hydrolyze Cer found in the membrane, as well as that one freely floating outside the cell. This is the reason why the primary function of neutral ceramidase is being a digestive enzyme that takes part in the degradation of

dietary SLs, and it is highly expressed in the villi throughout the small intestine[158]. Like AC, NC promotes cell survival and proliferation through decreasing Cer levels and increasing S1P effect. Thus, the inhibition of NC leads to cell cycle arrest and/or apoptosis[159].

2.2.1.3 Alkaline ceramidases

Three different types of alkaline CDases exist: ACER1, ACER2 and ACER3, which they are alike in that they have multiple transmembrane domains and being of similar molecular weights of approximately 31 kDa. Although, there is a great similarity in their protein sequence, each enzyme has its specific properties. As they differ in cell location, substrate specificity, tissue distribution and level of expression, ACERs are anticipated to play various roles in cellular signaling[160].

2.2.1.3.1 Alkaline ceramidase 1

Located in ER, ACER1 is a protein of multiple transmembrane domains[129]. The pH optima for the activity of ACER1 has been reported to be 8.5, and the absence of cations causes a dramatic decrease in its activity[129]. In addition, it has been reported[161] that very long-chain, unsaturated Cer (such as Cer C24:1) are the preferred substrates for ACER1. Initially, ACER1 was described as incapable of hydrolyzing neither dhCer nor phCer[129]. Later on, it has been revealed that ACER1 actually can hydrolyze unsaturated dhCer yielding dhSo species, however it cannot hydrolyze saturated dhCer[143]. This hydrolysis, however, occurs only in certain types of cells such as epidermal keratinocytes. In vitro, the activity of ACER1 increases exclusively with Ca^{2+}, but not other cations, suggesting that Ca^{2+} is a specific ionic activator for ACER1. Moreover, the generation of So in response to ACER1 overexpression is hindered under the treatment with Thapsigarin, which is a Ca^{2+} ATPase inhibitor that depletes ER Ca^{2+} levels[134]. This indicates that the cellular activity of ACER1 is regulated by the levels of Ca^{2+} in the ER.

ACER1 is mainly expressed in the skin[128], particularly in the upper layers of the epidermis. ACER1 is located in this tissue in which it plays its most significant role of regulating keratinocytes differentiation, the main epidermal cell type[162]. The differentiation of keratinocytes is promoted by the anti-proliferative properties of the bioactive lipid So. Thus, the growth arrest and induction of keratinocyte differentiation are caused as a result of the increased levels of So due to the activity of ACER1.

2.2.1.3.2 Alkaline ceramidase 2

Via the analysis of mRNA levels, ACER2 has been shown to be of high expression in the placenta, and of moderate expression in other tissues[135]. ACER2 and ACER1 have quite similar protein sequences, including several trans-membrane domains. However they differ in their subcellular location being ACER2 found in the Golgi apparatus[163]. Composed of odd transmembrane domains, the N-terminal tail is facing Golgi lumen and the C-terminus is oriented towards the cytosolic face. It has been shown that this arrangement is essential for its correct location in the Golgi, as well as for its CDase activity[130]. Its pH optima has been determined to be between 7 and 9, and it requires Ca^{2+} to optimally function in the Golgi lumen, both in vitro and in cells[130]. Similar to ACER1

substrate preference, ACER2 preferentially hydrolyzes Cer, over dhCer and phCer[163]. It has been reported that ACER2 catalyzes the hydrolysis of most mammalian Cer species, having a preference for unsaturated long-chain Cers[130]. Although both ACER1 and ACER2 prefer Cer as a substrate, they are also able to hydrolyze very long and unsaturated dhCer chains (C24:1), being considered the most abundant dhCer species in tumor cells[143]. In tumor cells, the CDase responsible for the generation of dhSo from dhCer is ACER2, since AC and NC are incapable of hydrolyzing dhCer, the activity of ACER1 is limited to keratinocytes[143] and ACER3 hydrolyzes low-abundance dhCers, as discussed in the next section.

Depending on its expression level, ACER2 either promotes cell proliferation or growth arrest. ACER2 moderate increased expression stimulates cell survival and proliferation, which is likely due to the decrease in Cer levels and the increased in S1P ones[163]. However, very high ACER2 expression may lead to the fragmentation of the Golgi apparatus, as it increases ceramide hydrolysis and therefore generating abnormally high So levels that lead to the inhibition of cell proliferation[163–165]. ACER2 also plays a key role in regulating protein glycosylation in Golgi[130]. Thus, the overexpression of ACER2 results in the inhibition of the glycosylation of the precursor of the β1 subunit of integrin, leading to the inhibition of cell adhesion to the extracellular matrix. In addition, a study conducted in HeLa cells has showed that ACER2 expression increases in response to serum deprivation. This increased expression has probably a protecting role by promoting cell survival since the knockdown of ACER2 in serum-free culture medium Hela cells led to the inhibition of cell proliferation, and caused apoptosis[163].

2.2.1.3.3 Alkaline ceramidase 3

ACER3, also known as alkaline phytoceramidase (aPHC) for its ability to hydrolyze the synthetic analogue of Cer D-ribo-C12-NBD-phytoceramide in vitro, was the first alkaline ceramidase to be cloned in mammmals[133]. ACER3 is located in both the ER and Golgi apparatus, and it is homologous to both ACER1 and ACER2, possessing multiple transmembrane domains[133]. Its optimum pH of activity is approximately 9.5, and it is stimulated by the presence of Ca^{2+} ions[133]. ACER3 is distinguished from other alkaline CDases by having a unique substrate specificity. As substrates, ACER1 and ACER2 utilize the long-chain Cer species abundant in mammals (such as C16, C24 and C24:1), whereas, ACER3 only hydrolyzes sparse Cer species such as mono- or poly-unsaturated Cer long chains (e.g. C18:1, C20:1 or C20:4), but is it incapable of hydrolyzing Cer long saturated chain (e.g. C18) or very long unsaturated chain (such as C24:1)[166]. Unlike other alkaline ceramidases (ACER1 and ACER2), ACER3 has the ability to hydrolyze Cer, dhCer and phytoceramides with similar efficacy in cells and in vitro[166]. It is important to note that non-mammalian polyunsaturated Cer and dhCer long chains are also substrates of ACER3[166].

Through the analysis of ACER3 mRNA levels in many cell lines via qPCR, an overexpression of this CDase was noted in fibroblasts, endothelial cells, hematopoietic cells and smooth muscles[166]. Moreover, mRNA levels were correlated with an increase in CDase activity. These results suggest that, among all other alkaline CDases, ACER3 is considered to be the most active in a wide range of cellular models. The knockdown of ACER3 leads to the inhibition of cell proliferation as a result of the activation of p21, a cyclin-dependent kinase inhibitor. Undoubtedly, this inhibition is due to

the accumulation of Cer, which in its turn alters cell growth. In addition, this gene knockout results in overexpression of ACER2, thus suggesting that ACER3 and ACER2 function coordinately to compensate for the loss of CDase activity, and therefore being able to regulate cell proliferation and control the levels of Cer, So and S1P[166].

2.2.1.4 Methods for the determination of ceramidase activity

The growing interest in CDases has led researchers to develop methods for the determination of their enzymatic activity. The first assay introduced used Cer radiolabeled with ^{3}H or ^{14}C. After the hydrolysis of these radiolabeled Cer, the levels of radioactivity in the reaction product and fatty acid were measured[167]. Due to the disadvantages of the use of radioactive substrates, fluorescent Cer analogues were the alternatives, such as Cer-NBD[168] or Cer-BODIPY[169]. The fluorophore in these substrates is linked to the end of the fatty acid chain of Cer, and under the action of CDases a fluorescent fatty acid is generated. Another testing approach to determining CDase activity is to evaluate the So generated after its derivatization with fluorescent compounds such as NDA (naphthalene-2,3-dialdehyde)[170]. To determine the enzymatic activity using the prior substrates it is necessary to separate the reagents and products via high-resolution liquid chromatography (HPLC) coupled to a fluorescent detector.

Given that CDases have been validated as being therapeutic targets, the development of inhibitors of CDases received increased attention. The majority of these inhibitors were rationally designed; however, many of them were discovered through the screening of compound libraries. Despite the existence of many procedures for the determination of CDase activity, only few of them can be employed in compound library screening, as the latter requires high-throughput screening (HTS) methodologies, which cannot be applied in most of these CDase activity assays (for example the ones requiring chromatographic separation of the substrate and the product). Among these handful methods suitable for HTS, one can find a FRET (fluorescence resonance energy transfer)-based assay that uses a Cer analogue labelled with two fluorophores, NBD and Nile Red. Changes in fluorescence emission upon hydrolysis allowed the determination of the enzymatic activity in real time[171]. Our group has also developed some CDase substrates suitable for HTS, such as the Cer coumarin analogues RBM14[172,173] (Figure 7).

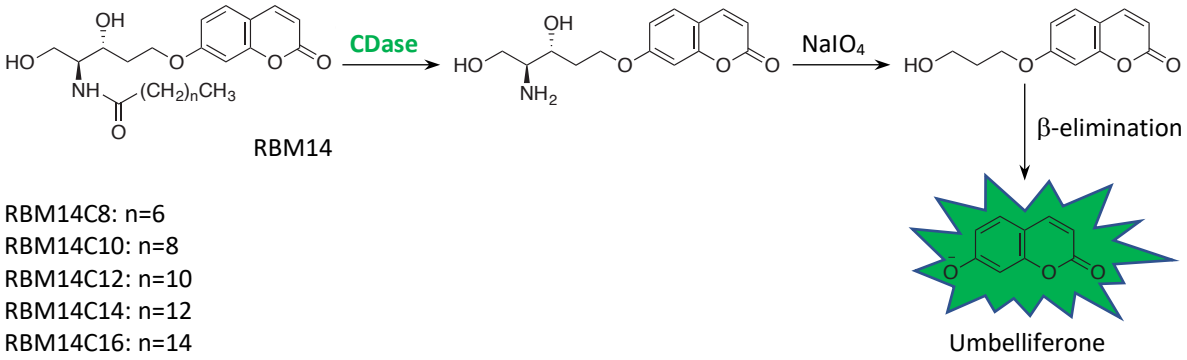

Figure 7: The hydrolysis of RBM14 by CDase and the release of fluorescent umbelliferone.

The different CDases can hydrolyze different RBM14 analogues, generating an aminodiol group which is subsequently oxidized to an aldehyde. The release of the fluorescent umbelliferon occurs as a result of spontaneous β-elimination, while attached to Cer, the umbelliferone does not emit fluorescence. As a representative example, RBM14C12[172] is a good substrate of AC and therefore can be used to determine AC activity. This compound has shown to be useful for the diagnosis of diseases related to altered AC activity such as Farber's disease, which is a genetic disease characterized by the deficiency of AC activity[172].

OBJECTIVES

The main goals of this PhD thesis are closely related within the field of CDases and their key role in the regulation of sphingolipid metabolism. Thus, the roles of ACER3 and AC in different human diseases are of valuable interest. However, research in this area has been hampered by the lack of specific inhibitors. For this reason, one of the objectives in this thesis was **the discovery of specific inhibitors for AC and ACER3 displaying activity in intact cells.**

AC is highly expressed in several types of cancer, and its deficiency is correlated with the Farber's disease. The existence of a method able to visualize the intracellular active form of AC, not the inactive one, is essential for the diagnosis of diseases associated with alterations in AC activity. Moreover, it is also important for the evaluation of the beneficial outcomes of therapeutic strategies. Hence, no methods have been yet presented to fulfill that aim, which hindered the development of therapeutic approaches based on chaperones due to the inability of imaging and following the existence of active AC in live cells. Activity-based probes (ABPs) have been proved useful in the visualization of active enzymes. Although few examples of ABPs for AC labelling have been reported, none of them was successfully used for live cell imaging of AC. Therefore, the other aim of this thesis was to **develop an optimal ABP able to visualize the catalytically active (AC) in intracellular compartments of living cells.**

RESULTS

ARTICLE 1

Discovery of deoxyceramide analogs as highly selective ACER3 inhibitors in live cells

Núria Bielsa [1], Mireia Casasampere [1], **Mazen Aseeri** [1], Josefina Casas [1,2], Antonio Delgado [1,3], José Luis Abad [1], Gemma Fabriàs [1,2]

[1] Institute for Advanced Chemistry of Catalonia (IQAC-CSIC), Jordi Girona 18, 08034 Barcelona, Spain.

[2] Department of Pharmacology, Toxicology and Medicinal Chemistry, Unit of Pharmaceutical Chemistry (Associated Unit to CSIC). Faculty of Pharmacy and Food Sciences. University of Barcelona. Avda. Joan XXIII 27-31, 08028 Barcelona, Spain.

[3] Liver and Digestive Diseases Networking Biomedical Research Centre (CIBEREHD). ISCIII. 28029 Madrid, Spain.

European Journal of Medicinal Chemistry (EJMECH). **2021** Apr 15;216:113296.

Impact factor: 6.514

The contribution of Mazen Aseeri to this work, corresponds to the design of experiments with alkaline ceramidase 3 and acid ceramidase obtaining and elaborating the data presented in Figures 2B and S1 (Series 2). He also contributed with the design of experiments whose results are shown in Figures 5, as well as with writing a first draft.

CASAS BRUGULAT JOSEFINA - DNI 40513738C
Firmado digitalmente por CASAS BRUGULAT JOSEFINA - DNI 40513738C
Fecha: 2023.01.24 13:17:50 +01'00'

TRIOLA GUILLEM GEMMA - DNI 40323105B
Digitally signed by TRIOLA GUILLEM GEMMA - DNI 40323105B
Date: 2023.01.25 17:41:43 +01'00'

Josefina Casas Brugulat and Gemma Triola Guillem

Thesis Directors

SUMMARY

Discovery of deoxyceramide analogs as highly selective ACER3 inhibitors in live cells

Objective: AC, NC and ACER3 are the most ubiquitous CDases, and targeting them for therapeutic purposes has been gaining interest in cancer treatment. Thus, the existence of specific and potent inhibitors for the different types of CDases is important for therapeutic use. Although, some inhibitors have been identified, yet nearly all are targets for AC, and few are for NC. However, well-characterized specific inhibitors for ACER3 do not exist. Therefore, and due to the lack or absence of specific inhibitors targeting CDases in intact cells, two small libraries of compounds were screened against AC, NC and ACER3.

Methodology: The determination of CDase activity was done by measuring the fluorescence released after the hydrolysis of RBM14 substrates. In 96-well plates, the assay was performed using the appropriate buffer for each CDase, according to the pH optima of its activity. To determine AC activity, Farber cell lysates stably overexpressing AC (FD-AC) were used. The activity of NC was evaluated in recombinant human NC (rhNC) enzyme, as well as in HT29 cell lysates. NC and ACER3 inhibition in intact cells was evaluated using two different cell lines (MEF-WT that display NC and ACER3 activity and ASAH2-null MEF that only display ACER but not NC activity) that combined enabled the identification of specific ACER3 inhibitors. All compounds and substates were incubated for the specified time required for each enzymatic reaction.

Results: The screening of the two libraries of compounds (series 1 and series 2) against AC, NC and ACER3, has led to discovering highly selective ACER3 inhibitors in intact cells. Compounds **8, 20, 20I and 20m** succeeded in inhibiting the activity of rhNC, however, they lost their inhibitory potency or were totally inactive when tested in cell lysates and intact cells. On the other hand, no significant inhibition was observed when the 4 compounds were tested against AC activity, in both cell lysates and intact cells. Compound **8** showed a very little inhibitory action over ACER3 activity in cell lysates, whereas compounds **20I** and **20m** showed significant inhibition in lysates and in intact cells. As a confirmatory step, the obtained inhibitory results of **20I** and **20m** over ACER3 activity in fluorescent assay, were reinforced by the analysis of Cer levels in treated cells using high-resolution mass spectrometry (HR-MS), which showed an increase in Cer levels in samples incubated with either of the two inhibitors.

Conclusions: In intact cells, compounds **20I** and **20m** are specific inhibitors of ACER3 activity and these results are confirmed by an increase in cellular Cer levels as detected by HR-MS. Interestingly, compounds **20I** and **20m** were highly cytotoxic when tested in the presence of methyl-β-cyclodextrin (MBCD). The mechanism by which such cytotoxicity occurs is still unknown. Overall, the results suggest that lysates and intact cells should be used when performing a screening of compounds against NC, and that the use of rhNC must be avoided.

European Journal of Medicinal Chemistry 216 (2021) 113296

Contents lists available at ScienceDirect

European Journal of Medicinal Chemistry

journal homepage: http://www.elsevier.com/locate/ejmech

Discovery of deoxyceramide analogs as highly selective ACER3 inhibitors in live cells

Núria Bielsa [a, 1], Mireia Casasampere [a, 1], Mazen Aseeri [a], Josefina Casas [a, b], Antonio Delgado [a, c], José Luis Abad [a, **], Gemma Fabriàs [a, b, *]

[a] Research Unit on BioActive Molecules, Department of Biological Chemistry, Institute for Advanced Chemistry of Catalonia (IQAC-CSIC), Jordi Girona 18, 08034, Barcelona, Spain
[b] Liver and Digestive Diseases Networking Biomedical Research Centre (CIBEREHD), ISCIII, 28029, Madrid, Spain
[c] Department of Pharmacology, Toxicology and Medicinal Chemistry, Unit of Pharmaceutical Chemistry (Associated Unit to CSIC). Faculty of Pharmacy. University of Barcelona (UB). Avda. Joan XXIII 27-31, 08028, Barcelona, Spain

ARTICLE INFO

Article history:
Received 6 November 2020
Received in revised form
27 January 2021
Accepted 12 February 2021
Available online 24 February 2021

Keywords:
Sphingolipid
Ceramide
Ceramidase
Inhibitor
Therapeutic target
Enzyme activity

ABSTRACT

Acid (AC), neutral (NC) and alkaline ceramidase 3 (ACER3) are the most ubiquitous ceramidases and their therapeutic interest as targets in cancer diseases has been well sustained. This supports the importance of discovering potent and specific inhibitors for further use in combination therapies. Although several ceramidase inhibitors have been reported, most of them target AC and a few focus on NC. In contrast, well characterized ACER3 inhibitors are lacking. Here we report on the synthesis and screening of two series of 1-deoxy(dihydro)ceramide analogs on the three enzymes. Activity was determined using fluorogenic substrates in recombinant human NC (rhNC) and both lysates and intact cells enriched in each enzyme. None of the molecules elicited a remarkable AC inhibitory activity in either experimental setup, while using rhNC, several compounds of both series were active as non-competitive inhibitors with K_i values between 1 and 5 μM. However, a dramatic loss of potency occurred in NC-enriched cell lysates and no activity was elicited in intact cells. Interestingly, several compounds of Series 2 inhibited ACER3 dose-dependently in both cell lysates and intact cells with IC_{50}'s around 20 μM. In agreement with their activity in live cells, they provoked a significant increase in the amounts of ceramides. Overall, this study identifies highly selective ACER3 activity blockers in intact cells, opening the door to further medicinal chemistry efforts aimed at developing more potent and specific compounds.

1. Introduction

Besides playing structural roles, sphingolipids are acknowledged as a family of bioactive lipids. Ceramides are the central molecules in sphingolipid metabolism. They can be generated *via* three different pathways, the *de novo* pathway, hydrolysis of complex sphingolipids, and the salvage pathway from sphingosine 1-phosphate [1]. The canonical *de novo* pathway begins with the condensation of palmitoyl CoA with L-serine catalyzed by serine palmitoyltransferase. Mutations in this enzyme induce a permanent shift in the substrate specificity of the enzyme from L-serine to L-alanine and glycine, resulting in increased production of 1-deoxysphingolipids [2].

After their synthesis, ceramides are converted to complex sphingolipids (sphingomyelin, ceramide 1-phosphate and glycosphingolipids) by substitution at the C1-hydroxyl group with polar groups. Due to the absence of this function, the addition of a head group to form complex sphingolipids is precluded in 1-deoxysphingolipids. Moreover, while ceramides are degraded to ethanolamine phosphate and a fatty aldehyde via sequential hydrolysis of ceramides, phosphorylation of the resulting long chain

Abbreviations: AC, acid ceramidase; ACER3, alkaline ceramidase 3; ASAH2, neutral ceramidase gene; C6-urea-ceramide, D-*erythro*-*N*-[2-(1,3-dihydroxy-4*E*-octadecene)]-*N*′-hexane-urea; D-e-DMAPP, (1*S*,2*R*)-D-*erythro*-2-(*N*-myristoylamino)-1-phenyl-1-propanol; LC/MS, liquid chromatography coupled to mass spectrometry; MEF, mouse embryonic fibroblasts; NC, neutral ceramidase; rhNC, recombinant human NC.

* Corresponding author. Research Unit on BioActive Molecules Department of Biological Chemistry Institute for Advanced Chemistry of Catalonia (IQAC-CSIC), Spain.
** Corresponding author.
E-mail addresses: joseluis.abad@iqac.csic.es (J.L. Abad), gemma.fabrias@iqac.csic.es (G. Fabriàs).
[1] Both authors contributed equally to this work.

https://doi.org/10.1016/j.ejmech.2021.113296
0223-5234/

base to the corresponding phosphate and final irreversible retro-aldolic cleavage by sphingosine-1-phosphate lyase [1], this pathway is not possible for 1-deoxysphingolipids, as the essential catabolic intermediate, sphingosine 1-phosphate, cannot be formed from the 1-deoxybases [2].

Hydrolysis of ceramides occurs by the action of ceramidases, which are encoded by five known genes and are distinguished by the pH required for optimal activity (acid ceramidase (AC, ASAH1), neutral ceramidase (NC, ASAH2) and alkaline ceramidases 1, 2 and 3 (ACER1, ACER2 and ACER3) [3]. Conversely, 1-deoxy(dihydro) ceramides are exclusively hydrolyzed by AC [4]. Amongst the five different enzymes, AC, NC and ACER3 are the most ubiquitous and their therapeutic interest as targets in cancer diseases has been well sustained [5].

AC is a glycosylated 50 kDa enzyme belonging to the N-terminal nucleophile (Ntn) superfamily of hydrolases. It is synthesized in the ER as an inactive proenzyme that is activated in the lysosome through autocleavage, rendering a mature heterodimeric enzyme containing α- and β-subunits [6]. The crystal structures have shown that the catalytic center is buried in the proenzyme, while autocleavage triggers a conformational change exposing the active site hydrophobic channel [7]. Genetic loss-of-function mutations in AC are the underlying cause of two severe rare diseases: Farber disease and spinal muscular atrophy with progressive myoclonic epilepsy [8]. Furthermore, changes in the expression levels of AC has been found to be relevant in melanoma [9–12], prostate cancer [13–16] and acute myeloid leukemia [17–19].

NC is a single transmembrane domain glycoprotein highly expressed in the small intestine and colon and it appears to regulate the levels of bioactive sphingolipid metabolites in the intestinal tract [20]. Its crystal structure revealed a catalytic domain, a short linker, and an immunoglobulin-like domain. The structure also revealed that the active site of human NC is composed of a narrow, 20 Å deep, hydrophobic pocket with a Zn^{2+} ion at the bottom [21]. Besides a few other roles [22–26], a function of NC in cancer is supported by the findings that NC downregulation is involved in gemcitabine-induced growth suppression [27] and by recent studies showing that NC regulates cell survival in colon cancer cells [28,29]. These studies demonstrated that inhibition of NC in a xenograft model delayed tumor growth and that mice lacking NC were protected from azoxymethane-induced tumor formation [28].

ACER3 is a seven-transmembrane domain with an intracellular N-terminus exposed to the cytoplasm and the C-terminus facing the lumen of the endoplasmic reticulum or Golgi apparatus. The protein contains functionally connected catalytic Zn^{2+} and Ca^{2+}-binding sites, providing a structural explanation for the known regulatory role of Ca^{2+} on ACER3 enzymatic activity [30,31]. Genetic ACER3 deficiency leads to progressive leukodystrophy in early childhood [32], a rare disease for which no treatment is available. Furthermore, ACER3 has been reported to contribute to hepatocellular carcinoma [33] and acute myeloid leukemia pathogenesis [34] and its downregulation has been shown to inhibit cell proliferation [35].

The role of ceramidases in human diseases is gaining increasing attention. However, current research in this field has been hampered by the lack of specific inhibitors for some of these enzymes. Although several inhibitors of ceramidases have been discovered [36], most of them target AC. Over the last two decades, a number of NC inhibitors have been reported, but their potency is low, their specificity has not been thoroughly investigated and none has reached clinical effect [36]. A recent article reports on a large (>650,000 small molecules) high-throughput screening assay for NC inhibitors that has resulted in interesting leads [37]. Unfortunately, no chemical structures are provided and further investigation of hits in cell free systems and intact cells has not been performed. On the other hand, only one inhibitor of alkaline ceramidases (ACER) has been reported, namely (1*S*,2*R*)-D-*erythro*-2-(*N*-myristoylamino)-1-phenyl-1-propanol (D-e-DMAPP) [38], but the specific ACER target has not been identified and a few articles claim that D-e-DMAPP inhibits also AC [39] and NC [40]. Thus, the identification of new tools should significantly advance our knowledge on the function of the different ceramidases, allow a better understanding of their role in the regulation of biological processes and in addition, may potentially lead to novel therapeutic strategies.

From the biological stand point, 1-deoxysphingolipids are relevant in diseases such as hereditary sensory and autonomic neuropathy, a genetic condition caused by mutations in serine palmitoyltransferase (see above). Furthermore, several clinical studies showed that 1-deoxysphingolipids are altered the metabolic syndrome and in type 2 diabetes [41]. Moreover, plasma 1-deoxysphingolipids are also elevated in von Gierke disease [42], and appear to be also relevant in the progress from hepatosteatosis to steatohepatitis [2].

In the light of these overall precedents, we envisioned that 1-deoxysphingolipid analogs might provide compounds with interesting biological properties. Herein, we report on the screening of 1-deoxysphingolipid analogs (Fig. 1) on AC, NC and ACER3 that yield to the identification of highly selective ACER3 inhibitors acting both in lysates and intact cells.

2. Materials and methods

2.1. Chemical synthesis

Synthesis and characterization of compounds is detailed in the supplementary materials.

2.2. Cell culture

The A375 cell line stably overexpressing ASAH1 under the control of a doxycycline-responsive promoter was kindly provided by Dr. Carmen Bedia and Prof. Thierry Levade. HT29 cells were obtained from ATCC, Farber disease (FD) cells transformed to stably overexpress AC (FD10X) were a kind gift of Prof. Jeff Medin and *ASAH2*$^{(-/-)}$ mouse embryonic fibroblasts (MEF) were kindly provided by Prof. Richard Proia. In the latter, experiments were conducted at least two weeks after thawing. All cells were maintained in DMEM (Dulbecco's Modified Eagle Medium) supplemented with 10% FBS (Fetal Bovine Serum). Cells were kept at 37 °C and 5% CO_2 and routinely grown up to 70% confluence.

2.3. Cell transfection

The antibiotic selection in the A375 cell line stably overexpressing ASAH1 under the control of a doxycycline-responsive promoter was performed with blasticidin (3 μg/mL) and hygromycin B (250 μg/mL). Ectopic expression of AC was induced with doxycycline at 1 μg/mL for 24 h before use.

Transient transfections with the ASAH2-containing plasmid were performed with Lipofectamine® 2000 (Invitrogen) in a 12-well plate format. One day before transfection, $3x10^5$ cells/mL were plated in growth medium without antibiotics, so that cells would be 90–95% confluent at the time of transfection. For each transfection sample, cDNA was diluted in 50 μL of Opti-MEM®I without serum; lipofectamine (2 μL) was diluted in 50 μL of Opti-MEM®I Medium and incubated for 5 min at 25 °C. Next, both solutions were combined, mixed gently, and incubated for 20 min at 25 °C. The resulting solution was mixed with 400 μL of medium and it was added to cells. After 4 h at 37 °C and 5% CO_2, 1 mL of medium

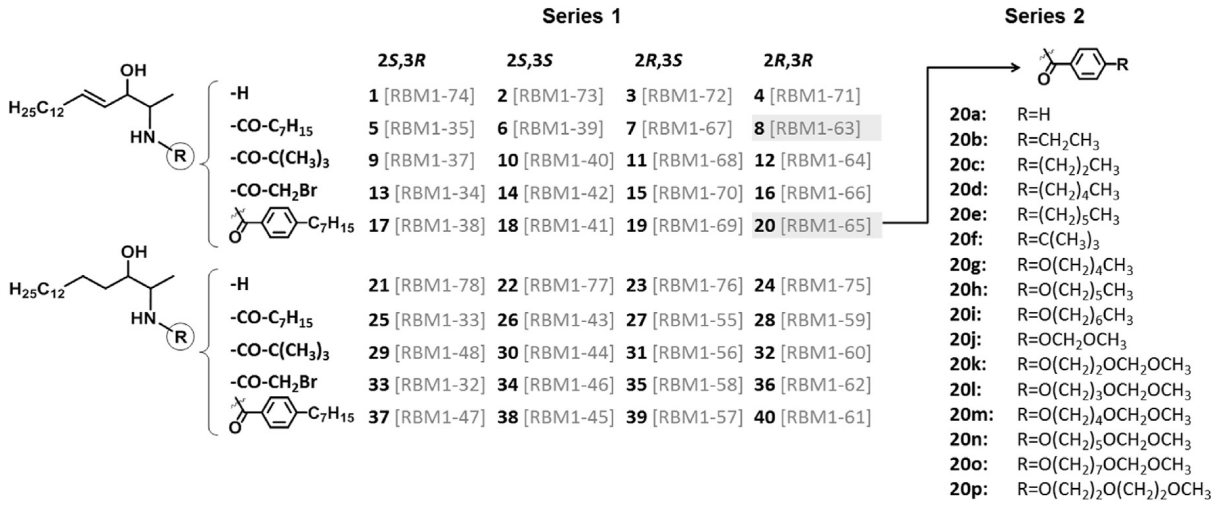

Fig. 1. Chemical structures of the 1-deoxyceramides studied in this work. Internal codes are shown in grey between brackets.

containing 10% FBS and tetracycline (10 ng/mL) was added. Cells were incubated for 24 h prior to testing for transgene expression and compounds addition for inhibitory activity determination.

2.4. Cell viability

Cells (0.1-0.25x10^6/ml) were seeded in 96 well plates (0.1 ml/well) and grown for 24 h. Cell viability was examined in triplicate samples by the MTT method after treatment with the indicated compounds or with the corresponding percentage of vehicle ($\leq$0.25% ethanol)

2.5. Fluorogenic ceramidase activity assay in vitro

Experiments with rhNC (R&D Systems, >95% pure) were carried out with 5 ng of protein (MW = 83 KDa) in 0.1 mL of buffer (see below), which affords a protein concentration of 0.6 nM for a substrate concentration of 20 μM. These conditions (substrate concentration much larger than protein concentration) are appropriate to use the Lineweaver-Burk plot to study the enzyme kinetics.

To prepare the lysates, cell pellets were resuspended in the appropriate volume of a 0.25 M saccharose solution containing the protease inhibitors aprotinin (1 mg/mL), leupeptin (1 mg/mL) and PMSF (100 mM). The suspension was submitted to three cycles of a 5 s sonication (probe) at 10 W/5 s resting on ice. The cell lysate was centrifuged at 600 *g* for 5 min. The supernatant was collected, and protein concentration was determined with BSA as a standard using a BCA protein determination kit (Thermo Scientific) according to the manufacturer's instructions.

All the enzyme activity assays were carried out in 96-well plates at a final volume of 100 μL/well. Reaction buffers were: 25 mM sodium acetate buffer pH 4.5 (AC), 25 mM phosphate buffer 150 mM NaCl 1% sodium cholate (NaChol) pH 7.4 (NC) and 50 mM HEPES 1 mM $CaCl_2$ pH 9 (ACERs). The reaction mixtures contained 25 μL/well of protein (5 ng recombinant NC or 25 μg cell lysate), 70 μL/well of substrate (prepared from 4 mM stock solutions in ethanol) and 5 μL/well of inhibitor (tested at concentrations indicated in the figure legends, prepared from 10 mM stock solutions in ethanol). The following fluorogenic substrates were used at the concentrations specified in the figure legends: for AC, RBM14C12 [43]; for NC, RBM14C24:1 [44] and for ACER, RBM14C16 [45]. Reaction mixtures were incubated at 37 °C for 1 h (recombinant NC) or 3 h (cell lysates). In all cases, reactions were stopped with 25 μL/well of MeOH and then 100 μL/well of $NaIO_4$ (2.5 mg/mL in 100 mM glycine-NaOH buffer, pH 10.6) was added. After incubation at 37 °C for 1 h in the dark, 100 μL/well of 100 mM glycine-NaOH buffer (pH 10.6) was added and fluorescence was measured spectrophotometrically at excitation and emission wavelengths of 355 and 460 nm, respectively. The same reaction mixtures without enzymes were used as blanks.

2.6. Fluorogenic ceramidase activity assay in intact cells

To determine ceramidase activity in intact cells, 2x10^4 cells/well were seeded in 96-well plates 24 h prior to the assay and maintained at 37 °C and 5% CO_2. Medium was replaced by 100 μL of fresh medium (DMEM 10% FBS) containing 10 μM of the corresponding RBM14 substrate and different concentrations of the indicated test compounds. The plate was incubated for 3 h at 37 °C in 5% CO_2. The reaction was stopped with 25 μL/well of MeOH and then 100 μL/well of $NaIO_4$ (2.5 mg/ml in glycine-NaOH buffer, pH 10.6) were added. After incubation at 37 °C for 1 h in the dark, 100 μL/well of 100 mM glycine-NaOH buffer (pH 10.6) were added and fluorescence was measured spectrophotometrically at excitation and emission wavelengths of 355 and 460 nm, respectively. The same reaction mixtures without cells were used as blanks. The following fluorogenic substrates were used at the concentrations specified in the figure legends: for AC, RBM14C12 [43] and for NC and ACER3, RBM14C16 [45]. Both substrates and test compounds were added simultaneously to the cell culture.

2.7. Lipid analysis

Cells were seeded at 0.2x10^6 cells/mL in 6 well plates (1 mL/well). After 24 h, medium was replaced with fresh medium containing either the treatment of interest or the corresponding vehicle as a control. After the indicated incubation times, medium was removed and cells were washed with PBS. Cells were collected by trypsinization. Ten μL of the cell suspension were used to count cells for each sample. Sphingolipid extracts, fortified with internal standards (*N*-dodecanoylsphingosine, *N*-dodecanoylglucosylsphingosine, *N*-dodecanoylsphingosylphosphorylcholine, C17-sphinganine (0.2 nmol each) were added and lipids were analyzed by LC/MS with the reported equipment and instrument conditions [46].

3. Results

3.1. Synthesis

Due to the interesting properties, biological activity and improved metabolically stability of 1-deoxysphingolipids, as well as to the finding that 1-deoxydihydroceramides with the natural stereochemistry are exclusively hydrolyzed by AC [4], a small library of derivatives was prepared based on the structure of 1-deoxysphingosine and 1-deoxysphinganine covering the four possible stereoisomers. The *N*-acyl moieties were chosen because of our previous reports showing that the corresponding (dihydro) ceramides are ceramidase inhibitors [15,47]. Sphingoid bases were prepared as previously reported [48] and deoxyceramide analogs (Fig. 1) were synthesized by amidation of the proper enantiopure sphingoid base with the corresponding acid derivative according to the previously described methodology (Scheme 1).

3.2. Studies in recombinant protein and cell lysates

Given the interest of AC, NC and ACER3 as therapeutic targets in cancer, Series 1 was first screened over these three enzymes at equimolar concentrations with the appropriate substrates. The activity over AC was tested in lysates from AC-overexpressing cells using RBM14C12, as the best AC fluorogenic substrate [43]. As shown in Figure S1, none of the compounds exhibited a remarkable inhibition of AC, even when the inhibitor/substrate molar ratio was increased to (2:1) (data not shown). Intriguingly, the bromoacetyl derivatives of 1-deoxysphingosine and 1-deoxysphinganine with the natural configuration (**13** and **33**, Fig. 1) did not inhibit AC, in contrast to their analogs containing the C1—OH, which are potent activity based irreversible AC inhibitors [15,49].

Activity over NC was initially tested using recombinant human NC (rhNC) and RBM14C16, as the best NC fluorogenic substrate [45]. Two compounds, **8** and **20**, completely blocked NC activity when tested at a substrate/inhibitor ratio of 1:1 (20 μM) and provoked a 70 and 90% inhibition, respectively, at 5 μM (20 μM substrate) (data not shown). Reducing **8** and **20** concentrations to 1 μM (substrate/inhibitor molar ratio of (20:1)) provoked a 50% and 70% inhibition of NC, respectively (Figure S1). It is worth noting that the two compounds are 1-deoxyceramides, while the corresponding saturated analogs were inactive at inhibiting NC, indicating that the C4-double bond is required for inhibition. Furthermore, they have a (2*R*,3*R*) configuration, different from that of the natural substrate (2*S*,3*R*), which agrees with a non-competitive inhibition where the inhibitor binds the enzyme at allosteric sites (see below).

Next, compounds were screened against ACER3 using lysates of *ASAH2*-null (*ASAH2*$^{(-/-)}$) mouse embryonic fibroblasts (MEF). These cells are considered a suitable model to screen ACER3 inhibitors since they lack NC, and ACER3 is the only alkaline ceramidase detected [45]. No significant ACER3 inhibition was elicited by these compounds at basic pH, in the presence of Ca^{2+} and at a substrate/inhibitor molar ratio of (1:1) (Figure S1).

Based on the structure of one of the most potent compound identified (**20**) as NC inhibitor, a focused library of analogs was next prepared including a set of more hydrophilic derivatives (Table S1) by modification of the benzene *para*-substituent by either shortening the chain length or introducing oxygen atoms. In this case, O-alkylbenzoic acids bearing a alkyl/polyoxygenated side chain were obtained by coupling of *p*-hydroxybenzoic acid methyl ester with the respective halogen derivatives using a two-step sequence (condensation and saponification) (Scheme 1).

Compounds belonging to this Series 2 were again screened against AC, NC and ACER3. None of the compounds inhibited AC at equimolar (Fig. S1) or two-fold molar (not shown) concentrations with the substrate (20 μM) when assayed in cell lysates from AC overexpressing cells. However, compounds **20** and **20l** were slightly inhibitory at 40 μM (Fig. 3A). Conversely, several inhibitors were also identified in the screening of Series 2 against recombinant NC, although none of them was more active than **20** (Fig. 2A). These results provided some insights into structure-activity relationships on the recombinant protein. Hence, decreasing the *p*-alkylphenyl substituent chain length (**20a**, **20b** and **20c**) resulted in reduction of the inhibitory activity, as compared to **20**, while compounds **20d** and **20e** had a similar activity to the reference compound. Introduction of one oxygen atom in the *p*-alkylphenyl substituent afforded compounds with similar inhibitory activity, while addition of two additional oxygen atoms resulted in reduction of activity (compare **20k** *vs* **20g**; **20l** *vs* **20h**, and **20m** *vs* **20i**). In addition, changing the oxygen position along the chain had also a negative effect on NC inhibitory activity (compare **20l** *vs* **20p**). Interestingly, the screening of the focused library on ACER3 also identified some inhibitors, mostly corresponding to the ω-methoxymethoxy family (Fig. 2B). Furthermore, activity against ACER3 was shown to be dose dependent for the two compounds examined (**20l** and **20m**) (Fig. 3C).

To get a deeper insight into the mode of inhibition against NC and ACER3, kinetic experiments were then conducted with **8**, **20, 20l and 20m**, two of the identified NC/ACER3 inhibitors[2]. Incubation of rhNC with different amounts of inhibitor at varied substrate concentrations resulted in modified V_{max} without significant changes in the K_m values (Fig. 4A), indicating that compounds **8**, **20**, **20l** and **20m** were non-competitive inhibitors of NC with K_i values of 2.0, 0.8, 5.4 and 3.6 μM, respectively. A similar outcome was observed for the two compounds active on ACER3, which behaved also as non-competitive inhibitors with apparent K_i values of 25.5 μM (**20l**) and 34.3 μM (**20m**) (Fig. 4B).

To compare the effects observed on ACER3 containing lysates (Fig. 2B), the inhibitory activity of **8**, **20**, **20l** and **20m** was then tested in lysates of HT29 cells transiently transfected to overexpress NC (Fig. 3B). A specific NC substrate, bearing a nervonic acid amide (RBM14C24:1) was employed in this case, thereby enabling only the measurement of NC activity [44]. Surprisingly, only **20l** and **20m** were shown to dose-dependently inhibit the hydrolysis of RBM14C24:1 (10 μM) at neutral pH (Fig. 3B) whereas no inhibition was observed with **8** and the parent compound **20**. Moreover, a remarkable reduction in potency was found in cell lysates, as compared to the recombinant enzyme, since a >40 μM concentration was necessary to achieve a 50% inhibition (Fig. 3B). A similar outcome occurred with the C6-urea-ceramide (D-*erythro*-*N*-[2-(1,3-dihydroxy-4*E*-octadecene)]-*N*′-hexane-urea-sphingosine), a reported NC inhibitor [50], which inhibited rhNC and NC from cell lysates with IC_{50}'s of 18 nM and 366 nM, respectively (Fig S2A). This decrease of potency observed when using cell lysates as compared to recombinant purified protein suggest that caution should be taken when interpreting data obtained with recombinant NC protein.

3.3. Studies in intact cells

Since cell-based assays consider the biological complexity of the cell and include factors, such as uptake and concentration by intracellular compartmentalization, that might have a positive impact on both inhibitory potency and selectivity, the activity of **8**,

[2] With the idea of testing the compounds in intact cells, we chose compounds **20l** and **20m** as they have similar lipophilicity to that of cell permeable *N*-octanoyl-sphingosine (Table S1) [56,57] with the lowest reduction in NC inhibitory activity, as compared to **20**.

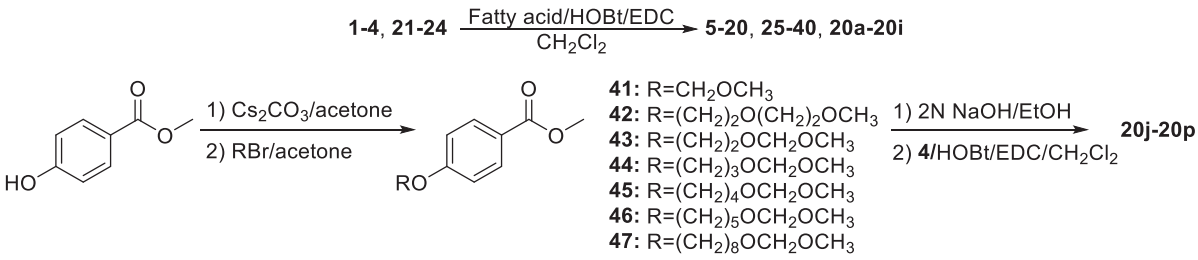

Scheme 1. Synthesis of compounds used in this study and shown in Fig. 1. The preparation of the free bases **1**–**4** and **21**–**24** was conducted as reported [48].

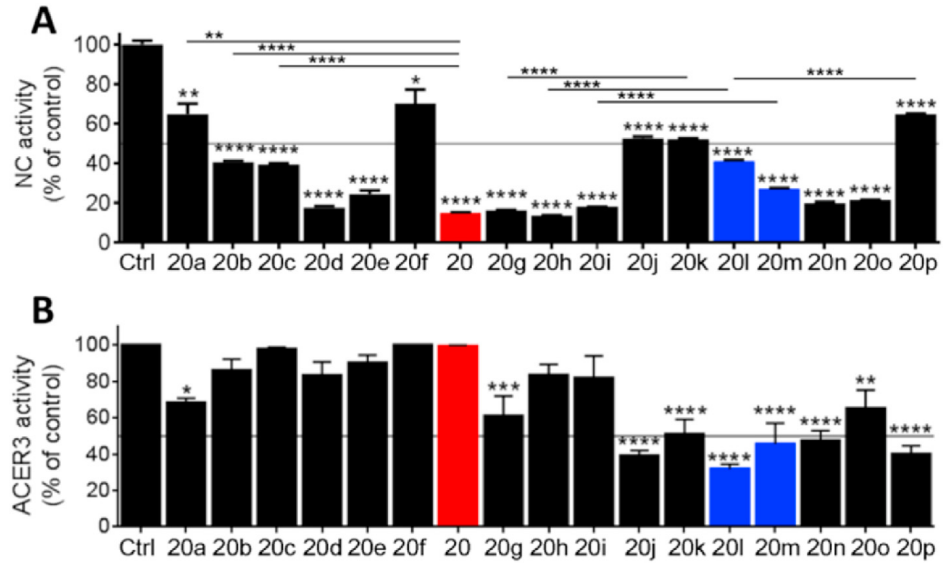

Fig. 2. Activity of Series 2 over rhNC (A) and ACER3 (ASAH2-null cell lysates) (B). Concentration of substrate was 20 μM (A) or 10 μM (B) and that of test compounds was 1 μM (A) and 20 μM (B). Suitable buffers and pH were used for each specific activity. Data (mean ± SD) were obtained from two to three experiments with triplicates. Asterisks above the SD bars denote statistical significance over controls at *, $p < 0.05$; **, $p < 0.01$; ***, $p < 0.001$; ****, $p < 0.0001$, while statistical significance between specific groups is indicated with asterisks above lines (One-way ANOVA followed by Dunnett's multiple comparisons test).

20, **20l** and **20m** was next examined in intact cells. Like in the studies with cell lysates, test compounds and substrates were added simultaneously to the appropriate cell lines and incubations proceeded for 3 h. By using similar conditions, both in lysates and intact cells, we could get an estimation of the global effects of uptake and compartmentalization of the compounds on their inhibitory activity. However, a real analysis of both factors would require the use of fluorescent derivatives and the study of their subcellular distribution to confirm that they reach the organelles containing the target enzymes.

Activity over AC was tested using AC overexpressing A375 cells (A375/+Dox) and the fluorogenic substrate RBM14C12. No inhibition could be observed with **20,** whereas **20l** and **20m** exhibited very weak AC inhibitory activity (IC50's > 200 μM) (Fig. 5A).

Preliminary experiments to investigate the compounds' effect on NC revealed that they were very toxic in the presence of methyl-β-cyclodextrin, the co-solvent required for the administration of the specific fluorogenic NC substrate (RBM14C24:1) in intact cells [44]. Since the NC specific substrate could not be used, RBM14C16 (substrate for both NC and ACER3) was employed and the inhibition experiments were carried out in ASAH2-null MEF (ACER3) and their wild type counterparts (WT-MEF) (NC and ACER3). Data comparison should allow discerning between NC and ACER3 inhibitory activity. As shown in Fig. 5B and C, compounds **8** and **20** exhibited insignificant inhibition of either NC or ACER3 while **20l** and **20m**, otherwise, both inhibited the hydrolysis of RBM14C16, and thereby umbelliferone production, in both cell lines (Fig. 5C). Statistical comparison of the dose-response data revealed that the four curves and their corresponding IC_{50} values were not statistically different ($P = 0.2206$). As the combined inhibition of both ACER and NC should result in higher inhibition rates in WT-MEF, these results, showing similar activities in both WT-MEF (which contain NC and ACER3 activity) and *ASAH2*-null MEF (lacking the NC gene), support that NC inhibition by **20l** and **20m** in intact cells is negligible and that ceramidase inhibition observed in intact cells is solely due to their action over ACER3 in both cell lines.

To confirm the effect of these two compounds on intracellular ceramide levels, a lipidomic analysis was performed in *ASAH2*-null MEF and in AC overexpressing A375 cells treated with either **20l** or **20m**. To this end, compounds were administered to cells and lipids were extracted and analyzed (LC/MS) after 3 h of treatment. Gratifyingly, in agreement with the results found with the fluorogenic assays, a significant 1.5-2-fold increase in the total amounts of ceramides was provoked by both **20l** and **20m** in *ASAH2*-null MEF, but no effect could be detected on sphingosine, sphingomyelin and glucosylceramide levels (Fig. 6A). Regarding the ceramides species, all of them were elevated by treatment with the compounds over vehicle controls, except for C24:0-ceramide, which was unaffected (Fig. 6B). Conversely, only a small effect on ceramide levels was provoked by **20l** in AC-overexpressing A375-cells (Fig. S3).

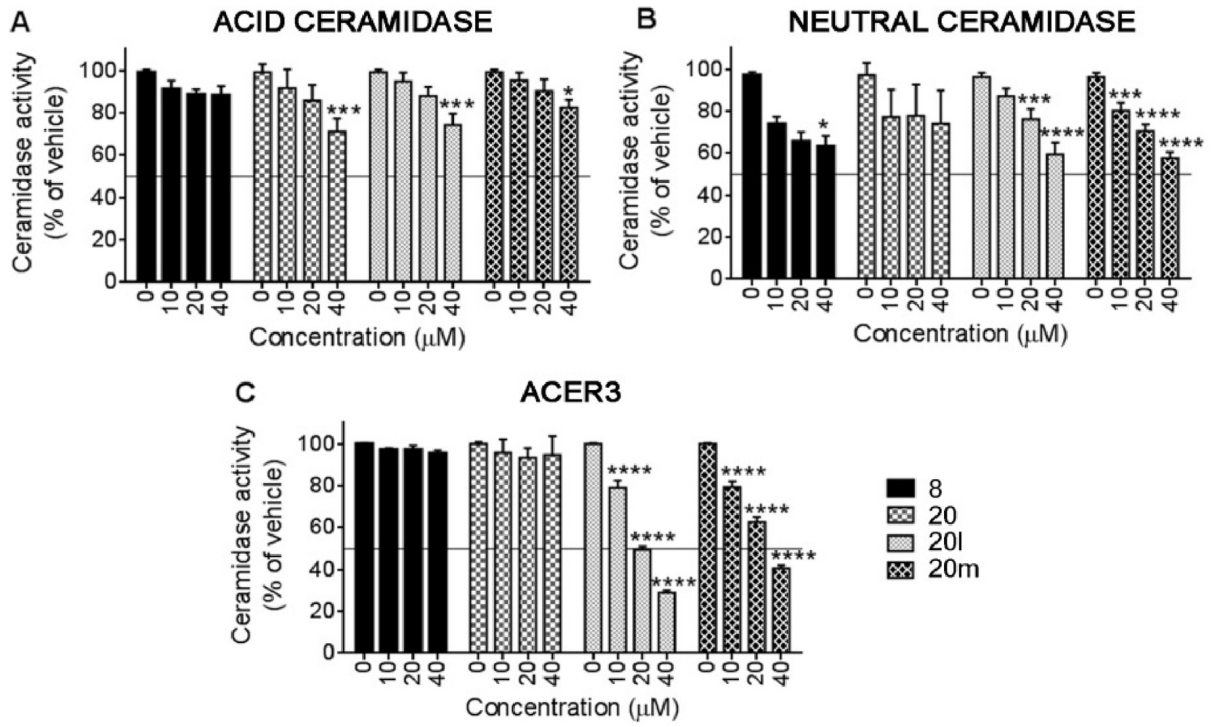

Fig. 3. Dose response of compounds on ceramidase activities in cell lysates. Experiments were carried out for 3 h (A, C) or 1 h (B) using 25 μg of lysates of AC overexpressing A375 cells (A), NC overexpressing HT29 cells (B) and ASAH2-null MEF (ACER3) (C), in 25 mM sodium acetate buffer, pH 4.5 (A), 25 mM phosphate buffer, 150 mM NaCl, 1% sodium cholate, pH 7.4 (B), or 50 mM HEPES 1 mM $CaCl_2$, pH 9 (C). Concentration of substrates (A, RBM14C12; B, RBM14C24:1; C, RBM14C16) was 10 μM. Data (mean ± SEM) was obtained from three to four experiments with triplicates. Asterisks denote statistical significance over controls at *, $p < 0.05$; **, $p < 0.01$; ***, $p < 0.001$; ****, $p < 0.0001$ (One-way ANOVA followed by Dunnett's multiple comparisons test).

4. Discussion

In our endeavour towards developing ceramidase inhibitors of pharmacological interest, two series of 1-deoxy(dihydro)ceramides were synthesized and screened against NC, AC and ACER3, the most ubiquitous ceramidases identified as therapeutic targets in cancer diseases [5]. Series 1 includes several diastereomeric *N*-acyl 1-deoxysphingosine and 1-deoxysphinganine amide derivatives, while Series 2 contains analogs of **20** with presumably improved bioavailability. An important feature of both libraries is their metabolic stability in front of enzymes acting at the C1—OH level to produce sphingomyelin, ceramide 1-phosphate, glycosphingolipids and the long chain base phosphates [51].

Whereas some compounds caused a significant and potent non-competitive inhibition of recombinant NC, studies performed in cell lysates with the most active inhibitors indicated a dramatic loss of potency, while several compounds of Series 2 inhibited ACER3. The identified selective ACER3 inhibitors, mostly belonging to the ω-methoxymethoxy family of Series 2, have a (2*R*,3*R*) configuration, different from that of the natural substrate (2*S*,3*R*), which suggests that the inhibitors bind the enzyme at allosteric sites in agreement with kinetic experiments showing that both **20l** and **20m** do not compete with the substrate active center.

This selective effect on ACER3 was further confirmed in studies with **20l** and **20m** using intact cells both in activity assays and after measurement of sphingolipid levels using mass-spectrometry methods, showing the expected increase in ceramides upon treatment with both compounds. However, no selective accumulation of long chain unsaturated ceramides was induced by **20l** and **20m**, which is at odds with reported data showing that ACER3 preferentially hydrolyzes these particular species [35] and that ACER3 upregulation prevents the buildup of C18:1-ceramide in mouse hepatocytes, while loss of ACER3 specifically augments C18:1-ceramide and C20:1-ceramide without affecting other ceramide species [52]. However, in another study showing that ACER3 is involved in aging-associated neurodegenerative disorders in humans [53], the effect of ACER3 knockout on the levels of ceramides and sphingosine was found to depend on both the age and the part of the brain examined, with the highest changes occurring in older tissues. However, no specific accumulation of long chain unsaturated ceramides was observed in ACER3 knockouts as compared to wild types.

On the other hand, neither **20l** nor **20m** provoked the expected reduction in the amounts of sphingosine. A similar outcome was observed in ACER3-knockout mouse hepatocytes [52] and in 6 week old brains of ACER3 knockout mice [53]. Conversely, the expected reduction in sphingosine [35] or its phosphate [33] was observed in other ACER3 knockout cell models. Overall, although C18:1-ceramide is clearly involved in some biological actions of ACER3, the effects of up- and downregulation of this enzyme on ceramide species and their catabolic products seem to depend on the cell type, the type of stimulus and the biological context.

It is worth noting that the three cell permeable compounds, namely **8**, **20l** and **20m**, were very toxic when tested in the presence of methyl-β-cyclodextrin, a cholesterol depleting agent, in HT29 cells overexpressing NC. A study reported by Romiti et al. [54] showed that endothelial cell treatment with cyclodextrin enhanced NC activity in caveolin-enriched membranes, indicating a negative role for cholesterol in NC regulation. It is possible that methyl-β-cyclodextrin removes cholesterol from membrane pools leading to NC activation, the inhibition of which by the compounds would lead to ceramide increases and subsequent cell death. However, ceramide analysis by LC/MS did not show the expected increase in cells treated with the compounds in the presence of methyl-β-

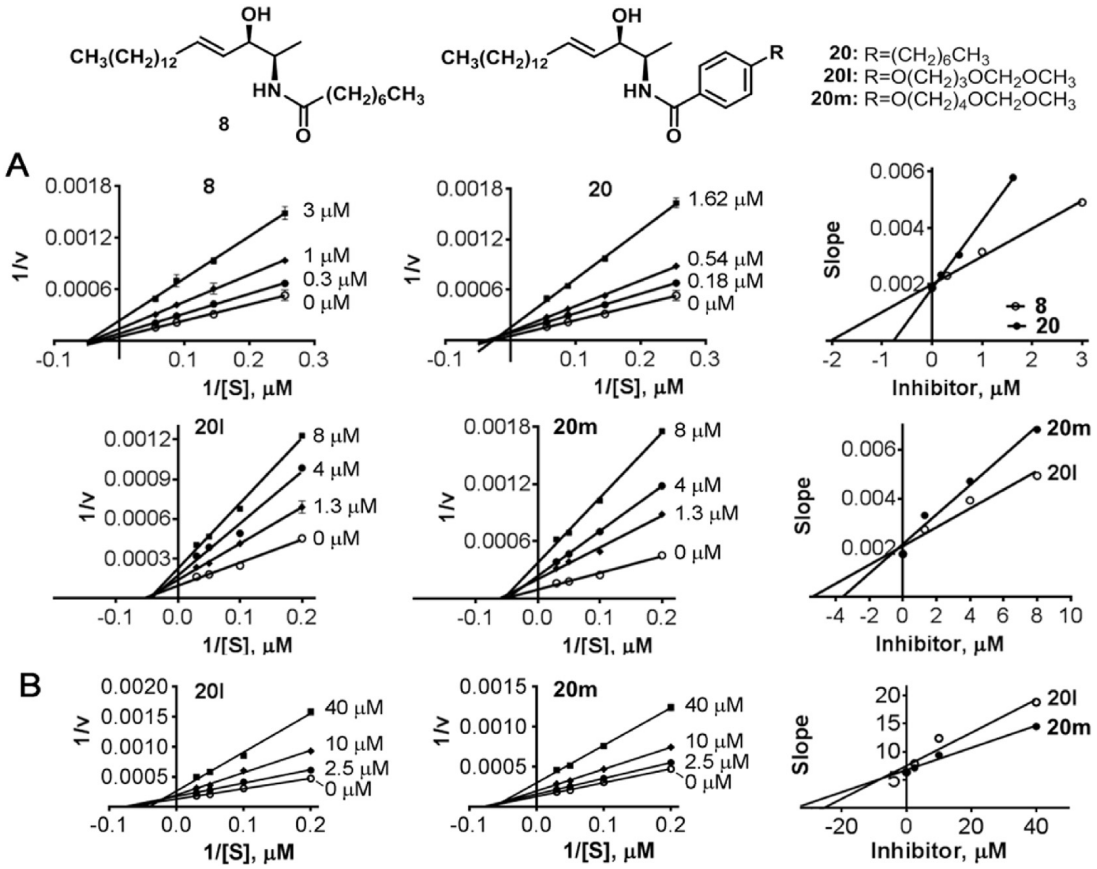

Fig. 4. Kinetics of inhibition of NC and ACER3 by **8**, **20**, **20l** and **20m**. Experiments were carried out using recombinant NC (5 ng, 0.6 nM) in 25 mM phosphate buffer, 150 mM NaCl, 1% sodium cholate, pH = 7.5 (A) or lysates from ASAH2-null MEFs (25 μg) in 50 mM HEPES 1 mM $CaCl_2$ pH 9 (B). Concentrations of substrate (RBM14C16) were 3.9, 6.9, 11.3 and 18 μM (**8** and **20**) and 5, 10, 20 and 40 μM (**20l** and **20m**). Data (mean ± SD) were obtained from four experiments with triplicates. K_i, as determined from the slope of the regression lines at each inhibitor concentration, were **8**, 2.0 μM; **20**, 0.8 μM; **20l**, 5.4 μM and **20m**, 3.6 μM in NC and **20l**, 25.5 μM and **20m**, 34.3 μM in ASAH2-null MEFs. Similar values were obtained using the x-intercept values.

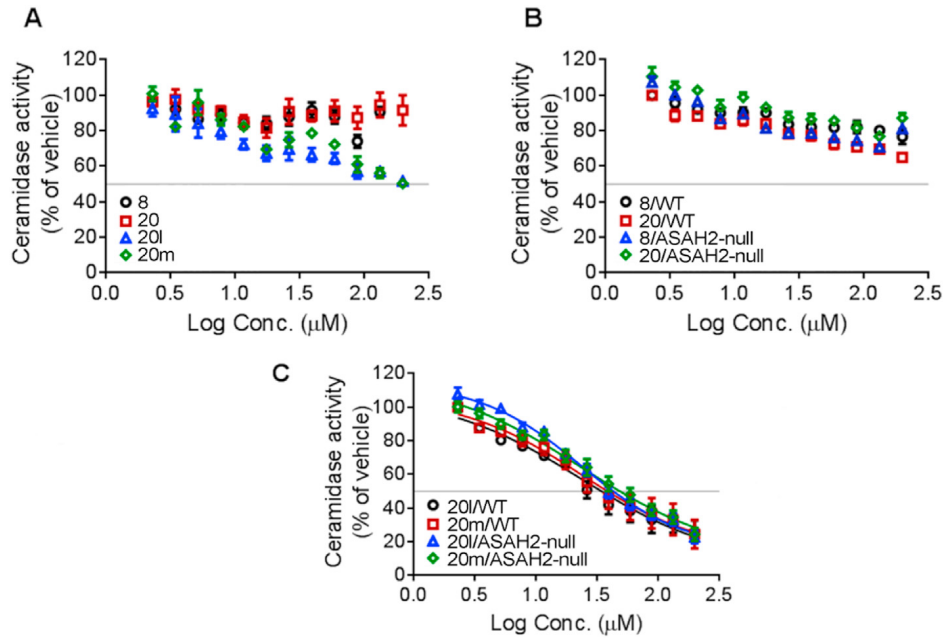

Fig. 5. Effect of inhibitors on umbelliferone production from fluorogenic substrates in intact cells. AC overexpressing A375 cells (A), WT-MEF (B,C) and ASAH2-null MEF (B,C) were incubated with the fluorogenic substrate (A, RBM14C12 (10 μM); B and C, RBM14C16 (10 μM)) and different concentrations of the specified compounds in DMEM 10% FBS for 3 h and enzyme activity was determined by the fluorogenic assay. Data were normalized by protein quantification (SRB assay, >90% cell viability). Data (mean ± SD) were obtained from three experiments with triplicates. In C, statistical comparison of fits concluded that the $LogIC_{50}$ was the same for all data sets ($p = 0.2206$) and the IC_{50} had a best fit value of 23.7 μM.

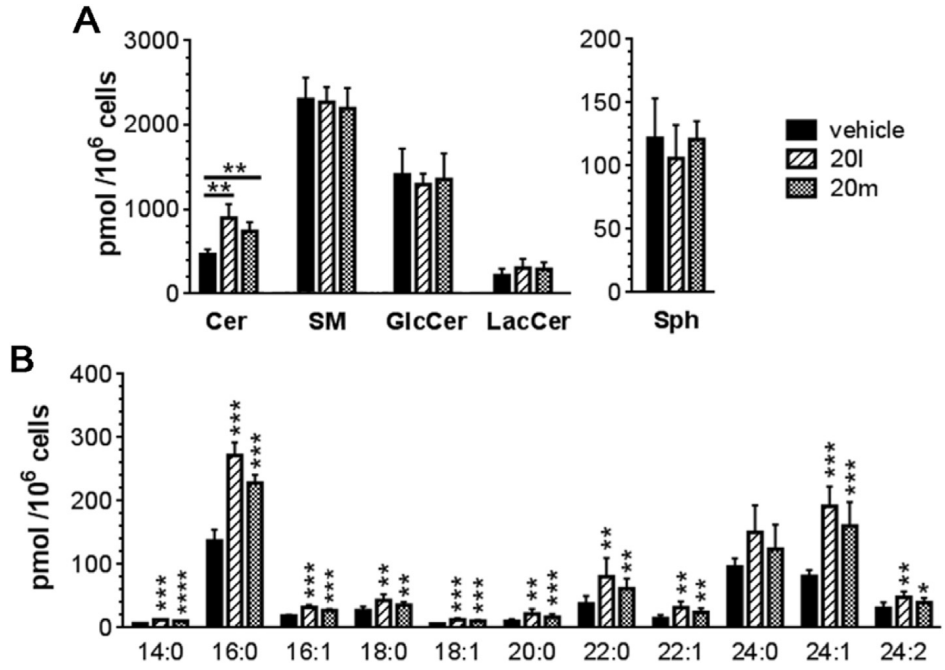

Fig. 6. Effect of inhibitors on sphingolipid levels in lysates of ASAH2-null MEF. Cells were treated with 50 μM of compound and vehicle (control) in DMEM 10% FBS. After 3 h, lipids were extracted and analyzed by LC/MS. Data (mean ± SD) were obtained from two experiments with triplicates. Asterisks indicate statistical significance over vehicle at *, $p < 0.05$; **, $p < 0.01$; ***, $p < 0.001$ (unpaired, two-tailed *t*-test). Total lipids are shown in A and ceramides species are represented in B.

cyclodextrin (data not shown). This suggests that cell death is provoked by the compounds independently of their effect on ceramide metabolism and that cells are sensitized to the molecules by the disturbance of cell membranes induced by cholesterol depletion.

An additional important finding of this article is the remarkable decrease of potency experienced by the NC inhibitors when used in NC-overexpressing cell lysates as compared to rhNC. Importantly, such activity reduction also occurred with C6-urea-ceramide, a competitive NC inhibitor [50], indicating that it is not exclusive to the non-competitive inhibitors reported here. The reason for this potency loss may lie in the structural differences between the commercially available rhNC and the natural enzyme. While NC is bound to the plasma membrane with a single transmembrane helix [21], rhNC lacks a part of the *N*-terminus that includes a few aminoacids of the transmembrane domain (Fig. S4). The truncated protein is soluble in aqueous buffers and it is possible that the inhibitor binding domain conformation in rhNC has a higher affinity for the inhibitors than in the membrane bound enzyme. In this regard, as an example, removal of the membrane anchor in calnexin to create a soluble protein resulted in changes in the profile of substrate binding [55]. In their library screening, Otsuka et al. [37] used secreted NC purified from Sf9 insect cells [21]. Their protein corresponds to the extracellular region (residues 99–780) of human NC with a C-terminal hexahistidine tag and an N-terminal secretory signal. Whether the inhibitors discovered in that high throughput screen retain activity over the natural protein in cell free systems or in live cells has not been reported. This would be interesting to know, as in case of activity reduction, it would alert against the convenience of using genetically modified soluble NC in screening programs and would sustain that studies in cell lysates or preferably live cells must be conducted to avoid false expectations in terms of inhibitory potency on the natural, membrane bound enzyme.

Efforts of numerous groups over the last two decades have enabled the identification of several ceramidase inhibitors. However, in contrast to the better-characterized AC or NC, selective inhibitors of ACER3 are still lacking. Herein, we report that the screening of two series of deoxy(dihydro)ceramides against AC, NC and ACER3 resulted in the discovery of highly selective ACER3 inhibitors in live cells and discloses a scaffold for further medicinal chemistry efforts aimed at improving the ACER3 inhibitory potency. Such efforts should lead compounds devoid of off-target activities in cellulo as expected for **20l** and **20m** due to the high concentrations required for activity in the cell-based assay. Docking studies against the crystal structure of ACER3 [31] should aid in the design of the best ligands for further use in the study or treatment of diseases linked to ACER3 alterations. These include enzyme blockers in the event of overexpression and chemical chaperones in case of genetic deficiencies. Our results also alert about the importance of performing NC inhibitors screening programs in cell free systems and preferably, intact cells, since the use of rhNC affords results which are not recapitulated over the endogenous enzyme.

Declaration of competing interest

The authors declare that they have no known competing financial interests or personal relationships that could have appeared to influence the work reported in this paper.

Acknowledgments

This work has been partly funded by the Spanish Ministry of Economy, Industry and Competitiveness (grant CTQ2017-85378-R) and Fundación BBVA (grant 35_2018). We thank Dr. Gemma Triola for critically reading the manuscript, and Alexandre Garcia, Pedro Rayo, Neus Roca and Eva Dalmau for their excellent technical assistance.

Appendix A. Supplementary data

Supplementary data to this article can be found online at https://doi.org/10.1016/j.ejmech.2021.113296.

References

[1] S.F. Morad, M.C. Cabot, Ceramide-orchestrated signalling in cancer cells, Nat. Rev. Canc. 13 (2013) 51–65, https://doi.org/10.1038/nrc3398.

[2] M.A. Lone, T. Santos, I. Alecu, L.C. Silva, T. Hornemann, 1-Deoxysphingolipids, Biochim. Biophys. Acta Mol. Cell Biol. Lipids 1864 (2019) 512–521, https://doi.org/10.1016/j.bbalip.2018.12.013.

[3] C. Mao, L.M. Obeid, Ceramidases: regulators of cellular responses mediated by ceramide, sphingosine, and sphingosine-1-phosphate, Biochim. Biophys. Acta 1781 (2008) 424–434.

[4] M. Casasampere, E. Izquierdo, J. Casas, J.L. Abad, X. Liu, R. Xu, C. Mao, Y.-T. Chang, A. Delgado, G. Fabrias, Click and count: specific detection of acid ceramidase activity in live cells, Chem. Sci. 11 (2020) 13044–13051, https://doi.org/10.1039/D0SC03166F.

[5] N. Coant, W. Sakamoto, C. Mao, Y.A. Hannun, Ceramidases, roles in sphingolipid metabolism and in health and disease, Adv. Biol. Regul. 63 (2017) 122–131, https://doi.org/10.1016/j.jbior.2016.10.002.

[6] N. Shtraizent, E. Eliyahu, J.-H.H. Park, X. He, R. Shalgi, E.H. Schuchman, Autoproteolytic cleavage and activation of human acid ceramidase, J. Biol. Chem. 283 (2008) 11253–11259, https://doi.org/10.1074/jbc.M709166200.

[7] A. Gebai, A. Gorelik, Z. Li, K. Illes, B. Nagar, Structural basis for the activation of acid ceramidase, Nat. Commun. 9 (2018) 1621, https://doi.org/10.1038/s41467-018-03844-2.

[8] F.P.S. Yu, S. Amintas, T. Levade, J.A. Medin, Acid ceramidase deficiency: Farber disease and SMA-PME, Orphanet J. Rare Dis. 13 (2018) 121, https://doi.org/10.1186/s13023-018-0845-z.

[9] C. Bedia, J. Casas, N. Andrieu-Abadie, G. Fabriàs, T. Levade, Acid ceramidase expression modulates the sensitivity of A375 melanoma cells to dacarbazine, J. Biol. Chem. 286 (2011) 28200–28209, https://doi.org/10.1074/jbc.M110.216382.

[10] N. Realini, F. Palese, D. Pizzirani, S. Pontis, A. Basit, A. Bach, A. Ganesan, D. Piomelli, Acid ceramidase in melanoma: expression, localization and effects of pharmacological inhibition, J. Biol. Chem. 291 (2016) 2422–2434, https://doi.org/10.1074/jbc.M115.666909.

[11] M. Lai, N. Realini, M. La Ferla, I. Passalacqua, G. Matteoli, A. Ganesan, M. Pistello, C.M. Mazzanti, D. Piomelli, Complete Acid Ceramidase ablation prevents cancer-initiating cell formation in melanoma cells, Sci. Rep. 7 (2017) 7411, https://doi.org/10.1038/s41598-017-07606-w.

[12] J. Leclerc, D. Garandeau, C. Pandiani, C. Gaudel, K. Bille, N. Nottet, V. Garcia, P. Colosetti, S. Pagnotta, P. Bahadoran, G. Tondeur, B. Mograbi, S. Dalle, J. Caramel, T. Levade, R. Ballotti, N. Andrieu-Abadie, C. Bertolotto, Lysosomal acid ceramidase ASAH1 controls the transition between invasive and proliferative phenotype in melanoma cells, Oncogene 38 (2018) 1282–1295, https://doi.org/10.1038/s41388-018-0500-0.

[13] X. Liu, J.C. Cheng, L.S. Turner, S. Elojeimy, T.H. Beckham, A. Bielawska, T.E. Keane, Y.A. Hannun, J.S. Norris, Acid ceramidase upregulation in prostate cancer: role in tumor development and implications for therapy, Expert Opin. Ther. Targets 13 (2009) 1449–1458, https://doi.org/10.1517/14728220903357512.

[14] T.H. Beckham, P. Lu, J.C. Cheng, D. Zhao, L.S. Turner, X. Zhang, S. Hoffman, K.E. Armeson, A. Liu, T. Marrison, Y.A. Hannun, X. Liu, Acid ceramidase-mediated production of sphingosine 1-phosphate promotes prostate cancer invasion through upregulation of cathepsin B, Int. J. Canc. 131 (2012) 2034–2043, https://doi.org/10.1002/ijc.27480.

[15] L. Camacho, O. Meca-Cortes, J.L. Abad, S. Garcia, N. Rubio, A. Diaz, T. Celia-Terrassa, F. Cingolani, R. Bermudo, P.L. Fernandez, J. Blanco, A. Delgado, J. Casas, G. Fabrias, T.M. Thomson, Acid ceramidase as a therapeutic target in metastatic prostate cancer, J. Lipid Res. 54 (2013) 1207–1220. https://doi.org/10.1194/jlr.M032375 [pii]10.1194/jlr.M032375 [doi].

[16] J.C. Cheng, A. Bai, T.H. Beckham, S.T. Marrison, C.L. Yount, K. Young, P. Lu, A.M. Bartlett, B.X. Wu, B.J. Keane, K.E. Armeson, D.T. Marshall, T.E. Keane, M.T. Smith, E.E. Jones, R.R.D. Jr, A. Bielawska, J.S. Norris, X. Liu, Radiation-induced acid ceramidase confers prostate cancer resistance and tumor relapse, J. Clin. Invest. 123 (2013) 4344–4358, https://doi.org/10.1172/JCI64791DS1.

[17] S.-F. Tan, X. Liu, T.E. Fox, B.M. Barth, A. Sharma, S.D. Turner, A. Awwad, A. Dewey, K. Doi, B. Spitzer, M.V. Shah, S.A.F. Morad, D. Desai, S. Amin, J. Zhu, J. Liao, J. Yun, M. Kester, D.F. Claxton, H.-G. Wang, M.C. Cabot, E.H. Schuchman, R.L. Levine, D.J. Feith, T.P. Loughran, Acid ceramidase is upregulated in AML and represents a novel therapeutic target, Oncotarget 7 (2016) 83208–83222, https://doi.org/10.18632/oncotarget.13079.

[18] S.F. Tan, W. Dunton, X. Liu, T.E. Fox, S.A.F. Morad, D. Desai, K. Doi, M.R. Conaway, S. Amin, D.F. Claxton, H.G. Wang, M. Kester, M.C. Cabot, D.J. Feith, T.P. Loughran, Acid ceramidase promotes drug resistance in acute myeloid leukemia through NF-κB-dependent P-glycoprotein upregulation, J. Lipid Res. 60 (2019) 1078–1086, https://doi.org/10.1194/jlr.M091876.

[19] J.M. Pearson, S.-F. Tan, A. Sharma, C. Annageldiyev, T.E. Fox, J.L. Abad, G. Fabrias, D. Desai, S. Amin, H.-G. Wang, M.C. Cabot, D.F. Claxton, M. Kester, D.J. Feith, T.P. Loughran, Ceramide analogue SACLAC modulates sphingolipid levels and MCL-1 splicing to induce apoptosis in acute myeloid leukemia, Mol. Canc. Res. 18 (2020) 352–363, https://doi.org/10.1158/1541-7786.MCR-19-0619.

[20] M. Kono, J.L. Dreier, J.M. Ellis, M.L. Allende, D.N. Kalkofen, K.M. Sanders, J. Bielawski, A. Bielawska, Y.A. Hannun, R.L. Proia, Neutral ceramidase encoded by the Asah2 gene is essential for the intestinal degradation of sphingolipids, J. Biol. Chem. 281 (2006) 7324–7331, https://doi.org/10.1074/jbc.M508382200.

[21] M.V. Airola, W.J. Allen, M.J. Pulkoski-Gross, L.M. Obeid, R.C. Rizzo, Y.A. Hannun, Structural basis for ceramide recognition and hydrolysis by human neutral ceramidase, Structure 23 (2015) 1482–1491, https://doi.org/10.1016/j.str.2015.06.013.

[22] S.A. Novgorodov, C.L. Riley, J. Yu, K.T. Borg, Y.A. Hannun, R.L. Proia, M.S. Kindy, T.I. Gudz, Essential roles of neutral ceramidase and sphingosine in mitochondrial dysfunction due to traumatic brain injury, J. Biol. Chem. 289 (2014) 13142–13154, https://doi.org/10.1074/jbc.M113.530311.

[23] K. Sundaram, A.R. Mather, S. Marimuthu, P.P. Shah, A.J. Snider, L.M. Obeid, Y.A. Hannun, L.J. Beverly, L.J. Siskind, Loss of neutral ceramidase protects cells from nutrient and energy deprivation-induced cell death, Biochem. J. 473 (2016) 743–755, https://doi.org/10.1042/BJ20150586.

[24] K. Tanaka, K. Tamiya-Koizumi, K. Hagiwara, H. Ito, A. Takagi, T. Kojima, M. Suzuki, S. Iwaki, S. Fujii, M. Nakamura, Y. Banno, R. Kannagi, T. Tsurumi, M. Kyogashima, T. Murate, Role of down-regulated neutral ceramidase during all-trans retinoic acid-induced neuronal differentiation in SH-SY5Y neuroblastoma cells, J. Biochem. 151 (2012) 611–620, https://doi.org/10.1093/jb/mvs033.

[25] A.J. Snider, B.X. Wu, R.W. Jenkins, J.A. Sticca, T. Kawamori, Y.A. Hannun, L.M. Obeid, Loss of neutral ceramidase increases inflammation in a mouse model of inflammatory bowel disease, Prostag. Other Lipid Mediat. 99 (2012) 124–130, https://doi.org/10.1016/j.prostaglandins.2012.08.003.

[26] Y. Osawa, H. Uchinami, J. Bielawski, R.F. Schwabe, Y.A. Hannun, D.A. Brenner, Roles for C16-ceramide and sphingosine 1-phosphate in regulating hepatocyte apoptosis in response to tumor necrosis factor-α, J. Biol. Chem. 280 (2005) 27879–27887, https://doi.org/10.1074/jbc.M503002200.

[27] B.X. Wu, Y.H. Zeidan, Y.A. Hannun, Downregulation of neutral ceramidase by gemcitabine: implications for cell cycle regulation, Biochim. Biophys. Acta Mol. Cell Biol. Lipids 1791 (2009) 730–739, https://doi.org/10.1016/j.bbalip.2009.03.012.

[28] M. Garcia-Barros, N. Coant, T. Kawamori, M. Wada, A.J. Snider, J.-P. Truman, B.X. Wu, H. Furuya, C.J. Clarke, A.B. Bialkowska, A. Ghaleb, V.W. Yang, L.M. Obeid, Y.A. Hannun, Role of neutral ceramidase in colon cancer, Faseb. J. 30 (2016) 4159–4171, https://doi.org/10.1096/fj.201600611R.

[29] N. Coant, M.G. Qifeng, Z. Lina, Y.A. Hannun, AKT as a key target for growth promoting functions of neutral ceramidase in colon cancer cells, Oncogene 37 (2018) 3852–3863, https://doi.org/10.1038/s41388-018-0236-x.

[30] W. Sun, R. Xu, W. Hu, J. Jin, H.A. Crellin, J. Bielawski, Z.M. Szulc, B.H. Thiers, L.M. Obeid, C. Mao, Upregulation of the human alkaline ceramidase 1 and acid ceramidase mediates calcium-induced differentiation of epidermal keratinocytes, J. Invest. Dermatol. 128 (2008) 389–397, https://doi.org/10.1038/sj.jid.5701025.

[31] I. Vasiliauskaité-Brooks, R.D. Healey, P. Rochaix, J. Saint-Paul, R. Sounier, C. Grison, T. Waltrich-Augusto, M. Fortier, F. Hoh, E.M. Saied, C. Arenz, S. Basu, C. Leyrat, S. Granier, Structure of a human intramembrane ceramidase explains enzymatic dysfunction found in leukodystrophy, Nat. Commun. 9 (2018) 5437, https://doi.org/10.1038/s41467-018-07864-w.

[32] S. Edvardson, J.K. Yi, C. Jalas, R. Xu, B.D. Webb, J. Snider, A. Fedick, E. Kleinman, N.R. Treff, C. Mao, O. Elpeleg, Deficiency of the alkaline ceramidase ACER3 manifests in early childhood by progressive leukodystrophy, J. Med. Genet. 53 (2016) 389–396, https://doi.org/10.1136/jmedgenet-2015-103457.

[33] Y. Yin, M. Xu, J. Gao, M. Li, Alkaline ceramidase 3 promotes growth of hepatocellular carcinoma cells via regulating S1P/S1PR2/PI3K/AKT signaling, Pathol. Res. Pract. 214 (2018) 1381–1387, https://doi.org/10.1016/j.prp.2018.07.029.

[34] C. Chen, Y. Yin, C. Li, J. Chen, J. Xie, Z. Lu, M. Li, Y. Wang, C.C. Zhang, ACER3 supports development of acute myeloid leukemia, Biochem. Biophys. Res. Commun. 478 (2016) 33–38, https://doi.org/10.1016/j.bbrc.2016.07.099.

[35] W. Hu, R. Xu, W. Sun, Z.M. Szulc, J. Bielawski, L.M. Obeid, C. Mao, Alkaline ceramidase 3 (ACER3) hydrolyzes unsaturated long-chain ceramides, and its down-regulation inhibits both cell proliferation and apoptosis, J. Biol. Chem. 285 (2010) 7964–7976, https://doi.org/10.1074/jbc.M109.063586.

[36] E.M. Saied, C. Arenz, Inhibitors of ceramidases, Chem. Phys. Lipids 197 (2016) 60–68, https://doi.org/10.1016/j.chemphyslip.2015.07.009.

[37] Y. Otsuka, M.V. Airola, Y.-M. Choi, N. Coant, J. Snider, C. Cariello, E.M. Saied, C. Arenz, T. Bannister, R. Rahaim, Y.A. Hannun, J. Shumate, L. Scampavia, J.D. Haley, T.P. Spicer, Identification of small-molecule inhibitors of neutral ceramidase (nCDase) via target-based high-throughput screening, SLAS discov, Adv. Sci. Drug Discov. (2020), https://doi.org/10.1177/2472555220945283, 2472555220945283.

[38] A. Bielawska, M.S. Greenberg, D. Perry, S. Jayadev, J.A. Shayman, C. McKay, Y.A. Hannun, (1S, 2R)-D-erythro-2-(N-myristoylamino)-1-phenyl-1-propanol as an inhibitor of ceramidase, J. Biol. Chem. 271 (1996) 12646–12654, accessed September 19, 2018, http://www.ncbi.nlm.nih.gov/pubmed/8647877.

[39] M. Raisova, G. Goltz, M. Bektas, A. Bielawska, C. Riebeling, A.M. Hossini,

J. Eberle, Y.A. Hannun, C.E. Orfanos, C.C. Geilen, Bcl-2 overexpression prevents apoptosis induced by ceramidase inhibitors in malignant melanoma and HaCaT keratinocytes, FEBS Lett. 516 (2002) 47–52, https://doi.org/10.1016/S0014-5793(02)02472-9.

[40] F. Thayyullathil, S. Pallichankandy, A. Rahman, J. Kizhakkayil, S. Chathoth, M. Patel, S. Galadari, Caspase-3 mediated release of SAC domain containing fragment from Par-4 is necessary for the sphingosine-induced apoptosis in Jurkat cells, J. Mol. Signal. 8 (2013) 2, https://doi.org/10.1186/1750-2187-8-2.

[41] J. Mwinyi, A. Boström, I. Fehrer, A. Othman, G. Waeber, H. Marti-Soler, P. Vollenweider, P. Marques-Vidal, H.B. Schiöth, A. Von Eckardstein, T. Hornemann, Plasma 1-deoxysphingolipids are early predictors of incident type 2 diabetes mellitus, PloS One 12 (2017), https://doi.org/10.1371/journal.pone.0175776.

[42] T. Hornemann, I. Alecu, N. Hagenbuch, A. Zhakupova, A. Cremonesi, M. Gautschi, H.H. Jung, F. Meienberg, S. Bilz, E. Christ, M.R. Baumgartner, M. Hochuli, Disturbed sphingolipid metabolism with elevated 1-deoxysphingolipids in glycogen storage disease type I – A link to metabolic control, Mol. Genet. Metabol. 125 (2018) 73–78, https://doi.org/10.1016/j.ymgme.2018.07.003.

[43] C. Bedia, L. Camacho, J.L. Abad, G. Fabrias, T. Levade, A simple fluorogenic method for determination of acid ceramidase activity and diagnosis of Farber disease, J. Lipid Res. 51 (2010) 3542–3547. https://doi.org/10.1194/jlr.D010033 [pii]10.1194/jlr.D010033 [doi].

[44] M. Casasampere, N. Bielsa, D. Riba, L. Bassas, R. Xu, C. Mao, G. Fabriàs, J.L. Abad, A. Delgado, J. Casas, New fluorogenic probes for neutral and alkaline ceramidases, J. Lipid Res. 60 (2019) 1174–1181, https://doi.org/10.1194/jlr.D092759.

[45] M. Casasampere, L. Camacho, F. Cingolani, J. Casas, M. Egido-Gabás, J.L. Abad, C. Bedia, R. Xu, K. Wang, D. Canals, Y.A. Hannun, C. Mao, G. Fabriàs, Activity of neutral and alkaline ceramidases on fluorogenic N -acylated coumarin-containing aminodiols, J. Lipid Res. 56 (2015) 2019–2028, https://doi.org/10.1194/jlr.D061564.

[46] J.M. Munoz-Olaya, X. Matabosch, C. Bedia, M. Egido-Gabás, J. Casas, A. Llebaria, A. Delgado, G. Fabriàs, Synthesis and biological activity of a novel inhibitor of dihydroceramide desaturase, ChemMedChem 3 (2008) 946–953, https://doi.org/10.1002/cmdc.200700325.

[47] C. Bedia, D. Canals, X. Matabosch, Y. Harrak, J. Casas, A. Llebaria, A. Delgado, G. Fabriás, Cytotoxicity and acid ceramidase inhibitory activity of 2-substituted aminoethanol amides, Chem. Phys. Lipids 156 (2008) 33–40, https://doi.org/10.1016/j.chemphyslip.2008.07.012.

[48] J.L. Abad, I. Nieves, P. Rayo, J. Casas, G. Fabrias, A. Delgado, Straightforward access to spisulosine and 4,5-dehydrospisulosine stereoisomers: probes for profiling ceramide synthase activities in intact cells, J. Org. Chem. 78 (2013) 5858–5866, https://doi.org/10.1021/jo400440z.

[49] Y.F. Ordóñez, J.L. Abad, M. Aseeri, J. Casas, V. Garcia, M. Casasampere, E.H. Schuchman, T. Levade, A. Delgado, G. Triola, G. Fabrias, Activity-based imaging of acid ceramidase in living cells, J. Am. Chem. Soc. 141 (2019) 7736–7742, https://doi.org/10.1021/jacs.8b11687.

[50] J. Usta, S. El Bawab, P. Roddy, Z.M. Szulc, Y.A. Hannun, A. Bielawska, Structural requirements of ceramide and sphingosine based inhibitors of mitochondrial ceramidase, Biochemistry 40 (2001) 9657–9668.

[51] S. Ballereau, T. Levade, Y. Genisson, N. Andrieu-Abadie, Alteration of ceramide 1-O-functionalization as a promising approach for cancer therapy, Anticancer. Agents Med. Chem. 12 (2012) 316–328, accessed April 15, 2014, http://www.ncbi.nlm.nih.gov/pubmed/21554198.

[52] K. Wang, C. Li, X. Lin, H. Sun, R. Xu, Q. Li, Y. Wei, Y. Li, J. Qian, C. Liu, Q. Zhang, S. Yu, Z. Cui, X. Huang, B. Zhu, J. Zhou, C. Mao, Targeting alkaline ceramidase 3 alleviates the severity of nonalcoholic steatohepatitis by reducing oxidative stress, Cell Death Dis. 11 (2020) 1–15, https://doi.org/10.1038/s41419-019-2214-9.

[53] K. Wang, R. Xu, J. Schrandt, P. Shah, Y.Z. Gong, C. Preston, L. Wang, J.K. Yi, C.-L. Lin, W. Sun, D.D. Spyropoulos, S. Rhee, M. Li, J. Zhou, S. Ge, G. Zhang, A.J. Snider, Y.A. Hannun, L.M. Obeid, C. Mao, Alkaline ceramidase 3 deficiency results in purkinje cell degeneration and cerebellar ataxia due to dyshomeostasis of sphingolipids in the brain, PLoS Genet. 11 (2015), e1005591, https://doi.org/10.1371/journal.pgen.1005591.

[54] E. Romiti, E. Meacci, G. Tanzi, L. Becciolini, S. Mitsutake, M. Farnararo, M. Ito, P. Bruni, Localization of neutral ceramidase in caveolin-enriched light membranes of murine endothelial cells, FEBS Lett. 506 (2001) 163–168, https://doi.org/10.1016/S0014-5793(01)02878-2.

[55] U.G. Danilczyk, M.F. Cohen-Doyle, D.B. Williams, Functional relationship between calreticulin, calnexin, and the endoplasmic reticulum luminal domain of calnexin, J. Biol. Chem. 275 (2000) 13089–13097, https://doi.org/10.1074/jbc.275.17.13089.

[56] J.W. Antoon, J. Liu, M.M. Gestaut, M.E. Burow, B.S. Beckman, M. Foroozesh, Design, synthesis, and biological activity of a family of novel ceramide analogues in chemoresistant breast cancer cells, J. Med. Chem. 52 (2009) 5748–5752, https://doi.org/10.1021/jm9009668.

[57] Y.C. Chang, Y. Fong, E.M. Tsai, Y.G. Chang, H.L. Chou, C.Y. Wu, Y.N. Teng, T.C. Liu, S.S. Yuan, C.C. Chiu, Exogenous C8-ceramide induces apoptosis by overproduction of ROS and the switch of superoxide dismutases SOD1 to SOD2 in human lung cancer cells, Int. J. Mol. Sci. 19 (2018) 3010, https://doi.org/10.3390/ijms19103010.

Discovery of deoxyceramide analogs as highly selective ACER3 inhibitors in live cells
N. Bielsa, M. Casasampere, M. Aseeri, J. Casas, A. Delgado, J. L. Abad and G. Fabriàs

SUPPLEMENTARY INFORMATION

SYNTHESIS OF COMPOUNDS

General Synthetic Methods

Unless otherwise stated, reactions were carried out under argon atmosphere. Dry solvents were obtained by passing through an activated alumina column on a Solvent Purification System (SPS). Commercially available reagents were used with no further purification. Benzoic acid, 4-etylbenzoic acid, 4-propylbenzoic acid, 4-pentylbenzoic acid, 4-hexylbenzoic acid 4-tert-butylbenzoic acid, 4-pentyloxybenzoic acid, 4-hexyloxybenzoic acid, 4-heptyloxybenzoic acid, methyl 4-hydroxybenzoate, bromomethyl methyl ether, bromoethyl methyl ether, and 1-bromo-2-(2-methoxyethoxy)ethane were obtained from commercial sources.

The following MOM bromides were prepared following reported protocols: 1-bromo-3-(methoxymethoxy)propane, 1-bromo-4-(methoxymethoxy)butane, 1-bromo-5-(methoxymethoxy)pentane, 1-bromo-7-(methoxymethoxy)heptane [1]. 1-Deoxysphingoid bases **1-4** and **21-24** were obtained according to described procedures [2].

All reactions were monitored by TLC analysis using Silica gel on precoated aluminum plates with fluorescent indicator at 254 nm (Sigma-Aldrich). UV light or a 5% (w/v) ethanolic solution of phosphomolybdic acid were used as the visualizing agents. Flash column chromatography was carried out with the indicated solvents using flash-grade silica gel (37-70 μm). Yields refer to chromatographically and spectroscopically pure compounds, unless otherwise stated. The purity of all synthesized (deoxy)ceramide analogs was >95% as estimated by ^{1}H NMR and TLC analysis. Specific rotations were recorded on a digital Perkin-Elmer 34 polarimeter at 25 ºC in a 1 mL cell. The lamp used was a sodium light lamp (589 nm). Results of specific optical rotation are reported in deg^{-1} cm^{3} g^{-1} ($[\alpha]^{20}_{D}$) and concentrations (c) are expressed in g/mL.

High Resolution Mass Spectrometry analyses were carried out on an Acquity UPLC system coupled to a LCT Premier orthogonal accelerated time-of-flight mass spectrometer (Waters) using electrospray ionization (ESI) technique.

Synthesis of *O*-alkylbenzoic acids: General method

Synthesis of polyether alkylbenzoic acids were carried out using two reaction steps.

Step A. Polyalkoxy chain coupling: This reaction was performed using the methodology described by Bost and Winstead with minor modifications [3]. In this case, cesium carbonate (720 mg, 2.21 mmol) was added portionwise over a solution of methyl *p*-hydroxybenzoate (150 mg, 0,98 mmol) in dry acetone (10 mL). A solution of the proper bromide in acetone (1.5 mmol/5 mL) was next added dropwise. After 8h reflux, the reaction mixture was cooled, the solids were removed by filtration and the recovered solution was evaporated to dryness to give an oil which was chromatographed using a gradient of hexanes/EtOAc (from 0 to 20%) to give the corresponding pure methyl O-alkyl benzoate esters in yields ranging between 75 and 90%.

Methyl 4-(methoxymethoxy)benzoate (41) [4]

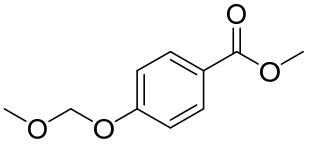

^{1}H NMR (400 MHz, $CDCl_3$) δ 7.99 (m, 2H), 7.05 (m, 2H), 5.22 (s, 2H), 3.89 (s, 3H), 3.48 (s, 3H).

^{13}C NMR (101 MHz, $CDCl_3$) δ 166.8, 161.0, 131.6, 123.7, 115.7, 94.1, 56.3, 51.9.

Methyl 4-(2-(2-methoxyethoxy)ethoxy)benzoate (42) [5]

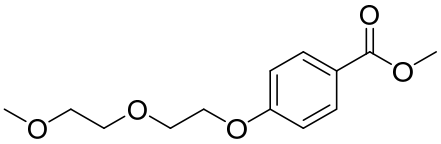

^{1}H NMR (400 MHz, $CDCl_3$) δ 7.97 (m, 2H), 6.92 (m, 2H), 4.19 (m, 2H), 3.89 (s + m, 5H), 3.71 (m, 2H), 3.57 (m, 2H), 3.38 (s, 3H).

^{13}C NMR (101 MHz, $CDCl_3$) δ 166.6, 162.4, 131.4, 122.6, 114.1, 71.8, 70.6, 69.4, 67.4, 58.9, 51.6.

Methyl 4-(2-(methoxymethoxy)ethoxy)benzoate (43)

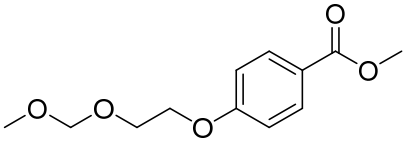

^{1}H NMR (400 MHz, $CDCl_3$) δ 7.99 (m, 2H), 6.94 (m, 2H), 4.72 (s, 2H), 4.20 (m, 2H), 3.92 (m, 2H), 3.88 (s, 3H), 3.40 (s, 3H).

^{13}C NMR (101 MHz, $CDCl_3$) δ 166.7, 162.5, 131.5, 122.8, 114.1, 96.6, 67.4, 65.7, 55.2, 51.8.

HRMS calcd. for $C_{12}H_{17}O_5^+$ ($[M+H]^+$): 241.1071, Found: 241.1074

Methyl 4-(3-(methoxymethoxy)propoxy)benzoate (44)

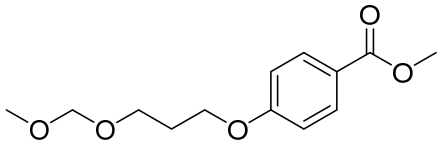

^{1}H NMR (400 MHz, $CDCl_3$) δ 7.98 (m, 2H), 6.92 (m, 2H), 4.63 (s, 2H), 4.13 (t, *J* = 6.5 Hz, 2H), 3.88 (s, 3H), 3.72 (t, *J* = 6.0 Hz, 2H), 3.34 (s, 3H), 2.09 (m, 2H).

^{13}C NMR (101 MHz, $CDCl_3$) δ 166.9, 162.8, 131.6, 122.5, 114.1, 96.5, 64.9, 63.9, 55.2, 51.8, 29.5.

HRMS calcd. for $C_{13}H_{19}O_5^+$ ($[M+H]^+$): 255.1227, Found: 255.1221

Methyl 4-(4-(methoxymethoxy)butoxy)benzoate (45)

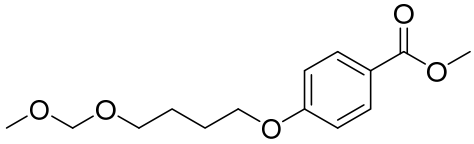

^{1}H NMR (400 MHz, $CDCl_3$) δ 7.98 (m, 2H), 6.90 (m, 2H), 4.64 (s, 2H), 4.05 (t, *J* = 6.0 Hz, 2H), 3.88 (s, 3H), 3.60 (t, *J* = 6.5 Hz, 2H), 3.37 (s, 3H), 1.90 (m, 2H), 1.79 (m, 2H).

^{13}C NMR (101 MHz, $CDCl_3$) δ 166.9, 162.9, 131.6, 122.5, 114.1, 96.5, 67.9, 67.3, 55.2, 51.9, 26.4, 26.1.

HRMS calcd. for $C_{14}H_{21}O_5^+$ ($[M+H]^+$): 269.1384, Found: 269.1391

Methyl 4-(5-(methoxymethoxy)pentyloxy)benzoate (46)

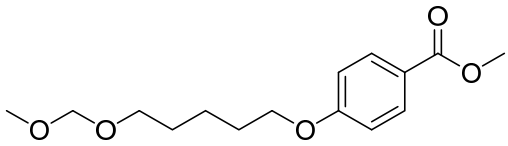

^{1}H NMR (400 MHz, $CDCl_3$) δ 7.97 (d, *J* = 8.5 Hz, 2H), 6.90 (d, *J* = 8.5 Hz, 2H), 4.62 (s, 2H), 4.02 (t, *J* = 6.5 Hz, 2H), 3.88 (s, 3H), 3.56 (t, *J* = 6.5 Hz, 2H), 3.36 (s, 3H), 1.84 (m, 2H), 1.66 (m, 2H), 1.57 (m, 2H).

^{13}C NMR (101 MHz, $CDCl_3$) δ 166.9, 162.9, 131.6, 122.4, 114.1, 96.5, 68.0, 67.6, 55.2, 51.9, 29.5, 28.9, 22.9.

HRMS calcd. for $C_{15}H_{23}O_5^+$ ($[M+H]^+$): 283.1540, Found: 283.1540

Methyl 4-(8-(methoxymethoxy)octyloxy)benzoate (47)

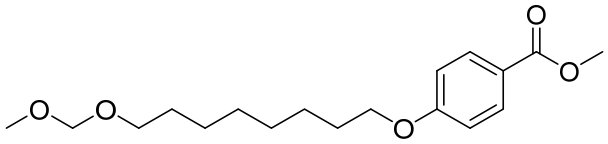

^{1}H NMR (400 MHz, $CDCl_3$) δ 7.97 (d, *J* = 8.5 Hz, 2H), 6.90 (d, *J* = 8.5 Hz, 2H), 4.62 (s, 2H), 4.02 (t, *J* = 6.5 Hz, 2H), 3.88 (s, 3H), 3.56 (t, *J* = 6.5 Hz, 2H), 3.36 (s, 3H), 1.84 (m, 2H), 1.66 (m, 2H), 1.57 (m, 2H).

^{13}C NMR (101 MHz, $CDCl_3$) δ 166.9, 162.9, 131.6, 122.4, 114.1, 96.5, 68.0, 67.6, 55.2, 51.9, 29.5, 28.9, 22.9.

HRMS calcd. for $C_{18}H_{29}O_5^+$ ($[M+H]^+$): 325.2010, Found:325.2019

Step B: **Saponification of the benzoate ester and condensation with the sphingoid bases**.

Saponification: General method. A solution of the corresponding benzoate ester (0.5 mmol) in EtOH (5 mL) was treated with aqueous 2*N* NaOH (5 mL). After stirring for 12h at rt, the reaction mixture was evaporated to dryness and the residue taken up in aqueous 1*N* HCl, extracted with CH_2Cl_2 (3 x 5 mL), dried ($MgSO_4$) and evaporated to give an oil, which was purified by flash chromatography (CH_2Cl_2-/MeOH from o to 3%) to afford the required acid in yields ranging from 85 to 95%

Acylation of the sphingoid bases: General method

To a solution of the corresponding benzoic acid derivative (0.11 mmol) and HOBt (0.13 mmol) in anhydrous CH_2Cl_2 (5 mL) was added EDC (0.14 mmol). The resulting mixture was stirred at rt for 5 min, and next added dropwise to a solution of the corresponding sphingoid base (0.1 mmol) and Et_3N (0.3 mmol) in anhydrous CH_2Cl_2 (5 mL). The reaction mixture was stirred at rt for 2 h and controlled by TLC. The mixture was next diluted by addition of CH_2Cl_2 (10 mL), and washed successively with 1*M* $NaHCO_3$ solution and brine (5 mL each). The organic layer was dried over $MgSO_4$, and filtered. Concentration under reduced pressure afforded crude compounds. Final products were purified by flash chromatography (hexanes/EtOAc, 7/3) to give the corresponding amides in 70-85% yield.

Compounds' characterization

33 [RBM1-32 (2*S*,3*R*-stereoisomer)] /// 35 [RBM1-58 (2*R*,3*S*-stereoisomer)]

^{1}H NMR (400 MHz, $CDCl_3$) δ 6.87 (d, *J* = 8.0 Hz, 1H), 4.09-3.98 (m, 1H), 4.05 (s, 2H), 3.68 (br s, 1H), 1.58 (br, 2H), 1.44 (m, 2H), 1.19 (br, 26H), 1.15 (d, *J* = 7.0 Hz, 3H), 0.88 (t, *J* = 8.0 Hz, 3H).

^{13}C NMR (101 MHz, $CDCl_3$) δ 165.7, 73.9, 49.8, 42.8, 33.9, 32.1, 29.9, 29.9, 29.8, 29.8, 29.7, 29.7, 29.5, 26.1, 22.8, 14.3, 13.7.

HRMS calcd. for $C_{20}H_{41}BrNO_2^+$ ($[M+H]^+$): 406.2315 (100.0%), 408.2295 (97.3%), Found: 406.2307, 408.2287

33 [RBM1-32] $[\alpha]_D$ -4.2 (c=1, $CHCl_3$); **35 [RBM1-58]** $[\alpha]_D$ +4.4 (c=1, $CHCl_3$).

25 [RBM1-33] (2*S*,3*R*-stereoisomer) /// 27 [RBM1-55] (2*R*,3*S*-stereoisomer)

^{1}H NMR (400 MHz, $CDCl_3$) δ 5.81 (m, 1H), 4.01 (m, 1H), 3.62 (m, 1H), 2.16 (t, *J* = 8.0 Hz, 2H), 1.62 (m, 2H), 1.48 (br, 1H), 1.39 (m, 2H), 1.19 (br, 34H), 1.09 (d, *J* = 8.0 Hz, 3H), 0.87 (t, *J* = 8.0 Hz, 6H).

^{13}C NMR (101 MHz, $CDCl_3$) δ 173.3, 74.5, 49.6, 37.1, 33.7, 32.1, 31.8, 29.8, 29.8, 29.8, 29.7, 29.7, 29.5, 29.4, 29.2, 26.2, 26.0, 22.8, 22.7, 14.3, 14.2.

HRMS calcd. for $C_{26}H_{54}NO_2^+$ ($[M+H]^+$): 412.4149 Found: 412.4153

25 [RBM1-33] $[\alpha]_D$ -11.6 (c=1, $CHCl_3$); **27 [RBM1-55]** $[\alpha]_D$ +11.4 (c=1, $CHCl_3$).

13 [RBM1-34] (2*S*,3*R*-stereoisomer) /// 15 [RBM1-70] (2*R*,3*S*-stereoisomer)

^{1}H NMR (400 MHz, $CDCl_3$) δ 6.75 (d, *J* = 8 Hz, 1H), 5.75 (dtd, *J* = 14.5, 8.0, 1.0 Hz, 1H), 5.45 (m, 1H), 4.17 (m, 1H), 4.10 (m, 1H), 4.05 (s, 2H), 2.06 (q, *J* = 7 Hz, 2H), 1.65 (broad, 1H), 1.37 (m, 2H), 1.19 (broad, 20H), 1.15 (d, *J* = 7.0 Hz, 3H), 0.88 (t, *J* = 7.0 Hz, 3H).

^{13}C NMR (101 MHz, $CDCl_3$) δ 166.0, 134.7, 128.1, 75.0, 50.3, 42.8, 32.5, 32.0, 29.8, 29.8, 29.8, 29.7, 29.6, 29.5, 29.3, 29.3, 22.8, 14.9, 14.2.

HRMS calcd. for $C_{20}H_{39}BrNO_2^+$ ($[M+H]^+$): 404.2159 (100.0%), 406.2138 (97.3%), Found: 404.2169, 406.2148

13 [RBM1-34] $[\alpha]_D$ -13.6 (c=1, $CHCl_3$); **15 [RBM1-70]** $[\alpha]_D$ +12.2 (c=1, $CHCl_3$).

5 [RBM1-36] (2*S*,3*R*-stereoisomer) /// 7 [RBM1-67] (2*R*,3*S*-stereoisomer)

^{1}H NMR (400 MHz, $CDCl_3$) δ 5.71 (m, 1H), 5.68 (d, *J* = 8 Hz, 1H), 5.41 (m, 1H), 4.11 (d, *J* = 6.5 Hz, 1H), 4.09 (m, 1H), 2.60 (br, 1H), 2.17 (t, *J* = 8.0 Hz, 2H), 2.03 (q, *J* = 7.0 Hz, 2H), 1.62 (m, 2H), 1.36 (m, 2H), 1.19 (br, 34H), 1.09 (d, *J* = 7.0 Hz, 3H), 0.87 (t, *J* = 7.0 Hz, 6H).

^{13}C NMR (101 MHz, $CDCl_3$) δ 174.0, 134.2, 128.3, 75.8, 50.2, 37.0, 32.5, 32.1, 29.8, 29.8, 29.8, 29.8, 29.6, 29.5, 29.4, 29.2, 26.8, 22.8, 22.7, 15.4, 14.3, 14.2.

HRMS calcd. for $C_{26}H_{52}NO_2^+$ ([M+H]$^+$): 410.3993 Found: 410.3989

5 [RBM1-36] $[\alpha]_D$ -31.2 (c=1, $CHCl_3$); **7 [RBM1-67]** $[\alpha]_D$ +30.4 (c=1, $CHCl_3$).

9 [RBM1-37] (2*S*,3*R*-stereoisomer) /// 11 [RBM1-68] (2*R*,3*S*-stereoisomer)

^{1}H NMR (400 MHz, $CDCl_3$) δ 5.78-5.64 (ca, 2H), 5.41 (m, 1H), 4.11 (d, *J* = 6.0 Hz, 1H), 4.09 (m, 1H), 2.54 (br, 1H), 2.04 (q, *J* = 7.0 Hz, 2H), 1.37 (m, 2H), 1.25 (broad s, 20H), 1.20 (s, 9H), 1.10 (d, *J* = 8 Hz, 3H), 0.87 (t, *J* = 7 Hz, 3H).

^{13}C NMR (101 MHz, $CDCl_3$) δ 179.4, 134.2, 128.2, 76.0, 50.2, 38.8, 32.5, 32.1, 29.8, 29.8, 29.8, 29.8, 29.6, 29.5, 29.4, 29.4, 27.7, 22.8, 15.6, 14.2.

HRMS calcd. for $C_{23}H_{46}NO_2^+$ ([M+H]$^+$): 368.3523 Found: 368.3526

9 [RBM1-37] $[\alpha]_D$ -34.0 (c=1, $CHCl_3$); **11 [RBM1-68]** $[\alpha]_D$ +33.2 (c=1, $CHCl_3$).

17 [RBM1-38] (2*S*,3*R*-stereoisomer) /// 19 [RBM1-69] (2*R*,3*S*-stereoisomer)

^{1}H NMR (400 MHz, $CDCl_3$) δ 7.67 (d, *J* = 8 Hz, 2H), 7.23 (d, *J* = 8 Hz, 2H), 6.25 (d, *J* = 8.0 Hz, 1H), 5.76 (dtd, *J* = 15.0, 7.0, 1.0 Hz, 1H), 5.49 (ddt, *J* = 15.5, 6.5, 1.5 Hz, 1H), 4.31 (ddt, *J* = 10.0, 8.0, 5.5 Hz, 1H), 4.24 (ddd, *J* = 6.5, 3.0, 1.0 Hz, 1H), 2.64 (t, *J* = 8 Hz, 2H), 2.06 (q, *J* = 7 Hz, 2H), 1.82 (Br, 1H), 1.61 (m, 2H), 1.32-1.09 (bs, 30H), 1.21 (d, *J* = 7 Hz, 3H), 0.88 (2x t, *J* = 6.5 Hz, 6H).

^{13}C NMR (101 MHz, $CDCl_3$) δ 168.0, 147.1, 134.3, 131.9, 128.7, 128.5, 127.1, 75.7, 50.6, 36.0, 32.5, 32.1, 31.9, 31.4, 29.8, 29.8, 29.8, 29.8, 29.6, 29.5, 29.4, 29.3, 29.3, 22.8, 22.7, 15.3, 14.3, 14.2.

HRMS calcd. for $C_{32}H_{56}NO_2^+$ ([M+H]$^+$): 486.4306, Found: 486.4299

17 [RBM1-38] $[\alpha]_D$ -9.2 (c=1, $CHCl_3$); **19 [RBM1-69]** $[\alpha]_D$ +9.4 (c=1, $CHCl_3$).

6 [RBM1-39] (2*S*,3*S*-stereoisomer) /// 8 [RBM1-63] (2*R*,3*R*-stereoisomer)

^{1}H NMR (400 MHz, $CDCl_3$) δ 5.71 (m, 1H), 5.68 (d, *J* = 8 Hz, 1H), 5.41 (m, 1H), 4.11 (d, *J* = 6.5 Hz, 1H), 4.09 (m, 1H), 2.60 (br, 1H), 2.17 (t, *J* = 8.0 Hz, 2H), 2.03 (q, *J* = 7.0 Hz, 2H), 1.62 (m, 2H), 1.36 (m, 2H), 1.19 (br, 34H), 1.09 (d, *J* = 7.0 Hz, 3H), 0.87 (t, *J* = 7.0 Hz, 6H).

^{13}C NMR (101 MHz, $CDCl_3$) δ 173.7, 134.2, 129.7, 76.2, 49.8, 37.1, 32.4, 32.1, 31.9, 29.8, 29.8, 29.8, 29.6, 29.7, 29.5, 29.4, 29.4, 29.3, 29.2, 26.0, 22.8, 22.8, 17.7, 14.3, 14.2.

HRMS calcd. for $C_{26}H_{52}NO_2^+$ ([M+H]$^+$): 410.3993 Found: 410.3999

6 [RBM1-39] $[\alpha]_D$ -22.4 (c=1, $CHCl_3$); **8 [RBM1-63]** $[\alpha]_D$ +20.2 (c=1, $CHCl_3$).

10 [RBM1-40] (2*S*,3*S*-stereoisomer) /// 12 [RBM1-64] (2*R*,3*R*-stereoisomer)

^{1}H NMR (400 MHz, $CDCl_3$) δ 5.82 (d, *J* = 8.0 Hz, 1H), 5.68 (dt, *J* = 14.0, 8.0 Hz, 1H), 5.43 (ddt, *J* = 15.5, 6.5, 1.5 Hz, 1H), 3.98 (m, 1H), 3.95 (m, 1H),), 2.25 (br, 1H) 2.02 (q, *J* = 7 Hz, 2H), 1.34 (m, 2H), 1.30-1.20 (br, 22H), 1.18 (s, 9H), 1.16 (d, *J* = 6.5 Hz, 3H), 0.87 (t, *J* = 7.0 Hz, 3H).

^{13}C NMR (101 MHz, $CDCl_3$) δ 178.9, 134.0, 129.7, 76.0, 49.5, 38.8, 32.4, 32.1, 29.8, 29.8, 29.8, 29.7, 29.6, 29.5, 29.4, 29.3, 27.7, 22.8, 17.5, 14.3.

HRMS calcd. for $C_{23}H_{46}NO_2^+$ ($[M+H]^+$): 368.3523 Found: 368.3532

10 [RBM1-40] $[\alpha]_D$ -26.4 (c=1, $CHCl_3$); **12 [RBM1-64]** $[\alpha]_D$ +25.2 (c=1, $CHCl_3$).

18 [RBM1-41] (2*S*,3*S*-stereoisomer) /// 20 [RBM1-65] (2*R*,3*R*-stereoisomer)

^{1}H NMR (400 MHz, $CDCl_3$) δ 7.67 (d, *J* = 8.0 Hz, 2H), 7.21 (d, *J* = 8.0 Hz, 2H), 6.37 (d, *J* = 8.0 Hz, 1H), 5.73 (dt, *J* = 15.0, 7.0 Hz, 1H), 5.52 (ddt, *J* = 15.5, 6.5, 1.5 Hz, 1H), 4.19 (m, 1H), 4.10 (m, 1H), 2.63 (t, *J* = 8 Hz, 2H), 2.34 (Br, 1H), 2.02 (q, *J* = 7 Hz, 2H), 1.61 (m, 2H), 1.36–1.18 (br, 32H), 0.88 (2x t, *J* = 7.0 Hz, 6H).

^{13}C NMR (101 MHz, $CDCl_3$) δ 167.8, 147.0, 134.2, 132.0, 129.7, 128.6, 127.1, 75.9, 50.2, 36.0, 32.4, 32.1, 31.9, 31.4, 29.8, 29.8, 29.8, 29.7, 29.6, 29.5, 29.3, 29.3, 29.3, 22.8, 22.8, 17.7, 14.2, 14.2.

HRM calcd. for $C_{32}H_{56}NO_2^+$ ($[M+H]^+$): 486.4306, Found: 486.4212

18 [RBM1-41] $[\alpha]_D$ +9.0 (c=1, $CHCl_3$); **20 [RBM1-65]** $[\alpha]_D$ -8.8 (c=1, $CHCl_3$).

14 [RBM1-42] (2*S*,3*S*-stereoisomer) /// 16 [RBM1-66] (2*R*,3*R*-stereoisomer)

^{1}H NMR (400 MHz, $CDCl_3$) δ 6.75 (d, *J* = 8.0 Hz, 1H), 5.73 (dt, *J* = 14.5, 8.0 Hz, 1H), 5.46 (m, 1H), 4.06 (m, 1H), 4.05 (s, 2H), 4.01 (m, 1H), 2.20 (broad, 1H), 2.03 (q, *J* = 7 Hz, 2H), 1.36 (m, 2H), 1.19 (broad, 20H), 1.22 (d, *J* = 6.5 Hz, 3H), 0.88 (t, *J* = 7.0 Hz, 3H).

^{13}C NMR (101 MHz, $CDCl_3$) δ 166.0, 134.9, 129.1, 75.5, 50.0, 42.9, 32.4, 32.1, 29.8, 29.8, 29.8, 29.8, 29.6, 29.5, 29.3, 29.3, 22.8, 17.4, 14.3.

HRMS calcd. for $C_{20}H_{39}BrNO_2^+$ ($[M+H]^+$): 404.2159 (100.0%), 406.2138 (97.3%), Found: 404.2166, 406.2145

14 [RBM1-42] $[\alpha]_D$ -6.2 (c=1, $CHCl_3$); **16 [RBM1-66]** $[\alpha]_D$ +5.4 (c=1, $CHCl_3$).

26 [RBM1-43] (2*S*,3*S*-stereoisomer) /// 28 [RBM1-59] (2*R*,3*R*-stereoisomer)

^{1}H NMR (400 MHz, $CDCl_3$) δ 5.78 (m, 1H), 3.96 (m, 1H), 3.51 (m, 1H), 2.44 (br, 1H), 2.17 (t, *J* = 8.0 Hz, 2H), 1.62 (m, 2H), 1.42 (m, 2H), 1.39 (m, 4H), 1.19 (br, 34H), 1.17 (d, *J* = 7.0 Hz, 3H), 0.87 (t, *J* = 8.0 Hz, 6H).

^{13}C NMR (101 MHz, $CDCl_3$) δ 173.5, 74.8, 48.9, 37.2, 34.7, 32.1, 31.9, 29.8, 29.8, 29.8, 29.8, 29.7, 29.5, 29.4, 29.2, 26.0, 25.8, 22.8, 22.7, 18.5, 14.2, 14.2.

HRMS calcd. for $C_{26}H_{54}NO_2^+$ ($[M+H]^+$): 412.4149 Found: 412.4150

26 [RBM1-43] $[\alpha]_D$ -11.0 (c=1, $CHCl_3$); **28 [RBM1-59]** $[\alpha]_D$ +9.6 (c=1, $CHCl_3$).

30 [RBM1-44] (2*S*,3*S*-stereoisomer) /// 32 [RBM1-60] (2*R*,3*R*-stereoisomer)

^{1}H NMR (400 MHz, $CDCl_3$) δ 5.91 (d, *J* = 8.5 Hz, 1H), 3.94 (m, 1H), 3.53 (m, 1H), 2.23 (br, 1H), 1.48-1.33 (4H), 1.25 (broad s, 26H), 1.19 (s, 9H), 1.17 (d, *J* = 7.0 Hz, 3H), 0.87 (t, *J* = 7.0 Hz, 3H).

^{13}C NMR (101 MHz, $CDCl_3$) δ 178.8, 74.9, 48.8, 38.9, 34.7, 32.1, 29.8, 29.8, 29.8, 29.8, 29.7, 29.5, 27.8, 25.8, 22.8, 18.4, 14.3.

HRMS calcd. for $C_{23}H_{48}NO_2^+$ ($[M+H]^+$): 370.3680, Found: 370.3688

30 [RBM1-44] $[\alpha]_D$ -14.0 (c=1, $CHCl_3$); **32 [RBM1-60]** $[\alpha]_D$ +13.0 (c=1, $CHCl_3$).

38 [RBM1-45] (2*S*,3*S*-stereoisomer) /// 40 [RBM1-61] (2*R*,3*R*-stereoisomer)

^{1}H NMR (400 MHz, $CDCl_3$) δ 7.69 (d, *J* = 8.0 Hz, 2H), 7.21 (d, *J* = 8.0 Hz, 2H), 6.49 (d, *J* = 8.5 Hz, 1H), 4.18 (m, 1H), 3.63 (m, 1H), 2.63 (t, *J* = 8.0 Hz, 3H), 1.60 (m, 2H), 1.55 – 1.38 (4H), 1.34-1.20 (broad, 36H), 1.29 (d, 3H), 0.88 (2 x t, *J* = 7.0 Hz, 6H).

^{13}C NMR (101 MHz, $CDCl_3$) δ 167.7, 146.9, 132.1, 128.7, 127.1, 102.7, 74.9, 49.4, 35.9, 34.8, 32.1, 31.9, 31.4, 29.9, 29.8, 29.8, 29.8, 29.7, 29.5, 29.3, 29.3, 25.9, 22.8, 22.8, 18.6, 14.2, 14.2.

HRMS calcd. for $C_{32}H_{58}NO_2^+$ ($[M+H]^+$): 488.4462, Found: 488.4462

38 [RBM1-45] $[\alpha]_D$ +8.4 (c=1, $CHCl_3$); **40 [RBM1-61]** $[\alpha]_D$ -8.0 (c=1, $CHCl_3$).

34 [RBM1-46] (2*S*,3*S*-stereoisomer) /// 36 [RBM1-62] (2*R*,3*R*-stereoisomer)

^{1}H NMR (400 MHz, $CDCl_3$) δ 6.80 (d, *J* = 8.5 Hz, 1H), 4.06 (s, 2H), 4.00 (m, 2H), 3.58 (m, 1H), 1.98 (broad, 1H), 1.52–1.34 (4H), 1.34-1.19 (broad, 27H), 0.88 (t, *J* = 7.0 Hz, 3H).

^{13}C NMR (101 MHz, $CDCl_3$) δ 166.0, 74.5, 49.4, 42.9, 34.6, 32.1, 29.8, 29.8, 29.8, 29.8, 29.7, 29.7, 29.7, 29.5, 25.8, 22.8, 18.3, 14.3.

HRMS calcd. for $C_{20}H_{41}BrNO_2^+$ ($[M+H]^+$): 406.2315 (100.0%), 408.2295 (97.3%), Found: 406.2314, 408.2294

34 [RBM1-46] $[\alpha]_D$ -4.8 (c=1, $CHCl_3$); **36 [RBM1-62]** $[\alpha]_D$ +4.0 (c=1, $CHCl_3$).

37 [RBM1-47] (2*S*,3*R*-stereoisomer) /// 39 [RBM1-57] (2*R*,3*S*-stereoisomer)

^{1}H NMR (400 MHz, $CDCl_3$) δ 7.69 (d, *J* = 8.0 Hz, 1H), 7.21 (d, *J* = 8.0 Hz, 1H), 6.50 (d, *J* = 8.0 Hz, 1H), 4.21 (m, 1H), 3.75 (m, 1H), 2.63 (t, *J* = 8.0 Hz, 2H), 1.61 (m, 2H), 1.56–1.36 (4H), 1.36–1.15 (broad, 34H), 1.20 (t, *J* = 7.0 Hz, 3H), 0.88 (2 x t, *J* = 7.0 Hz, 6H).

^{13}C NMR (101 MHz, $CDCl_3$) δ 167.4, 147.0, 132.0, 128.7, 127.1, 74.5, 50.0, 36.0, 33.9, 32.1, 31.9, 31.4, 29.8, 29.8, 29.8, 29.8, 29.7, 29.5, 29.3, 29.3, 26.2, 22.8, 22.8, 14.3, 14.2, 14.1.

HRMS calcd. for $C_{32}H_{58}NO_2^+$ ($[M+H]^+$): 488.4462, Found: 488.4471

37 [RBM1-47] $[\alpha]_D$ +5.0 (c=1, $CHCl_3$); **39 [RBM1-57]** $[\alpha]_D$ -4.8 (c=1, $CHCl_3$).

29 [RBM1-48] (2*S*,3*R*-stereoisomer) /// 31 [RBM1-56] (2*R*,3*S*-stereoisomer)

^{1}H NMR (400 MHz, $CDCl_3$) δ 5.89 (d, *J* = 8.0 Hz, 1H), 3.99 (m, 1H), 3.61 (m, 1H), 2.03 (br, 1H), 1.54-1.30 (4H), 1.30-1.20 (broad s, 24H), 1.20 (s, 9H), 1.09 (d, *J* = 7.0 Hz, 3H), 0.88 (t, *J* = 7.0 Hz, 3H).

^{13}C NMR (101 MHz, $CDCl_3$) δ 178.6, 74.5, 49.5, 38.7, 33.8, 32.1, 29.8, 29.8, 29.8, 29.7, 29.7, 29.5, 27.7, 26.1, 22.8, 14.2, 14.2.

HRMS calcd. for $C_{23}H_{48}NO_2^+$ ($[M+H]^+$): 370.3680, Found: 370.3686

29 [RBM1-48] $[\alpha]_D$ -15.0 (c=1, $CHCl_3$); **31 [RBM1-56]** $[\alpha]_D$ +14.6 (c=1, $CHCl_3$).

20a [RBM1-65a]

^{1}H NMR (400 MHz, $CDCl_3$) δ 7.76 (m, 2H), 7.50 (m, 1H), 7.43 (m, 2H), 6.34 (d, *J* = 8 Hz, 1H), 5.75 (dt, *J* = 14.0, 6.5 Hz, 1H), 5.53 (dd, *J* = 15.5, 7.0 Hz, 1H), 4.21 (m, 1H), 4.12 (m, 1H), 2.03 (q, *J* = 7.0 Hz, 2H), 1.39-1.20 (broad, 24H), 1.30 (d, *J* = 7.0 Hz, 3H), 0.88 (t, *J* = 7.0 Hz, 3H).

^{13}C NMR (101 MHz, $CDCl_3$) δ 167.8, 134.7, 134.4, 131.6, 129.7, 128.6, 127.1, 75.9, 50.2, 32.4, 32.1, 29.8, 29.8, 29.8, 29.7, 29.6, 29.5, 29.3, 29.3, 22.8, 17.8, 14.3.

HRMS calcd. for $C_{25}H_{42}NO_2^+$ ($[M+H]^+$): 388.3210, Found: 388.3219

$[\alpha]_D$ -3.8 (c=1, $CHCl_3$)

20b [RBM1-65b]

^{1}H NMR (400 MHz, $CDCl_3$) δ 7.69 (d, *J* = 8.0 Hz, 2H), 7.25 (d, *J* = 8.0 Hz, 2H), 6.29 (d, *J* = 8.0 Hz, 1H), 5.74 (dt, *J* = 14.0, 7.0 Hz, 1H), 5.52 (dd, *J* = 15.5, 7.5 Hz, 1H), 4.20 (m, 1H), 4.10 (m, 1H), 2.69 (q, *J* = 7.5 Hz, 2H), 2.02 (q, *J* = 7.0 Hz, 2H), 1.36-1.29 (m, 2H), 1.27 (d, 3H), 1.26-1.19 (br, 24H), 0.86 (t, *J* = 7.0 Hz, 3H).

^{13}C NMR (101 MHz, $CDCl_3$) δ 167.8, 148.2, 134.3, 132.1, 129.7, 128.1, 127.2, 76.0, 50.2, 32.5, 32.1, 29.8, 29.8, 29.8, 29.8, 29.7, 29.6, 29.5, 29.3, 29.3, 28.9, 22.8, 17.7, 15.5, 14.3.

HRMS calcd. for $C_{27}H_{46}NO_2^+$ ([M+H]$^+$): 416.3523, Found: 416.3515

$[\alpha]_D$ -8.2 (c=1, $CHCl_3$)

20c [RBM1-65c]

^{1}H NMR (400 MHz, $CDCl_3$) δ 7.68 (d, *J* = 8.0 Hz, 2H), 7.23 (d, *J* = 8.0 Hz, 2H), 6.29 (d, *J* = 8.5 Hz, 1H), 5.74 (dt, *J* = 14.0, 7.0 Hz, 1H), 5.52 (dd, *J* = 15.5, 7.0 Hz, 1H), 4.20 (m, 1H), 4.11 (m, 1H), 2.63 (t, *J* = 8.0 Hz, 2H), 2.03 (q, *J* = 7.0 Hz, 2H), 1.65 (m, 2H), 1.33 (m, 2H), 1.29 (d, *J* = 7.0 Hz, 3H), 1.31-1.21 (m, 20H), 0.94 (t, *J* = 7.5 Hz, 3H), 0.88 (t, *J* = 7.0 Hz, 3H).

^{13}C NMR (101 MHz, $CDCl_3$) δ 167.8, 146.7, 134.3, 132,1, 129.7, 128.7, 127,1, 76.0, 50.2, 38.0, 32.5, 32.1, 29.8, 29.8, 29.8, 29.7, 29.6, 29.5, 29.3, 29.3, 24.5, 22.8, 17.7, 14.3, 13.9.

HRMS calcd. for $C_{28}H_{48}NO_2^+$ ([M+H]$^+$): 430.3680, Found: 430.3674

$[\alpha]_D$ -8.4 (c=1, $CHCl_3$)

20d [RBM1-65d]

^{1}H NMR (400 MHz, $CDCl_3$) δ 7.68 (d, *J* = 8.0 Hz, 2H), 7.23 (d, *J* = 8.0 Hz, 2H), 6.30 (d, *J* = 8.0 Hz, 1H), 5.74 (dt, *J* = 14.0, 7.0 Hz, 1H), 5.52 (dd, *J* = 15.5, 7.0 Hz, 1H), 4.20 (m, 1H), 4.10 (m, 1H), 2.64 (t, *J* = 8.0 Hz, 2H), 2.02 (q, *J* = 7.0 Hz, 2H), 1.68-1.54 (m, 4H), 1.39-1.19 (ca, 27H), 0.90 (t, *J* = 8.0 Hz, 3H), 0.88 (t, *J* = 8.0 Hz, 3H).

^{13}C NMR (101 MHz, $CDCl_3$) δ 167.8, 147.0, 134.3, 132.1, 129.7, 128.7, 127.1, 76.0, 50,2, 35.9, 32.5, 32.1, 31,5, 31.0, 29.8, 29.8, 29.8, 29.7, 29.6, 29.5, 29.3, 29.3, 22.8, 22.6, 17.7, 14.2, 14.1.

HRMS calcd. for $C_{30}H_{52}NO_2^+$ ([M+H]$^+$): 458.3993, Found: 458.4004

$[\alpha]_D$ -8.6 (c=1, $CHCl_3$)

20e [RBM1-65e]

^{1}H NMR (400 MHz, $CDCl_3$) δ 7.62 (d, *J* = 8.0 Hz, 2H), 7.22 (d, *J* = 8.0 Hz, 2H), 6.33 (d, *J* = 8.0 Hz, 1H), 5.74 (dt, *J* = 14.0, 7.0 Hz, 1H), 5.52 (dd, *J* = 15.5, 7.0 Hz, 1H), 4.19 (m, 1H), 4.10 (m, 1H), 2.64 (t, *J* = 8.0 Hz, 2H), 2.02 (q, *J* = 7.0 Hz, 2H), 1.61 (m, 2H), 1.39-1.19 (ca, 31H),0.88 (2xt, *J* = 7.0 Hz, 6H).

^{13}C NMR (101 MHz, $CDCl_3$) δ 167.8, 147.0, 134.3, 132.1, 129.7, 128.6, 127.1, 76.0, 50.2, 36.0, 32.5, 32.1, 31.80 31.3, 29.8, 29.8, 29.8, 29.7, 29.6, 29.5, 29.3, 29.3, 29.0, 22.8, 22.7, 17.7, 14.2, 14.2.

HRMS calcd. for $C_{31}H_{54}NO_2^+$ ([M+H]$^+$): 472.4149, Found: 472.4139

$[\alpha]_D$ -8.6 (c=1, $CHCl_3$)

20f [RBM1-65f]

^{1}H NMR (400 MHz, $CDCl_3$) δ 7.70 (d, *J* = 8.5 Hz, 2H), 7.43 (d, *J* = 8.5 Hz, 2H), 6.40 (d, *J* = 8.0 Hz, 1H), 5.73 (dt, *J* = 14.0, 7.0 Hz, 1H), 5.52 (dd, *J* = 15.5, 7.0 Hz, 1H), 4.19 (m, 1H), 4.10 (m, 1H), 2.70 (broad, 1H), 2.01 (q, *J* = 7.0 Hz, 2H), 1.33 (s, 9H), 1.33-1.19 (broad, 24H), 0.87 (t, *J* = 7.0 Hz, 3H).

^{13}C NMR (101 MHz, $CDCl_3$) δ 167.7, 155.1, 134.3, 131.8, 129.7, 126.9, 125.6, 76.0, 50.1, 35.0, 32.4, 32.1, 31.3, 29.8, 29.8, 29.8, 29.7, 29.6, 29.5, 29.3, 29.3, 22.8, 17.7, 14.3.

HRMS calcd. for $C_{29}H_{50}NO_2^+$ ($[M+H]^+$): 444.3836, Found: 444.3832

$[\alpha]_D$ -9.0 (c=1, $CHCl_3$)

20g [RBM1-65g]

^{1}H NMR (400 MHz, $CDCl_3$) δ 7.71 (m, 2H), 6.90 (m, 2H), 6.22 (d, *J* = 8.0 Hz, 1H), 5.73 (dt, *J* = 14.0, 7.0 Hz, 1H), 5.52 (dd, *J* = 15.5, 7.0 Hz, 1H), 4.18 (m, 1H), 4.09 (m, 1H), 3.99 (t, *J* = 6.5 Hz, 2H), 2.02 (q, *J* = 7.0 Hz, 2H), 1.83-1.72 (broad, 1H), 1.80 (m, 2H), 1.47-1.35 (m, 4H), 1.35-1.28 (m, 2H), 1.28 (d, *J* = 7 Hz, 3H), 1.25-1.19 (broad, 20H), 0.94 (t, *J* = 7.0 Hz, 3H), 0.88 (t, *J* = 7.0 Hz, 3H).

^{13}C NMR (101 MHz, $CDCl_3$) δ 167.5, 161.9, 134.2, 129.8, 128.9, 126.6, 114.3, 76.1, 68.3, 50.2, 32.4, 32.1, 29.8, 29.8, 29.8, 29.8, 29.7, 29.6, 29.5, 29.3, 29.3, 29.0, 28.3, 22.8, 22.6, 17.8, 14.2, 14.1.

HRMS calcd. for $C_{30}H_{52}NO_3^+$ ($[M+H]^+$): 474.3942, Found: 474.3951

$[\alpha]_D$ -9.0 (c=1, $CHCl_3$)

20h [RBM1-65h]

^{1}H NMR (400 MHz, $CDCl_3$) δ 7.71 (m, 2H), 6.90 (m, 2H), 6.24 (br d, *J* = 8.0 Hz, 1H), 5.73 (dt, *J* = 14.0, 7.0 Hz, 1H), 5.52 (dd, *J* = 15.5, 7.0 Hz, 1H), 4.18 (m, 1H), 4.09 (m, 1H), 3.99 (t, *J* = 6.5 Hz, 2H), 2.02 (q, *J* = 7.0 Hz, 2H), 2.20-1.85 (broad, 1H), 1.79 (m, 2H), 1.40-1.31 (m, 6H), 1.28 (d, *J* = 7 Hz, 3H), 1.25-1.19 (broad, 20H), 0.91 (t, *J* = 7.0 Hz, 3H), 0.88 (t, *J* = 7.0 Hz, 3H).

^{13}C NMR (101 MHz, $CDCl_3$) δ 167.5, 161.9, 134.2, 129.8, 128.9, 126.6, 114.3, 76.1, 68.3, 50.2, 32.4, 32.1, 31.7, 29.8, 29.8, 29.8, 29.8, 29.7, 29.6, 29.5, 29.3, 29.3, 29.2, 25.8, 22.8, 22.7, 17.8, 14.2, 14.1.

HRMS calcd. for $C_{31}H_{54}NO_3^+$ ($[M+H]^+$): 488.4098 , Found: 488.4086

$[\alpha]_D$ -8.8 (c=1, $CHCl_3$)

20i [RBM1-65i]

^{1}H NMR (400 MHz, $CDCl_3$) δ 7.71 (m, 2H), 6.90 (m, 2H), 6.21 (d, *J* = 8.0 Hz, 1H), 5.74 (dt, *J* = 14.0, 7.0 Hz, 1H), 5.52 (dd, *J* = 15.5, 7.0 Hz, 1H), 4.18 (m, 1H), 4.09 (m, 1H), 3.99 (t, *J* = 6.5 Hz, 2H), 2.02 (q, *J* = 7.0 Hz, 2H), 1.84-1.55 (broad, 1H), 1.79 (m, 2H), 1.40-1.31

(m, 6H), 1.28 (d, *J* = 7 Hz, 3H), 1.25-1.19 (broad, 22H), 0.90 (t, *J* = 7.0 Hz, 3H), 0.88 (t, *J* = 7.0 Hz, 3H).

^{13}C NMR (101 MHz, $CDCl_3$) δ 167.5, 161.9, 134.2, 129.8, 128.9, 126.6, 114.3, 76.1, 68.3, 50.2, 32.4, 32.1, 31.7, 29.8, 29.8, 29.8, 29.8, 29.7, 29.6, 29.5, 29.3, 29.3, 29.3, 29.2, 26.1, 22.8, 22.7, 17.8, 14.2, 14.2.

HRMS calcd. for $C_{32}H_{56}NO_3^+$ ($[M+H]^+$): 502.4255, Found: 502.4246

$[\alpha]_D$ -7.4 (c=1, $CHCl_3$)

20j [RBM1-65j]

^{1}H NMR (400 MHz, $CDCl_3$) δ 7.72 (m, 2H), 7.06 (m, 2H), 6.24 (d, *J* = 8.0 Hz, 1H), 5.74 (dt, *J* = 14.0, 7.0 Hz, 1H), 5.52 (dd, *J* = 15.5, 7.0 Hz, 1H), 5.21 (s, 2H), 4.18 (m, 1H), 4.10 (m, 1H), 3.48 (s, 3H), 2.02 (q, *J* = 7.0 Hz, 2H), 1.28 (d, *J* = 7 Hz, 3H), 1.24 (broad, 25H), 0.88 (t, *J* = 7.0 Hz, 3H).

^{13}C NMR (101 MHz, $CDCl_3$) δ 167.3 159.9, 134.2, 129.7, 128.8, 128.1, 115.9, 94.3, 76.0, 56.3, 50.2, 32.4, 32.0, 29.8, 29.8, 29.8, 29.7, 29.6, 29.5, 29.3, 29.3, 22.8, 17.8, 14.2.

HRMS calcd. for $C_{27}H_{46}NO_4^+$ ($[M+H]^+$): 448.3421, Found: 448.3421

$[\alpha]_D$ -9.2 (c=1, $CHCl_3$)

20k [RBM1-65k]

^{1}H NMR (400 MHz, $CDCl_3$) δ 7.72 (d, *J* = 8.5 Hz, 2H), 6.94 (d, *J* = 8.5 Hz, 2H), 6.25 (d, *J* = 8.0 Hz, 1H), 5.74 (dt, *J* = 14.0, 7.0 Hz, 1H), 5.52 (dd, *J* = 15.5, 7.0 Hz, 1H), 4.72 (s, 2H), 4.23-4.12 (m, 3H), 4.10 (m, 1H), 3.91 (m, 2H), 3.40 (s, 3H), 2.02 (q, *J* = 7.0 Hz, 2H), 1.27 (d, *J* = 7 Hz, 3H), 1.39-1.15 (22H), 0.88 (t, *J* = 7.0 Hz, 3H).

^{13}C NMR (101 MHz, $CDCl_3$) δ 167.3 161.5, 134.3, 129.8, 128.9, 127.2, 114.4, 96.7, 76.1, 67.5, 65.9, 55.4, 50.2, 32.4, 32.0, 29.8, 29.8, 29.8, 29.7, 29.6, 29.5, 29.3, 29.3, 22.8, 17.8, 14.2.

HRMS calcd. for $C_{29}H_{50}NO_5^+$ ($[M+H]^+$): 492.3684, Found: 492.3688

$[\alpha]_D$ -9.6 (c=1, $CHCl_3$)

20l [RBM1-65l]

^{1}H NMR (400 MHz, $CDCl_3$) δ 7.72 (d, *J* = 8.5 Hz, 2H), 6.94 (d, *J* = 8.5 Hz, 2H), 6.25 (d, *J* = 8.0 Hz, 1H), 5.74 (dt, *J* = 14.0, 7.0 Hz, 1H), 5.52 (dd, *J* = 15.5, 7.0 Hz, 1H), 4.72 (s, 2H), 4.23-4.12 (m, 3H), 4.10 (m, 1H), 3.91 (m, 2H), 3.40 (s, 3H), 2.09 (m, 2H), 2.02 (q, *J* = 7.0 Hz, 2H), 1.27 (d, *J* = 7 Hz, 3H), 1.39-1.15 (22H), 0.88 (t, *J* = 7.0 Hz, 3H).

^{13}C NMR (101 MHz, $CDCl_3$) δ 167.4 161.7, 134.3, 129.8, 128.9, 126.9, 114.3, 96.6, 76.1, 65.0, 64.1, 55.3, 50.2, 32.4, 32.0, 29.8, 29.8, 29.8, 29.7, 29.6, 29.6, 29.5, 29.3, 29.3, 22.8, 17.8, 14.2.

HRMS calcd. for $C_{30}H_{52}NO_5^+$ ([M+H]$^+$): 506.3840, Found: 506.3829

$[\alpha]_D$ -9.0 (c=1, $CHCl_3$)

20m [RBM1-65m]

^{1}H NMR (400 MHz, $CDCl_3$) δ 7.72 (d, *J* = 8.5 Hz, 2H), 6.91 (d, *J* = 8.5 Hz, 2H), 6.22 (d, *J* = 8.0 Hz, 1H), 5.74 (dt, *J* = 14.0, 7.0 Hz, 1H), 5.52 (dd, *J* = 15.5, 7.0 Hz, 1H), 4.64 (s, 2H), 4.18 (m, 1H), 4.09 (m, 1H), 4.03 (t, *J* = 6.0 Hz, 2H), 3.60 (t, *J* = 6.0 Hz, 2H), 3.37 (s, 3H), 2.02 (q, *J* = 7.0 Hz, 2H), 1.90 (m, 2H), 1.79 (m, 2H), 1.28 (d, *J* = 7 Hz, 3H), 1.39-1.15 (22H), 0.88 (t, *J* = 7.0 Hz, 3H).

^{13}C NMR (101 MHz, $CDCl_3$) δ 167.4 161.8, 134.2, 129.8, 128.9, 126.8, 114.3, 96.5, 76.1, 67.9, 67.4, 55.3, 50.2, 32.4, 32.0, 29.8, 29.8, 29.8, 29.7, 29.6, 29.5, 29.3, 29.3, 26.5, 26.2, 22.8, 17.8, 14.2.

HRMS calcd. for $C_{31}H_{54}NO_5^+$ ([M+H]$^+$): 520.3997, Found: 520.3979

$[\alpha]_D$ -9.0 (c=1, $CHCl_3$)

20n [RBM1-65n]

^{1}H NMR (400 MHz, $CDCl_3$) δ 7.71 (d, *J* = 8.5 Hz, 2H), 6.90 (d, *J* = 8.5 Hz, 2H), 6.22 (d, *J* = 8.0 Hz, 1H), 5.74 (dt, *J* = 14.0, 7.0 Hz, 1H), 5.52 (dd, *J* = 15.5, 7.0 Hz, 1H), 4.63 (s, 2H), 4.18 (m, 1H), 4.09 (m, 1H), 4.01 (t, *J* = 6.5 Hz, 2H), 3.56 (t, *J* = 6.5 Hz, 2H), 3.37 (s, 3H), 2.02 (q, *J* = 7.0 Hz, 2H), 1.84 (m, 2H), 1.68 (m, 2H), 1.57 (m, 2H), 1.28 (d, *J* = 7 Hz, 3H), 1.39-1.15 (22H), 0.88 (t, *J* = 7.0 Hz, 3H).

^{13}C NMR (101 MHz, $CDCl_3$) δ 167.4 161.8, 134.2, 129.8, 128.8, 126.7, 114.3, 96.5, 76.1, 68.1, 67.7, 55.3, 50.2, 32.4, 32.0, 29.8, 29.8, 29.8, 29.7, 29.6, 29.6, 29.5, 29.3, 29.3, 29.1, 22.9, 22.8, 17.8, 14.2.

HRMS calcd. for $C_{32}H_{56}NO_5^+$ ([M+H]$^+$): 534.4153, Found: 534.4166

$[\alpha]_D$ -8.8 (c=1, $CHCl_3$)

20o [RBM1-65o]

^{1}H NMR (400 MHz, $CDCl_3$) δ 7.71 (d, *J* = 8.5 Hz, 2H), 6.90 (d, *J* = 8.5 Hz, 2H), 6.22 (d, *J* = 8.0 Hz, 1H), 5.74 (dt, *J* = 14.0, 7.0 Hz, 1H), 5.52 (dd, *J* = 15.5, 7.0 Hz, 1H), 4.62 (s, 2H), 4.17 (m, 1H), 4.09 (m, 1H), 3.99 (t, *J* = 6.5 Hz, 2H), 3.52 (t, *J* = 6.5 Hz, 2H), 3.36 (s, 3H), 2.02 (q, *J* = 7.0 Hz, 2H), 1.79 (m, 2H), 1.68-1.52 (br, 6H), 1.46 (m, 2H), 1.42-1.20 (28H), 0.88 (t, *J* = 7.0 Hz, 3H).

^{13}C NMR (101 MHz, $CDCl_3$) δ 167.4 161.9, 134.3, 129.8, 128.8, 126.7, 114.3, 96.5, 76.2, 68.3, 68.0, 55.2, 50.2, 32.4, 32.0, 29.9, 29.8, 29.8, 29.8, 29.7, 29.6, 29.5, 29.5, 29.4, 29.3, 29.3, 29.3, 26.3, 26.1, 22.8, 17.8, 14.3.

HRMS calcd. for $C_{35}H_{62}NO_5^+$ ([M+H]$^+$): 576.4623, Found: 576.4630

$[\alpha]_D$ -8.7 (c=1, $CHCl_3$)

20p [RBM1-65p]

^{1}H NMR (400 MHz, $CDCl_3$) δ 7.71 (d, *J* = 8.5 Hz, 2H), 6.93 (d, *J* = 8.5 Hz, 2H), 6.26 (br s, 1H), 5.73 (dt, *J* = 14.0, 6.5 Hz, 1H), 5.51 (dd, *J* = 15.5, 7.0 Hz, 1H), 4.23-4.12 (3H), 4.08 (m, 1H), 3.87 (m, 2H), 3.72 (m, 2H), 3.58 (m, 2H), 3.39 (s, 3H), 2.10 (broad, 1H, OH), 2.02 (q, *J* = 7.0 Hz, 2H), 1.42-1.15 (broad, 26H), 0.88 (t, *J* = 7.0 Hz, 3H).

^{13}C NMR (101 MHz, $CDCl_3$) δ 167.3, 161.4, 134.1, 129.8, 128.8, 127.1, 114.4, 76.0, 72.0, 70.9, 69.7, 67.6, 59.2, 50.2, 32.4, 32.0, 29.8, 29.8, 29.7, 29.7, 29.6, 29.5, 29.3, 29.3, 22.8, 17.7, 14.2.

HRMS calcd. for $C_{30}H_{52}NO_5^+$ ([M+H]$^+$): 506.3840, Found: 506.3850

$[\alpha]_D$ -9.4 (c=1, $CHCl_3$)

Synthesis of (2*S*,3*R*)-*N*-[2-(1,3-dihydroxy-4*E*-octadecene)]-*N*-hexane-urea (C6-urea-Cer).

To a solution of (2*S*,3*R*,4*E*)-sphingosine (21 mg, 0.07 mmol) and NEt_3 (10 µL) in anhydrous CH_3CN (4 mL) and anhydrous methyl tert-butyl ether (2 mL), hexyl isocyante (17 µL, 0.181 mmol) was added, and the mixture was stirred at room temperature under N_2 for 4 h. After evaporation of the solvents under a reduced pressure, residue was dissolved in CH_2Cl_2 (10 mL) washed with H_2O (2 x 3 mL) and concentrated to dryness. Flash chromatography purification with silica gel using a stepwise solvent gradient (CH_2Cl_2/MeOH, 0-4%) gave the pure urea isoster of ceramide (27 mg, 86% yield); TLC (CH_2Cl_2-MeOH, 10:1, v/v; Rf 0.5)

^{1}H NMR ($CDCl_3$) 5.73 (dt, *J* =15.5, 7.0 Hz, 1H), 5.49 (dd, *J* = 15.5, 6.5 Hz, 1H), 4.22 (m, 1H), 3.78 (m, 1H), 3.72 (m, 1H), 3.67 (m, 1H), 3.11 (t, *J* = 7 Hz, 1H), 2.02 (m, 2H), 1.46 (m, 2H), 1.20 (m, 2H), 1.41-1.19 (brs, 28H), 0.88 (t, *J* =7.0 Hz, 3H), 0.87 (t, *J* =7.0 Hz, 3H).

^{13}C NMR (101 MHz, $CDCl_3$) δ 159.4, 133.9, 128.9, 77.5, 77.2, 76.8, 74.6, 63.0, 56.0, 40.8, 32.6, 32.1, 31.7, 30.3, 29.9, 29.8, 29.8, 29.7, 29.5, 29.4, 26.8, 22.8, 22.8, 14.3, 14.2.

SUPPLEMENTARY TABLE

Table S1. CLogP values of analogs of compound 20.[a]

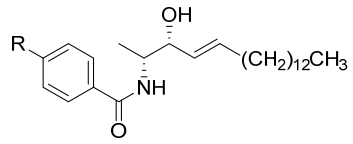

Name	R	CLogP	Name	R	CLogP
20a	-H	7.03	**20i**	$-O(CH_2)_6CH_3$	9,39
20b	$-CH_2CH_3$	7.93	**20j**	$-OCH_2OCH_3$	7,02
20c	$-(CH_2)_2CH_3$	8.35	**20k**	$-O(CH_2)_2OCH_2OCH_3$	6,86
20d	$-(CH_2)_4CH_3$	9.18	**20l**	$-O(CH_2)_3OCH_2OCH_3$	6,97
20e	$-(CH_2)_5CH_3$	9.6	**20m**	$-O(CH_2)_4OCH_2OCH_3$	7,42
20	$-(CH_2)_6CH_3$	10.02	**20n**	$-O(CH_2)_5OCH_2OCH_3$	7,84
20f	$-C(CH_3)_3$	8.73	**20o**	$-O(CH_2)_8OCH_2OCH_3$	8,68
20g	$-O(CH_2)_4CH_3$	8.56	**20p**	$-O(CH_2)_2O(CH_2)_2OCH_3$	6,59
20h	$-O(CH_2)_5CH_3$	8.98	*N*-octanoylsphingosine		7.01

[a]CLogP were determined using the calculation algorithm included in ChemDraw Professional 15.0.

SUPPLEMENTARY FIGURES

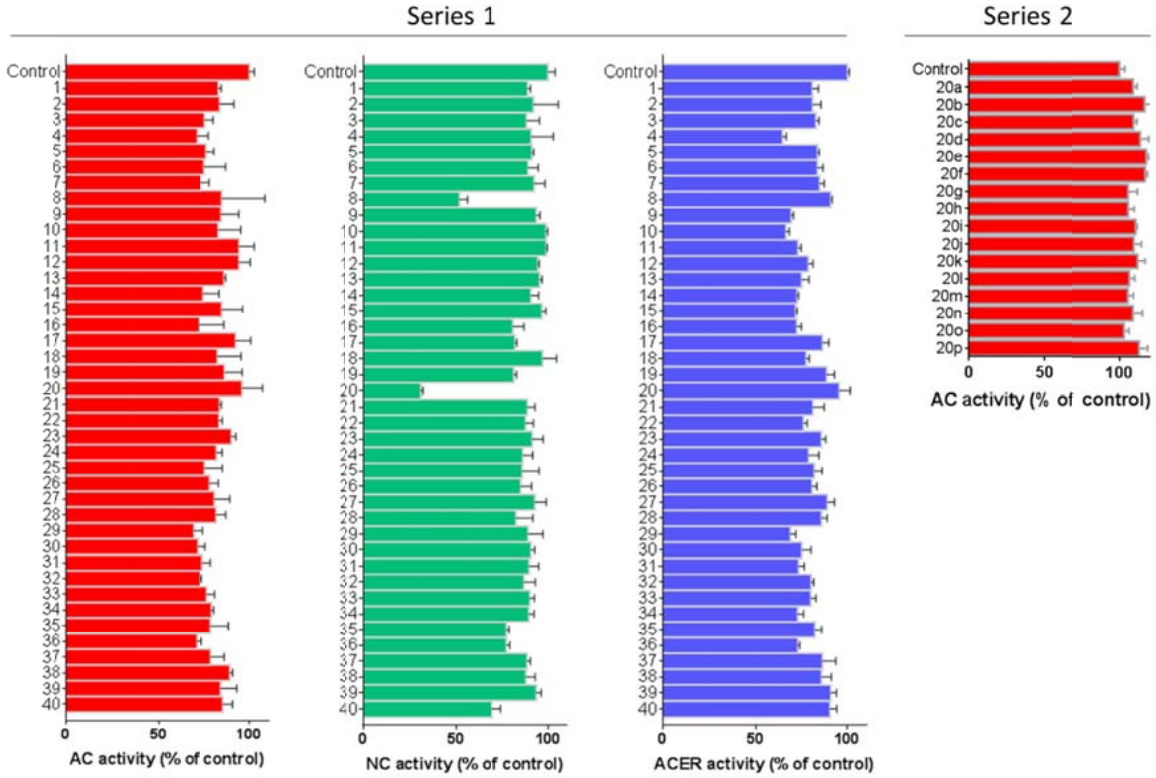

Figure S1. Activity of compounds on ceramidases. Experiments were carried out using recombinant NC, lysates of AC overexpressing Farber cells or lysates of MEF from ASAH2-null mice. The suitable buffers and pH were used for each specific activity. Concentration of substrate was 20 µM and those of test compounds were: 1 µM for NC and 20 µM for AC and ACER. Data (mean ± SD) were obtained from two experiments with triplicates.

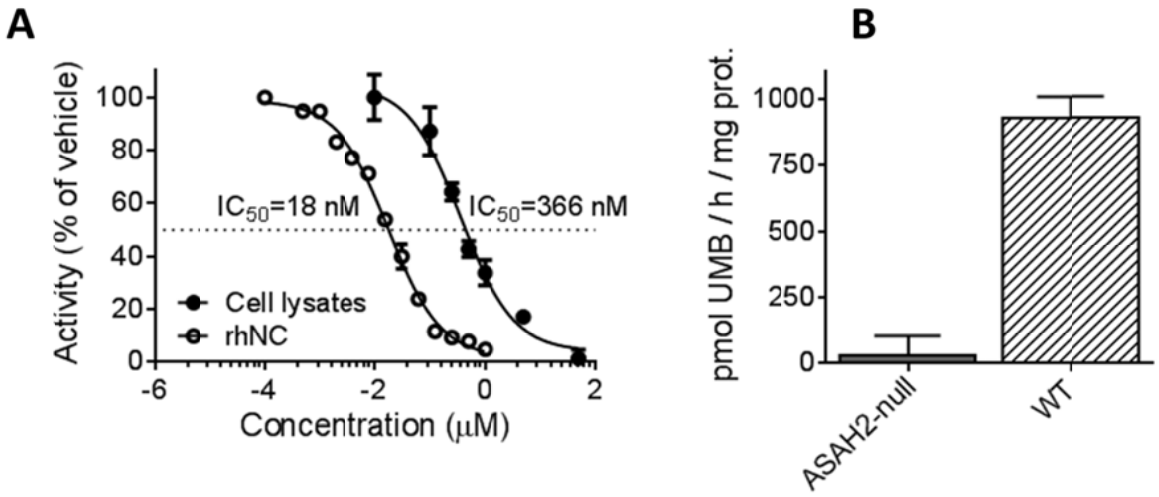

Figure S2. A. Activity of C6-urea-Cer on NC. Experiments were carried out using rhNC (5 ng) or lysates (25 μg) of WT-MEF using 25 mM phosphate buffer, 150 mM NaCl, 1% NaChol (sodium cholate), pH 7.4. and the specific NC substrate (RBM14C24:1, 10 μM) and 3h incubation time. Lysates were obtained from ASAH2-null (B) and wild type (WT) MEF (A and B) cells that had been growing for at least 14 days after thawing. Data (mean ± SD) were obtained from two experiments with triplicates. Data adjustment with the four parameter logistic equation (GraphPad Prism 6) afforded the indicated IC_{50} values. B. NC activity in ASAH2-null and wild type (WT) MEF (mean ± SD, n=6 (two experiments with triplicates)).

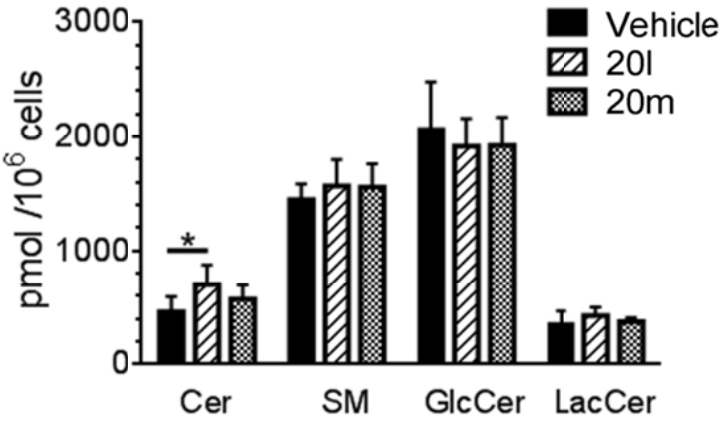

Figure S3. Effect of compounds 20l and 20m on sphingolipid levels in lysates of AC-overexpressing A375 cells. Cells were treated with 50 μM of compound and vehicle (control) in DMEM 10% FBS. After 3 h, lipids were extracted and analysed by LC/MS. Data (mean ± SD) were obtained from two experiments with triplicates. Asterisks indicate statistical significance at *, p = 0,052 (unpaired, two-tailed *t* test).

A

MSAITVALLSLLFITSGTIENHKDLGGHFFSTTQSPPATQGSTAAQRSTATQHSTATQSSTATQTSPVPLTPESPLF
QNFSGYHIGVGRADCTGQVADINLMGYGKSGQNAQGILTRLYSRAFIMAEPDGSNRTVFVSIDIGMVSQRLRLE
VLNRLQSKYGSLYRRDNVILSGTHTHSGPAGYFQYTVFVIASEGFSNQTFQHMVTGILKSIDIAHTNMKPGKIFIN
KGNVDGVQINRSPYSYLQNPQSERARYPSNTDKEMIVLKMVDLNGDDLGLISWFAIHPVSMNNSNHLVNSDN
VGYASYLLEQEKNKGYLPGQGPFVAAFASSNLGDVSPNILGPRCINTGESCDNANSTCPIGGPSMCIAKGPGQD
MFDSTQIIGRAMYQRAKELYASASQEVTGPLASAHQWVDMTDVTVWLNSTHASKTCKPALGYSFAAGTIDGV
GGLNFTQGKTEGDPFWDTIRDQILGKPSEEIKECHKPKPILLHTGELSKPHPWHPDIVDVQIITLGSLAITAIPGEFT
TMSGRRLREAVQAEFASHGMQNMTVVISGLCNVYTHYITTYEEYQAQRYEAASTIYGPHALSAYIQLFRNLAKAI
ATDTVANLSRGPEPPFFKQLIVPLIPSIVDRAPKGRTFGDVLQPAKPEYRVGEVAEVIFVGANPKNSVQNQTHQT
FLTVEKYEATSTSWQIVCNDASWETRFYWHKGLLGLSNATVEWHIPDTAQPGIYRIRYFGHNRKQDILKPAVILS
FEGTSPAFEVVTI

B

HHHHHHSGTIENHKDLGGHFFSTTQSPPATQGSTAAQRSTATQHSTATQSSTATQTSPVPLTPESPLFQNFSGY
HIGVGRADCTGQVADINLMGYGKSGQNAQGILTRLYSRAFIMAEPDGSNRTVFVSIDIGMVSQRLRLEVLNRLQ
SKYGSLYRRDNVILSGTHTHSGPAGYFQYTVFVIASEGFSNQTFQHMVTGILKSIDIAHTNMKPGKIFINKGNVDG
VQINRSPYSYLQNPQSERARYPSNTDKEMIVLKMVDLNGDDLGLISWFAIHPVSMNNSNHLVNSDNVGYASYL
LEQEKNKGYLPGQGPFVAAFASSNLGDVSPNILGPRCINTGESCDNANSTCPIGGPSMCIAKGPGQDMFDSTQII
GRAMYQRAKELYASASQEVTGPLASAHQWVDMTDVTVWLNSTHASKTCKPALGYSFAAGTIDGVGGLNFTQ
GKTEGDPFWDTIRDQILGKPSEEIKECHKPKPILLHTGELSKPHPWHPDIVDVQIITLGSLAITAIPGEFTTMSGRRL
REAVQAEFASHGMQNMTVVISGLCNVYTHYITTYEEYQAQRYEAASTIYGPHALSAYIQLFRNLAKAIATDTVAN
LSRGPEPPFFKQLIVPLIPSIVDRAPKGRTFGDVLQPAKPEYRVGEVAEVIFVGANPKNSVQNQTHQTFLTVEKYE
ATSTSWQIVCNDASWETRFYWHKGLLGLSNATVEWHIPDTAQPGIYRIRYFGHNRKQDILKPAVILSFEGTSPAF
EVVTI

C

FSGYHIGVGRADCTGQVADINLMGYGKSGQNAQGILTRLYSRAFIMAEPDGSNRTVFVSIDIGMVSQRLRLEVL
NRLQSKYGSLYRRDNVILSGTHTHSGPAGYFQYTVFVIASEGFSNQTFQHMVTGILKSIDIAHTNMKPGKIFINKG
NVDGVQINRSPYSYLQNPQSERARYSSNTDKEMIVLKMVDLNGDDLGLISWFAIHPVSMNNSNHLVNSDNVG
YASYLLEQEKNKGYLPGQGPFVAAFASSNLGDVSPNILGPRCINTGESCDNANSTCPIGGPSMCIAKGPGQDMF
DSTQIIGRAMYQRAKELYASASQEVTGPLASAHQWVDMTDVTVWLNSTHASKTCKPALGYSFAAGTIDGVGGL
NFTQGKTEGDPFWDTIRDQILGKPSEEIKECHKPKPILLHTGELSKPHPWHPDIVDVQIITLGSLAITAIPGEFTTMS
GRRLREATLSAYIQLFRNLAKAIATDTVANLSRGPEPPFFKQLIVPLIPSIVDRAPKGRTFGDVLQPAKPEYRVGEV
AEVIFVGANPKNSVQNQTHQTFLTVEKYEATSTSWQIVCNDASWETRFYWHKGLLGLSNATVEWHIPDTAQP
GIYRIRYFGHNRKQDILKPAVILSFEGTSPAFEVVTIHHHHHH

Figure S4. Comparison of amino acid sequences of human NC (>AAF86240.1 mitochondrial ceramidase [Homo sapiens]) (A), the commercial rhNC used in this study (B) and the crystalized NC (C) as reported by Airola et al. [6] (>pdb|4wgk|A B). The signal/anchor sequence is highlighted in blue and the mucin-like domain is highlighted in green. The genetically introduced hexahistidine tags are in red. In the commercial rhNC, the MSAITVALLSLLFIT sequence from the natural protein (Accession # AAF86240) is replaced with a 6His tag. The crystalized protein lacks both anchor sequence and mucin-like domain sequences.

REFERENCES

[1] J.L. Abad, G. Fabriás, F. Camps, Synthesis of dideuterated and enantiomers of monodeuterated tridecanoic acids at C-9 and C-10 positions, J. Org. Chem. 65 (2000) 8582–8588. https://doi.org/10.1021/jo000957k.

[2] J.L. Abad, I. Nieves, P. Rayo, J. Casas, G. Fabrias, A. Delgado, Straightforward access to spisulosine and 4,5-dehydrospisulosine stereoisomers: probes for profiling ceramide synthase activities in intact cells., J. Org. Chem. 78 (2013) 5858–5866. https://doi.org/10.1021/jo400440z.

[3] R.W. Bost, M.B. Winstead, The Preparation of Some Polyalkoxy Ethers of the Isomeric Hydroxybenzoic Acids, J. Am. Chem. Soc. 74 (1952) 1821–1824. https://doi.org/10.1021/ja01127a058.

[4] Y. Xia, Z. Mo, L. Sun, L. Zou, W. Zhang, J. Zhang, L. Wang, First total synthesis of quiquesetinerviusin A, J. Chem. Res. 41 (2017) 296–300. https://doi.org/10.3184/174751917X14931195075599.

[5] C.P. Collier, J.O. Jeppesen, Y. Luo, J. Perkins, E.W. Wong, J.R. Heath, J.F. Stoddart, Molecular-based electronically switchable tunnel junction devices, J. Am. Chem. Soc. 123 (2001) 12632–12641. https://doi.org/10.1021/ja0114456.

[6] M. V. Airola, W.J. Allen, M.J. Pulkoski-Gross, L.M. Obeid, R.C. Rizzo, Y.A. Hannun, Structural Basis for Ceramide Recognition and Hydrolysis by Human Neutral Ceramidase, Structure. 23 (2015) 1482–1491. https://doi.org/10.1016/j.str.2015.06.013.

ARTICLE 2

Activity-Based Imaging of Acid Ceramidase in Living Cells

Yadira F Ordóñez [1], José Luís Abad [1], **Mazen Aseeri** [1], Josefina Casas [1,2], Virginie Garcia [3], Mireia Casasampere [1], Edward H Schuchman [4], Thierry Levade [3,5], Antonio Delgado [1,6], Gemma Triola [7], Gemma Fabrias [1,2]

[1] Research Unit on Bioactive Molecules (RUBAM), Department of Biological Chemistry , Institute for Advanced Chemistry of Catalonia (IQAC-CSIC) , Jordi Girona, 18 , 08034 Barcelona , Spain.

[2] Liver and Digestive Diseases Networking Biomedical Research Centre (CIBER-EHD) , 28029 Madrid , Spain.

[3] INSERM, UMR1037 CRCT , 31037 Toulouse , France.

[4] Department of Genetics and Genomic Sciences, Icahn School of Medicine at Mount Sinai , New York 10029 , United States.

[5] Laboratoire de Biochimie Métabolique , Institut Fédératif de Biologie, CHU Purpan , 31300 Toulouse , France.

[6] Unit of Pharmaceutical Chemistry (Associated Unit to CSIC), Department of Pharmacology, Toxicology and Medicinal Chemistry, Faculty of Pharmacy and Food Sciences , University of Barcelona, 08028 Barcelona , Spain.

[7] Chemical Biology group, Department of Biological Chemistry, Institute for Advanced Chemistry of Catalonia (IQAC-CSIC), Jordi Girona, 18, 08034 Barcelona, Spain.

Journal of the American Chemical Society (JACS). **2019** May 15;141(19):7736-7742.

Impact factor: 14.695

The contribution of Mazen Aseeri to this work, corresponds to the design, performance and data analysis of experiments which are presented in Figures 3, 4, 5, S2, S6, S7 and S8. He also contributed to the writing of the initial draft and the preparation of the published work.

CASAS BRUGULAT JOSEFINA - DNI 40513738C Firmado digitalmente por CASAS BRUGULAT JOSEFINA - DNI 40513738C Fecha: 2023.01.24 13:18:17 +01'00'

TRIOLA GUILLEM GEMMA - DNI 40323105B Digitally signed by TRIOLA GUILLEM GEMMA - DNI 40323105B Date: 2023.01.25 17:42:38 +01'00'

Josefina Casas Brugulat and Gemma Triola Guillem

Thesis Directors

SUMMARY

Activity-Based Imaging of Acid Ceramidase in Living Cells

Objective: Acid ceramidase (AC) is overexpressed in many types of cancer and Alzheimer's disease, and its genetic deficiency leads to the manifestation of various diseases, for which no treatment yet exists. These pathological alterations in AC activity should be intracellularly monitored for diagnostic purposes, as well as to follow-up treatment approaches. This requires a method capable of specific labelling of active AC in living cells. Activity-based probes (ABPs) proved useful for visualizing active enzymes, yet no ABPs were successfully used for AC imaging in living cells. Therefore, this work aimed at the development of an ABP that could be employed for the intracellular detection of AC.

Methodology: Analogues of SABRAC, a previously reported irreversible AC inhibitor, were synthesized by our group, and were found to be highly potent AC inhibitors. And because the analogue SOBRAC was the most potent among all, its fluorescent-derivative BODIPY-SOBRAC was first synthesized to explore enzyme labelling in Farber fibroblast (FD1), which contains zero AC activity, and the same FD1 cells transduced to overexpress AC (FD1/AC). AC labelling was not seen in FD1 lysates, whereas a band corresponding to labelled AC was clearly visualized in FD1/AC extracts. Although, BODIPY-SOBRAC succeeded in labelling active AC in lysates, it resulted in unspecific background staining possibly due side-reactions with intracellular electrophiles. Therefore, BODIPY-SOCLAC was next synthesized and investigated as it contains a less reactive chloroacetyl moiety. The reactivity of BODIPY-SOCLAC with Cys143 was first confirmed by mass spectrometry. BODIPY-SOCLAC was then tested in lysates from cells transfected with wild-type (WT) ASAH1 cDNA and ASAH1 mutant, in which the active-site cysteine was replaced by serine (C143S). Both plasmids (WT and mutated) were transiently transfected in cells using Lipofectamine 2000. Following the successful detection of AC using BODIPY-SOCLAC in cells transfected with ASAH1, the probe was then tested in cell lysates from A549, fibroblasts, FD1/AC, FD1 and three different homozygous Farber fibroblast FD2-FD4, displaying null or very low AC activity. The activity of AC was first determined by measuring the fluorescence released after the hydrolysis of RBM14C12 substrate. Next, AC labelling was performed by exposing cell lysates to 0.5 µM and 1 µM of BODIPY-SOCLAC probe for 5 min at 37˚C while shaking. Selective target binding of BODIPY-SOCLAC was assessed in FD1/AC and confirmed after competition experiments in the presence of unlabeled SOCLAC. Briefly, lysates from FD1/AC cells were preincubated for 5 min with the specified concentrations of SOCLAC (competitor) followed by 5 min incubation with 1 µM probe. The reaction mixtures were then quenched with 6.25 µL of Laemmli 4× buffer, and proteins were resolved on 12.5% SDS-PAGE. Gels were stained with Coomassie blue to confirm that equal amounts of protein were loaded. In-gel visualization of the fluorescent bands was performed in

the wet gel slabs using a Typhoon 5 Biomolecular Imager. AC labelling in intact cells was performed by adding a medium containing 75 nM LysoTracker Red DND-99 to culture medium of cell lines for 1 h at 37˚C, followed by the addition of 1 µM BODIPY-SOCLAC for 5 min. Staining was viewed with a Leica TCS-SP2 Laser Scanning Confocal microscope, and the images were analyzed using Fiji-ImageJ software.

Results: BODIPY-SOCLAC was able to detect AC in lysates of cells transfected with WT-ASAH1, but not in those transfected with ASAH1-mutant. Western blot detected both WT and mutant proteins in previous samples, which confirms the labeling ability of BODIPY-SOCLAC in distinguishing between the active and inactive forms of AC. Unlike labelling with BODIPY-SOBRAC, and as it was anticipated, BODIPY-SOCLAC did not result in background staining, and exclusively detected one band corresponding to labelled AC. The probe was also successful in detecting endogenous levels of AC in lysates of different cell lines. In intact cells, BODIPY-SOCLAC achieved excellent imaging of varying levels of AC expression, contained in different intact cell lines, with a labelling intensity matching the AC activity detected in those cells.

Conclusions: Novel ABPs were developed based on the structure of SABRAC, an AC irreversible inhibitor reported previously. The in-gel labelling of AC with the probe proved useful at submicromolar concentrations and short incubation times and the probe also succeeded in detecting endogenous levels of the active enzyme. Importantly, labelling of AC was not seen in denatured protein, indicating that the probe specifically detects active protein folding. Although an ABP for AC labelling was reported earlier, BODIPY-SOCLAC is distinguished in that it unprecedently permitted the exclusive detection of active AC, not the inactive, in the lysosomes of living cells. Overall, the outcomes of this work could be of biomedical interest in visualizing and tracking intracellular active AC, as well as in evaluating new chaperone treatments for diseases with altered AC activity.

JACS
JOURNAL OF THE AMERICAN CHEMICAL SOCIETY
Article
Cite This: J. Am. Chem. Soc. 2019, 141, 7736−7742
pubs.acs.org/JACS

Activity-Based Imaging of Acid Ceramidase in Living Cells

Yadira F. Ordóñez,[†,○,¶] José Luís Abad,[†,¶] Mazen Aseeri,[†] Josefina Casas,[†,‡] Virginie Garcia,[§] Mireia Casasampere,[†] Edward H. Schuchman,[∥] Thierry Levade,[§,⊥] Antonio Delgado,[†,#] Gemma Triola,*[,▽] and Gemma Fabrias*[,†,‡]

[†]Research Unit on Bioactive Molecules (RUBAM), Department of Biological Chemistry, Institute for Advanced Chemistry of Catalonia (IQAC−CSIC), Jordi Girona, 18, 08034 Barcelona, Spain

[‡]Liver and Digestive Diseases Networking Biomedical Research Centre (CIBER-EHD), 28029 Madrid, Spain

[§]INSERM, UMR1037 CRCT, 31037 Toulouse, France

[∥]Department of Genetics and Genomic Sciences, Icahn School of Medicine at Mount Sinai, New York 10029, United States

[⊥]Laboratoire de Biochimie Métabolique, Institut Fédératif de Biologie, CHU Purpan, 31300 Toulouse, France

[#]Unit of Pharmaceutical Chemistry (Associated Unit to CSIC), Department of Pharmacology, Toxicology and Medicinal Chemistry, Faculty of Pharmacy and Food Sciences, University of Barcelona, 08028 Barcelona, Spain

[▽]Chemical Biology group, Department of Biological Chemistry, Institute for Advanced Chemistry of Catalonia (IQAC−CSIC), Jordi Girona, 18, 08034 Barcelona, Spain

Supporting Information

ABSTRACT: Acid ceramidase (AC) hydrolyzes ceramides into sphingoid bases and fatty acids. The enzyme is overexpressed in several types of cancer and Alzheimer's disease, and its genetic defect causes different incurable disorders. The availability of a method for the specific visualization of catalytically active AC in intracellular compartments is crucial for diagnosis and follow-up of therapeutic strategies in diseases linked to altered AC activity. This work was undertaken to develop activity-based probes for the detection of AC. Several analogues of the AC inhibitor SABRAC were synthesized and found to act as very potent (two-digit nM range) irreversible AC inhibitors by reaction with the active site Cys143. Detection of active AC in cell-free systems was achieved either by using fluorescent SABRAC analogues or by click chemistry with an azide-substituted analogue. The compound affording the best features allowed the unprecedented labeling of active AC in living cells.

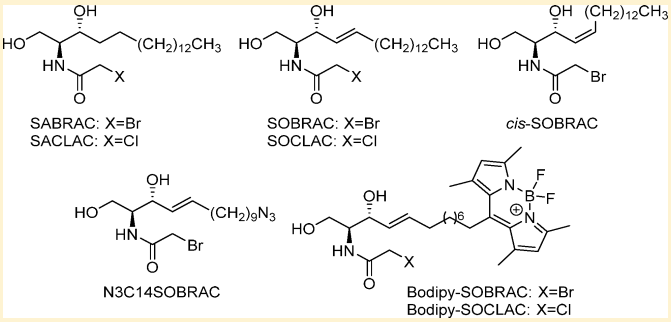

INTRODUCTION

Acid ceramidase (AC) is a ubiquitously expressed lysosomal enzyme that hydrolyzes ceramide into a sphingoid base and a fatty acid in a key reaction that regulates the balance between antimitogenic (ceramides and sphingoid bases) and mitogenic (sphingosine 1-phosphate) lipids. AC is a heterodimeric glycoprotein with a molecular weight of ∼50 kDa. Under reducing conditions, AC dissociates into two disulfide bond-linked subunits: a nonglycosylated 13 kDa α-subunit and a glycosylated 40 kDa β-subunit. The biosynthesis of AC starts with the expression of a single precursor polypeptide of ∼53−55 kDa that is subsequently processed to the mature, heterodimeric enzyme in the endosomes/lysosomes. Mechanistically, AC belongs to the N-terminal nucleophile hydrolase family. These enzymes, which are characterized by their ability to cleave nonpeptide amide bonds, have the common feature of having an active site-terminal nucleophile. In AC, the nucleophilic thiol of Cys143 is exposed at the N-terminus of the β-subunit after autoproteolytic cleavage of the precursor protein.[1]

From the pathological perspective, overexpression of AC has been reported in some cancers[2−4] and Alzheimer's disease brain.[5,6] On the other hand, genetic deficiency in AC activity results in two very rare autosomal recessive disorders: Farber disease (FD)[7] and spinal muscular atrophy with progressive myoclonic epilepsy (SMA-PME),[8] both showing accumulation of lysosomal ceramide. To date, at least 20 different Farber disease-linked mutations have been described in the acid ceramidase ASAH1 gene. These mutations often cause protein misfolding and misrouting and its degradation by the endoplasmic reticulum-associated degradation (ERAD) pathway. Nowadays, therapy for FD is mainly palliative, and severely affected patients die at an early age. Current treatment trials include bone marrow or hematopoietic stem cell

Received: October 30, 2018
Published: April 28, 2019

transplantation[9] and gene therapy,[10] but results are still far from satisfactory. Enzyme replacement therapy and the use of pharmacological chaperones[11] are expected to emerge as promising therapeutic approaches. Pharmacological chaperones are small molecules able to serve as molecular scaffolds of misfolded mutant proteins, thus promoting their proper folding, ERAD escape, and correct trafficking to their site of action. The capability of small compounds to act as pharmacological chaperones, has been investigated in several sphingolipidoses,[12−14] but it has not been examined in FD. In addition, progress in the discovery of pharmacological chaperones is hampered by the lack of small molecules able to stain and follow active proteins in the intracellular compartments of living cells.

Activity-based probes (ABPs) have proved useful to visualize active enzymes,[15−17] including glucocerebrosidase in Gaucher fibroblasts.[18] Moreover, ABPs have a wide range of applications. These include, apart from assessing the beneficial effects of a potential chaperone on the amount and correct localization of mutant proteins, the profiling of changes in enzyme activity in healthy and disease samples and the screening of inhibitors in a cellular environment.

Despite this growing interest, very few examples of ABP for AC detection can be found. Recently, a fluorescent analogue of the AC inhibitor carmofur has been reported as an ABP for AC detection in Gaucher tissue homogenates.[19] However, no ABP has been successfully used for live cell imaging of AC. Herein, we describe the development of a novel ABP that allows for detection of active AC in intact cells.

EXPERIMENTAL SECTION

Materials. Dulbecco's modified Eagle medium (DMEM), fetal bovine serum, doxycycline, penicillin/streptomycin, and trypsin-EDTA were purchased from Sigma. Blasticidin and hygromycin B were from Invitrogen. Polyvinylidene difluoride (PVDF) membrane was purchased from Roche. ECL Prime Western Blotting Detection reagent was purchased from GE Healthcare. Laemmli buffer and acrylamide were purchased from BioRad, and sodium dodecyl sulfate (SDS) was from Fluka. Mass spectrometry-grade trypsin for digestion was from ThermoFisher. In Figure 3, rabbit anti-AC polyclonal antibody was from ORIGENE (reference TA306621) and antirabbit IgG secondary antibody was from GE Healthcare (reference NA934 V). In Figure 3C, a rabbit anti-AC antiserum kindly provided by Prof. K. Sandhoff (University of Bonn, Germany) and a goat antirabbit coupled to horseradish peroxidase (Cell Signaling, Ozyme, France) were used. Recombinant human acid ceramidase was purified from the media of overexpressing Chinese hamster ovary cells according to previously published methods.[20] DBCO-PEG$_4$5/6-TAMRA was purchased from Jena Bioscience.

NMR spectra were recorded at room temperature on a Varian Mercury 400 instrument. The chemical shifts (δ) are reported in ppm relative to the solvent signal, and coupling constants (J) are reported in Hertz (Hz). Deuterated solvents were used as internal standards ($CDCl_3$: δ = 7.26 ppm for ^{1}H, δ = 77.16 ppm for ^{13}C; acetone-d_6: δ = 2.05 ppm for ^{1}H, δ = 29.84 ppm for ^{13}C; CD_3OD: δ = 3.31 ppm for ^{1}H, δ = 49.00 ppm for ^{13}C; and trifluoroacetic acid (TFA) (external standard) for ^{19}F). Chemical shift (δ) values are reported in ppm. Signal characterization is described using the following abbreviations: s (singlet), d (doublet), t (triplet), q and m (multiplet). High-resolution mass spectrometry analyses were carried out on an Acquity ultraperformance liquid chromatography (UPLC) system coupled to a LCT Premier orthogonal accelerated time-of-flight mass spectrometer (Waters) using electrospray ionization (ESI) technique.

Synthesis of Probes. BODIPY-sphingosine,[21] Z-So,[22] ω-N3C14So,[23] and SABRAC[24] were obtained following reported protocols. The haloacetamide probes were obtained by acylation of the corresponding sphingoid base with bromoacetic acid, following a reported protocol,[24] or with bromoacetyl bromide or chloroacetyl chloride (1.2 equiv/mol) in CH_2Cl_2/Et_3N at room temperature for 12 h. Evaporation of the solvent afforded a crude product that was purified by flash chromatography on silica gel CH_2Cl_2/MeOH gradient (from 0−7%) to afford pure amides in 70−85% yield.

(2S,3R,E)-2-Bromo-N-[1,3-dihydroxyoctadec-4-en-13-(4,4-difluoro-4-bora-3a,4a-diaza-s-indacene-8-yl)2-yl]acetamide (BODIPY-SOBRAC). High-resolution mass spectrometry (HRMS) calculated for $C_{28}H_{40}BBrF_2N_3O_3^-$ [M − 1]: 594.2319, found 594.2413. ^{1}H NMR (400 MHz, $CDCl_3$) δ 1.20−1.40 (broad, 10H), 1.61 (m, 2H), 2.04 (m, 2H), 2.39 (s, 6H), 2.49 (s, 6H), 2.91 (broad, 2H), 3.70 (dd, J = 11.4, 3.2 Hz, 2H), 3.84 (m, 1H), 3.88 (s, 2H), 3.98 (dd, J = 11.4, 3.4 Hz, 1H), 4.35 (broad, 1H), 5.50 (dt, J = 14.6, 7.2 Hz, 2H), 5.77 (tt, J = 13.9, 6.5 Hz, 2H), 6.03 (s, 2H), 7.20 (d, J = 8.1 Hz, 1H). ^{13}C NMR (101 MHz, $CDCl_3$) δ 165.93, 153.69, 140.24, 134.42, 128.53, 121.54, 77.30, 76.98, 76.67, 74.19, 61.87, 54.84, 32.17, 31.88, 30.35, 29.35, 29.09, 28.99, 28.45, 16.36, 14.41. ^{19}F NMR: −146.67 (m).

(2S,3R,E)-2-Chloro-N-[1,3-dihydroxyoctadec-4-en-13-(4,4-difluoro-4-bora-3a,4a-diaza-s-indacene-8-yl)2-yl]acetamide (BODIPY-SOCLAC). HRMS calculated for $C_{28}H_{42}BClF_2N_3O_3^+$ [M + 1]: 552.2971, found 552.2953. ^{1}H NMR (400 MHz, $CDCl_3$): δ 1.20−1.65 (12H), 2.04 (broad, 2H), 2.38 (s, 6H), 2.50 (s, 6H), 2.89 (broad, 2H), 3.71 (broad d, 1H), 3.89 (broad, 1H), 3.99 (broad d, 1H), 4.06 (s, 2H), 4.34 (broad, 1H), 5.52 (m, 1H), 5.77 (m, 1H), 6.03 (broad, 2H), 7.27 (broad, 1H). ^{13}C NMR (101 MHz, $CDCl_3$) δ 166.44, 153.65, 146.63, 140.29, 134.40, 131.39, 128.52, 121.53, 74.00, 61.86, 54.67, 42.65, 32.18, 31.86, 30.34, 29.33, 29.08, 29.02, 28.42, 16.34, 14.40.

(2S,3R,E)-N-(14-Azido-1,3-dihydroxytetradec-4-en-2-yl)-2-bromoacetamide (N_3C_{14}-SOBRAC). HRMS calculated for $C_{16}H_{30}BrN_4O_3^+$ [M + 1]: 405.1496, found 405.1512. ^{1}H NMR (400 MHz, $CDCl_3$): δ 1.20−1.35 (broad, 14H), 1.58 (broad, 2H), 2.03 (broad, 2H), 3.24 (t, 2H), 3.71 (dd, 1H, J = 11.4, 3.6), 3.89 (broad, 1H), 3.98 (dd, 1H, J = 11.4, 3.5), 4.06 (s, 2H), 4.33 (broad, 1H), 5.50 (dd, 1H, J = 14.9, 6.4), 5.78 (m, 1H), 7.27 (d, 1H, J = 6.6). ^{13}C NMR (101 MHz, $CDCl_3$) δ 166.41, 134.61, 128.44, 74.12, 61.90, 54.65, 51.44, 42.65, 32.20, 29.34, 29.28, 29.07, 29.00, 28.78, 26.65.

(2S,3R)-2-Chloro-N-(1,3-dihydroxyoctadecan-2-yl)acetamide (SACLAC). HRMS calculated for $C_{20}H_{41}ClNO_3^+$ [M + 1]: 378.2769, found 378.2764. ^{1}H NMR (400 MHz, $CDCl_3$, CD_3OD, 9:1): δ 0.85 (t, 3H), 1.23 (broad, 28 H), 1.51 (broad, 2H), 3.71 (dd, 1H, J = 11.6, 3.4 Hz), 3.72 (m, 1H), 3.80 (m, 1H), 3.96 (dd, 1H, J = 11.6, 3.4 Hz), 4.05 (s, 2H), 7.4 (d, 1H, J = 8.4). ^{13}C NMR (101 MHz, $CDCl_3$, CD_3OD, 9:1) δ 166.48, 73.27, 61.48, 54.08, 42.56, 34.25, 31.86, 29.6−29.3, 25.85, 22.62, 14.03.

(2S,3R,E)-2-Bromo-N-(1,3-dihydroxyoctadec-4-en-2-yl)-acetamide (SOBRAC). HRMS calculated for $C_{20}H_{39}BrNO_3^+$ [M + 1]: 420.2108, found 420.2125. ^{1}H NMR (400 MHz, $CDCl_3$): δ 0.85 (t, J = 6.7 Hz, 3H), 1.23 (broad, 23H), 1.35 (broad, 2H), 2.04 (q, J = 7.1 Hz, 2H), 3.71 (dd, J = 11.4, 3.6 Hz, 1H), 3.89 (s, 2H), 3.83−3.92 (m, 1H), 3.97 (dd, J = 11.4, 3.6 Hz, 1H), 4.33 (t, J = 5.4 Hz, 1H), 5.54−5.46 (m, 1H), 5.83−5.74 (m, 1H), 7.19 (d, J = 8.0 Hz, 1H). ^{13}C NMR (101 MHz, $CDCl_3$): δ 166.03, 134.75, 128.30, 74.12, 61.88, 54.91, 32.25, 31.89, 29.66, 29.65, 29.62, 29.58, 29.45, 29.32, 29.18, 29.08, 29.06, 22.65, 14.08.

(2S,3R,E)-2-Chloro-N-(1,3-dihydroxyoctadec-4-en-2-yl)-acetamide (SOCLAC). HRMS calculated for $C_{20}H_{39}ClNO_3^+$ [M + 1]: 376.2613, found 376.2604. ^{1}H NMR (400 MHz, $CDCl_3$): δ 0.86 (t, J = 6.8 Hz, 3H). 1.39−1.32 (m, 2H), 1.24 (s, 22H), 2.05 (q, J = 6.9 Hz, 2H), 3.72 (dd, J = 11.4, 3.4 Hz, 1H), 3.90 (dq, J = 7.8, 3.6 Hz, 1H), 4.00 (dd, J = 11.4, 3.5 Hz, 1H), 4.37−4.33 (m, 1H), 4.07 (s, 2H), 5.52 (dd, J = 15.4, 6.5 Hz, 1H), 5.85−5.75 (m, 1H), 7.28 (broad d, 1H). ^{13}C NMR (101 MHz, $CDCl_3$): δ 166.48, 134.71, 128.33, 74.00, 69.20, 61.86, 54.89, 54.70, 42.65, 32.25, 31.88, 29.64, 29.62, 29.58, 29.45, 29.32, 29.18, 29.07, 27.85, 22.65, 14.08.

(2S,3R,Z)-2-Bromo-N-(1,3-dihydroxyoctadec-4-en-2-yl)-acetamide (cis-SOBRAC). HRMS calculated for $C_{20}H_{39}BrNO_3^+$ [M + 1]: 420.2108, found 420.2123. ^{1}H NMR (400 MHz, $CDCl_3$): δ 0.88 (t, J = 6.7 Hz, 3H), 1.25 (broad, 22H), 2.10 (m, 2H), 3.76 (broad dd, 1H), 3.88 (m, 1H), 4.06 (broad dd, 1H), 4.07 (s, 2H), 4.70 (dd, J =

DOI: 10.1021/jacs.8b11687
J. Am. Chem. Soc. 2019, 141, 7736−7742

8.1, 4.6 Hz, 1H), 5.67−5.57 (m, 1H), 5.53−5.45 (m, 1H), 7.31 (d, J = 7.7 Hz, 1H). ^{13}C NMR (101 MHz, $CDCl_3$): δ 166.54, 135.22, 128.27, 69.50, 62.16, 55.02, 42.82, 32.06, 29.83, 29.82, 29.80, 29.73, 29.70, 29.67, 29.50, 29.44, 28.03, 22.83, 14.26.

Cell Culture. The A375 cell line stably overexpressing *ASAH1* under the control of a tetracycline/doxycycline-responsive promoter was kindly provided by Dr. Carmen Bedia.[25] The antibiotic selection of this cell line was performed with blasticidin (3 μg/mL) and hygromycin B (250 μg/mL). Ectopic expression of AC was induced with doxycycline at 1 μg/mL for 24 h before use. Farber disease fibroblasts FD1−FD4 were from Laboratoire de Biochimie Métabolique (CHU Touluse, France). FD1 cells do not produce either precursor or proteolytically processed mature protein.[26] FD2 harbors products of normal size with a transition *ASAH1* mutation c.107A>G, resulting in the p.Y36C substitution, which has been reported to result in <5% residual enzyme activity.[30] FD3 has a c.833C>T substitution that leads to p.P278L replacement.[7] Finally, FD4 contains a c.502G>T substitution, which leads to p.G168W replacement and a very low enzyme activity. All cells were grown in a humidified 5% CO_2 atmosphere at 37 °C in DMEM medium supplemented with 10% fetal bovine serum and 100 ng/mL each of penicillin and streptomycin.

Construction of the *ASAH1* Mutant. The pcDNA5TO plasmid encoding the wild-type (WT) sequence of the human cDNA of *ASAH1* was prepared as reported.[25] The same vector encoding the mutated sequence (C143S) of the human cDNA was constructed using the above plasmid containing the WT sequence, the GeneArt Site-Directed Mutagenesis PLUS kit (Life Technologies), and the following pair of primers: Fw 5′GAATTATTTACCATTTCTACTTCAATAGTAGC3′ and Rv 5′GCTACTATTGAAGTAGAAATGGTAAATAATTC3′. The vector sequence was confirmed by Sanger sequencing. Both plasmids (WT and mutated) were transiently transfected in HEK293T cells using Lipofectamine 2000 (Life Technologies).

Cell Lysis and Protein Determination. Cells were suspended in 0.25 M sucrose (2×10^6 cells/0.3 mL), sonicated with a 3 mm probe (3 cycles of 5 s/9 W on ice), and centrifuged at 2300g for 5 min. Supernatants were collected and protein concentration was measured with bicinchoninic acid-based protein assay.

AC Activity. AC activity was measured using a fluorogenic substrate as reported.[27]

Mass Spectrometry Analysis of AC Adducts. Recombinant purified human AC (50 μg) was incubated with dithiothreitol (DTT) (3 mM in 100 mM acetate buffer, pH 4.5; 100 μL final volume) for 1 h at 37 °C. Then either EtOH (control, 1 μL) or inhibitor (SABRAC, SOBRAC, or N_3C_{14}SOBRAC; 1 μL from 10 mM stocks in ethanol, 100 μM final concentration) was added, and the mixture was incubated for 20 min at 37 °C. After incubation, the reaction was stopped by adding 100 μL of cold (4 °C) acetone. After 10 min on ice, the tubes were vortexed and centrifuged at 5000g for 10 min at 4 °C. The supernatant was then discarded, and the resulting pellet was carefully dried under a nitrogen stream and resuspended in 50 μL of 50 mM $(NH_4)_2CO_3$, pH 8, for trypsin digestion. Proteomic-grade trypsin was then added in 1:50 w/w ratio with the protein. After an overnight incubation at 37 °C, the sample was diluted with 100 μL of methanol and the resulting peptides were analyzed on a Waters Aquity UPLC system connected to a Waters LCT Premier Orthogonal Accelerated Time of Flight Mass Spectrometer (Waters, Milford, MA), operated in positive electrospray ionization mode. Full scan spectra from 50 to 1500 Da were obtained. Mass accuracy and reproducibility were maintained by using an independent reference spray via LockSpray. A 100 mm × 2.1 mm i.d., 1.7 mm C18 Acquity UPLC BEH (Waters) analytical column was used. The two mobile phases were acetonitrile (phase A) and water (phase B), both with 0.1% of formic acid. The gradient was as follows: 0 min, 95% A; 11 min, 100% A; 12 min, 95% A. In both cases, the flow rate was 0.3 mL/min. The column was run at 30 °C. Positive identification of compounds will be based on the accurate mass measurement with an error <5 ppm and its LC retention time.

Strain Promoted Alkyne−Azide Cycloaddition-Based Labeling of Recombinant Purified Human AC. Recombinant purified human AC (5 μg) was incubated with N_3C_{14}SOBRAC (100 μM) in the presence of different concentrations of C2Cer (0, 20, 50, 100, and 200 μM) for 20 min at pH 4.5 (100 mM acetate buffer; 10 μL final volume) at 37 °C. Then the adducts were reacted with 500 μM DBCO-PEG$_4$5/6-TAMRA (10 μL of a 1 mM solution in methanol) for 1 h at 37 °C. After incubation, the reaction was stopped by adding two volumes of cold (4 °C) acetone. The tubes were vortexed and centrifuged at 5000g for 10 min at 4 °C. The supernatants were discarded, and the resulting pellets were dried under a nitrogen stream. The pellet was suspended in 18.75 μL of phosphate-buffered saline (PBS) and 6.25 μL of Laemmli 4× buffer and resolved on 12.5% SDS-PAGE (sodium dodecyl sulfate polyacrylamide gel electrophoresis) at 140 V/1 h. In-gel visualization of the fluorescence labeling was performed in the wet gel slabs using a Typhoon 5 Biomolecular imager (Amersham) with the Cy3/TAMRA settings. A sampel of recombinant purified human AC (60 ng) was loaded in a parallel lane, cut, and submitted to Western blot analysis as detailed in the Western Blotting section.

Strain Promoted Alkyne−Azide Cycloaddition-Based Labeling of Cell Lysates. Cell lysates (9 μL, 2.8 mg/mL protein, 25 μg of protein) were diluted in assay buffer (100 mM sodium acetate, 150 mM NaCl, 0.1% Igepal, 3 mM DTT, pH = 4.5, 25 μL) and incubated with 0.5 μM N_3C_{14}SOBRAC for 5 min at 37 °C. In competition experiments, lysates were exposed to the specified concentrations of SOBRAC for 5 min at 37 °C prior to N_3C_{14}SOBRAC addition. Iodoacetamide (IAA) was added (3 μL, 35 mg/mL, 15 mM final concentration) and incubated for 5 min at room temperature to block free thiol groups. Following this, DBCO-PEG$_4$5/6-TAMRA was added (3 μL of a 6.4 μM solution in methanol, 0.5 μM final concentration), and the mixture was incubated for 10 min at 37 °C while shaking. The reaction mixtures were then quenched with 6.25 μL of Laemmli 4× buffer, and proteins were resolved on 12.5% SDS-PAGE. In-gel visualization of the fluorescent bands was performed in the wet gel slabs using a Typhoon 5 Biomolecular Imager (Amersham) with the Cy3/TAMRA settings.

AC Labeling with BODIPY-Labeled Probes in Cell Lysates. Cell lysates (10 μL, 2.5 mg/mL protein, 25 μg protein) were diluted in assay buffer (100 mM sodium acetate, 150 mM NaCl, 0.1% Igepal, 3 mM DTT, pH = 4.5, 25 μL) and exposed to the indicated concentration of the BODIPY-labeled probe for 5 min at 37 °C while shaking. In competition experiments, samples were preincubated for 5 min at 37 °C with the competitor (0.1 μM final concentration unless otherwise indicated). The reaction mixtures were then quenched with 6.25 μL of Laemmli 4× buffer, and proteins were resolved on 12.5% SDS-PAGE. In-gel visualization of the fluorescent bands was performed in the wet gel slabs using a Typhoon 5 Biomolecular Imager (Amersham) with the Cy3/TAMRA settings.

AC Labeling in Intact Cells. Cells (5000 cells per well) were seeded on glass-bottom 4-well plates and allowed to adhere for 24 h. Then the medium was replaced with fresh medium containing 75 nM LysoTracker Red DND-99 (L7528; Invitrogen), and cells were incubated for 1 h at 37 °C. After this time, BODIPY-SOBRAC or BODIPY-SOCLAC (1 μM final concentration) was directly added, and cells were incubated for 5 min. Then cells were washed twice with PBS, phenol red-free DMEM was added, and cells were kept in the incubator for the specified times. If long incubation times were required, LysoTracker was added 1 h prior to microscope analysis. Staining was viewed with a Leica TCS-SP2 Laser Scanning Confocal microscope, and the images were analyzed using Fiji-ImageJ software.

Western Blotting. Proteins were extracted from cell pellets using Cell Lysis Buffer (Cell Signaling), 1 mM phenylmethanesulfonyl fluoride (PMSF), and a protease inhibitor mixture (Roche Applied Science) and brief sonication. Protein concentration was determined, and 50 μg of proteins were separated on a 12.5% SDS-PAGE gel. Proteins were then transferred onto a nitrocellulose membrane (Amersham Protan) (Figure 3C) or PVDF membrane (Figure S4A). Unspecific binding sites were blocked with 5% milk in Tris-buffered saline, 0.1% Tween 2 (TBST) (1 h at room temperature). The

DOI: 10.1021/jacs.8b11687
J. Am. Chem. Soc. 2019, 141, 7736−7742

polyclonal anti-AC antibody was diluted 1:5000 in 5% bovine serum albumin (BSA) in TBST. Membranes were incubated overnight at 4 °C under gentle agitation. After washing with TBST, membranes were probed with the secondary antirabbit antibody diluted 1:5000 in 5% milk in TBST for 1 h at room temperature (Figure 3C) or diluted 1:1000 in 3% milk in TBST overnight at 4 °C (Figure S4A) under gentle agitation. Antibody excess was eliminated by washing with TBST, and protein detection was carried out using enhanced chemiluminescence (ECL) and membrane scanning with LI-COR C-DiGit Blot Scanner. Band intensities were quantified by LI-COR Image Studio Lite Software.

RESULTS AND DISCUSSION

The probes were designed based on the structure of the reported irreversible AC inhibitor SABRAC (Figure 1),[28] a

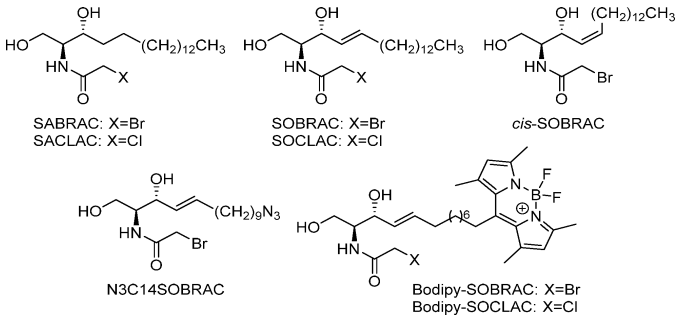

Figure 1. Compounds used in this study.

Table 1. Kinetic Analysis of Covalent Inhibition of AC

inhibitor	k_{inact}[a] (min^{-1})	K_i[a] (nM)	k_{inact}/K_i[a] (min^{-1} mM^{-1})
SOBRAC	0.034 ± 0.003	29.7 ± 3.1	1139.5 ± 112.2
N_3C_{14}SOBRAC	0.017 ± 0.002	35.7 ± 3.2	463.7 ± 48.7
BODIPY-SOBRAC	0.033 ± 0.003	26.7 ± 2.2	1217.4 ± 132.2
SACLAC	0.019 ± 0.002	97.1 ± 9.0	196.0 ± 18.9
SOCLAC	0.017 ± 0.002	40.2 ± 3.8	418.5 ± 40.9
BODIPY-SOCLAC	0.038 ± 0.004	98.8 ± 9.2	393.7 ± 39.4

[a]Kinetic parameters (mean ± SD) were obtained from 2 independent determinations with triplicates. Graphs are shown in Figure S2.

ceramide analogue modified at the amide linkage with a 2-bromoacetyl moiety. The compounds were prepared by standard amidation of suitable bases. SOBRAC, *cis*-SOBRAC, SACLAC, and SOCLAC were first synthesized and found to inhibit wild-type AC activity with very high potencies (Figure S1). Because the compounds are covalent enzyme inhibitors and their activity depends on the incubation time, the IC_{50} values were only used for preliminary comparative purposes. Because, under identical experimental conditions, SOBRAC was the most potent inhibitor, its fluorescent (BODIPY-SOBRAC) and azide-tagged (N_3C_{14}SOBRAC) derived probes were synthesized for enzyme labeling. Kinetic analysis showed that the 5 compounds (*cis*-SOBRAC was not investigated further) are effective AC inhibitors (k_{inact}/K_i = 200−1220 min^{-1} mM^{-1}) (Table 1 and Figure S2). All of them exhibited similar specific reactivities (k_{inact} = 0.017−0.034 min^{-1}), while SOCLAC and the three bromo-derivatives showed similar affinities (K_i = 27−40 nM). SACLAC, with a saturated long-chain base, had a lower affinity for AC (K_i = 97.1 nM), in

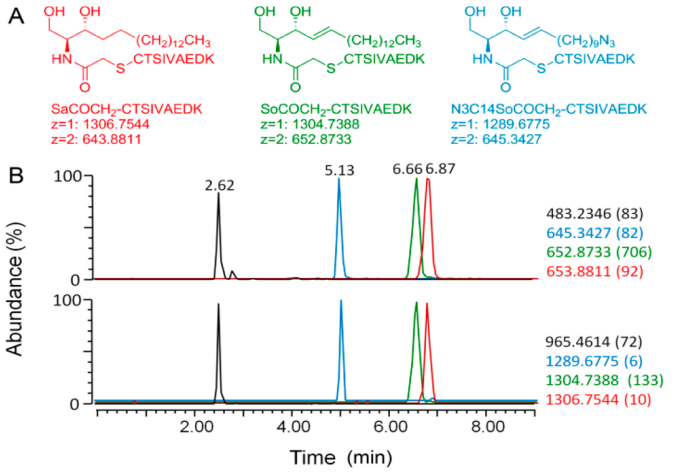

Figure 2. Covalent modification of acid ceramidase Cys-143 by SABRAC, SOBRAC, and N_3C_{14}SOBRAC. (A) Structure of the modified Cys-143 containing tryptic peptides showing the expected exact masses for monocharged and doubly charged peptides. (B) Extracted-ion chromatograms of doubly charged (top) and monocharged native peptide from a control incubation with ethanol (CTSIVAEDK, *m/z*: 483.2346 and 965.4614, black trace) and the same peptide covalently modified by N_3C_{14}SOBRAC (*m/z*: 645.3427 and 1289.6775, blue trace), SOBRAC (*m/z*: 652.8733 and 1304.7388, green trace), and SABRAC (*m/z*: 653.8811 and 1306.7544, red trace). Numbers between parentheses correspond to the peak area.

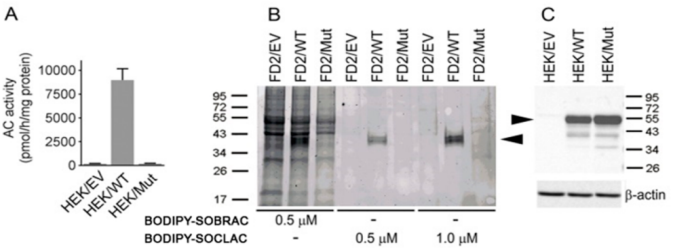

Figure 3. In vitro labeling of acid ceramidase with BODIPY-SOCLAC. Cell lysates were incubated with the indicated concentrations of the specified probes for 5 min, and the reaction mixtures were resolved on SDS-PAGE before in-gel fluorescence analysis. Protein extracts were from HEK293T (HEK) cells or Farber FD2 cells transfected with an empty vector (EV), wild-type AC (WT), or an inactive AC mutant (C143S) (Mut). AC activity of lysates used in panel C are shown in A. WB detection of AC is shown in C. Arrows indicate labeled AC. The gel stained with Coomassie blue (loading control) is shown in Figure S6.

agreement with the enzyme preference for ceramides over dihydroceramides.[3]

SABRAC and its analogues were expected to form adducts with the catalytic Cys143 by displacement of the halogen atom by the Cys thiolate function. Consistent with this model, and as previously found for SABRAC,[28] time-dependence of enzyme inactivation supports that SABRAC analogues act as irreversible inhibitors of AC (Figure S2). Formation of covalent adducts has been confirmed here by mass spectrometry analysis of the peptides resulting from trypsin digestion of recombinant human AC (rhAC) exposed to the inhibitors.

As shown in Figure 2, the presence in the extracts of the expected lipid-modified CTSIVAEDK peptide (Figure S3)

DOI: 10.1021/jacs.8b11687
J. Am. Chem. Soc. 2019, 141, 7736−7742

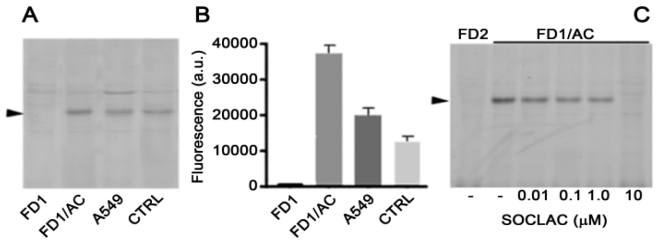

Figure 4. (A) In vitro labeling of endogenous acid ceramidase with BODIPY-SOCLAC. Cell lysates (34 μg of protein) were incubated with the probe (1 μM/5 min), and the reaction mixtures were resolved on SDS-PAGE before in-gel fluorescence analysis. CRTL, fibroblasts from a healthy individual. (B) AC activity of samples used in gel A, as determined with the fluorogenic assay. (C) Competition with unlabeled ligand. Lysates from FD1/AC cells were preincubated for 5 min with the specified concentrations of SOCLAC (competitor) followed by 5 min incubation with 1 μM probe. The gel of panel C stained with Coomassie blue (loading control) is shown in Figure S7.

after treatment with each inhibitor and the absence of these peptides in control incubations, which showed only the native unmodified peptide, supported that ceramide analogues with the 2-bromoacetyl unit at the amide linkage might be useful as AC ABPs.

Next, AC detection was attempted. Two approaches were possible: a two-step, strain promoted alkyne–azide cycloaddition (SPAAC)-enzyme labeling using N_3C_{14}SOBRAC and DBCO-PEG$_4$5/6-TAMRA as alkyne partner and a one-step labeling using BODIPY-tagged probes. The first approach allowed the detection of rhAC by in-gel fluorescence analysis as a band at the expected molecular weight for the β-subunit (ca. 40 kDa). The same band mobility was observed when AC was detected by Western blot (Figure S4A). Specificity of the click-based detection was demonstrated by competition with *N*-acetylsphingosine (C2Cer), which reduced the band intensity corresponding to the AC-probe adduct in a concentration-dependent manner (Figure S4A).

We next treated cell lysates from AC-overexpressing A375 melanoma cells with N_3C_{14}SOBRAC and DBCO-PEG$_4$5/6-TAMRA. Although AC labeling was achieved after short incubation times and with low concentrations of both reagents (Figure S4B), high unspecific labeling was observed. In agreement with reports showing that thiol–yne addition with reduced peptidylcysteines is responsible for most of the azide-independent polypeptide labeling and that undesired thiol–yne reactions can be prevented by alkylating peptidylcysteine thiols with iodoacetamide (IAA),[29] we found that addition of IAA prior to incubation with DBCO-PEG$_4$5/6-TAMRA reduced the unspecific labeling (Figure S4C). Selective target binding was also shown by competition of N_3C_{14}SOBRAC with untagged SOBRAC (Figure S4D).

To simplify the AC detection protocol and minimize unspecific labeling, AC labeling with BODIPY-SOBRAC was attempted. Using lysates from AC-overexpressing A375 cells, time-course experiments showed that successful AC (β-subunit) detection occurred after only 5 min of reaction with the probe and that increasing the incubation time did not augment the band intensity but led to augmented unspecific labeling (Figure S5A). Importantly, the band corresponding to the AC-lipid adduct was less visible in lysates from A375 cells not overexpressing the enzyme (cells not induced with doxycycline) (Figure S5A). Next, the BODIPY-SOBRAC labeling method was applied to detect AC in extracts of

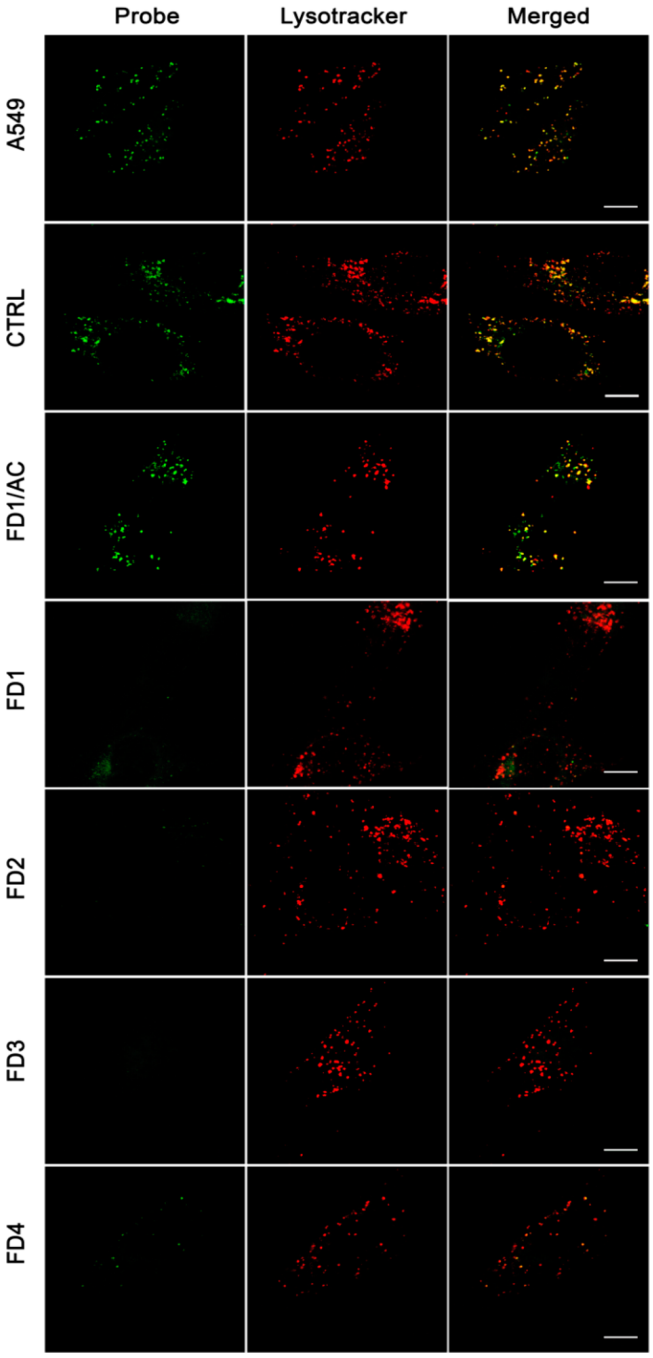

Figure 5. In situ AC labeling. Representative fluorescence micrographs of cells with different levels of AC, namely, lung adenocarcinoma A549, skin fibroblasts of a healthy individual (CTRL), FD1 cells transduced to overexpress AC (FD1/AC), and different Farber cells (FD1–FD4). Cells were treated with BODIPY-SOCLAC (1 μM/5 min). Then they were washed and placed back in the incubator, and images were taken after 2 (A549), 3.5 (CTRL), and 5 h (FD1–FD4 and FD1/AC). LysoTracker (75 nM/60 min) was added 1 h prior to visualization. AC activity of these cells is shown in Figure S9. Scale 10 μm.

Farber fibroblasts FD1, which do not produce either precursor or proteolytically processed mature protein,[26] and the same FD1 cells transduced to overexpress AC (FD1/AC). No band corresponding to labeled AC was detected in FD1 lysates, while fluorescently labeled AC was clearly visualized in FD1/

DOI: 10.1021/jacs.8b11687
J. Am. Chem. Soc. 2019, 141, 7736–7742

AC extracts (Figure S5B). These results correlated well with AC activity (Figure S5C). Target binding was also demonstrated in this case in competition experiments with SOBRAC (Figure S5B), which decreased AC labeling concentration dependently.

As observed in Figures S4 and S5, the successful labeling of AC with BODIPY-SOBRAC also gave rise to certain background staining, likely resulting from unspecific reaction with intracellular electrophiles. The lower reactivity of chlorine over bromine as nucleophile was expected to reduce this observed background signal.[30] Therefore, BODIPY-SOCLAC was next synthesized and investigated. The reactivity of BODIPY-SOCLAC with Cys143 was first confirmed by mass spectrometry (data not shown). Kinetic analysis showed that, despite the lower nucleophilic reactivity of chlorine over bromine,[30] in the enzyme's environment this compound and BODIPY-SOBRAC exhibited a similar k_i for AC (Table 1 and Figure S2). In contrast, although both BODIPY derivatives contain the same long-chain base, the affinity of BODIPY-SOCLAC for AC is 3.5-fold weaker than that of BODIPY-SOBRAC. Because SOBRAC and SOCLAC affinities for AC are similar, the coexistence of both chlorine and BODIPY in the same molecule appears to provoke the AC affinity decrease. Consequently, BODIPY-SOCLAC exhibits an overall 3-fold lower biochemical potency than BODIPY-SOBRAC. This probe was then tested in lysates from cells transfected with wild-type (WT) ASAH1 cDNA and an ASAH1 mutant in which the active-site cysteine was replaced by serine (C143S). As expected, this mutation provoked the loss of AC activity, while the enzyme was active in cells transfected with the WT gene (Figure 3A). In-gel fluorescence analysis after labeling with BODIPY-SOCLAC revealed a band only in extracts from cells transfected with the WT but not the mutant, ASAH1 cDNA (Figure 3B). In contrast, both WT and mutant proteins were detected by Western blot (WB) (Figure 3C), highlighting a promising feature of the probe: unlike antibodies, which react with both inactive and active AC, BODIPY-SOCLAC can clearly detect the active form of AC and distinguish it from the inactive enzyme. Importantly, the use of BODIPY-SOCLAC resulted in a remarkable reduction of nontarget labeling as compared to BODIPY-SOBRAC treatment (Figure 3B), with the band corresponding to labeled AC being the almost exclusive one.

Encouraged by these results, the detection of endogenous AC by BODIPY-SOCLAC was examined in lysates of cell lines with different levels of endogenous enzyme expression. As shown in Figure 4A, the protein was detected in both A549 cells and fibroblasts from a healthy individual, and the level of detection correlated well with the enzyme activity (Figure 4B), thus indicating that the probe can be employed to label endogenous levels of acid ceramidase. As found with BODIPY-SOBRAC, increasing the incubation time with BODIPY-SOCLAC (1 μM) beyond 5 min did not augment the AC band intensity but led to increased unspecific labeling (Figure S8A). This observation agrees with the time-dependence of AC inactivation by BODIPY-SOCLAC, showing that only 10% of activity remained after a 15 min incubation with a 0.2 nM concentration (5-fold lower than that used in the labeling experiment) (Figure S2). This rapid and efficient reaction with the target prevents off-target labeling. We next determined the selectivity of target binding by competition with the unlabeled ligand. As depicted in Figure 4C, AC labeling decreased concentration dependently as SOCLAC concentration augmented.

Because BODIPY-SOCLAC afforded an excellent labeling of AC in cell lysates, we next investigated whether labeling of AC in intact cells was also feasible. To this end, BODIPY-SOCLAC (1 μM/5 min) was added to the culture medium of cell lines with different levels of AC expression, and labeling was analyzed by confocal scanning microscopy. As shown in Figure 5, intracellular compartment staining was observed upon treatment of A549, fibroblasts, and FD1/AC cells with BODIPY-SOCLAC. Colocalization with LysoTracker indicated that BODIPY-SOCLAC was contained in the lysosomes, in agreement with the lysosomal location of AC, the probe target.

In FD1 cells, BODIPY-SOCLAC did not afford a vesicular pattern colocalizing with LysoTracker, in agreement with the absence of AC in this cell line. No lysosomal labeling was observed after BODIPY-SOCLAC treatment of three different homozygous Farber fibroblasts (FD2−FD4) producing mutant proteins (Figure 5). The impact of these mutations on AC activity using the fluorogenic assay is depicted in Figure S9. Interestingly, some lysosome labeling occurred with BODIPY-SOCLAC in FD4 cells, which are those retaining some AC activity (Figure S9).

CONCLUSIONS

In conclusion, we have reported on novel ABPs for AC arising from the previously reported AC irreversible inhibitor SABRAC. The presence of the sphingoid base scaffold is expected to provide selectivity toward enzymes of sphingolipid metabolism, of which only AC has been reported to be a cysteine amidase.[1] The probes proved useful for in-gel AC detection at submicromolar concentrations and short incubation times, and they successfully stained endogenous levels of active enzyme. Moreover, no AC labeling occurred after protein denaturation (data not shown), showing that the correct protein folding is a labeling requirement (as it is for activity). Importantly, although an ABP for AC has been previously reported,[19] BODIPY-SOCLAC represents a major advantage in that it allowed the unprecedented lysosomal staining of active, but not inactive, AC in intact cells. These overall results might be of biomedical relevance to visualize the location and monitor the trafficking of active AC, as well as for the analysis of novel pharmacological chaperones for the treatment of FD and SMA-PME. All in all, our findings suggest that BODIPY-SOCLAC may be a valuable tool for the study of AC activity and open up novel opportunities for therapeutics in diseases characterized by an aberrant expression of AC.

ASSOCIATED CONTENT

Supporting Information

The Supporting Information is available free of charge on the ACS Publications website at DOI: 10.1021/jacs.8b11687.

Inhibition of AC by 2-haloacetamides, time-dependence of AC activity inhibition by different concentrations of inhibitors, amino acid sequence of AC, SPAAC-based AC labelling, in vitro labelling of acid ceramidase with Bodipy-SOBRAC, gels stained with Coomassie blue to confirm that equal amounts of protein were loaded, time-course of in vitro labelling of acid ceramidase with Bodipy-SOCLAC, AC activity of cells, and NMR spectra of compounds (PDF)

DOI: 10.1021/jacs.8b11687
J. Am. Chem. Soc. 2019, 141, 7736−7742

AC extracts (Figure S5B). These results correlated well with AC activity (Figure S5C). Target binding was also demonstrated in this case in competition experiments with SOBRAC (Figure S5B), which decreased AC labeling concentration dependently.

As observed in Figures S4 and S5, the successful labeling of AC with BODIPY-SOBRAC also gave rise to certain background staining, likely resulting from unspecific reaction with intracellular electrophiles. The lower reactivity of chlorine over bromine as nucleophile was expected to reduce this observed background signal.[30] Therefore, BODIPY-SOCLAC was next synthesized and investigated. The reactivity of BODIPY-SOCLAC with Cys143 was first confirmed by mass spectrometry (data not shown). Kinetic analysis showed that, despite the lower nucleophilic reactivity of chlorine over bromine,[30] in the enzyme's environment this compound and BODIPY-SOBRAC exhibited a similar k_i for AC (Table 1 and Figure S2). In contrast, although both BODIPY derivatives contain the same long-chain base, the affinity of BODIPY-SOCLAC for AC is 3.5-fold weaker than that of BODIPY-SOBRAC. Because SOBRAC and SOCLAC affinities for AC are similar, the coexistence of both chlorine and BODIPY in the same molecule appears to provoke the AC affinity decrease. Consequently, BODIPY-SOCLAC exhibits an overall 3-fold lower biochemical potency than BODIPY-SOBRAC. This probe was then tested in lysates from cells transfected with wild-type (WT) ASAH1 cDNA and an ASAH1 mutant in which the active-site cysteine was replaced by serine (C143S). As expected, this mutation provoked the loss of AC activity, while the enzyme was active in cells transfected with the WT gene (Figure 3A). In-gel fluorescence analysis after labeling with BODIPY-SOCLAC revealed a band only in extracts from cells transfected with the WT but not the mutant, ASAH1 cDNA (Figure 3B). In contrast, both WT and mutant proteins were detected by Western blot (WB) (Figure 3C), highlighting a promising feature of the probe: unlike antibodies, which react with both inactive and active AC, BODIPY-SOCLAC can clearly detect the active form of AC and distinguish it from the inactive enzyme. Importantly, the use of BODIPY-SOCLAC resulted in a remarkable reduction of nontarget labeling as compared to BODIPY-SOBRAC treatment (Figure 3B), with the band corresponding to labeled AC being the almost exclusive one.

Encouraged by these results, the detection of endogenous AC by BODIPY-SOCLAC was examined in lysates of cell lines with different levels of endogenous enzyme expression. As shown in Figure 4A, the protein was detected in both A549 cells and fibroblasts from a healthy individual, and the level of detection correlated well with the enzyme activity (Figure 4B), thus indicating that the probe can be employed to label endogenous levels of acid ceramidase. As found with BODIPY-SOBRAC, increasing the incubation time with BODIPY-SOCLAC (1 μM) beyond 5 min did not augment the AC band intensity but led to increased unspecific labeling (Figure S8A). This observation agrees with the time-dependence of AC inactivation by BODIPY-SOCLAC, showing that only 10% of activity remained after a 15 min incubation with a 0.2 nM concentration (5-fold lower than that used in the labeling experiment) (Figure S2). This rapid and efficient reaction with the target prevents off-target labeling. We next determined the selectivity of target binding by competition with the unlabeled ligand. As depicted in Figure 4C, AC labeling decreased concentration dependently as SOCLAC concentration augmented.

Because BODIPY-SOCLAC afforded an excellent labeling of AC in cell lysates, we next investigated whether labeling of AC in intact cells was also feasible. To this end, BODIPY-SOCLAC (1 μM/5 min) was added to the culture medium of cell lines with different levels of AC expression, and labeling was analyzed by confocal scanning microscopy. As shown in Figure 5, intracellular compartment staining was observed upon treatment of A549, fibroblasts, and FD1/AC cells with BODIPY-SOCLAC. Colocalization with LysoTracker indicated that BODIPY-SOCLAC was contained in the lysosomes, in agreement with the lysosomal location of AC, the probe target.

In FD1 cells, BODIPY-SOCLAC did not afford a vesicular pattern colocalizing with LysoTracker, in agreement with the absence of AC in this cell line. No lysosomal labeling was observed after BODIPY-SOCLAC treatment of three different homozygous Farber fibroblasts (FD2−FD4) producing mutant proteins (Figure 5). The impact of these mutations on AC activity using the fluorogenic assay is depicted in Figure S9. Interestingly, some lysosome labeling occurred with BODIPY-SOCLAC in FD4 cells, which are those retaining some AC activity (Figure S9).

CONCLUSIONS

In conclusion, we have reported on novel ABPs for AC arising from the previously reported AC irreversible inhibitor SABRAC. The presence of the sphingoid base scaffold is expected to provide selectivity toward enzymes of sphingolipid metabolism, of which only AC has been reported to be a cysteine amidase.[1] The probes proved useful for in-gel AC detection at submicromolar concentrations and short incubation times, and they successfully stained endogenous levels of active enzyme. Moreover, no AC labeling occurred after protein denaturation (data not shown), showing that the correct protein folding is a labeling requirement (as it is for activity). Importantly, although an ABP for AC has been previously reported,[19] BODIPY-SOCLAC represents a major advantage in that it allowed the unprecedented lysosomal staining of active, but not inactive, AC in intact cells. These overall results might be of biomedical relevance to visualize the location and monitor the trafficking of active AC, as well as for the analysis of novel pharmacological chaperones for the treatment of FD and SMA-PME. All in all, our findings suggest that BODIPY-SOCLAC may be a valuable tool for the study of AC activity and open up novel opportunities for therapeutics in diseases characterized by an aberrant expression of AC.

ASSOCIATED CONTENT

Supporting Information

The Supporting Information is available free of charge on the ACS Publications website at DOI: 10.1021/jacs.8b11687.

Inhibition of AC by 2-haloacetamides, time-dependence of AC activity inhibition by different concentrations of inhibitors, amino acid sequence of AC, SPAAC-based AC labelling, in vitro labelling of acid ceramidase with Bodipy-SOBRAC, gels stained with Coomassie blue to confirm that equal amounts of protein were loaded, time-course of in vitro labelling of acid ceramidase with Bodipy-SOCLAC, AC activity of cells, and NMR spectra of compounds (PDF)

DOI: 10.1021/jacs.8b11687
J. Am. Chem. Soc. 2019, 141, 7736−7742

Activity-Based Imaging of Acid Ceramidase in Living Cells

Yadira F. Ordóñez, José Luís Abad, Mazen Aseeri, Josefina Casas, Virginie Garcia, Mireia Casasampere, Edward H. Schuchman, Thierry Levade, Antonio Delgado, Gemma Triola* and Gemma Fabrias*.

SUPPLEMENTARY FIGURES

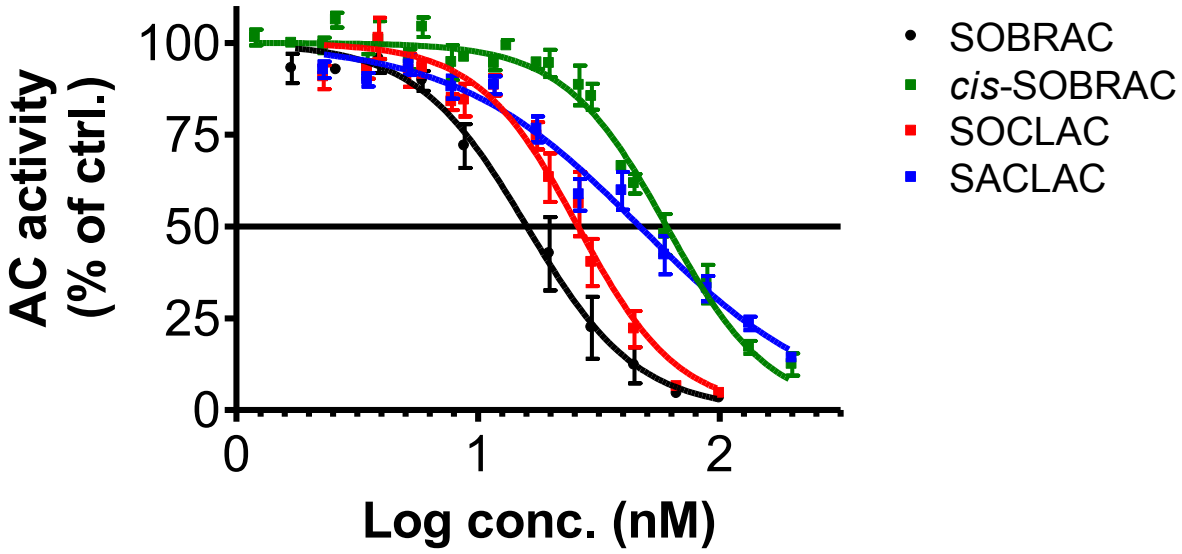

Figure S1. Inhibition of AC by 2-haloacetamides. Dose-response curves were determined on AC-overexpressing A375 cell lysates, which were preincubated for 15 min before the substrate addition (the inhibitor remained in the reaction mixture until the end of the assay). Data are expressed as mean ± SD of three independent experiments with triplicates. Curve adjustments with the four parameter logistic equation afforded the following IC_{50} values (95% confidence intervals): SOBRAC, 15.9 nM (13.9 to 17.3 nM); *cis*-SOBRAC, 60.4 nM (56.4 to 64.7 nM); SOCLAC, 25.9 nM (23.8 to 28.3 nM) and SACLAC, 46.7 nM (42.2 to 51.8 nM) Chemical structures of inhibitors are given in Figure 1.

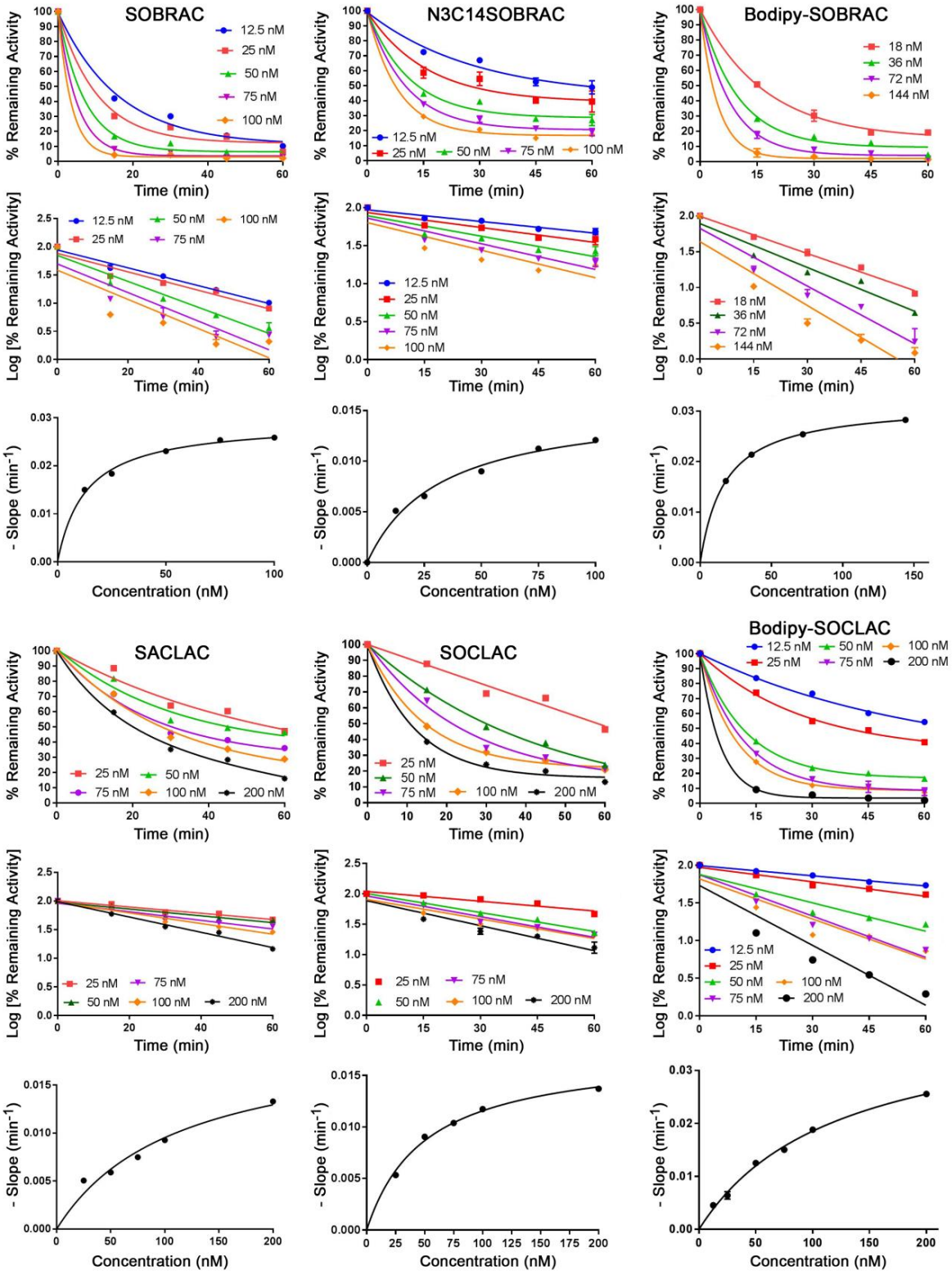

Figure S2. Time-dependence of AC activity inhibition by different concentrations of inhibitors. Reaction mixtures containing 400 ng of protein, substrate (20 μM) and either vehicle (control) or the test compounds were incubated at 37 °C for 15, 30, 45 and 60 min in 96-well plates. Reactions were stopped and the formation of umbelliferone was measured as reported. Experiments were carried out twice with triplicates. The –Slope *vs* concentration curves were fitted with GraphPad Michaelis-Menten equation.

MPGRSCVALVLLAAAVSCAVAQHAPPWTEDCRKSTYPPSGPTYRGAVPWYT
INLDLPPYKRWHELMLDKAPMLKVIVNSLKNMINTFVPSGKVMQVVDEKLP
GLLGNFPGPFEEEMKGIAAVTDIPLGEIISFNIFYELFTICTSIVAEDKKG
HLIHGRNMDFGVFLGWNINNDTWVITEQLKPLTVNLDFQRNNKTVFKASSF
AGYVGMLTGFKPGLFSLTLNERFSINGGYLGILEWILGKKDAMWIGFLTRT
VLENSTSYEEAKNLLTKTKILAPAYFILGGNQSGEGCVITRDRKESLDVYE
LDAKQGRWYVVQTNYDRWKHPFFLDDRRTPAKMCLNRTSQENISFETMYDV
LSTKPVLNKLTVYTTLIDVTKGQFETYLRDCPDPCIGW

Figure S3. Amino acid sequence of AC. The α-subunit is shown in blue and the β-subunit is shown in red. The active site Cys-143-containing peptide fragment resulting from trypsin digestion is shown highlighted in yellow.

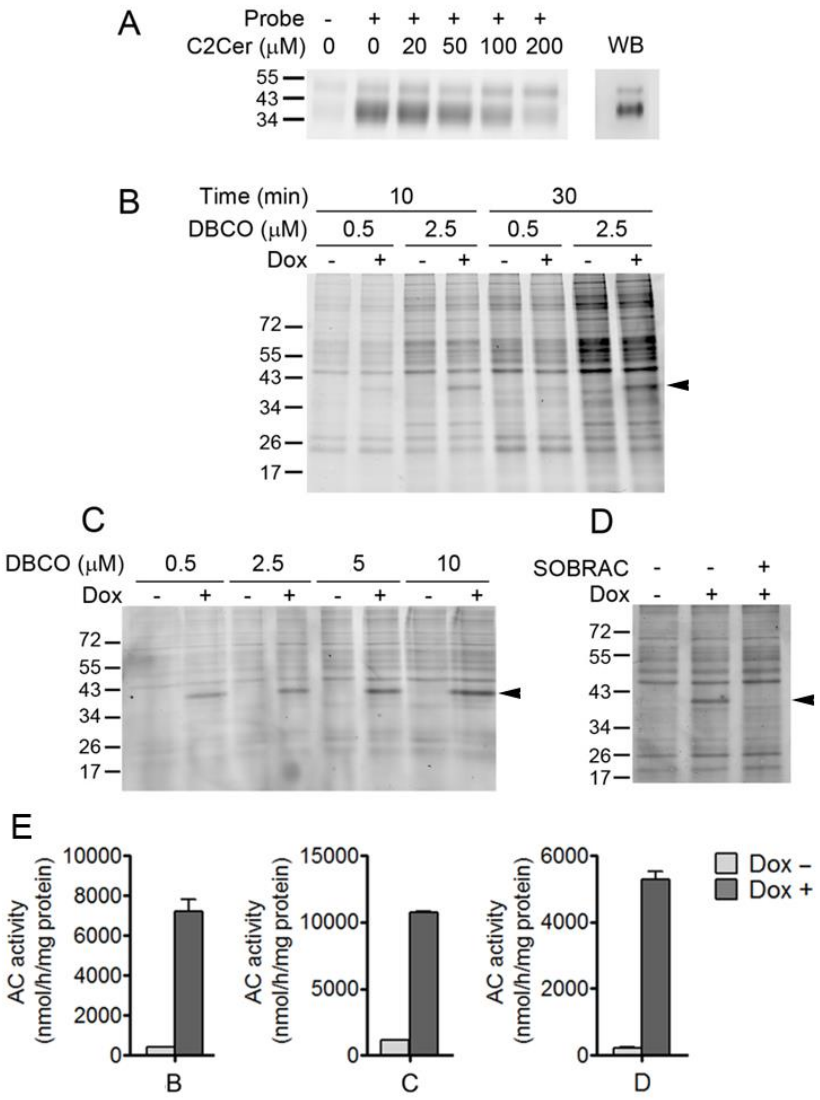

Figure S4. Strain Promoted Alkyne-Azide Cycloaddition **(**SPAAC)-based AC labelling. A. Recombinant purified human AC (5 μg) was allowed to react with 100 μM N3C14SOBRAC in the presence of different concentrations of C2Cer (0, 20, 50, 100 and 200 μM) and then adducts were reacted with DBCO-PEG$_4$5/6-TAMRA (500 μM). B. Cells lysates of A375 cells overexpressing (Dox +) or not (Dox -) AC were incubated with N3C14SOBRAC (0.5 μM/5 min/37 ºC) and DBCO-PEG$_4$5/6-TAMRA (DBCO) was added at the specified concentrations and incubated for the indicated times (37°C). C. Same as in B, but IAA (15 mM final concentration) was added and incubated for 5 min at 37 °C prior to incubation (10 min/37 °C) with DBCO-PEG$_4$5/6. D. Same as in C, but cell lysates were preincubated or not with 0.1 μM SOBRAC (5 min/37°C) prior to N3C14SOBRAC addition. In all cases, the reaction mixtures were resolved on SDS-PAGE and in-gel fluorescence analysis was carried out as detailed in the experimental section. In A, a sample of recombinant purified human AC (5 μg) was loaded in a parallel lane and submitted to Western blot analysis. Arrows indicate labelled AC. The AC activity of the lysates used to generate the gels (mean ± SD, n=3) is shown in E. The letter in the *x* axis indicates the reference gel.

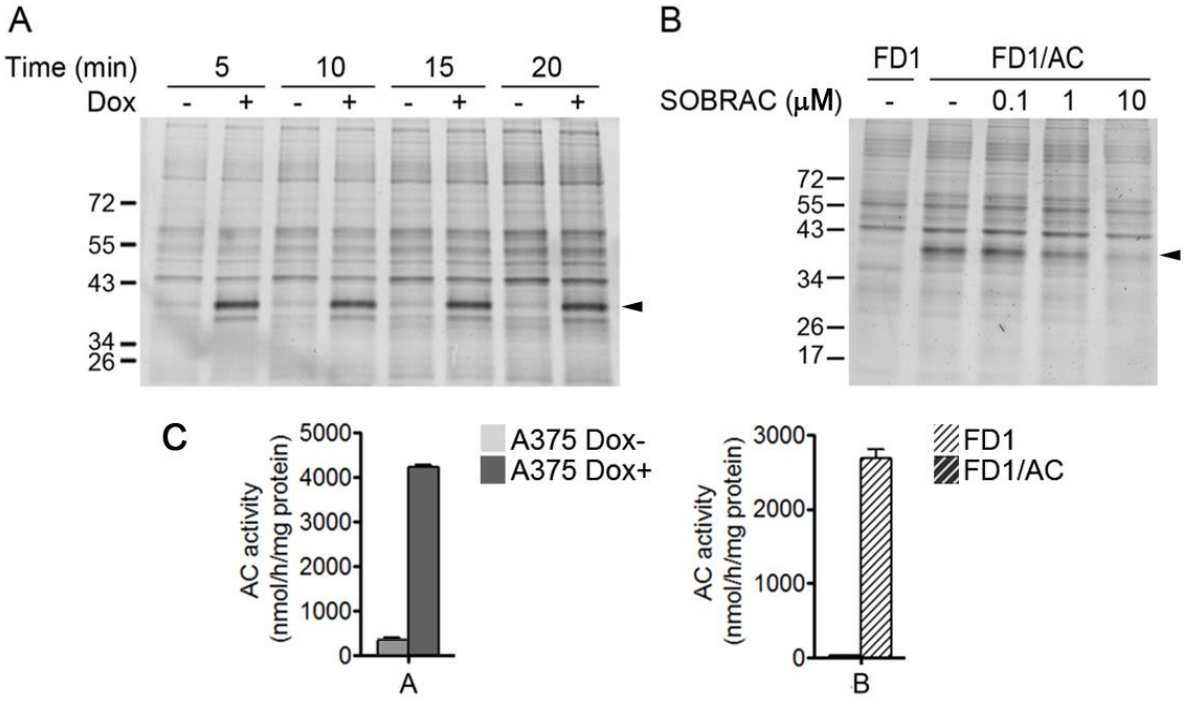

Figure S5. In vitro labelling of acid ceramidase with Bodipy-SOBRAC. Cell lysates were incubated with the probe (0.5 μM) for the specified times and the reaction mixtures were resolved on SDS-PAGE before in-gel fluorescence analysis. In (B), lysates were preincubated for 5 min with the specified concentrations of SOBRAC (competitor) followed by 5 min incubation with 0.5 μM probe. Protein extracts were from: A, A375 cells induced (Dox +) or not (Dox -) to overexpress AC; B, FD1 Farber cells and FD1/AC cells (Farber Cells overexpressing AC). Arrows indicate labelled AC. The AC activity of the lysates used to generate the gels (mean ± SD, n=3) is shown in C. The letter in the *x* axis indicates the reference gel.

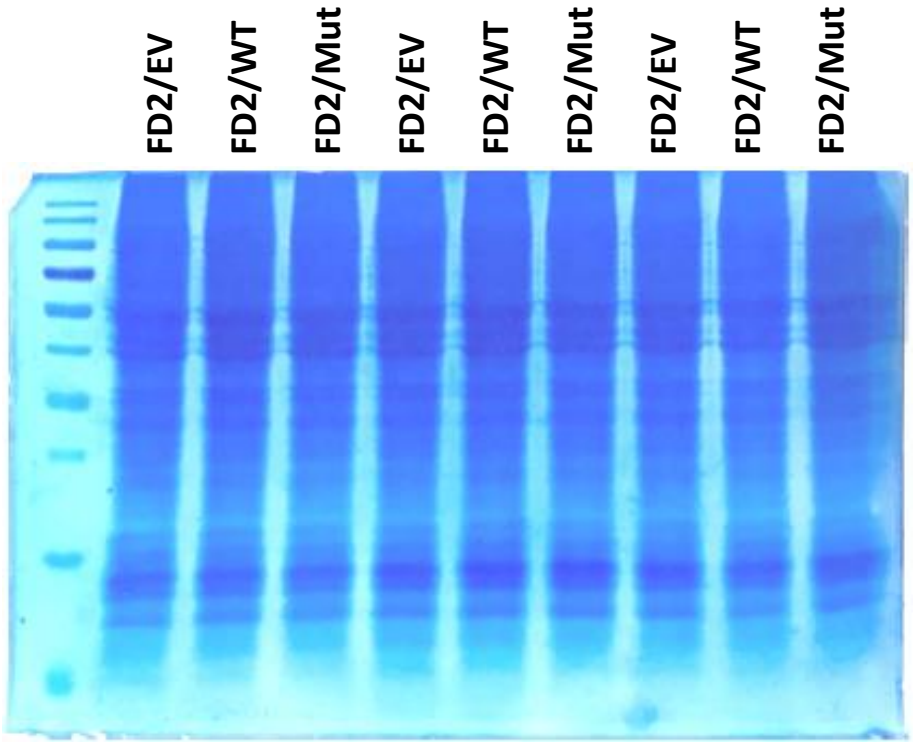

Figure S6. The same gel shown in figure 3 was stained with Coomassie blue to confirm that equal amounts of protein were loaded.

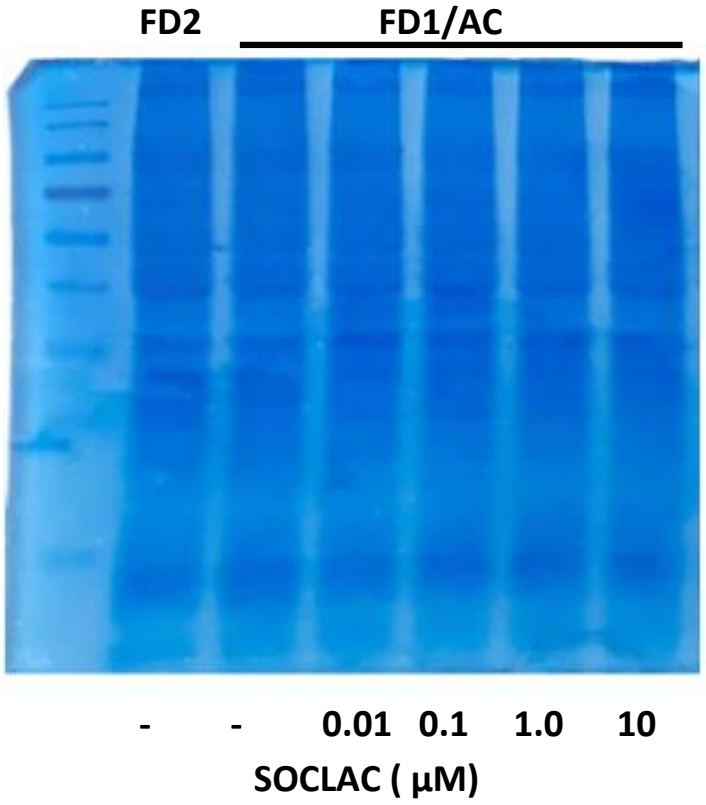

Figure S7. The same gel shown in figure 4C was stained with Coomassie blue to confirm that equal amounts of protein were loaded.

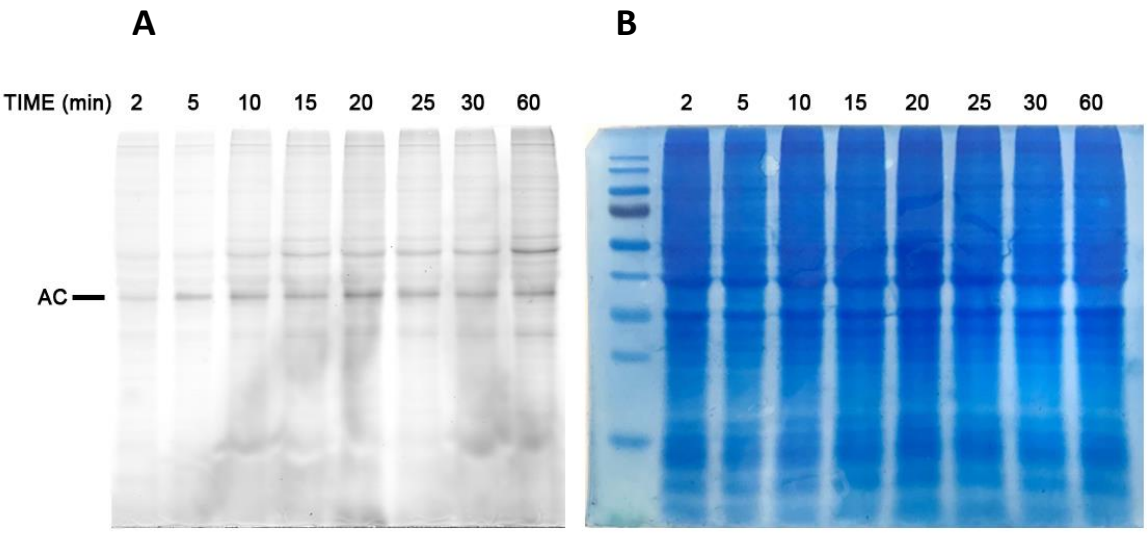

Figure S8. Time course of *in vitro* labelling of acid ceramidase with Bodipy-SOCLAC. Lysates from control fibroblasts (25 µg of protein) were incubated with the probe (1 µM) for the specified times and the reaction mixtures were resolved on SDS-PAGE before in-gel fluorescence analysis (left) or stained with Coomassie blue (right) to assess loading.

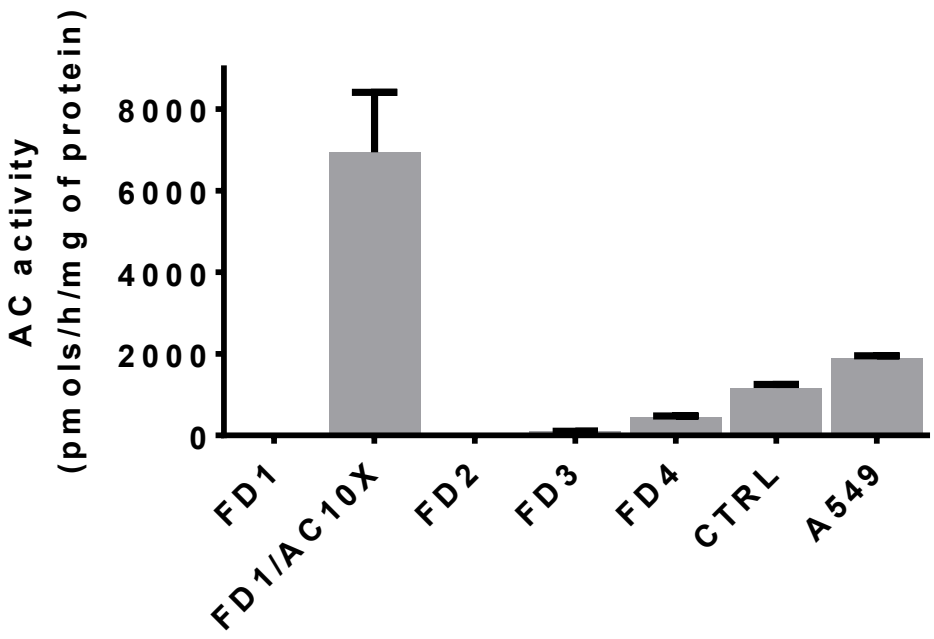

Figure S9. AC activity of cells imaged in Figure 5. Activity was determined in cell lysates at pH 4.5 following the standard fluorogenic protocol (see main text). FD refers to Farber cells and CTRL refers to skin fibroblasts of a healthy individual. Data (mean ± SD, n=4) were obtained from two experiments with triplicates.

NMR SPECTRA

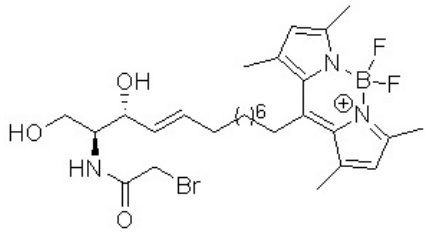
OH
HO
HN
Br
O
F
B
F
N
N
6

0.45
1.00
0.68
0.81
0.60
0.54
1.98
0.79
0.82
3.55
3.05
1.21
1.45
1.04
9.77
9.5
9.0
8.5
8.0
7.5
7.0
6.5
6.0
5.5
5.0
4.5
4.0
3.5
3.0
2.5
2.0
1.5
1.0
0.5

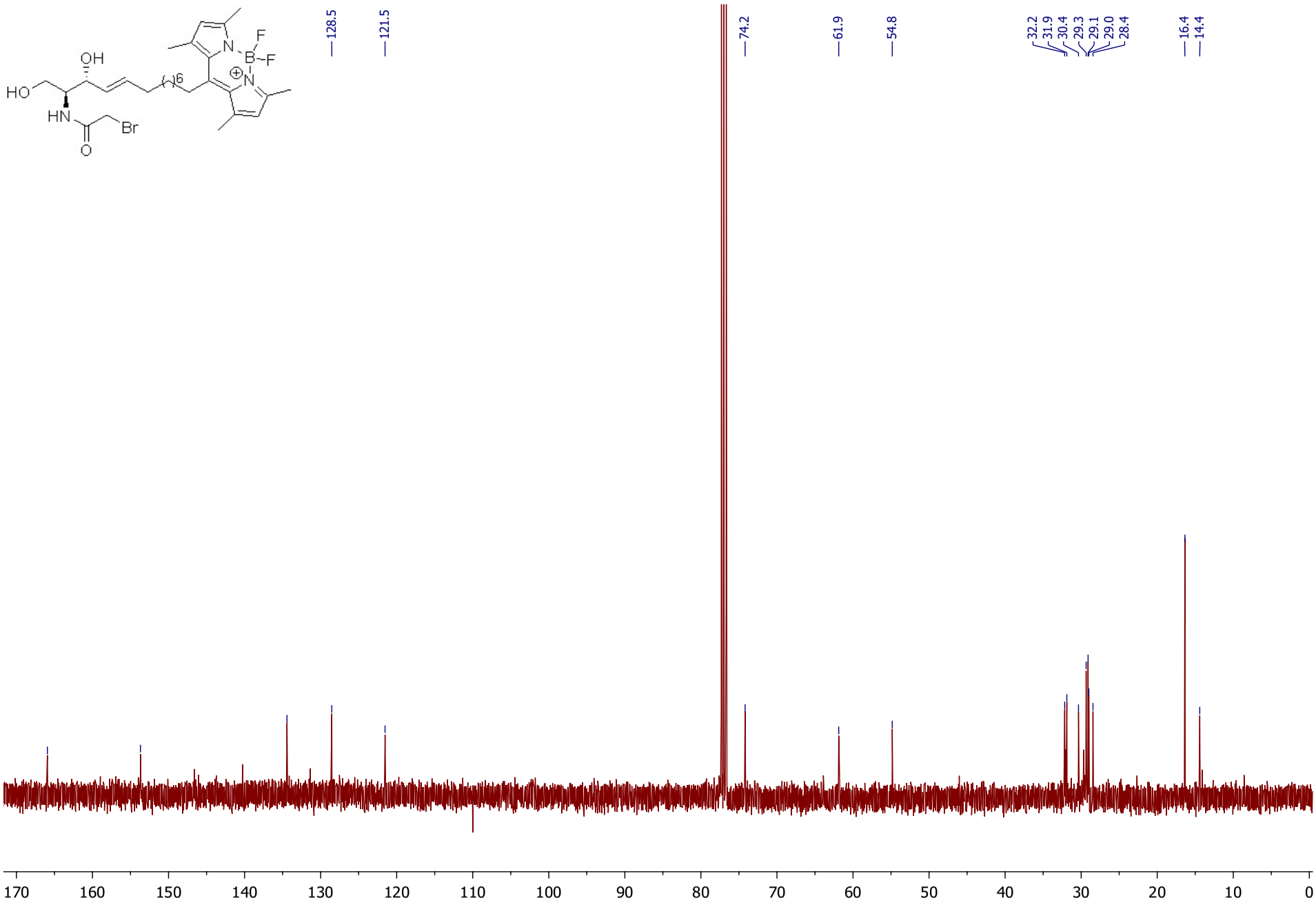
128.5
121.5
74.2
61.9
54.8
32.2
31.9
30.4
29.3
29.1
29.0
28.4
16.4
14.4
OH
HO
HN
Br
O
F
B
F
N
N
6
170
160
150
140
130
120
110
100
90
80
70
60
50
40
30
20
10
0

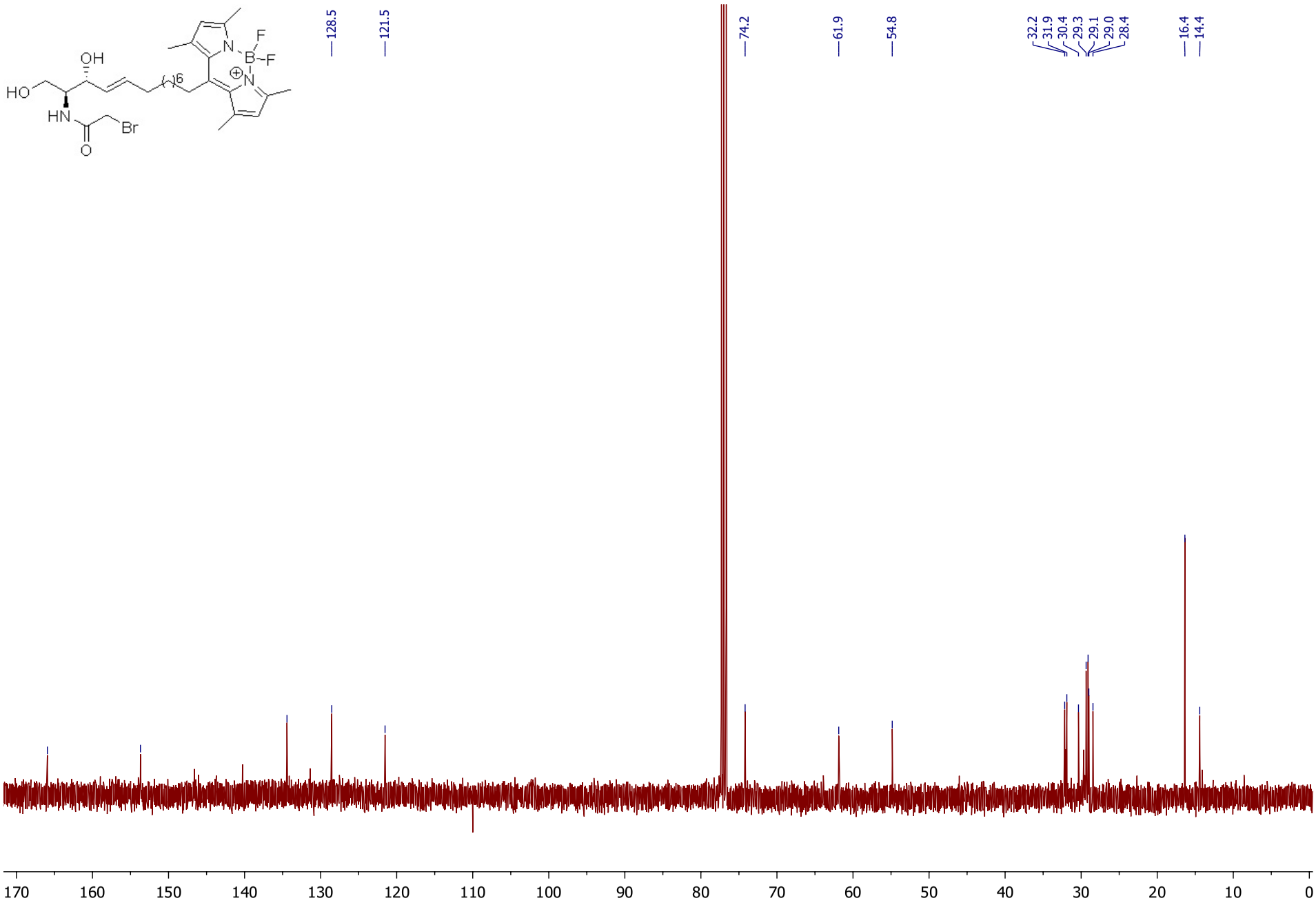
128.5
121.5
74.2
61.9
54.8
32.2
31.9
30.4
29.3
29.1
29.0
28.4
16.4
14.4
OH
HO
HN
Br
O
F
B
F
N
N
6
170
160
150
140
130
120
110
100
90
80
70
60
50
40
30
20
10
0

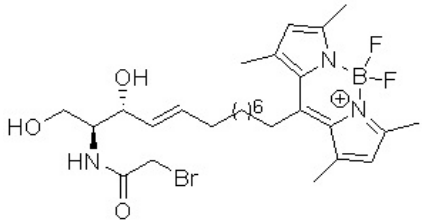

-143.87

-146.51
-146.59
-146.68
-146.76
-146.85

-142.0 -142.5 -143.0 -143.5 -144.0 -144.5 -145.0 -145.5 -146.0 -146.5 -147.0 -147.5 -148.0 -148.5 -149.0 -149.5 -15

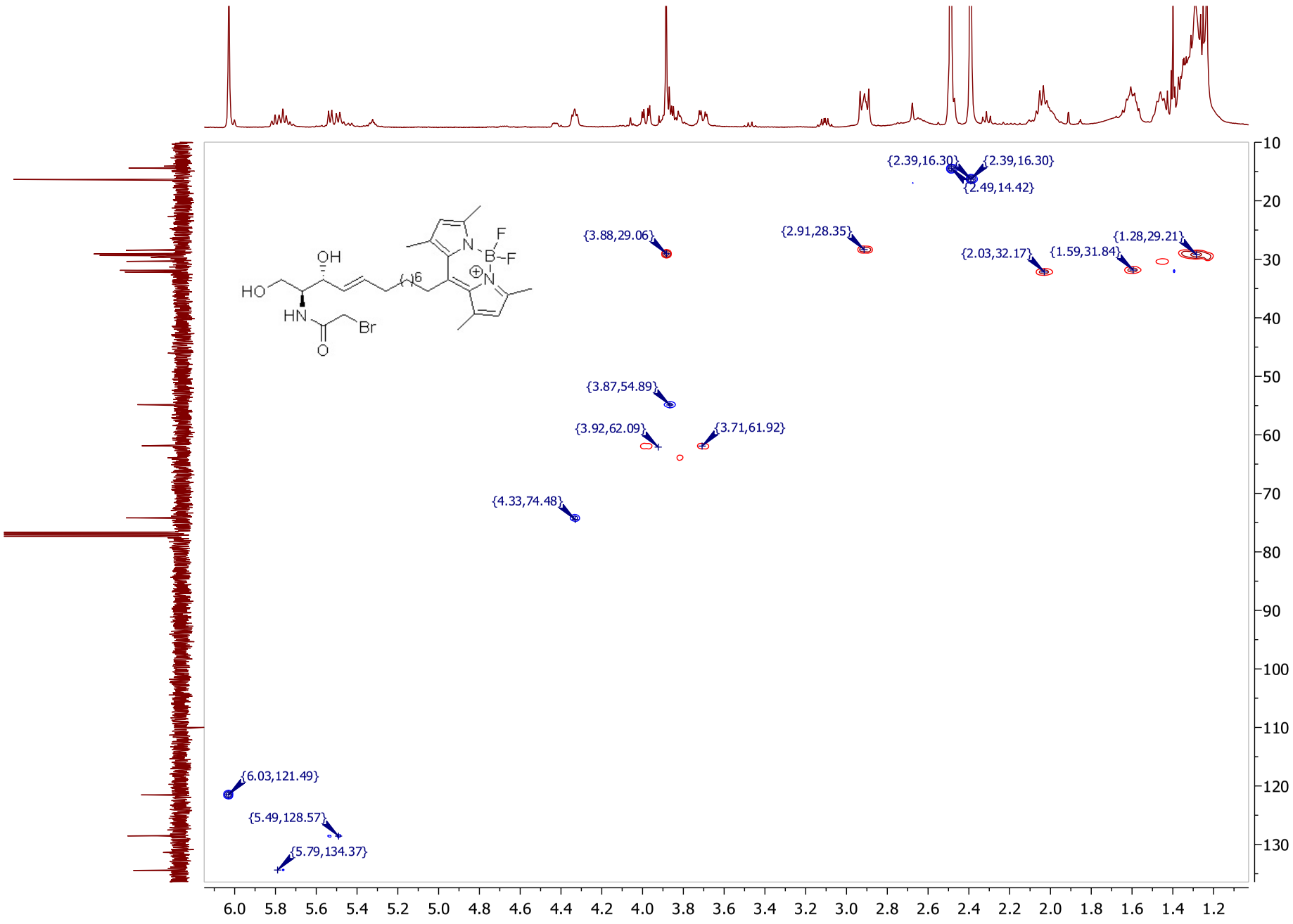
{2.39,16.30}
{2.39,16.30}
{2.49,14.42}
{3.88,29.06}
{2.91,28.35}
{2.03,32.17}
{1.59,31.84}
{1.28,29.21}
{3.87,54.89}
{3.92,62.09}
{3.71,61.92}
{4.33,74.48}
{6.03,121.49}
{5.49,128.57}
{5.79,134.37}
OH
HO
HN
Br
O
F
B
F
N
6
10
20
30
40
50
60
70
80
90
100
110
120
130
6.0
5.8
5.6
5.4
5.2
5.0
4.8
4.6
4.4
4.2
4.0
3.8
3.6
3.4
3.2
3.0
2.8
2.6
2.4
2.2
2.0
1.8
1.6
1.4
1.2

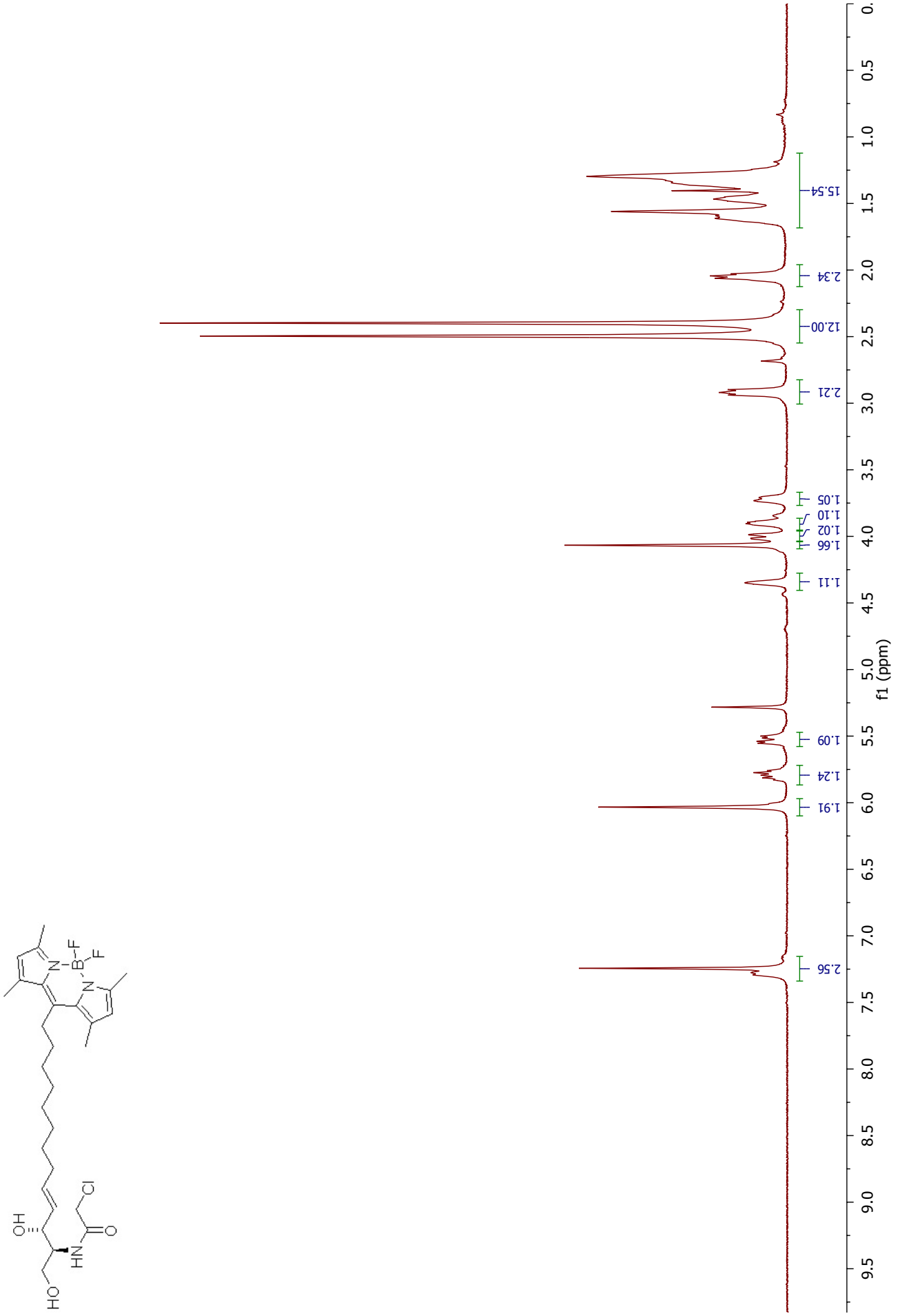
15.54
2.34
12.00
2.21
1.05
1.10
1.02
1.66
1.11
1.09
1.24
1.91
2.56
f1 (ppm)

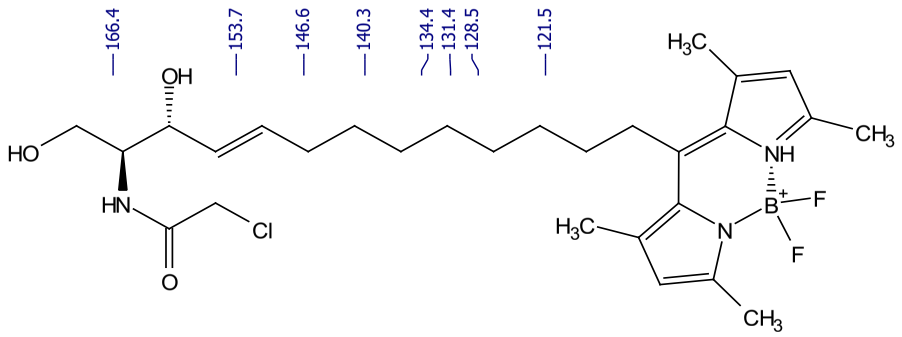

166.4 153.7 146.6 140.3 134.4 131.4 128.5 121.5 74.0 61.9 54.7 42.6 32.2 31.9 30.3 29.3 29.1 29.0 28.4 16.3 14.4

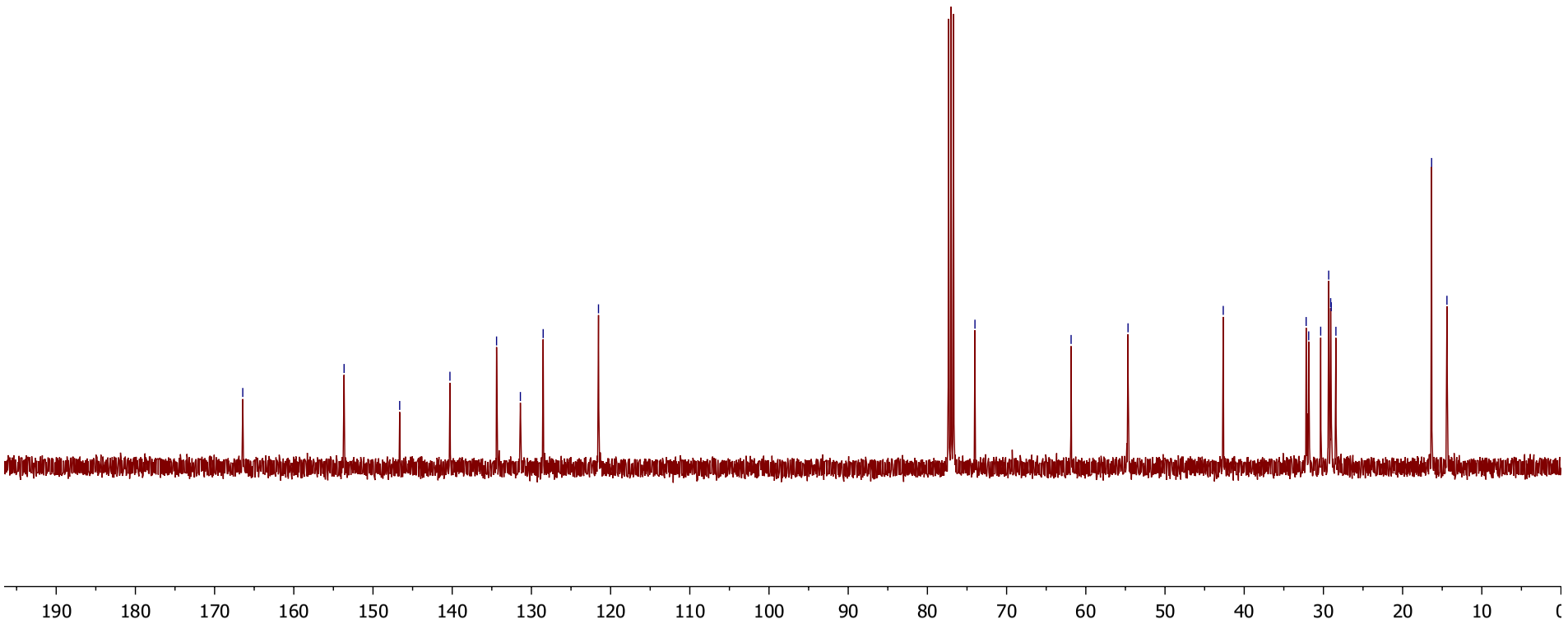

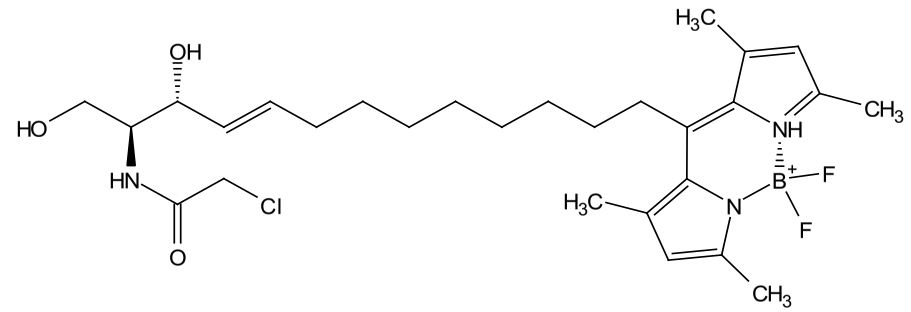

-143.92

-146.54
-146.63
-146.72
-146.80
-146.89

-137 -138 -139 -140 -141 -142 -143 -144 -145 -146 -147 -148 -149 -150 -151 -152 -153 -154

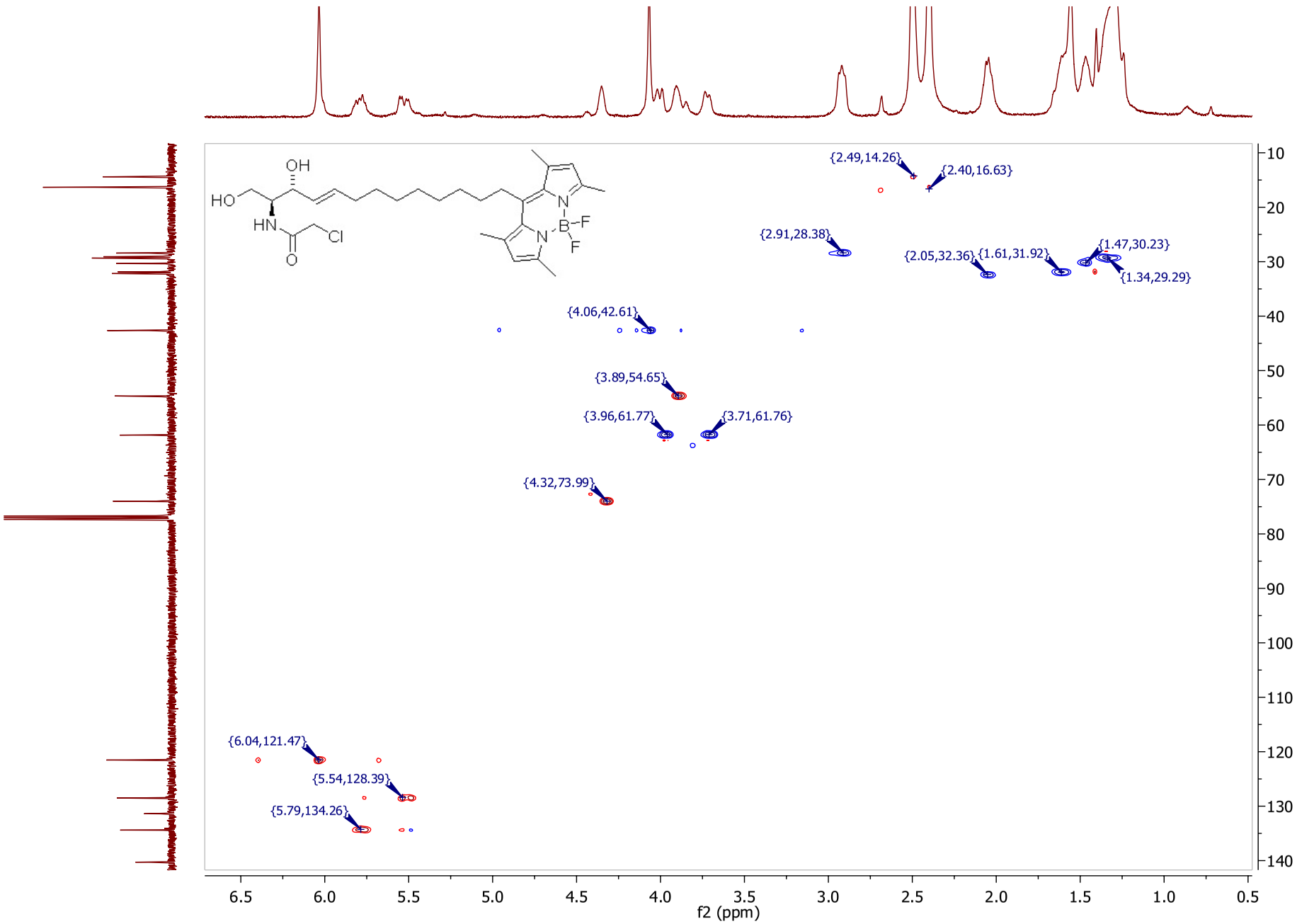
OH
HO
HN
Cl
O
N
B
F
F
{2.49,14.26}
{2.40,16.63}
{2.91,28.38}
{2.05,32.36}
{1.61,31.92}
{1.47,30.23}
{1.34,29.29}
{4.06,42.61}
{3.89,54.65}
{3.96,61.77}
{3.71,61.76}
{4.32,73.99}
{6.04,121.47}
{5.54,128.39}
{5.79,134.26}
6.5
6.0
5.5
5.0
4.5
4.0
3.5
3.0
2.5
2.0
1.5
1.0
0.5
f2 (ppm)
10
20
30
40
50
60
70
80
90
100
110
120
130
140

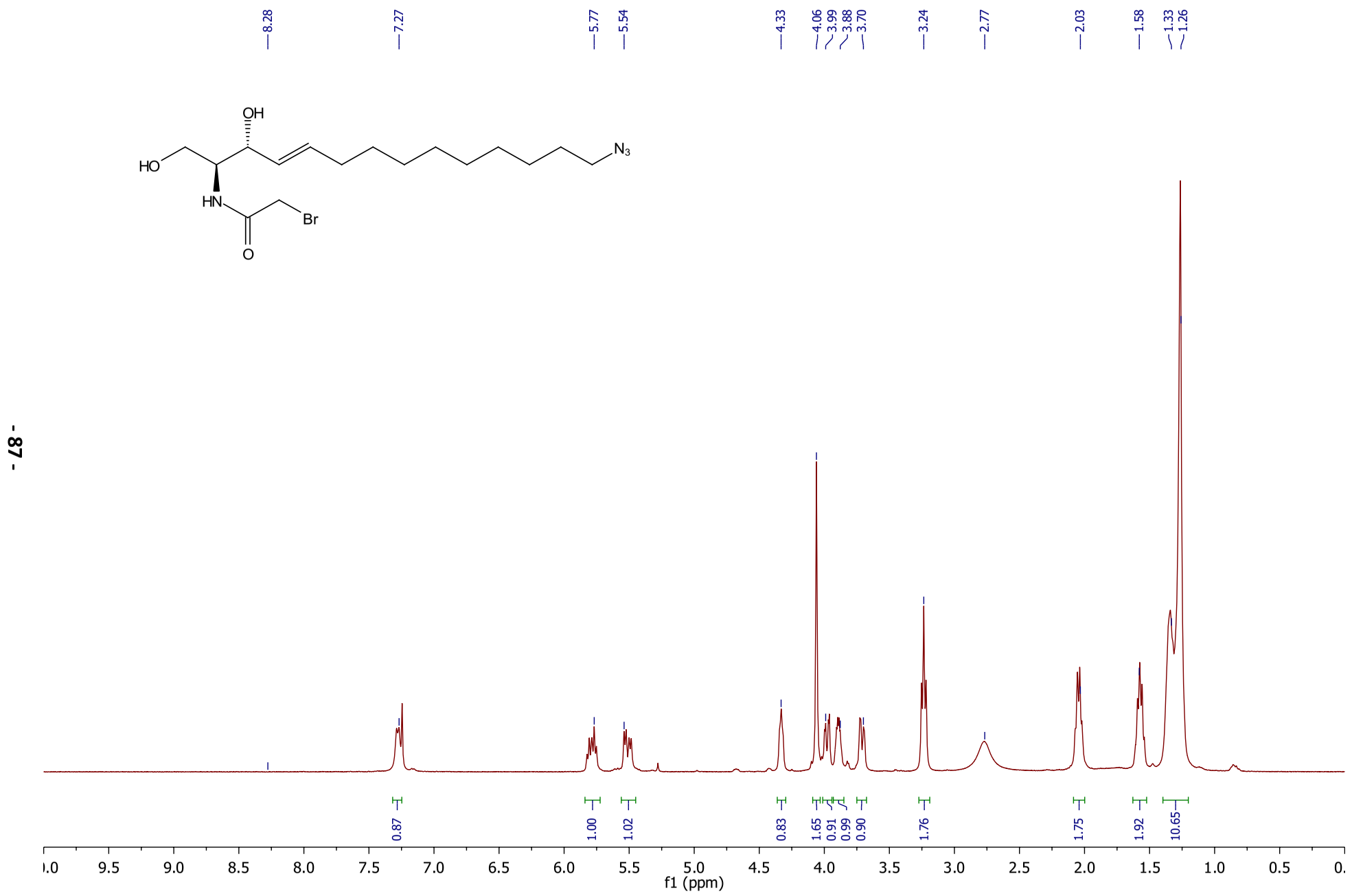
8.28
7.27
5.77
5.54
4.33
4.06
3.99
3.88
3.70
3.24
2.77
2.03
1.58
1.33
1.26
OH
HO
HN
Br
O
N3
0.87
1.00
1.02
0.83
1.65
0.91
0.99
0.90
1.76
1.75
1.92
10.65
f1 (ppm)

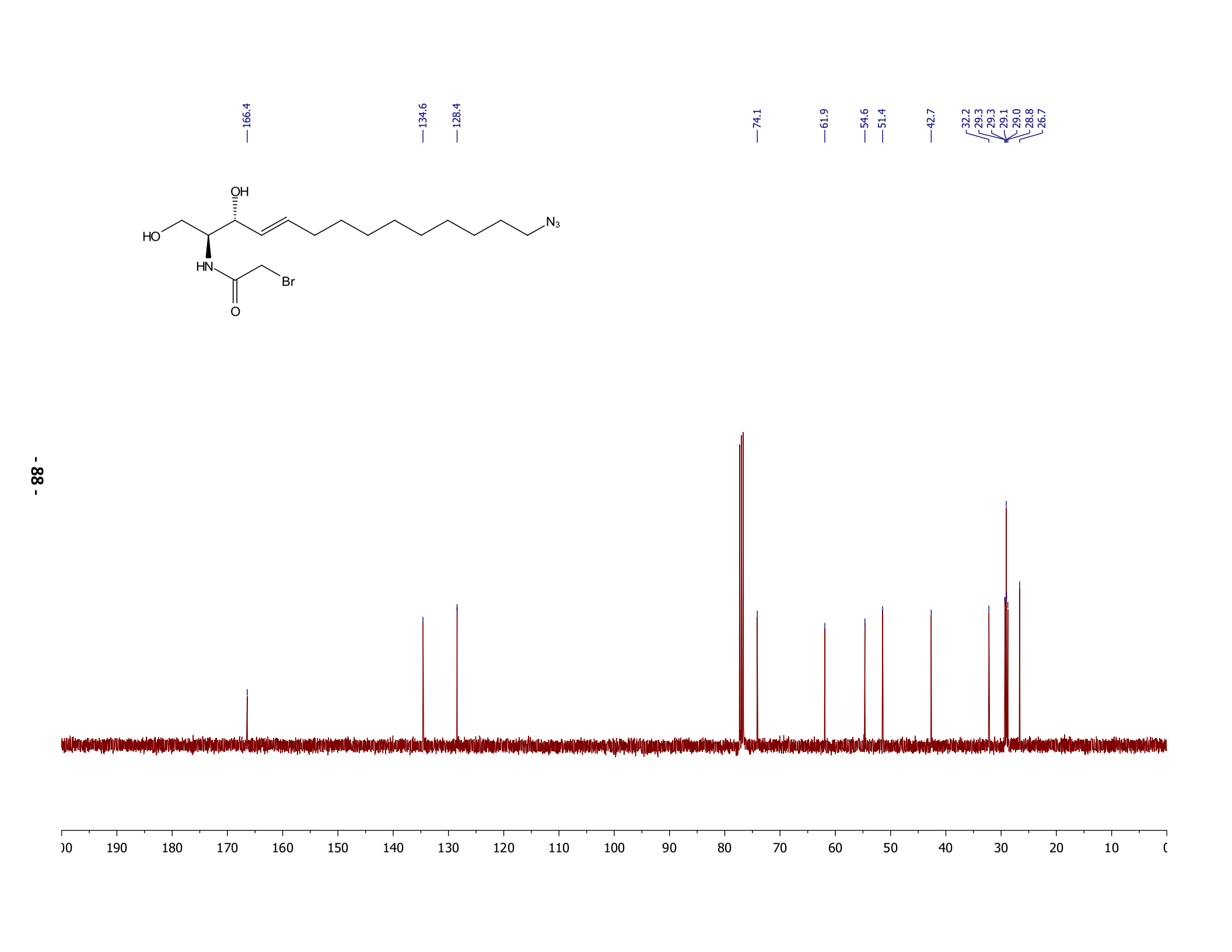
166.4
134.6
128.4
74.1
61.9
54.6
51.4
42.7
32.2
29.3
29.3
29.1
29.0
28.8
26.7
OH
HO
HN
Br
O
N3
- 88 -
190
180
170
160
150
140
130
120
110
100
90
80
70
60
50
40
30
20
10

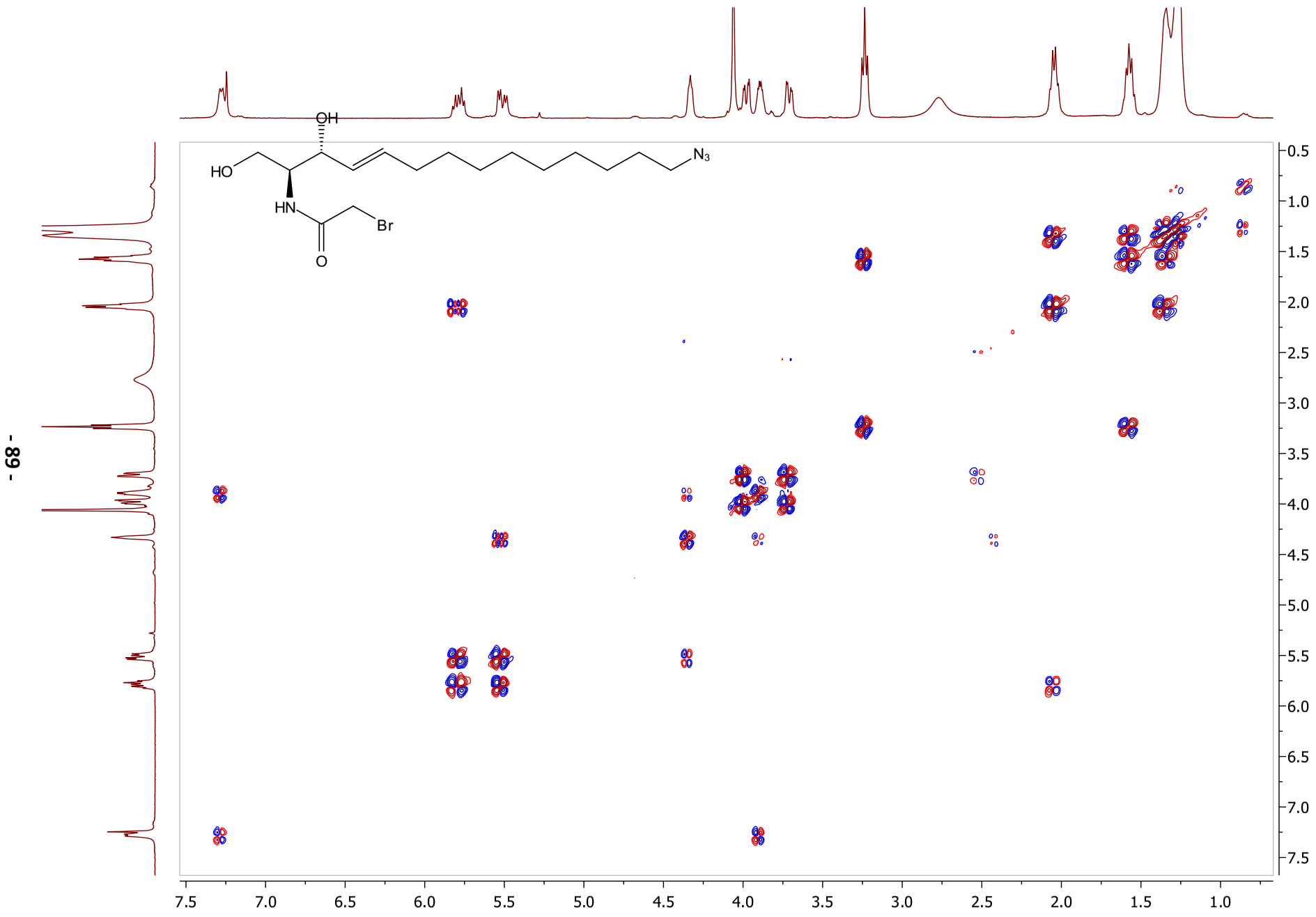
OH
HO
HN
Br
O
N3
7.5
7.0
6.5
6.0
5.5
5.0
4.5
4.0
3.5
3.0
2.5
2.0
1.5
1.0
0.5

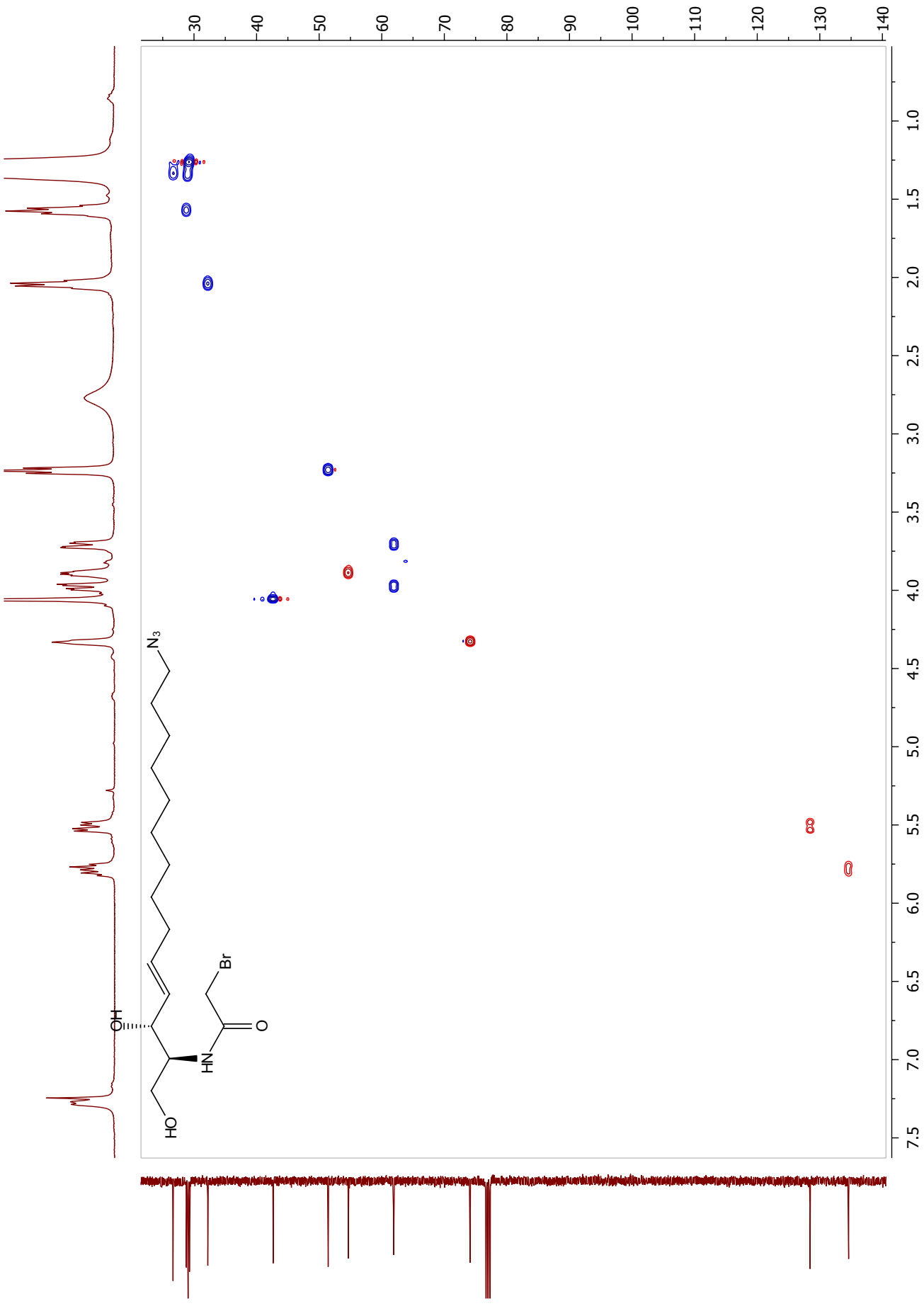
30
40
50
60
70
80
90
100
110
120
130
140
1.0
1.5
2.0
2.5
3.0
3.5
4.0
4.5
5.0
5.5
6.0
6.5
7.0
7.5
N3
OH
HN
O
Br
HO

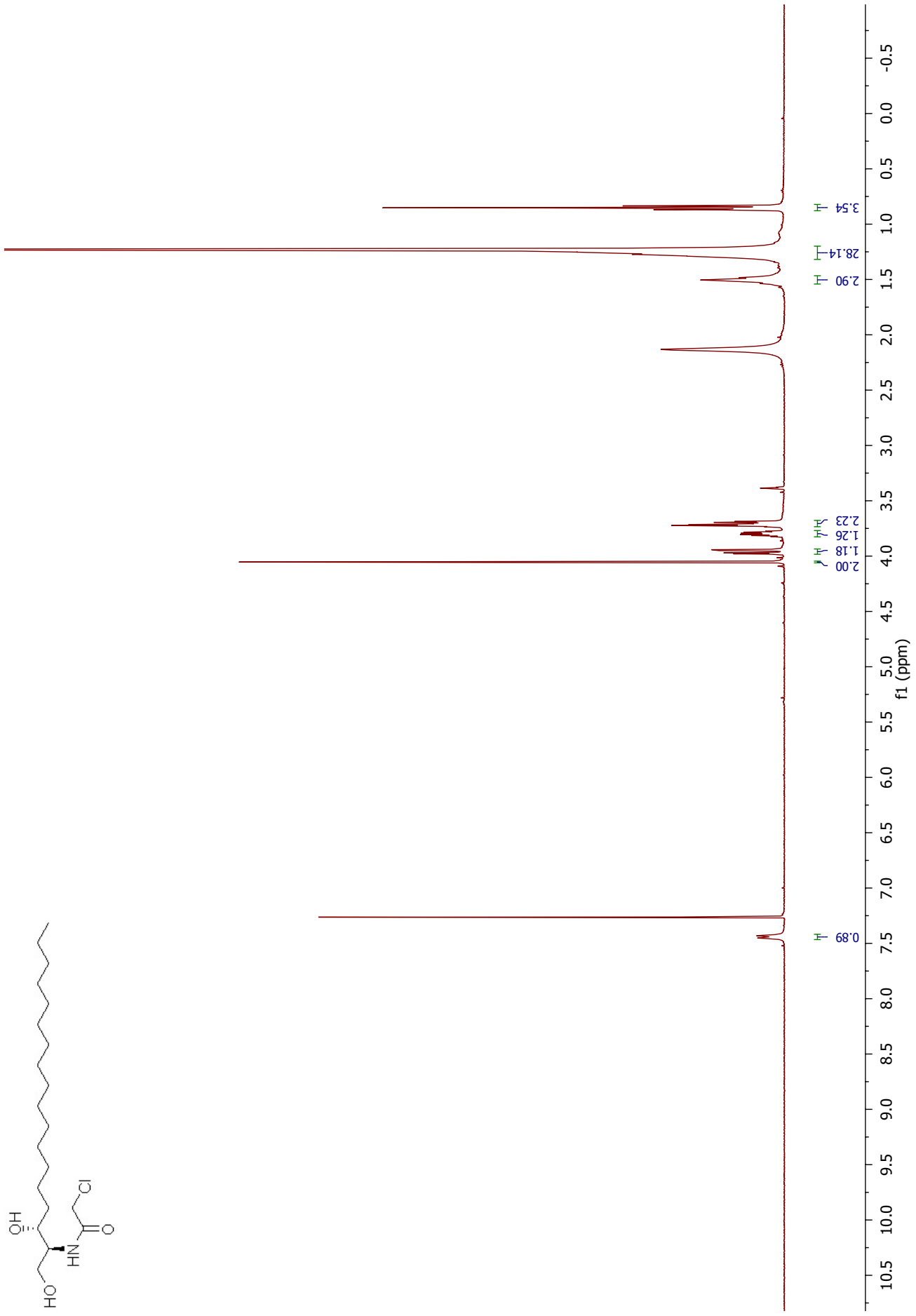
3.54
28.14
2.90
2.23
1.26
1.18
2.00
0.89
f1 (ppm)

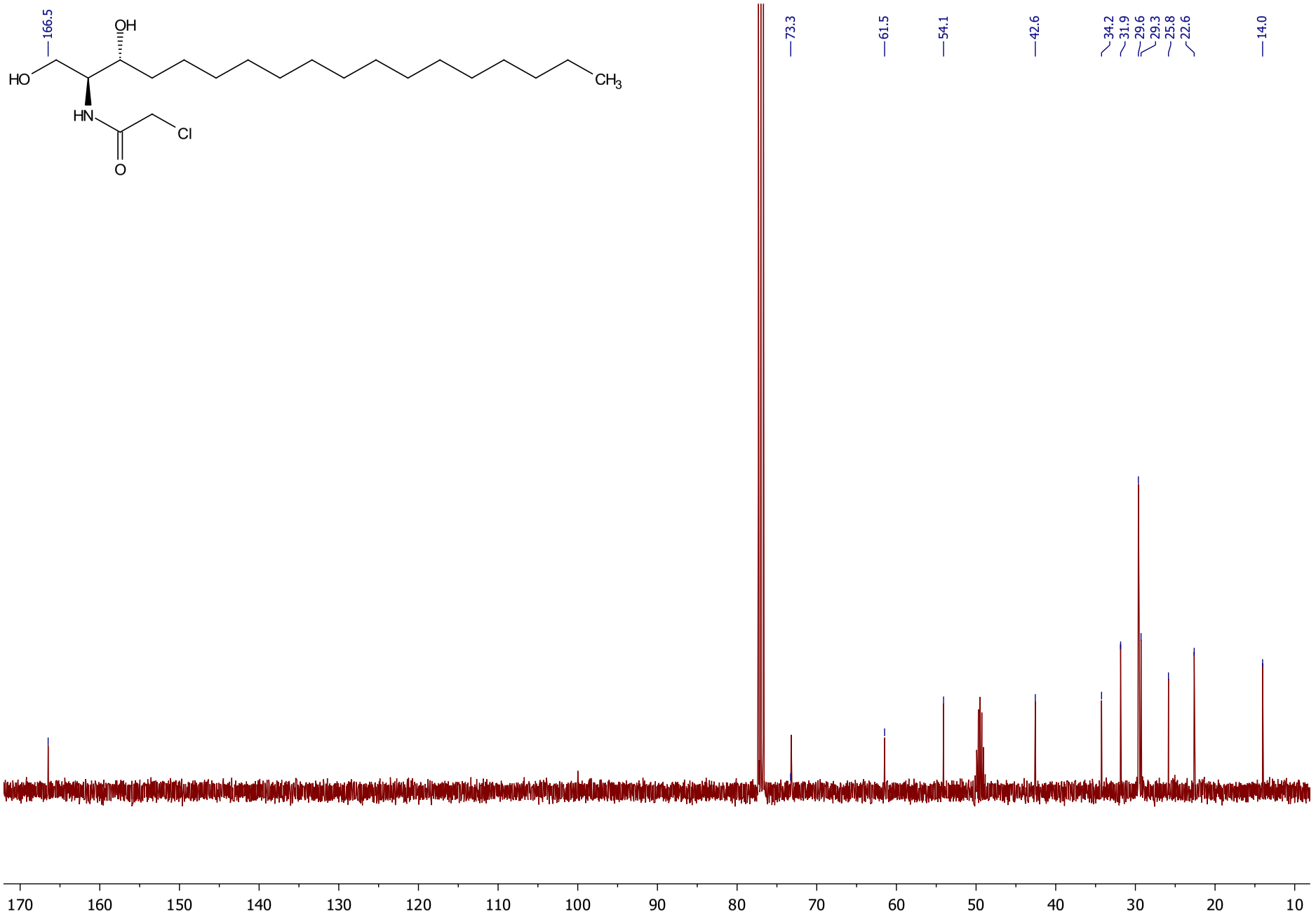
166.5
73.3
61.5
54.1
42.6
34.2
31.9
29.6
29.3
25.8
22.6
14.0
OH
HO
HN
Cl
O
CH3
170
160
150
140
130
120
110
100
90
80
70
60
50
40
30
20
10

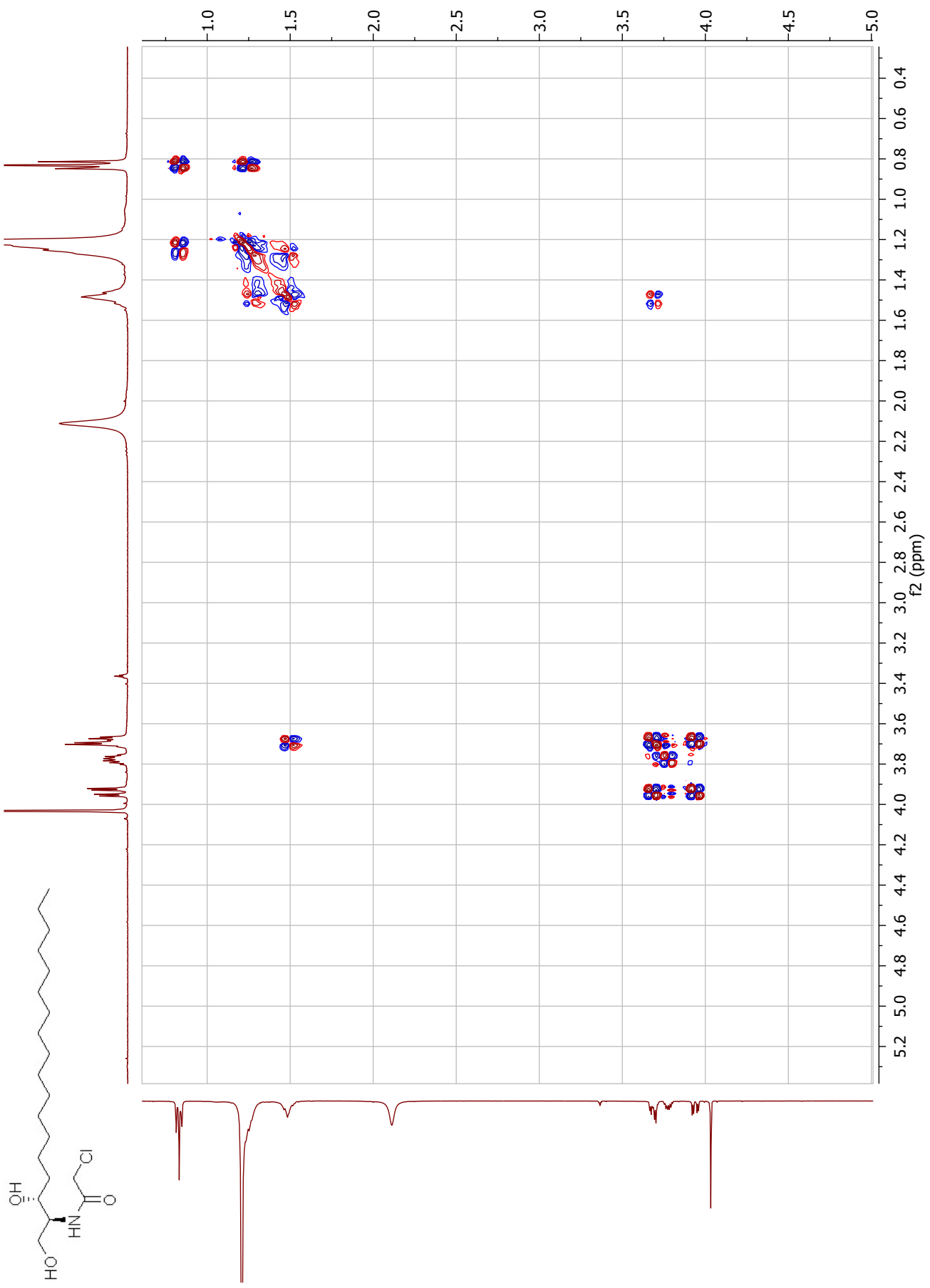
OH
HN
O
Cl
HO
1.0
1.5
2.0
2.5
3.0
3.5
4.0
4.5
5.0
5.2
5.0
4.8
4.6
4.4
4.2
4.0
3.8
3.6
3.4
3.2
3.0
2.8
2.6
2.4
2.2
2.0
1.8
1.6
1.4
1.2
1.0
0.8
0.6
0.4
f2 (ppm)

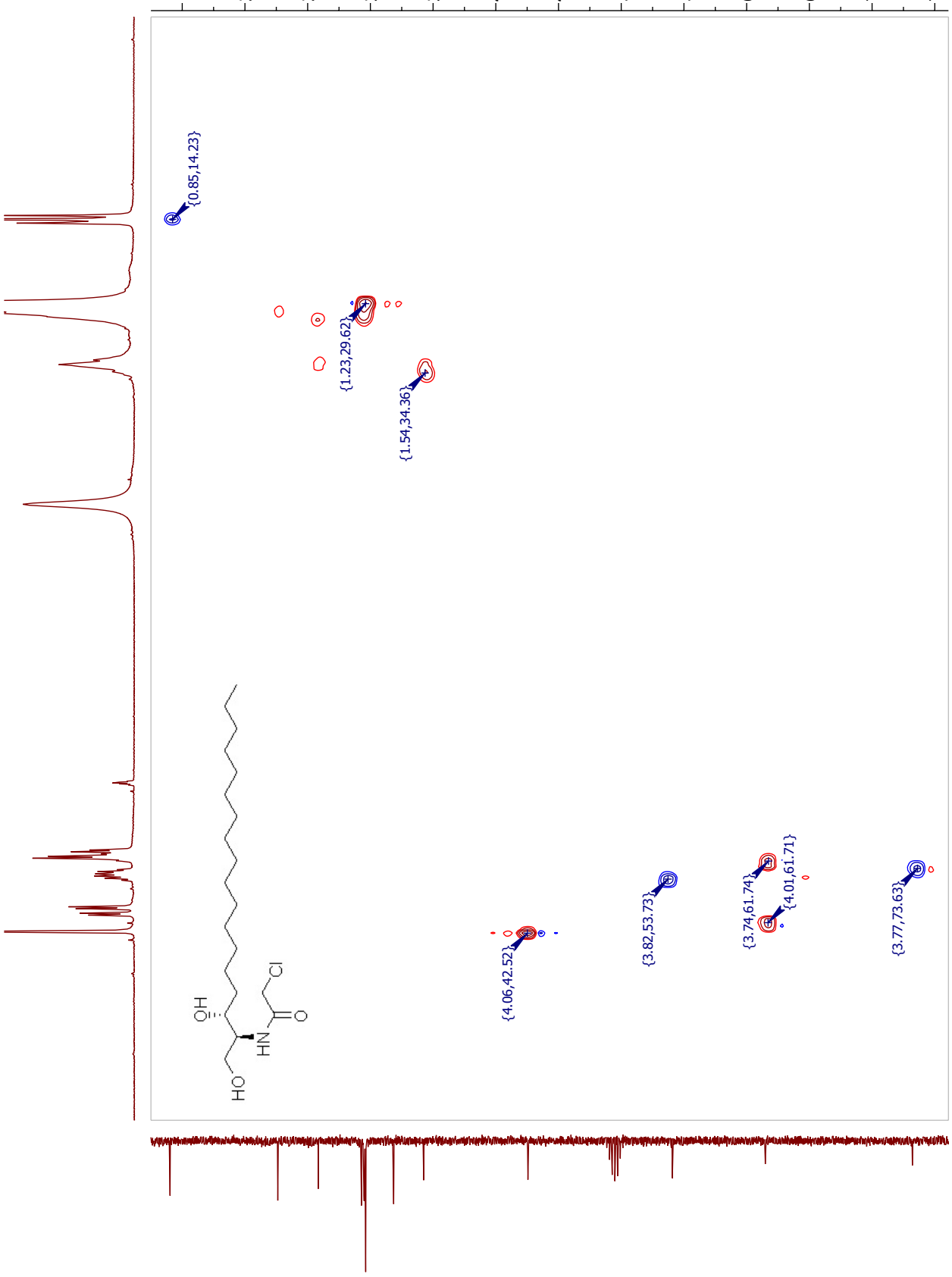
{0.85,14.23}
{1.23,29.62}
{1.54,34.36}
{4.06,42.52}
{3.82,53.73}
{3.74,61.74}
{4.01,61.71}
{3.77,73.63}
OH
HO
HN
O
Cl

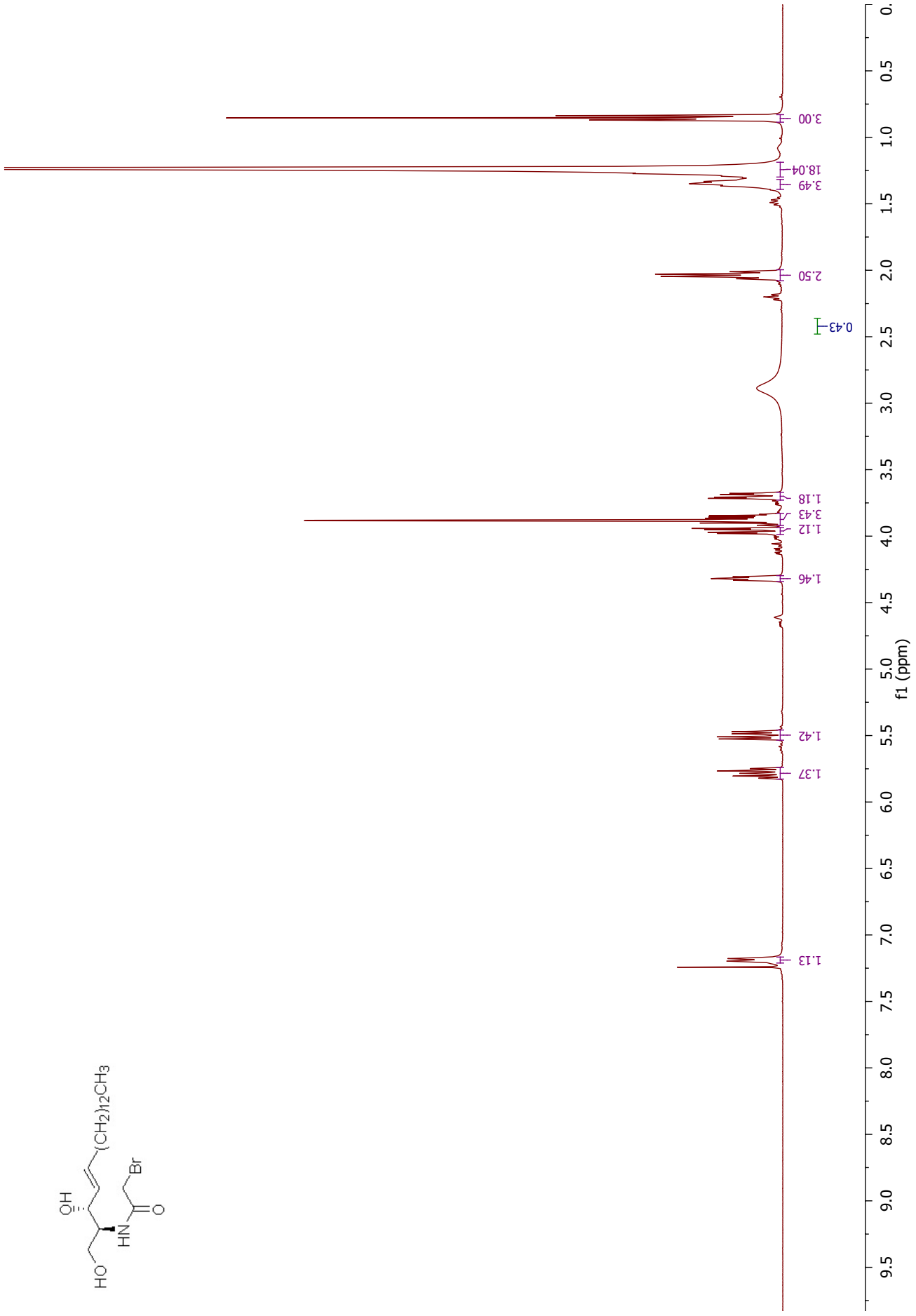
3.00
18.04
3.49
2.50
0.43
1.18
3.43
1.12
1.46
1.42
1.37
1.13
f1 (ppm)

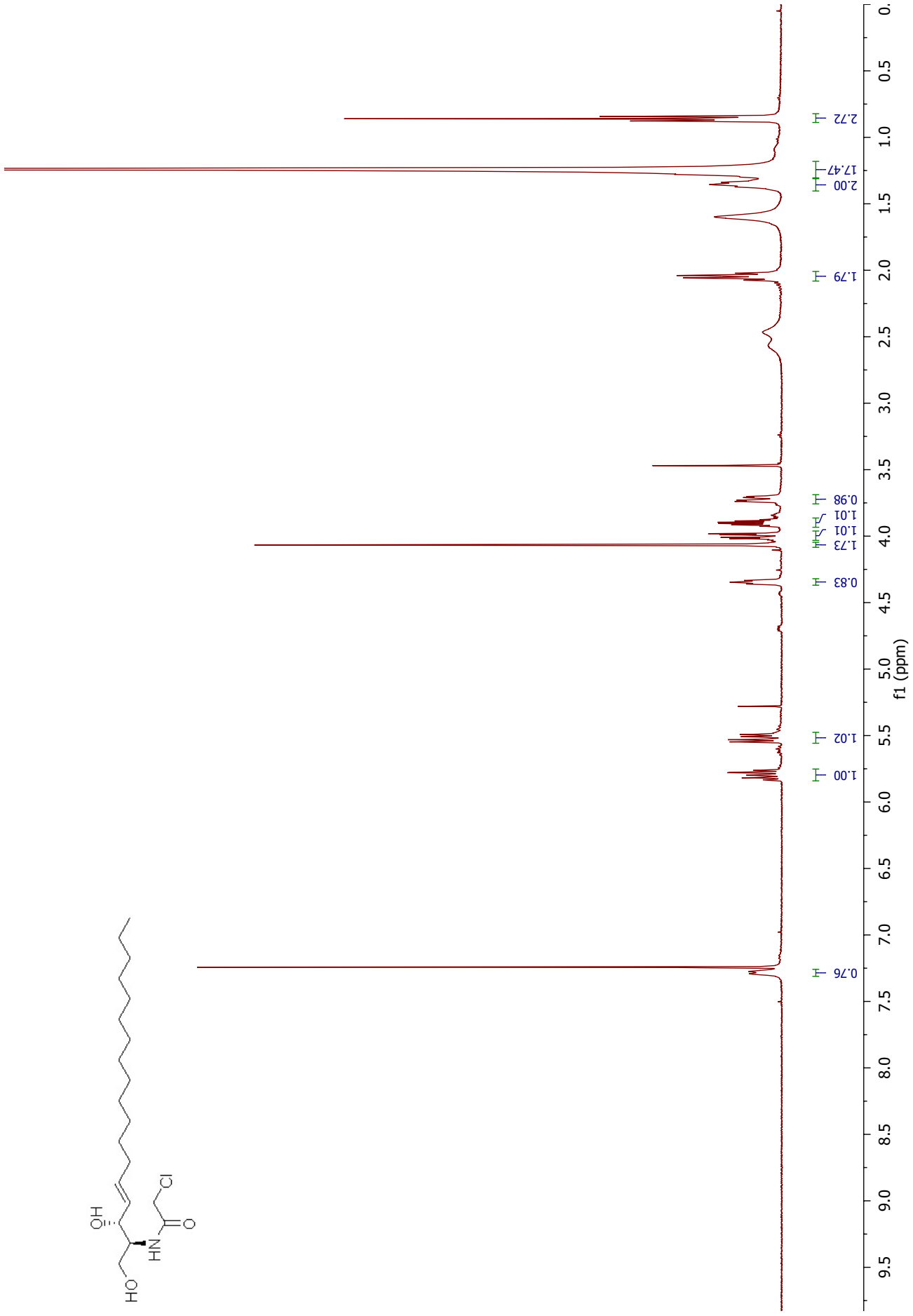
2.72
17.47
2.00
1.79
0.98
1.01
1.01
1.73
0.83
1.02
1.00
0.76
f1 (ppm)

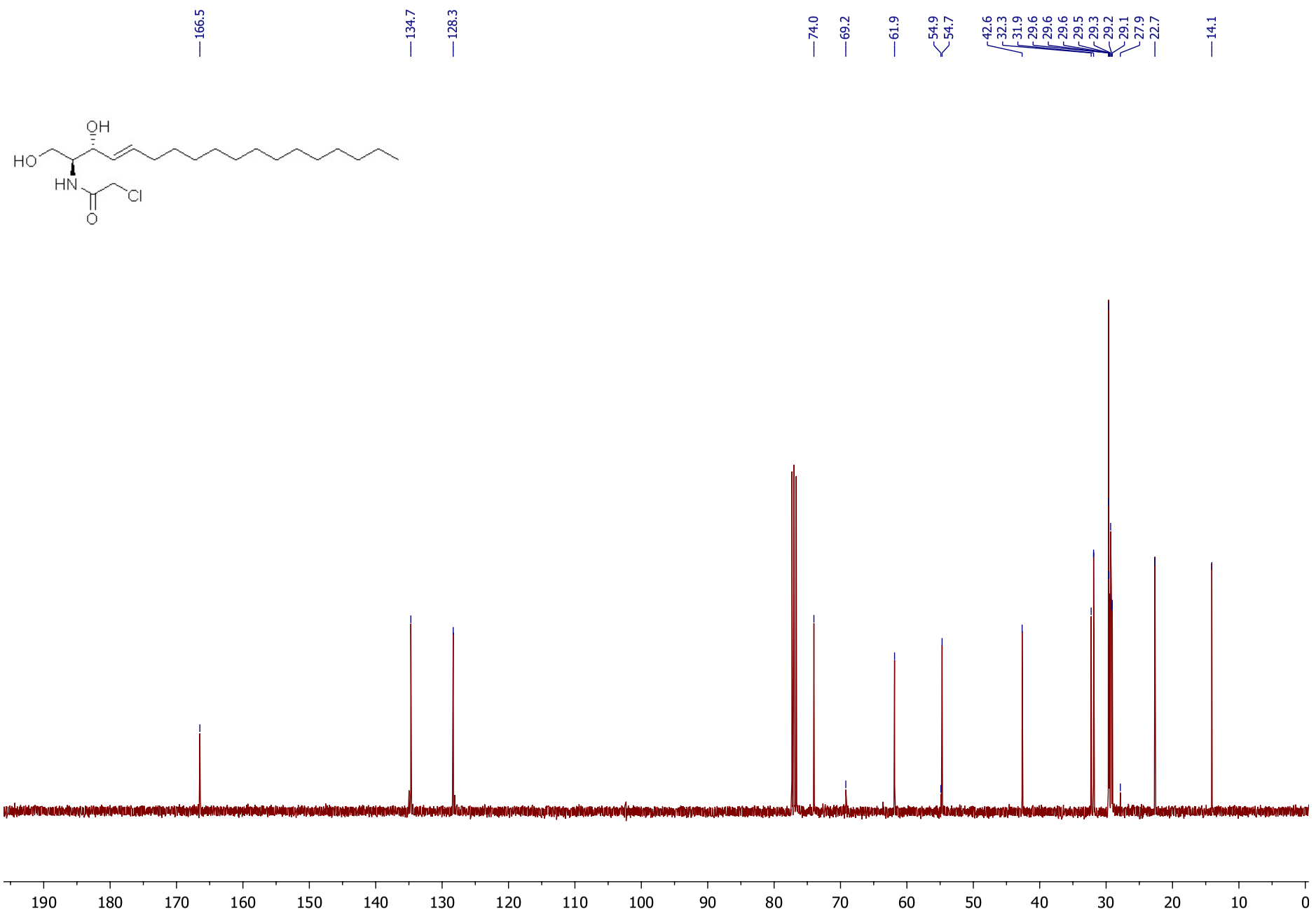
166.5
134.7
128.3
74.0
69.2
61.9
54.9
54.7
42.6
32.3
31.9
29.6
29.6
29.6
29.5
29.3
29.2
29.1
27.9
22.7
14.1
OH
HO
HN
Cl
O
190
180
170
160
150
140
130
120
110
100
90
80
70
60
50
40
30
20
10
0

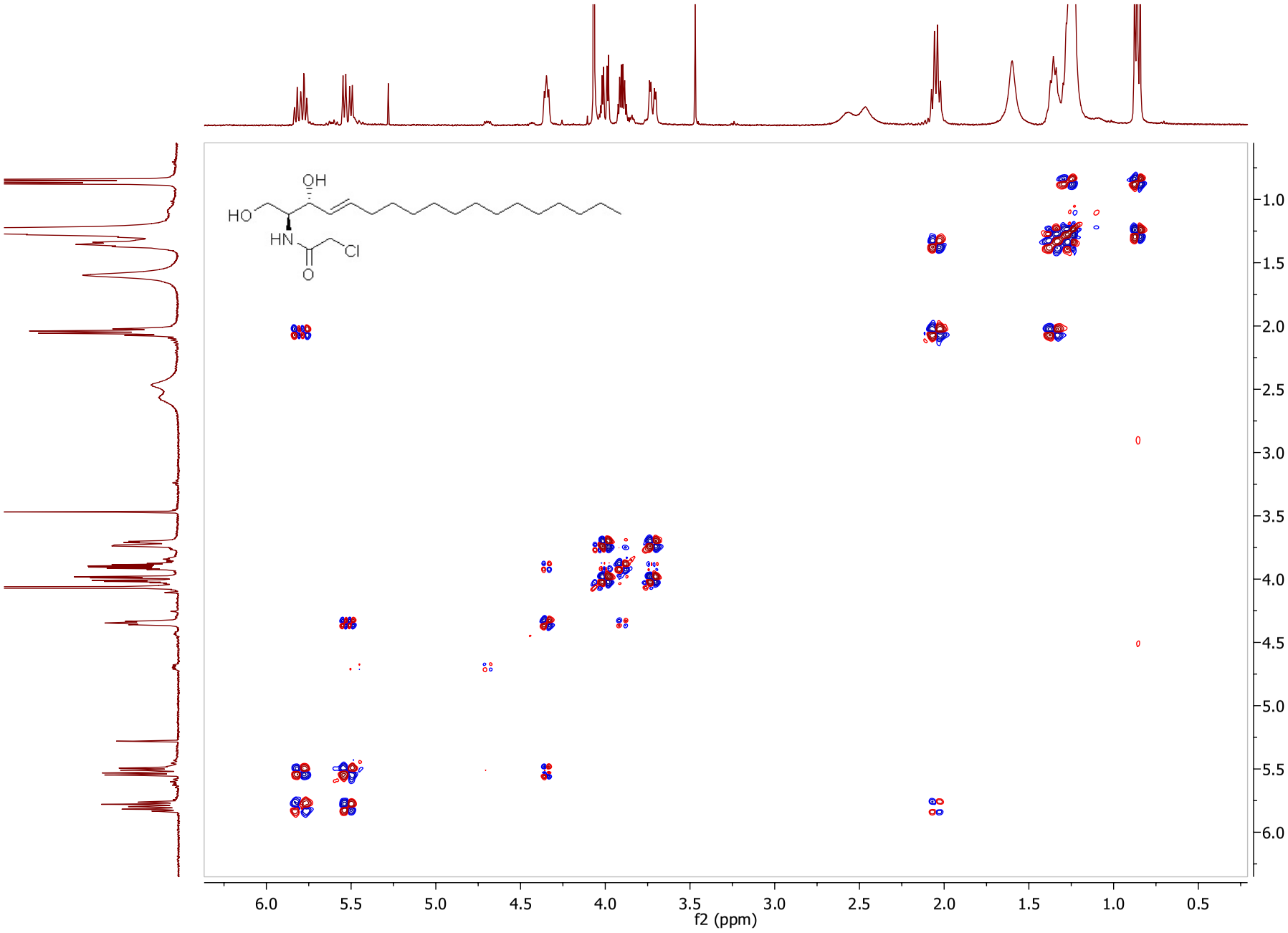
OH
HO
HN
Cl
O
1.0
1.5
2.0
2.5
3.0
3.5
4.0
4.5
5.0
5.5
6.0
6.0
5.5
5.0
4.5
4.0
3.5
3.0
2.5
2.0
1.5
1.0
0.5
f2 (ppm)

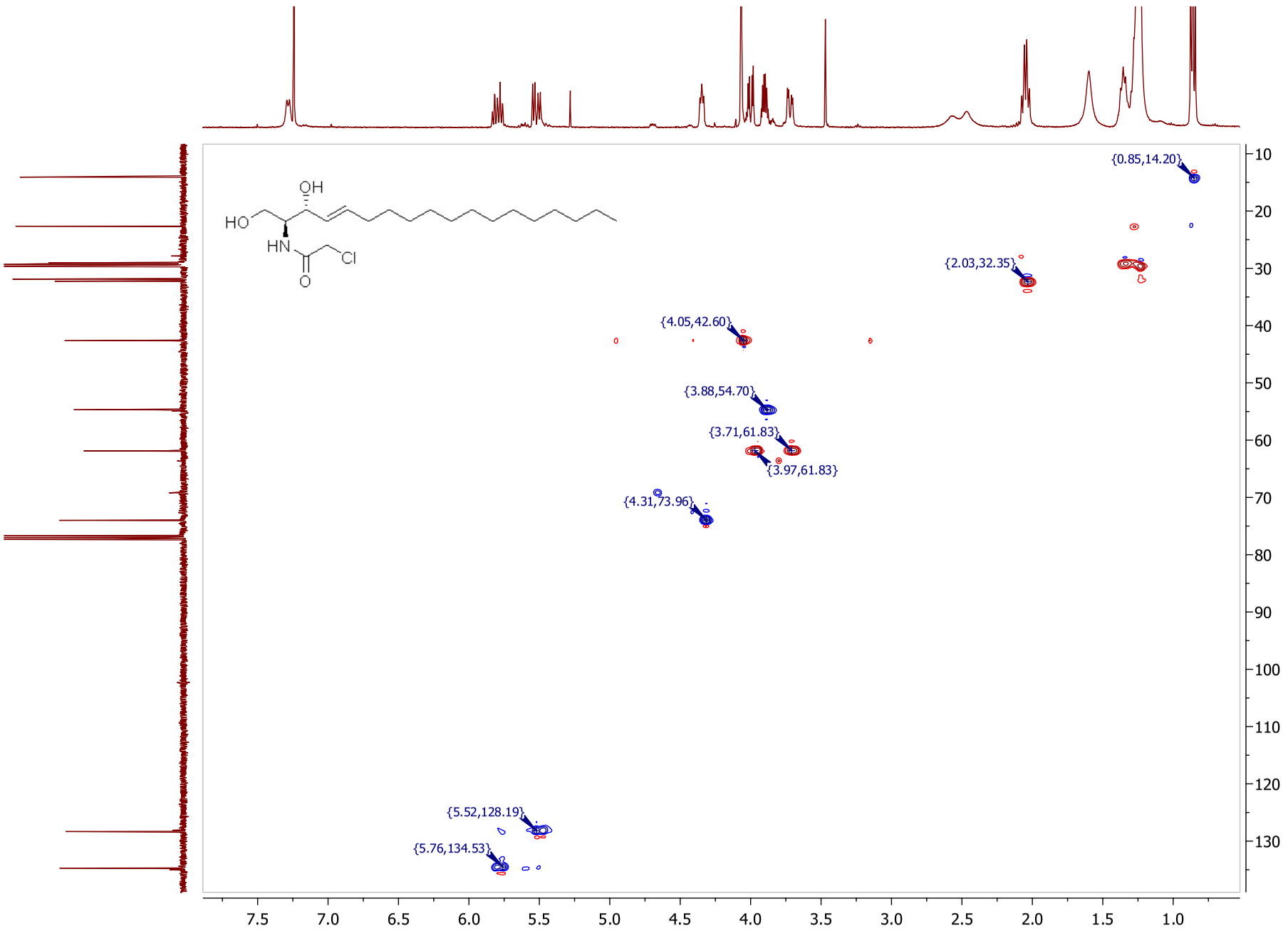
OH
HO
HN
Cl
O
{0.85,14.20}
{2.03,32.35}
{4.05,42.60}
{3.88,54.70}
{3.71,61.83}
{3.97,61.83}
{4.31,73.96}
{5.52,128.19}
{5.76,134.53}
7.5
7.0
6.5
6.0
5.5
5.0
4.5
4.0
3.5
3.0
2.5
2.0
1.5
1.0
10
20
30
40
50
60
70
80
90
100
110
120
130

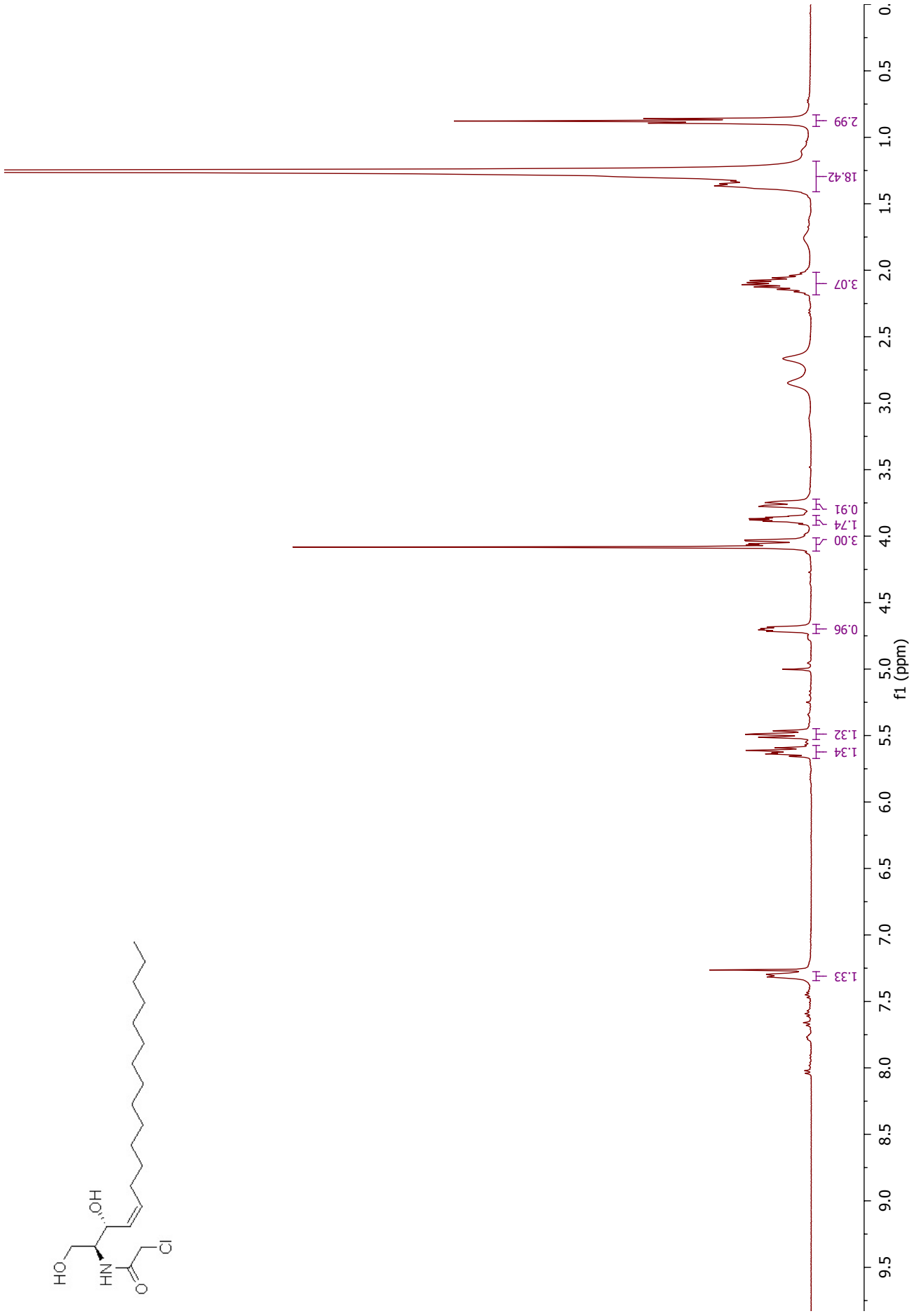
2.99
18.42
3.07
0.91
1.74
3.00
0.96
1.32
1.34
1.33
f1 (ppm)

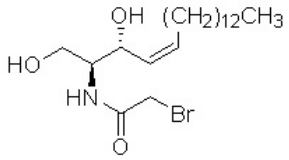

166.5
135.2
128.3
77.5 cdcl3
77.2 cdcl3
76.8 cdcl3
69.5
62.2
55.0
42.8
32.1
29.8
29.8
29.8
29.7
29.7
29.7
29.5
29.4
28.0
22.8
14.3

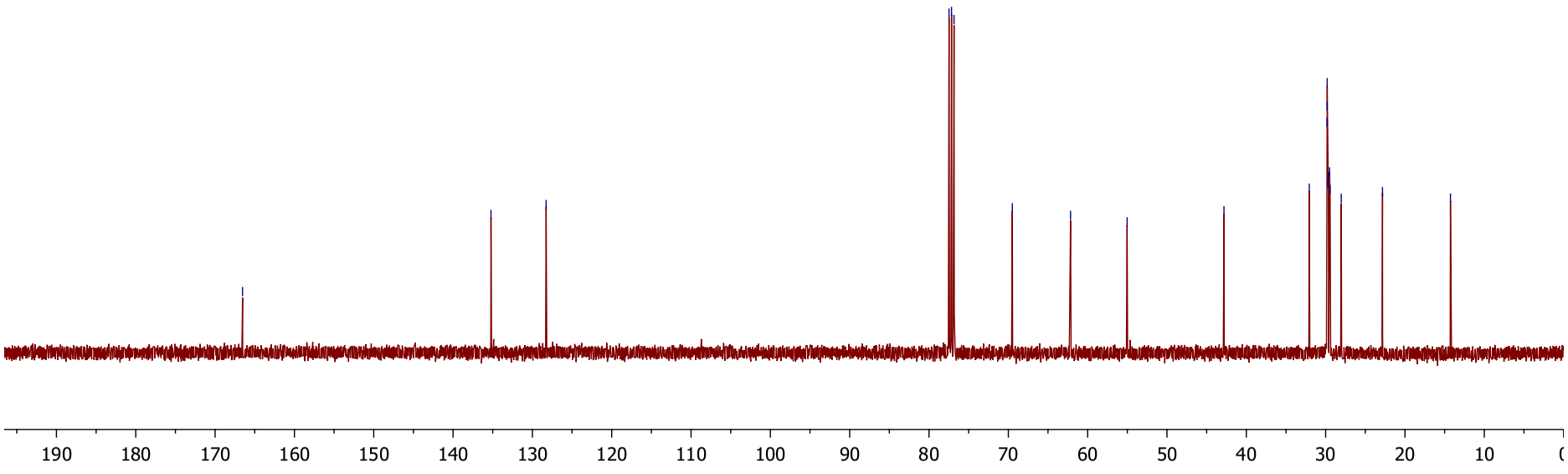

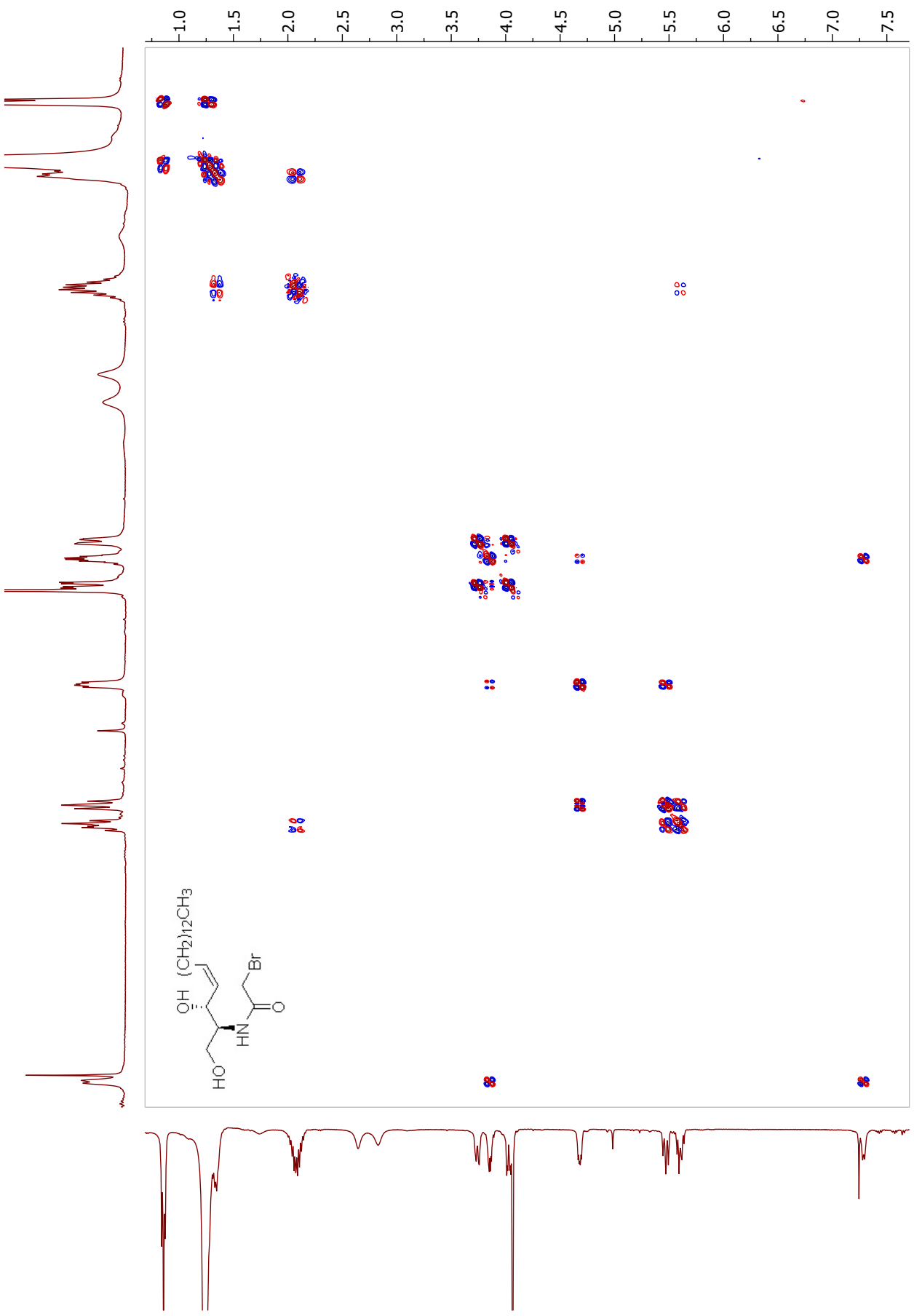
1.0
1.5
2.0
2.5
3.0
3.5
4.0
4.5
5.0
5.5
6.0
6.5
7.0
7.5
OH
(CH2)12CH3
HN
O
Br
HO

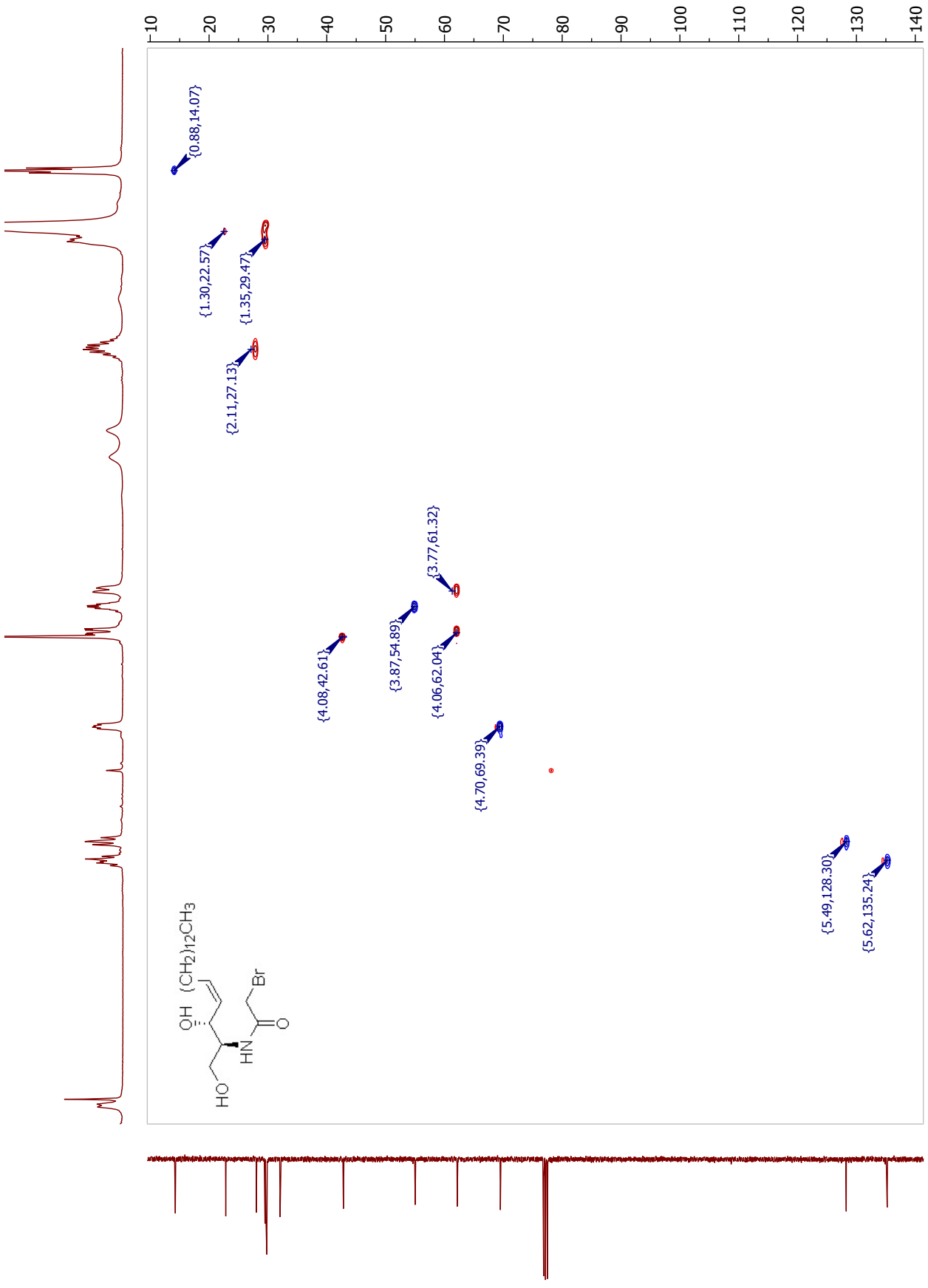
{0.88,14.07}
{1.30,22.57}
{1.35,29.47}
{2.11,27.13}
{3.77,61.32}
{3.87,54.89}
{4.06,62.04}
{4.08,42.61}
{4.70,69.39}
{5.49,128.30}
{5.62,135.24}
OH
(CH2)12CH3
HN
O
Br
HO

ARTICLE 3

High-throughput discovery of novel small-molecule inhibitors of acid Ceramidase

Mazen Aseeri [1], José Luis Abad [1], Antonio Delgado [1,2], Gemma Fabriàs [1,3], Gemma Triola [1] and Josefina Casas [1,3]

[1] Department of Biological Chemistry. Institute for Advanced Chemistry of Catalonia (IQAC-CSIC), Research Unit on Bioactive Molecules (RUBAM), 08034 Barcelona, Spain.

[2] Liver and Digestive Diseases Networking Biomedical Research Centre (CIBEREHD, ISCIII), 28029 Madrid, Spain.

[3] University of Barcelona (UB), Faculty of Pharmacy and Food Sciences, Department of Pharmacology, Toxicology and Medical Chemistry, Pharmaceutical Chemistry Unit (Unit associated with the CSIC), 08028 Barcelona, Spain.

Journal of Enzyme Inhibition and Medicinal Chemistry (JEIMC). **2023** 38(1):343-348.

Impact factor: 5.668

The contribution of Mazen Aseeri to this work, corresponds to the design, performance and data analysis of all experiments. He also contributed to the writing of the initial draft and the preparation of the published work.

CASAS BRUGULAT JOSEFINA - DNI 40513738C
Firmado digitalmente por CASAS BRUGULAT JOSEFINA - DNI 40513738C
Fecha: 2023.01.24 13:19:09 +01'00'

TRIOLA GUILLEM GEMMA - DNI 40323105B
Digitally signed by TRIOLA GUILLEM GEMMA - DNI 40323105B
Date: 2023.01.25 17:43:04 +01'00'

Josefina Casas Brugulat and Gemma Triola Guillem

Thesis Directors

SUMMARY

High-throughput discovery of novel small-molecule inhibitors of acid ceramidase

Objective: Acid ceramidase (AC) is highly expressed in many types of cancer, and the identification of selective AC has attracted increasing interest. However, the discovery of novel AC inhibitors has been hampered by the lack of high-density formats suitable for the screening of large compound libraries. Thus, efforts were made to overcome this drawback by adapting a fluorogenic assay to a 384-well plate format and employ it to screen the inhibitory effect of a library of 4100 compounds over AC activity.

Methodology: A fluorescent-based assay in a 96-well format was previously set up in our group and applied to measure acid ceramidase activity using cell lysates and intact cells as a source of enzyme. The assay is based on the coumarinic substrate RBM14-C12, that shows a high affinity and specificity for AC over neutral and alkaline ceramidases. AC activity is determined by measuring the fluorescence released after the hydrolysis of RBM14-C12 substrate. This assay has been largely used by our group and others to identify novel ceramidase inhibitors. However, assays with increased capacity are required to allow the rapid high-throughput screening (HTS) of large chemical libraries, thereby accelerating the drug discovery process as well as reducing the associated costs. Therefore, the AC assay was optimally miniaturized to a 384-well format and employed for the identification of new acid ceramidase inhibitors. The robustness and assay performance of the miniaturized assay were validated and assessed by the screening of a 4100 compound library. AC-overexpressing A375 melanoma cell line was used as a source of protein and cells. The activity of the identified hits over NC was tested using recombinant human NC (rhNC) and a specific NC substrate bearing a nervonic acid amide (RMB14-C24:1). Together, compounds and substates were incubated for the specified time required for the enzymatic reaction.

Results: As a first validation step, a control run consisting of 60 wells representing AC activity and 60 wells representing the signal in absence of the enzyme. The results revealed excellent separation between high and low control wells resulting in a signal-to-background ratio >8 and a Z´factor of 0.72. The calculated coefficients of variation (CV) for both the high and low controls were 6.08% and 17.1% respectively. These data demonstrated that the assay was very robust, stable and possessed minimal well-to-well variability and therefore it is appropriate for HTS to identify AC inhibitors. After having successfully established the optimal reaction conditions in a 384-well format, this newly miniaturized AC assay was employed in a pilot screen against a library of 4100 compounds. A total of 116 compounds of the 4100 screened in duplicates at a single dose of 20 μM met the active criterion, based on the hit cut-off at % inhibition >40, in the single-point primary screen, what resulted in a hit rate of 2.8%. The inhibitory activity of these hits was then validated in an additional assay performed at a single-point concentration in triplicates. To confirm

the results from the primary screening, top hits were cherry-picked and tested in a concentration-dependent response assay with triplicates per sample. Thus, 101 compounds were then subjected to 8-points two-fold dilution series starting at a maximum concentration of 200 micromolar. Among them, nine exhibited dose-dependent inhibition of AC with IC_{50} values in the range of 6 and 49 µM, whereas 92 compounds showed a higher IC_{50} value or did not yield a concentration-dependent inhibition. Remarkably, the identified nine hits were proven selective in inhibiting AC over neutral ceramidase (NC). In intact AC overexpressing A375 cells, only two of the 9 tested compounds exhibited significant inhibition of AC activity when tested in triplicates at a single-point concentration of 20 µM: W000113402_C12 with a 53% inhibition and W000113414_H19 with a weaker 32% inhibition, whereas slight effects were observed for the other hits. Dose-dependent inhibition could be also confirmed for W000113402_C12 in the cell-based assay displaying an IC_{50} value of 32 µM.

Conclusions: HTS is still the primary hit-finding strategy both in academia and industry. However, the identification of novel AC inhibitors has been hampered by the unavailability of appropriate screening platforms. Herein, we report a robust and cost-effective assay for the determination of AC activity that enables the rapid profile of large compound libraries. The screening platform has been employed to evaluate a 4100 compound library leading to the identification of 9 novel compound classes targeting AC activity with low micromolar IC_{50}. Dose-dependent inhibition was confirmed for the primary hits identified in the screening campaign and now they can serve as a basis for hit-to-lead optimization through chemical modifications, thereby opening new venues in the field of AC inhibition. Moreover, the reported technique can be considered an attractive drug-screening platform with great potential to identify novel AC modulators. As several diseases are linked to altered AC activity, novel compounds modulating its activity should allow progress in drug discovery and expand our knowledge of the essential role of this enzyme.

JOURNAL OF ENZYME INHIBITION AND MEDICINAL CHEMISTRY
2023, VOL. 38, NO. 1, 343–348
https://doi.org/10.1080/14756366.2022.2150183

Taylor & Francis
Taylor & Francis Group

BRIEF REPORT

OPEN ACCESS Check for updates

High-throughput discovery of novel small-molecule inhibitors of acid Ceramidase

Mazen Aseeri[a], José Luis Abad[a], Antonio Delgado[a,b], Gemma Fabriàs[a,c], Gemma Triola[a] and Josefina Casas[a,c]

[a]Department of Biological Chemistry, Institute for Advanced Chemistry of Catalonia (IQAC-CSIC), Barcelona, Spain; [b]Department of Pharmacology, Toxicology and Medicinal Chemistry, Unit of Pharmaceutical Chemistry (Associated Unit to CSIC), Faculty of Pharmacy and Food Sciences, University of Barcelona, Barcelona, Spain; [c]Liver and Digestive Diseases Networking Biomedical Research Centre (CIBEREHD), ISCIII, Madrid, Spain

ABSTRACT

Ceramide has a key role in the regulation of cellular senescence and apoptosis. As Ceramide levels are lowered by the action of acid ceramidase (AC), abnormally expressed in various cancers, the identification of AC inhibitors has attracted increasing interest. However, this finding has been mainly hampered by the lack of formats suitable for the screening of large libraries. We have overcome this drawback by adapting a fluorogenic assay to a 384-well plate format. The performance of this optimised platform has been proven by the screening a library of 4100 compounds. Our results show that the miniaturised platform is well suited for screening purposes and it led to the identification of several hits, that belong to different chemical classes and display potency ranges of 2–25 μM. The inhibitors also show selectivity over neutral ceramidase and retain activity in cells and can therefore serve as a basis for further chemical optimisation.

ARTICLE HISTORY
Received 3 October 2022
Revised 3 November 2022
Accepted 13 November 2022

KEYWORDS
Sphingolipids; ceramide; acid ceramidase; inhibitor

Introduction

Sphingolipids (SLs) are a major class of cellular lipids. Besides playing a structural role in cellular membranes, several members of the SLs family are also involved in the regulation of a variety of cellular processes. The metabolic hub in SLs biosynthesis and catabolism is ceramide, a bioactive lipid intimately involved in the regulation of stress response[1], inflammation[2], apoptosis[3] and cancer cell death[4].

In the recent years, there is more and more evidence that maintaining a tight regulation of ceramide levels is key to cells and strongly contributes to cell fate decisions. Moreover, altered ceramide levels are a hallmark in the manifestation of several pathological processes such as Alzheimer disease[5], metabolic disorders[6] or cancer[7], in which lower levels of this lipid are inversely correlated with the degree of malignant progression[8]. Consequently, tremendous efforts have been devoted to identifying small molecules targeting the enzymes involved in ceramide biosynthesis and degradation.

Ceramide can be generated *de novo* from serine and palmitate, by the degradation of sphingomyelin catalysed by sphingomyelinases and by the acylation of sphingosine in the salvage pathway. Ceramide degradation is in turn mediated by the actions of different ceramidases that are distinguished by the pH required for optimal activity, i.e. acid ceramidase (AC, ASAH1), neutral ceramidase (NC, ASAH2) and alkaline ceramidases 1, 2 and 3 (ACER1, ACER2 and ACER3)[9]. Different functions and cellular roles, probably defined by their intracellular localisation and substrate specificity, have been suggested for these ceramidases. Hence, NC overexpression has been related to colon carcinogenesis[10], whereas ACER3 has been reported to contribute to hepatocellular carcinoma[11] and to acute myeloid leukaemia pathogenesis[12].

AC is one of the better-characterized ceramidases and its role in cancer initiation and progression has been largely studied. Abnormally elevated AC expression has been reported in various type of cancer including prostate cancer[13], colon adenocarcinoma[14], head and neck cancer[15], glioblastoma[16] and melanoma[17]. Moreover, whereas AC overexpression renders the cells more resistant to chemo and radiotherapy[18], inhibition of the enzyme sensitises the cell to treatment[19], thereby suggesting a role of AC in drug resistance associated to therapy. As a result, AC inhibition has emerged as an attractive target to improve the efficacy and lower the resistance to cancer treatments, and the identification of novel and selective AC inhibitors has gained increasing interest. Tremendous efforts have been done during the last two decades to develop AC modulators. However, most of the reported inhibitors are structurally related to ceramide, which has a negative impact on their selectivity, potency and drug-like properties[20]. Thus, the discovery of ceramide-unrelated hits would be highly desirable. Some potent and structurally unrelated inhibitors of AC have already been described. Representative examples of this class of compounds are carmofur, identified after the screening of a commercial library using a LC/MS-based assay[14], and the related dioxypyrimidine and benzoxazolone carboxamides[21–23]. Despite these relevant examples, there is still a great need for the identification of novel molecules that can expand the toolbox for AC inhibitors.

One of the best alternatives to identify structurally diverse inhibitors is through the screening of large compound libraries. However, this approach requires a powerful, robust and cost-

CONTACT Gemma Triola gemma.triola@iqac.csic.es, Josefina Casas fina.casas@iqac.csic.es Department of Biological Chemistry, Institute for Advanced Chemistry of Catalonia (IQAC-CSIC), Jordi Girona 18, Barcelona, 08034, Spain

Supplemental data for this article is available online at https://doi.org/10.1080/14756366.2022.2150183.

effective HTS assay, allowing the rapid and reliable testing of large number of compounds. Recently, we described a flow-cytometry-based assay that uses a deoxyceramide analog to monitor AC activity in intact cells. This assay could be potentially useful in the future for screening purposes, but it would require proper optimisation and the use of high-throughput flow cytometry platforms[24]. Herein, we report a fluorescence-based AC assay that has been adapted to a 384-well format. Once validated, it has been employed to evaluate a 4100 compound library leading to the identification of novel compound classes targeting AC activity. Remarkably, the identified inhibitors also show selectivity over NC and retain activity in cellular studies.

Results and discussion

The screening for specific and potent AC inhibitors requires the availability of a high-throughput screening assay (HTS) capable of examining relatively large number of compounds simultaneously. A fluorescent-based assay in a 96-well format was previously set up in our group and applied to measure acid ceramidase activity using cell lysates and intact cells as a source of enzyme. The assay is based on the coumarinic substrate RBM14-C12[25], that shows a high affinity and specificity for AC over neutral and alkaline ceramidases. Briefly, hydrolysis of the amide bond of RBM14-C12 by AC yields an aminodiol that can be then oxidised upon treatment with sodium periodate. The resulting aldehyde undergoes a β-elimination reaction to release the fluorescent product umbelliferone (Scheme 1). The assay has been largely used by our group and others to identify novel ceramidase inhibitors[21,26,27]. However, assays with increased capacity are required to allow the rapid high-throughput screening (HTS) of large chemical libraries, thereby accelerating the drug discovery process as well as reducing the associated costs. Remarkably, recent advances have been performed in this area of research. Thus, a HTS screening assay for the identification of neutral ceramidase inhibitors was recently established by Spicer et al. using an analogous substrate RBM14-C16, developed in our group[28]. Moreover, Granier et al. synthesised a suite of doubly fluorophore-modified ceramides as turn-on probes for the direct FRET-based analysis of ceramidase activity in real-time. Although ACER3 was able to hydrolyse one of the probes, no synthetic substrates were hydrolysed by AC[29]. Therefore, although the Granier's method has the advantage of monitoring ceramidase activity in real-time, it cannot be applied to AC until suitable FRET ceramide substrates are discovered for this enzyme. Herein, we report the miniaturisation of an AC assay to a 384-well format and we employ it for the identification of new acid ceramidase inhibitors. The robustness and assay performance of the miniaturised assay were validated and assessed by the screening of a 4100 compound library, leading to the identification of novel AC inhibitors (Figure 1).

Optimisation and miniaturisation of the AC HTS assay

To start with, the final reaction volume was adapted from 100 µL (96-well-format) to 32 µL (384 well-format) with a final concentration of substrate of 20 µM. Next, protein concentration was adjusted using cell lysates of AC-overexpressing A375 melanoma cells. Ideally, the optimal amount of protein is the one that ensures reaction linearity over a period of time together with less than 10% of substrate depletion, in order to assume that the enzyme operates at steady-state conditions. Thus, different amounts of cell lysates were mixed with the substrate and product formation was measured over 1 h. Figure 2(A) displays the reaction progress curve for the hydrolysis of RBM14-C12 by AC obtained at a range of protein concentrations. Finally, an amount of 0.4 µg of protein was chosen, as higher amounts of proteins were not in the linear portion whereas lower amounts would compromise the signal window. The optimal incubation time of the reaction mixture was next explored. Although a higher signal was witnessed at 2 h reaction time, a final reaction time of 1 h was chosen since it exhibited an excellent signal window. As a first validation step, we performed a control run consisting of 60 wells representing AC activity and 60 wells representing the signal in absence of the enzyme. Figure 2(B) depicts the results and reveals excellent separation between high and low control wells resulting in a signal-to-background ratio >8 and a *Z'*factor of

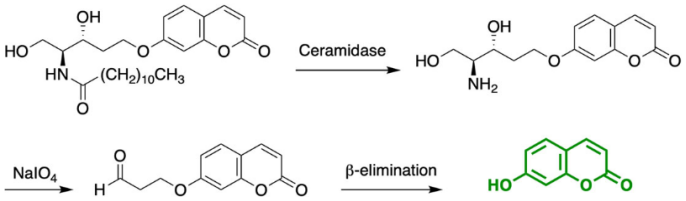

Scheme 1. Enzymochemical transformation of RBM14-C12 into fluorescent umbelliferone.

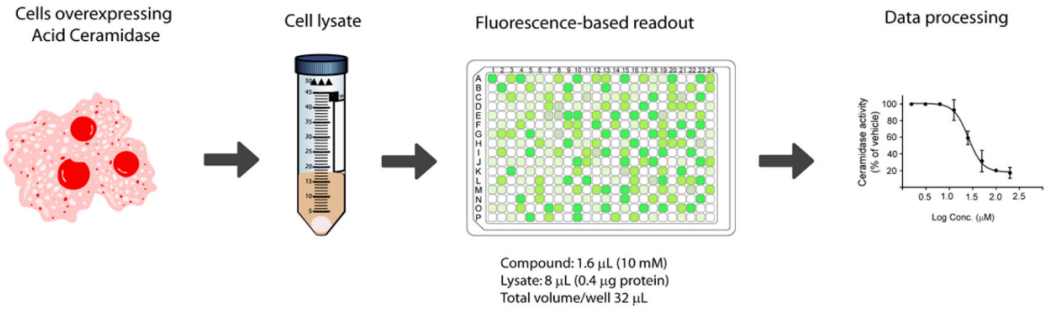

Figure 1. Workflow for acid ceramidase activity screening in the 384-well HTS format.

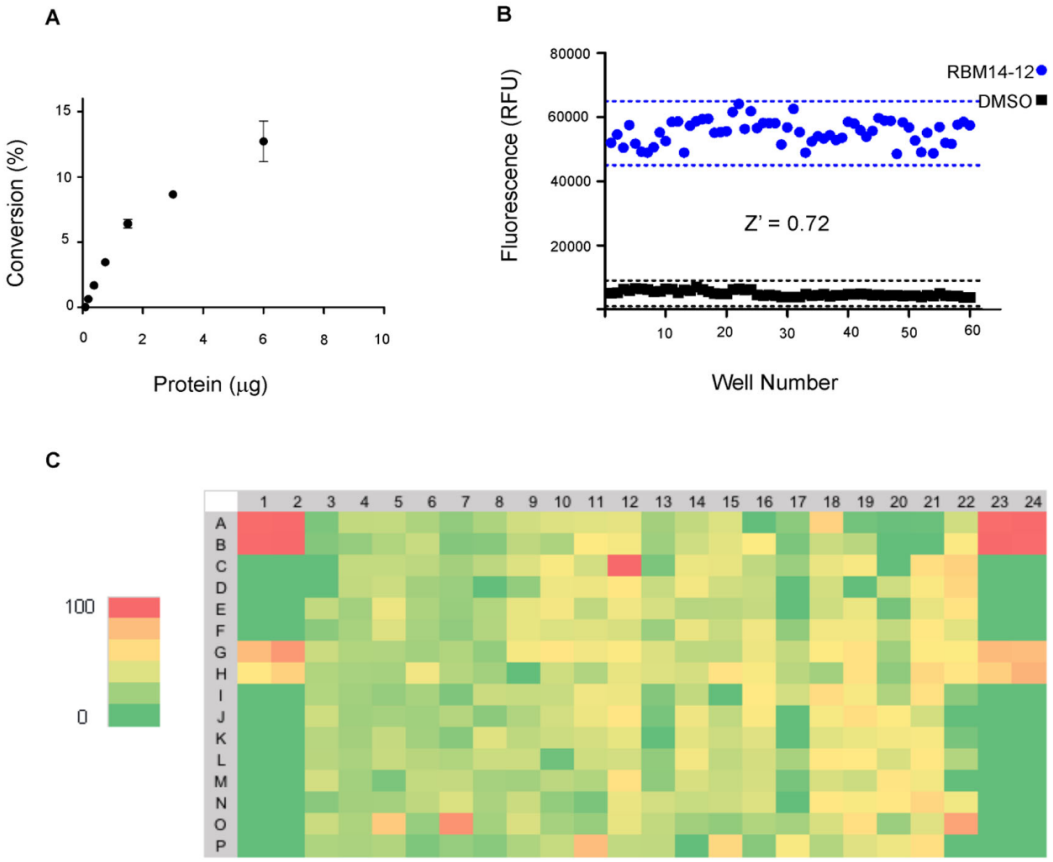

Figure 2. (A) Percentage of substrate conversion obtained using different amounts of AC (measured as µg of total protein). (B) Determination of the *Z'*-factor (*Z'*) of the AC assay in the 384-well plate format. Solid black squares and solid blue circles represent negative (without protein) and positive reaction, respectively. (C) Representative results for one 384-well plate. Each plate contained 8 negative controls, 16 positive controls and 8 samples with the known AC inhibitor SOCLAC. A colour gradient heat map, with red to green colours indicating high to low percentage of inhibition has been applied to the well values.

0.72. The calculated coefficients of variation (CV) for both the high and low controls were 6.08% and 17.1% respectively. These data demonstrated that the assay was very robust, stable and possessed minimal well-to-well variability and therefore it is appropriate for HTS to identify AC inhibitors.

Screening of a compound library

After having successfully established the optimal reaction conditions in a 384-well format, we employed this newly miniaturised AC assay in a pilot screen against a library of 4100 compounds. The screen was carried out at a single dose of 20 µM for each library compound in 6% DMSO (v/v) and in duplicate. The acid ceramidase inhibitor SOCLAC was used as a pharmacological control for the assay[26]. The Z'-factor per plate were consistent with those obtained during the initial validation. A total of 116 compounds of the 4100 screened at 20 µM met the active criterion, based on the hit cut-off at % inhibition >40, in the single-point primary screen, what resulted in a hit rate of 2.8%. An example hit map from one screening plate is shown (Figure 2(C)). The inhibitory activity of these hits was then validated in an additional assay performed at a single-point concentration in triplicates.

To confirm the results from the primary screening, top hits were cherry-picked and tested in a concentration-dependent response assay with triplicates per sample. Thus, 101 compounds were then subjected to 8-points two-fold dilution series starting at a maximum concentration of 200 micromolar. Among them, nine exhibited dose-dependent inhibition of AC with IC_{50} values in the range of 6 and 49 µM (Table 1, Figure 3), whereas 92 compounds showed a higher IC_{50} value or did not yield a concentration-dependent inhibition (structures not disclosed).

Table 1. The hit molecules identified through the primary assay performed at a single-point concentration of 20 µM were dose-titrated to establish their IC_{50} values (95% confidence interval).

Unique ID	% Inhibition	IC_{50} (µM)
W000113414_I13	67.39	6.6 (9.5–12.9)
W000113402_O07	53.75	7.9 (6.9–9.0)
W000113403_I18	63.38	10.6 (9.5–11.7)
W000113402_C12	75.46	10.6 (9.3–12.0)
W000113414_H19	61.39	11.1 (9.5–12.9)
W000113400_H06	41.71	15.8 (11.1–22.8)
W000113407_J11	59.17	23.9 (20.1–28.4)
W000113414_D15	60.38	36.7 (30.2–45.5)
W000113414_C16	58.95	48.9 (41.9–57.5)

Values shown are means of three replicates experiments.

Inhibition of neutral ceramidase

As mentioned above, hydrolysis of ceramides occurs by the action of ceramidases which are encoded by five known genes and are distinguished by the pH required for optimal activity[9]. A common problem with AC inhibitors, especially those one with a scaffold related to the structure of ceramide, is the lack of selectivity over other ceramidases. Thus, to discard a selectivity issue, the activity

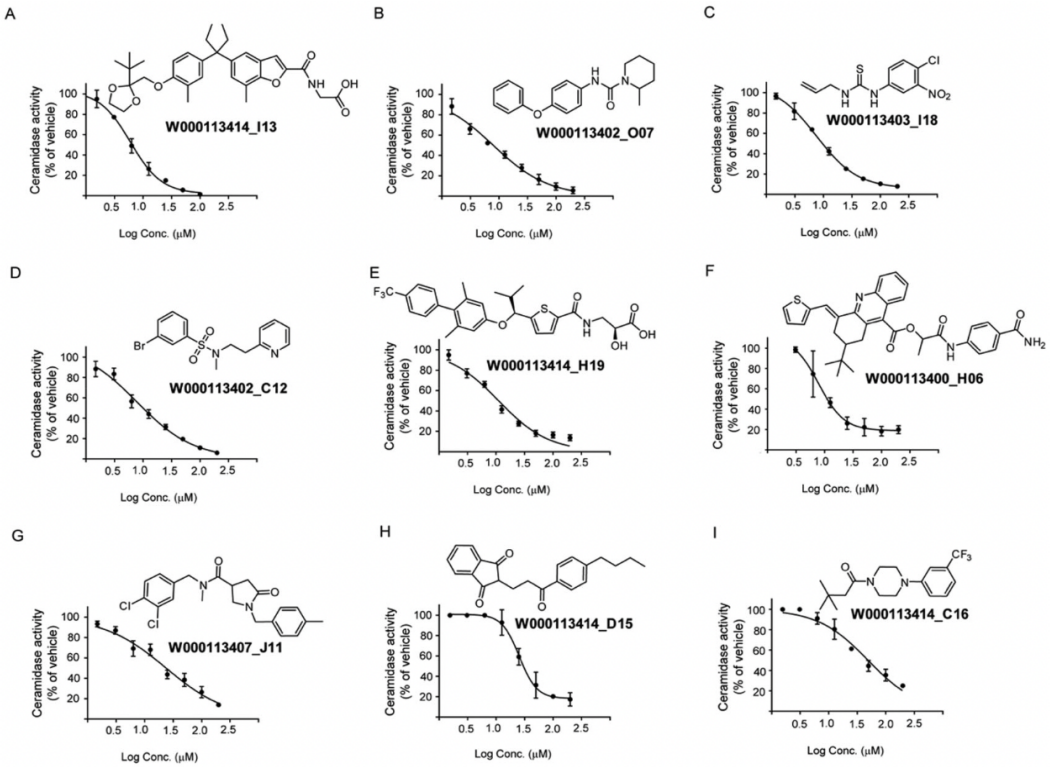

Figure 3. Structure of the identified inhibitors and their concentration-response curves. Active compounds were dose-tritiated to establish the corresponding IC_{50} values ($N = 3$ well per replicate point, errors bars are shown).

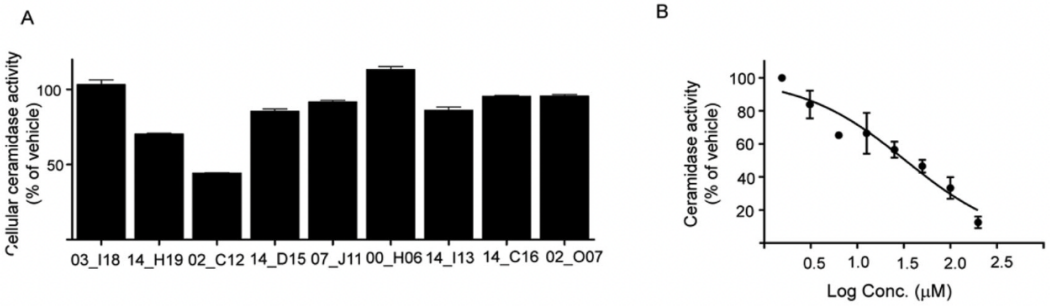

Figure 4. (A) Cellular validation of hit compounds on acid ceramidase. The hit molecules identified during the primary validation were investigated using a cellular assay. Values shown are mean of three replicates and results are expressed as percentage of activity compared to vehicle control. Compounds are identified with the last 5 letters/numbers of their unique code (B) Concentration-response curve of the most potent hit molecule W000113402_C12 in a cellular assay.

of nine detected hits against neutral ceramidase was next explored at 50 μM. Activity over NC was tested using recombinant human NC (rhNC) and a specific NC substrate bearing a nervonic acid amide (RBM14-C24:1)[30]. Remarkably, none of the molecules elicited a significant inhibitory activity, thereby confirming the selective inhibition of AC over NC (Supplemental Table 1).

Cellular inhibition of acid ceramidase

Cell-based assays allow evaluating biological activity in a more physiologically relevant system that also considers additional factors that might have a positive impact on inhibitory potency such as permeabilization through cellular membranes, metabolisation or concentration by intracellular compartmentalisation. Thus, the activity of the nine selected hits was next examined in intact cells using AC overexpressing A375 cells and the fluorogenic substrate RBM14-C12. First, compounds were tested in a primary screening assay. Measurements were performed in triplicated at a single-point concentration of 20 μM. The results showed that only two of the 9 tested compounds exhibited a significant inhibition of AC activity at this concentration: W000113402_C12 with a 53% inhibition and W000113414_H19 with a weaker 32% inhibition, whereas slight effects were observed for the other hits (Figure 4(A)). Dose-dependent inhibition could be also confirmed for W000113402_C12 in the cell-based assay displaying an IC_{50} of value of 32 μM (24.3–44.7) (Figure 4(B)).

Summary and conclusions

HTS is still the primary hit-finding strategy both in academia and industry. However, the identification of novel AC inhibitors has been hampered by the unavailability of appropriate screening platforms. Herein, we report a robust and cost-effective assay for the determination of AC activity that enables the rapid profile of

large compound libraries. The screening platform has been employed to evaluate a 4100 compound library leading to the identification of 9 novel compound classes targeting AC activity with low micromolar IC_{50}. Dose-dependent inhibition was confirmed for the primary hits identified in the screening campaign and now they can serve as a basis for hit-to-lead optimisation through chemical modifications, thereby opening new venues in the field of AC inhibition. Moreover, the reported technique can be considered an attractive drug-screening platform with a great potential to identify novel AC modulators. To further validate hits obtained in HTS campaigns of large libraries, an orthogonal assay using a different detection method (e.g. C12-Ceramide Bodipy and HPLC-based detection of substrate and reaction product) could be applied to discard potential interference of compounds on the fluorescence-based assay[31]. As several diseases are linked to altered AC activity, novel compounds modulating its activity should allow progress in drug discovery and expand our knowledge in the essential role of this enzyme.

Materials and methods

Compound library

A library containing 4100 compounds was obtained from Eli Lilly. Compounds were distributed in triplicates in 384-well microtiter plates at a 10 mM concentration in DMSO (0.4 µL). Compounds were identified with a unique code. Plates were stored at −20 °C until use. Immediately prior to use, plates were withdrawn from −20 °C storage, thawed an ambient temperature and centrifuged.

Cell culture

The A375 cell line stably overexpressing *ASAH1* under the control of a tetracycline/doxycycline-responsive promoter was kindly provided by Dr. Carmen Bedia and Prof. Thierry Levade[17]. The antibiotic selection of this cell line was performed with blasticidin (3 µg/mL) and hygromycin B (250 µg/mL). Ectopic expression of AC was induced with doxycycline at 1 µg/mL for 24 h before use. Cells were suspended in the appropriate volume of a 0.25 M saccharose solution with the proteases inhibitors aprotinin (1 mg/mL), leupeptin (1 mg/mmL) and PMSF (100 mM). The suspension was submitted to three cycles of a 5 s sonication (probe) at 10 watts/5 s resting on ice. The cell lysate was centrifuged at 600 g for 5 min. The supernatant was collected and protein concentration was determined with BSA as a standard using the bicinchoninic acid (BCA) protein determination kit (Thermo Scientific) according to the manufacturer's instructions.

Acid ceramidase HTS assay

A previously described 96-well plate assay[25] was miniaturised into a 384-well plate format with a final reaction volume of 32 µL. Plated compounds were diluted with a mixture of DMSO/H_2O (1.6 µL/18 µL), and after centrifugation, 3.2 µL were dispensed into a new 384-well plate, so that the final concentration of the compound in the final reaction volume of 32 µL was 20 µM and the DMSO content of the assay was 1%. Next, 20.8 µL of a substrate solution of RBM14-C12 in sodium acetate buffer (25 mM, pH 4.5) was added for a final concentration of 20 µM, followed by the addition of 8 µL of a 0.25 M sucrose solution of cell lysates from AC-overexpressing A375 melanoma cells containing 0.4 µg of protein The reaction was terminated after 60 min incubation at 37 °C by adding 8 µL of methanol. Oxidation was performed by treatment with 32 µL of a [2.5 mg/mL] solution of NaIO4 in 100 mM glycine-NaOH buffer (pH 10.6). The plates were incubated at 37 °C in the dark for another 1 h. Finally, 32 µL of 100 mM glycine-NaOH buffer (pH 10.6) were added and fluorescence was measured spectrophotometrically at excitation and emission wavelength of 355 and 460 nm, respectively. Blank reactions contained the same constituents as the test reactions except the cell lysates.

Neutral ceramidase assay

The NC assay was performed in 96-well plates at a final volume of 100 µL/well. Reaction buffers was 25 mM phosphate buffer 150 mM NaCl 1% (NaChol) pH 7.4. The reaction mixtures contained 25 µL/well of protein (5 ng recombinant NC R&D Systems, >95% pure), 70 µL/well of substrate (prepared from 4 mM stock solutions in ethanol) and 5 µL/well of inhibitor (prepared from 1 mM stock solutions in DMSO/H_2O). Reaction mixtures were incubated at 37 °C for 1 h and reactions were stopped with 25 µL/well of MeOH followed by 100 µL/well of NaIO4 (2.5 mg/mL in 100 mM glycine-NaOH buffer, pH 10.6). After incubation at 37 °C for 1 h in the dark, 100 µL/well of 100 mM glycine-NaOH buffer (pH 10.6) was added and fluorescence was measured spectrophotometrically at excitation and emission wavelenght of 355 and 460 nm, respectively. The same reaction mixtures without enzymes were used as blanks.

Fluorogenic ceramidase activity assay in intact cells

To determine activity in intact cells, 2×10^4 cells/well were seeded in 96-well plates 24 h prior to the assay and maintained at 37 °C and 5% CO_2. Overexpression of AC was induced with doxycycline at 1 µg/mL for 24 h. Medium was replaced by 100 µL of fresh medium (DMEM 10% FBS) containing 20 µM of the substrate and different concentrations of the indicated test compounds. Both substrates and test compounds were added simultaneously to the cell culture. The plate was incubated for 3 h at 37 °C in 5% CO2. The reaction was stopped with 25 µL/well of MeOH and then 100 µL/well of $NaIO_4$ (2.5 mg/mL in glycine-NaOH buffer, pH 10.6) were added. After incubation at 37 °C for 1 h in the dark, 100 µL/well of 100 mM glycine-NaOH buffer (pH 10.6) were added and fluorescence was measured spectrophotometrically at excitation and emission wavelengths of 355 and 460 nm, respectively. The same reaction mixtures without cells were used as blanks.

Disclosure statement

No potential conflict of interest was reported by the author(s).

Funding

This work was supported by the Ministerio de Economica, Industria y Competitividad under the Grant CTQ2017-85378-R. The authors thank Eli Lilly for providing the compounds tested in this study. Mazen Aseeri was financially supported by a scholarship from the Saudi Arabian Ministry of Higher Education.

ORCID

José Luis Abad http://orcid.org/0000-0002-8343-9611
Antonio Delgado http://orcid.org/0000-0003-4586-6070
Gemma Fabriàs http://orcid.org/0000-0001-7162-3772
Gemma Triola http://orcid.org/0000-0003-4177-8989
Josefina Casas http://orcid.org/0000-0002-7926-5209

References

1. Hannun YA, Obeid LM. The ceramide -centric universe of lipid-mediated cell regulation: stress encounters of the lipid kind. J Biol Chem 2002;277:25847–50.
2. MacEyka M, Spiegel S. Sphingolipid metabolites in inflammatory disease. Nature 2014;510:58–67.
3. Obeid LM, Linardic CM, Karolak L, Hannun YA. Programmed cell-death is mediated by ceramide. Clin Res 1993;41:A240.
4. Nganga R, Oleinik N, Ogretmen B. Mechanisms of ceramide-dependent cancer cell death. Adv Cancer Res 2018;140:1–25.
5. Filippov V, Song MA, Zhang K, et al. Increased ceramide in brains with Alzheimer's and other neurodegenerative diseases. J Alzheimers Dis 2012;29:537–47.
6. Turpin-Nolan SM, Brüning JC. The role of ceramides in metabolic disorders: when size and localization matters. Nat Rev Endocrinol 2020;16:224–33.
7. Ogretmen B, Hannun YA. Biologically active sphingolipids in cancer pathogenesis and treatment. Nat Rev Cancer 2004;4:604–16.
8. Riboni L, Campanella R, Bassi R, et al. Ceramide levels are inversely associated with malignant progression of human glial tumors. Glia 2002;39(2):105–13.
9. Mao C, Obeid LM. Ceramidases: regulators of cellular responses mediated by ceramide, sphingosine, and sphingosine-1-phosphate. Biochim Biophys Acta Mol Cell Biol Lipids 2008;1781:424–34.
10. García-Barros M, Coant N, Kawamori T, et al. Role of neutral ceramidase in colon cancer. FASEB J 2016;30:4159–71.
11. Yin Y, Xu M, Gao J, Li M. Alkaline ceramidase 3 promotes growth of hepatocellular carcinoma cells via regulating S1P/S1PR2/PI3K/AKT signaling. Pathol Res Pract 2018;214:1381–7.
12. Chen C, Yin Y, Li C, et al. ACER3 supports development of acute myeloid leukemia. Biochem Biophys Res Commun 2016;478:33–8.
13. Saad AF, Meacham WD, Bai A, et al. The functional effects of acid ceramidase overexpression in prostate cancer progression and resistance to chemotherapy. Cancer Biol Ther 2007;6:1455–60.
14. Realini N, Solorzano C, Pagliuca C, et al. Discovery of highly potent acid ceramidase inhibitors with in vitro tumor chemosensitizing activity. Sci Rep 2013;3:1035.
15. Mehta S, Blackinton D, Omar I, et al. Combined cytotoxic action of paclitaxel and ceramide against the human Tu138 head and neck squamous carcinoma cell line. Cancer Chemother Pharmacol 2000;46:85–92.
16. Doan NB, Alhajala H, Al-Gizawiy MM, et al. Acid ceramidase and its inhibitors: a de novo drug target and a new class of drugs for killing glioblastoma cancer stem cells with high efficiency. Oncotarget 2017;8:112662–74.
17. Bedia C, Casas J, Andrieu-Abadie N, et al. Acid ceramidase expression modulates the sensitivity of A375 melanoma cells to dacarbazine. J Biol Chem 2011;286:28200–9.
18. Mahdy AEM, Cheng JC, Li J, et al. Acid ceramidase upregulation in prostate cancer cells confers resistance to radiation: AC inhibition, a potential radiosensitizer. Mol Ther 2009;17:430–8.
19. Gouazé-Andersson V, Flowers M, Karimi R, et al. Inhibition of acid ceramidase by a 2-substituted aminoethanol amide synergistically sensitizes prostate cancer cells to N-(4-hydroxyphenyl) retinamide. Prostate 2011;71:1064–73.
20. Saied EM, Arenz C. Inhibitors of ceramidases. Chem Phys Lipids 2016;197:60–68.
21. Pizzirani D, Bach A, Realini N, et al. Benzoxazolone carboxamides: potent and systemically active inhibitors of intracellular acid ceramidase. Angew Chemie - Int Ed. 2015;54:485–9.
22. Bach A, Pizzirani D, Realini N, et al. Benzoxazolone carboxamides as potent acid ceramidase inhibitors: synthesis and structure-activity relationship (SAR) studies. J Med Chem. 2015;58:9258–72.
23. Di Martino S, Tardia P, Cilibrasi V, et al. Lead optimization of benzoxazolone carboxamides as orally bioavailable and CNS penetrant acid ceramidase inhibitors. J Med Chem 2020;63:3634–64.
24. Casasampere M, Izquierdo E, Casas J, et al. Click and count: specific detection of acid ceramidase activity in live cells. Chem Sci 2020;11:13044–51.
25. Bedia C, Casas J, Garcia V, et al. Synthesis of a novel ceramide analogue and its use in a high-throughput fluorogenic assay for ceramidases. Chembiochem 2007;8:642–8.
26. Bielsa N, Casasampere M, Aseeri M, et al. Discovery of deoxyceramide analogs as highly selective ACER3 inhibitors in live cells. Eur J Med Chem 2021;216:113296.
27. Ordóñez YF, Abad JL, Aseeri M, et al. Activity-based imaging of acid ceramidase in living cells. J Am Chem Soc 2019;141:7736–42.
28. Otsuka Y, Airola MV, Choi YM, et al. Identification of small-molecule inhibitors of neutral ceramidase (NCDase) via target-based high-throughput screening. SLAS Discov 2021;26:113–21.
29. Healey RD, Saied EM, Cong X, et al. Discovery and mechanism of action of small molecule inhibitors of ceramidases**. Angew Chemie Int Ed 2022;61:e202109967.
30. Casasampere M, Bielsa N, Riba D, et al. New fluorogenic probes for neutral and alkaline ceramidases. J Lipid Res 2019;60:1174–81.
31. He X, Li C, Park J, Dagan A, et al. A fluorescent-based high performance liquid chromarographic assay to determine acid ceramidase activity. Anal Biochem 1999;274:264–9.

Supplementary Table

Unique ID	% Inhibition Neutral Ceramidase
W000113414_I13	22.9
W000113402_O07	8.5
W000113403_I18	23.4
W000113402_C12	-5.9
W000113414_H19	-8.9
W000113400_H06	35.6
W000113407_J11	20.8
W000113414_D15	-1.3
W000113414_C16	-4.1

Sup Table 1. The hit molecules in the acid ceramidase assay were investigated in a neutral ceramidase assay performed at a single-point concentration of 50 μM. Values shown are means of three replicates experiments.

SUMMARY OF THE RESULTS

The family of sphingolipids (SLs) includes a wide range of complex lipids. SLs have an important structural role in membranes and they have also emerged as critical modulators of several cellular processes such as inflammation, aging or apoptosis, among others. The bioactive lipid ceramide is the central molecule in the sphingolipid metabolic network and its generation and metabolism are key to controlling its levels and proapoptotic effects. Hence, ceramide can be generated through the de novo pathway starting from L-serine and palmitoyl-CoA, by hydrolysis of complex sphingolipids and through the recycling pathway by acylation of sphingosine. Alternatively, ceramide degradation occurs through the combined action of different ceramidases, classified according to the pH optima for their activities: acid ceramidase (AC), neutral ceramidase (NC) and three alkaline ceramidases (ACER 1-3) [134].

The thesis has mainly focused on the role of these ceramidases. To obtain potent and selective inhibitors of ceramidases has been a challenge for the last two decades. Several groups have contributed to this field of research with important advances. However, some limitations still persist and there is a need to increase the toolbox of available ligands and approaches to characterize them. The work performed in the scope of this PhD thesis focuses on the development of tools and molecules to study and modulate alkaline and acid ceramidases. In the first chapter, we report the identification of small molecule inhibitors that selectively block ACER3. Chapter 2 and 3 focuses on the development of tools to study AC. In a first approach, we have developed an Activity-based probe (ABP) to specifically label AC and then we have set up a powerful activity-screening assay, which allows the testing of a large number of compounds thereby leading to the identification of AC inhibitors belonging to new compound classes.

ACER3 is an ubiquitously expressed protein, yet very little information is known about its structure at the molecular level[132]. It is an intramembrane enzyme with a seven-transmembrane domain architecture[132]. Intracellularly, its N-terminus is exposed to the cytoplasm and the C-terminus faces the lumen of either the endoplasmic reticulum or Golgi apparatus[132]. ACER3 harbors in its core two catalytic Zn^{2+} and Ca^{2+}-binding sites, which structurally explains the known dependence of ACER3 enzymatic activity on Ca^{2+} [129]. Genetic deficiency of ACER3 causes progressive leukodystrophy at a young age, a rare disease with no available treatment[174], while ACER3 high expression was found to contribute to hepatocellular carcinoma[175] and acute myeloid leukemia[176] pathogenesis. The downregulation of ACER3 expression has shown successful inhibition of both cell proliferation and apoptosis[166]. Despite its important role in diseases, only one alkaline ceramidase (ACER) inhibitor has been reported, namely (1S,2R)-D-erythro- 2-(N-myristoylamino)-1-phenyl-1-propanol (D-e-DMAPP)[177], and the targeted ACER type has not been identified. Moreover, some studies claim that D-e-DMAPP also inhibits AC[177] and NC[178]. Thus, the identification of new compounds with properties of relevant biological interest should advance existing knowledge on ACER3 and other ceramidases, and most importantly may give rise to novel therapeutic approaches for diseases linked to aberrant ACER3 activity.

1-deoxysphingolipids (1-deoxySLs) are atypical sphingolipids differ structurally from canonical ones in that they lack the C1-hydroxyl group, which is essential in the synthesis of complex sphingolipids and for their final degradation to phosphoethanolamine and hexadecenal[28]. As such, 1-deoxySLs conversion to complex sphingolipids and their degradation via the canonical catabolic

pathway, are both not possible[28]. 1-deoxySLs are produced by mutations in the de novo pathway enzyme SPT, resulting in an increased preference for L-alanine as a substrate rather than L-serine[28,29]. Pathologically, high levels of 1-deoxySLs are of clinical relevance in hereditary sensory and autonomic neuropathy (HSAN1) or type 2 diabetes[29].

Our group has previously worked in the synthesis and biological evaluation of a set of 1-deoxySL analogs against NC, that yielded two potent NC inhibitors when tested against recombinant human NC (rhNC). Based on the structure of the most potent one (**20**), a small library of 17 analogues was next prepared. Although many compounds inhibited NC activity when screened against rhNC, two of the most potent identified inhibitors showed a remarkable reduction in potency when tested in NC-overexpressing cell lysates, suggesting that the recombinant enzyme may not be a correct model. In this thesis, and as a continuation of the work and results obtained earlier by members of our group, the 17 analogues were screened against AC and ACER3 in cell lysates. Firstly, the analogues were screened against AC at equimolar or two-fold molar concentrations compared to the substrate. The activity over AC was assayed in lysates from AC-overexpressing A375 cells using 20 µM of RBM14-C12[172]. None of the compounds elicited AC inhibition under these conditions. Next, compounds were screened against ACER3 in lysates of *ASAH2*-null mouse embryonic fibroblasts (MEFs). These cells are considered a suitable model to screen ACER3 inhibitors since they lack NC, and ACER3 is the only alkaline ceramidase detected. At basic pH, in the presence of Ca^{2+}, and at a substrate/inhibitor molar ratio of (1:2), the effect of the analogues over ACER3 activity was tested using 10 µM of the substrate RBM14-C16[179]. Interestingly, two inhibitors of ACER3 were identified **20l** and **20m**, mostly corresponding to the ω-methoxymethoxy family (Figure 8). These results suggest that inhibition activity should be always performed in cells and the use or rhNC should be avoided to discard the identification of false positive inhibitors. Moreover, this approach has enabled the identification of a compound class showing specific inhibitory activity of ACER3 (Figure 8).

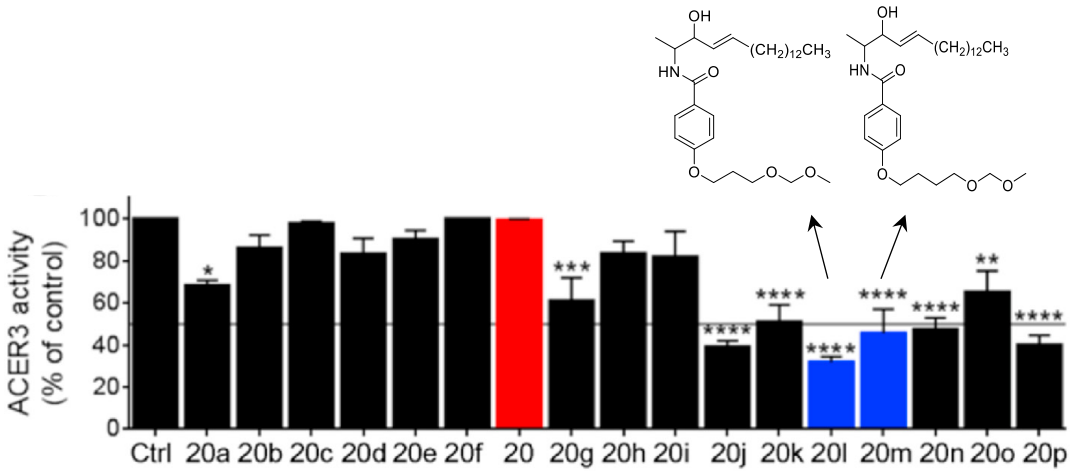

Figure 8: Activity of the 17 analogues over ACER3 (ASAH2-null cell lysates). Concentration of substrate (RBM14-C16) was 10 µM and that of the test compounds was 20 µM. Suitable buffer and pH were used. Data (mean ± SD) were obtained from two to three experiments with triplicates. Asterisks above the SD bars denote statistical significance over controls at *, $p < 0.05$; **, $p < 0.01$; ***, $p < 0.001$; ****, $p < 0.0001$, while statistical significance between specific groups is indicated with asterisks above lines (One-way ANOVA followed by Dunnett's multiple comparisons test). Compounds 20I and 20m showed the highest inhibition over ACER3 activity (Chemical structures are demonstrated).

The second part of this thesis has dealt with the development of tools to study and manipulate AC, the enzyme responsible for the cleavage of ceramide at acid pH. AC initially synthesized as a single precursor polypeptide of ~53 kDa. Later, in the lysosomes, it dissociates into α and β disulfide linked subunits (of 13 and 40 kDa, respectively), forming the mature heterodimeric active enzyme[180]. AC autocleavage and activation mechanisms resemble those of the N-terminal nucleophile hydrolases, which are enzymes characterized by breaking nonpeptide amide bonds and containing an active site-terminal nucleophile[181]. And after the dissociation of the AC precursor, the nucleophilic Cys143 is exposed at the N-terminal side of the β subunit, acting as the active site of the enzyme.

AC is among several other enzymes that degrade ceramide within mammalian cells, thus regulating its intracellular levels[182]. It hydrolyses ceramide into sphingosine and free fatty acid in the lysosome[183]. The level of ceramide, as it degrades into its metabolites, drops within cells; while the level of sphingosine rises[184]. This increased sphingosine level will then be phosphorylated by sphingosine kinase and converted into sphingosine-1-phosphate (S1P). Ceramide induces apoptosis if it accumulates in cells. On the other hand, its metabolite S1P is anti-apoptotic in nature. This rheostat between the proapoptotic and the antiapoptotic agents, if not maintained, contributes to the pathology of many diseases. Due to the overexpression of AC observed in several types of cancer, the identification of potent and selective inhibitors is an emerging field of research. Apart from its implication in cancer development, deficiency in AC activity caused by genetic mutations in *ASAH1* gene that encodes AC results in rare disorders among which is Farber's disease (FD), also known as Farber's lipogranulomatosis[185–187]. This is a rare lysosomal storage disorder characterized by decreased AC activity, which in turn leads to ceramide accumulation and diverse pathological manifestations[186–188]. Different mutations in *ASAH1* gene have been reported to be linked to the manifestation of FD[189–195]. They often result in misfolded and misrouted proteins, which are ultimately degraded via the endoplasmic reticulum-associated degradation (ERAD) pathway. To date, treatment for FD is primarily palliative, and severely affected patients die at a very young age. Ongoing clinical trials entail hematopoietic stem cells[196] or bone marrow transplantation[197] and gene therapy[198], however the therapeutic outcomes are still far away from satisfactory. Enzyme replacement therapy (ERT) and pharmacological chaperone therapy (PCT)[199,200] are emerging as promising therapeutic approaches. PCT is based on the use of small chaperone molecules designed to promote proper folding of mutated enzymes and facilitate their correct trafficking to their site of action[201,202]. The applicability of this treatment approach has been studied in many lysosomal storage disease[203–205], but not yet in FD. One attractive tool to study the effect of chaperones are activity-based probes (ABPs), small molecules able to label and therefore follow the localization of active enzymes in living cells. ABPs have proved its utility in visualizing several enzymes[206–208], including glucocerebrosidase in Gaucher fibroblasts[209]. Furthermore, ABPs have a broad range of additional uses[210]. Besides evaluating the beneficial outcomes of a potential PCT on the quantity and proper localization of mutant enzymes, they are used in the profiling of variations in enzyme activity in healthy and diseased cells, as well as the screening of inhibitors in live cells. Thus, ABP can assess enzyme activity and inhibition in a cell environment, thereby showing a considerable advantage over classical enzymatic assays such as displaying information about cell permeability or direct target engagement. Despite all these useful applications, very few ABPs for AC detection have been reported. Recently, a fluorescent

analogue of the AC inhibitor carmofur has been reported and it has been employed for AC detection in Gaucher tissue homogenates[211]. However, no ABP has been successfully applied for imaging AC in live cells.

Previous efforts of our group were taken to design probes based on the structure of the reported irreversible AC inhibitor SABRAC; a ceramide analogue modified at the amide linkage with a 2-bromoacetyl moiety. The SABRAC analogues were synthesized and found to inhibit wild-type AC activity with very high potencies. Due to the fact that in preliminary experiments SOBRAC was the most potent among all other SABRAC analogues, its fluorescent (BODIPY-SOBRAC) and an azide-tagged (N_3C_{14}SOBRAC) derived probes were synthesized for enzyme labelling. SABRAC and its analogues were expected to form adducts with the catalytic Cys143 by displacement of the halogen atom by the Cys thiolate function. Formation of covalent adducts was confirmed in the group by mass spectrometry analysis of the peptides resulting from trypsin digestion of recombinant human AC (rhAC) exposed to the inhibitors.

Later, AC detection was performed using a two-step and a one-step labelling protocols. In the two-step approach, strain promoted alkyne–azide cyclo-addition (SPAAC)-enzyme labeling using N_3C_{14}SOBRAC and DBCO-$PEG_4$5/6-TAMRA as alkyne partner allowed in-gel fluorescence labelling of rhAC as a single band at the expected molecular weight of β-subunit (i.e. 40 kDa). Successful labelling of AC was also seen in cell lysates of AC-overexpressing A375 melanoma cells, however high unspecific staining was observed. To discard potential unspecific labelling of DBCO-$PEG_4$5/6-TAMRA, the simple one-step labeling approach using BODIPY-SOBRAC was subsequently applied. Although AC labelling in AC-overexpressing A375 cell lysates using BODIPY-SOBRAC was successful with short incubation times, the background staining continued to appear (Figure 9B). The AC labelling was achieved in this case after only 5 min of reaction with the probe and increasing the incubation time did not augment the band intensity but did augment the unspecific labelling. Similarly, unspecific BODIPY-SOBRAC labelling was observed in-gel fluorescence analysis of lysates from Farber fibroblasts FD1, with zero AC activity, and the same one transduced to overexpress AC (FD1/AC) (Figure 9B). No band corresponding to labeled AC was detected in FD1 lysates, while fluorescently labeled AC was clearly visualized in FD1/AC extracts (Figure 9B). This background staining is likely due to unspecific reaction of SOBRAC high reactive bromine with intracellular electrophiles. SOCLAC, another SABRAC analogue, bearing a less reactive chlorine, was then nominated for fluorescent-probe designing as a potentially more specific AC labeler. Once synthesized, the reactivity of BODIPY-SOCLAC with Cys143 was first confirmed by mass spectrometry analysis of the protein exposed to the inhibitor followed by tryptic digestion.

In this study, and as a continuation of the previous work and results obtained by a member of our group, labelling of AC using BODIPY-SOCLAC was attempted in lysates from HEK293T (HEK) or Farber FD2 cells transfected with empty vector (EV), wild-type AC (WT) and an in active AC mutant (Mut), in which the active-site cysteine was replaced by serine (C143S). The activity of AC contained in these transfected cells has been measured (Figure 9A). As expected, this mutation provoked the loss of AC activity, while the enzyme was active in cells transfected with the WT gene. In-gel fluorescence analysis after labeling with BODIPY-SOCLAC, revealed a band only in extracts from cells transfected with the WT but not in the one transfected with the mutant vector

(Figure 9B). Conversely, both WT and mutant proteins were detected by Western blot (WB) (Figure 9C), highlighting a promising feature of the probe: unlike antibodies, which recognize both inactive and active AC, BODIPY-SOCLAC can clearly detect the active form of AC and distinguish it from the inactive enzyme. Importantly, the use of BODIPY-SOCLAC resulted in a remarkable reduction of nontarget labeling as compared to BODIPY-SOBRAC treatment, with the band corresponding to labeled AC being the almost exclusive one (Figure 9B). Coomassie blue staining was performed on the gel to confirm that equal amounts of protein were loaded (Figure 10).

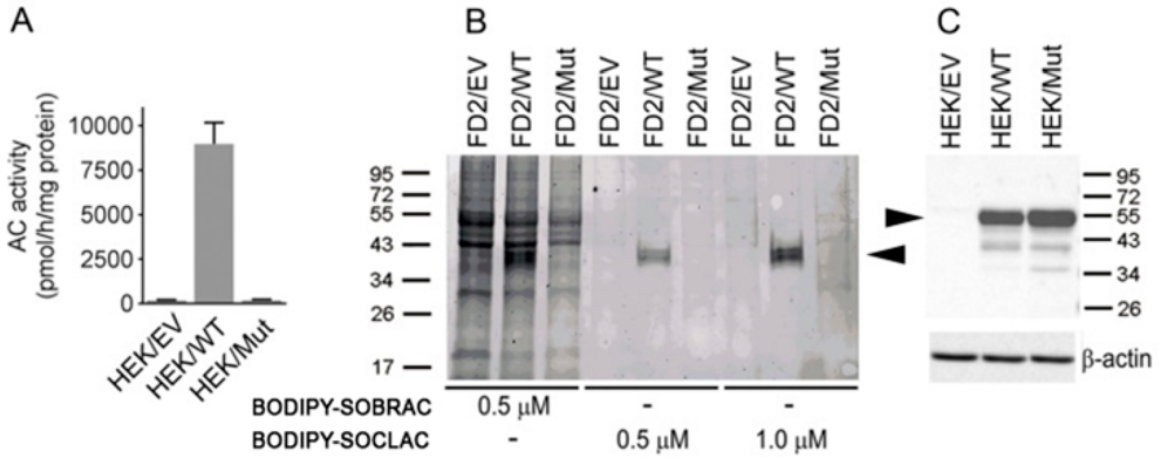

Figure 9: In vitro labeling of AC with BODIPY- SOCLAC. Cell lysates were incubated with the indicated concentrations of the specified probes for 5 min, and the reaction mixtures were resolved on SDS-PAGE before in-gel fluorescence analysis. Protein extracts were from HEK293T (HEK) cells or Farber FD2 cells transfected with an empty vector (EV), wild-type AC (WT), or an inactive AC mutant (C143S) (Mut). AC activity of lysates used in panel C are shown in A. WB detection of AC is shown in C. Arrows indicate labeled AC.

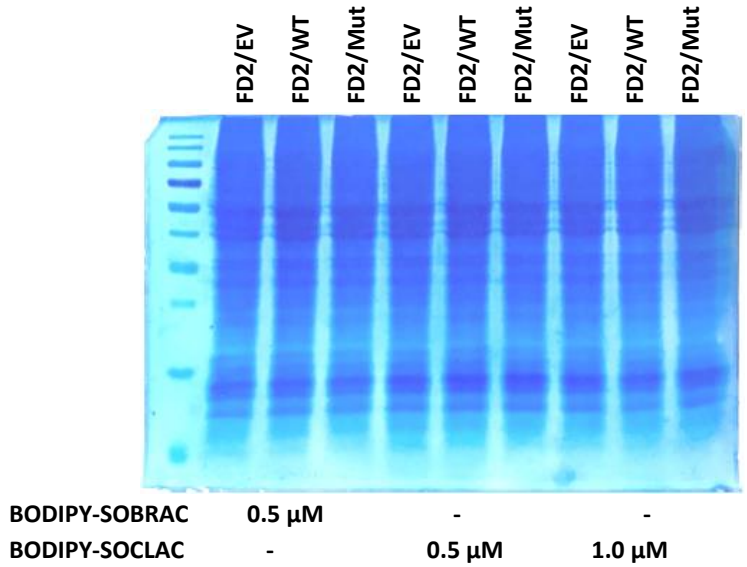

Figure 10: The same gel shown in figure 9 was stained with Coomassie blue to confirm that equal amounts of protein were loaded.

Encouraged by these results, the detection of endogenous AC by BODIPY-SOCLAC was examined in lysates of cell lines with different levels of AC expression (Figure 11A). The protein was detected in both A549 cells and fibroblasts from a healthy individual (CTRL), and the level of detection correlated well with the AC enzymatic activity contained in every cell line (Figure 11A and 11B), thus indicating that the probe can be employed to label endogenous levels of AC. As found with BODIPY- SOBRAC, increasing the incubation time with BODIPY- SOCLAC (1 µM) beyond 5 min did not augment the AC band intensity but led to increased unspecific labeling (Figure 12A). This observation agrees with the time-dependence of AC inactivation by BODIPY-SOCLAC, showing that only 10% of activity remained after a 15 min incubation with a 0.2 nM concentration (5-fold lower than that used in the labeling experiment). The gel was stained with Coomassie blue to reveal the equal protein quantities loaded in each sample (Figure 12B). This rapid and efficient reaction with the target prevents off-target labeling. We next determined the selectivity of target binding by competition with the unlabeled ligand (Figure 11C). AC labeling decreased concentration dependently as SOCLAC concentration augmented (Figure 11C). Again, the gel was stained with Coomassie blue for ensuring equal protein loading assessment (Figure 13).

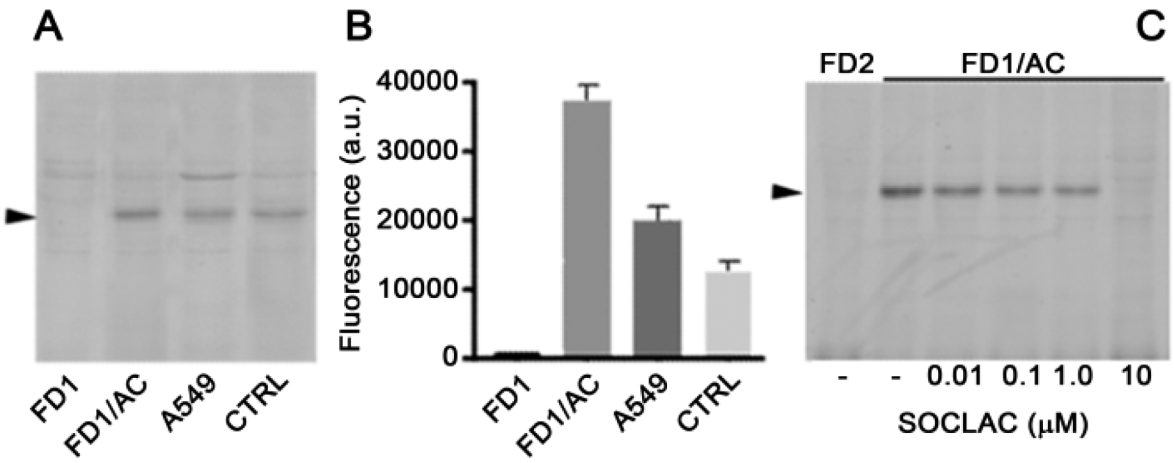

Figure 11: (A) In vitro labeling of endogenous AC with BODIPY-SOCLAC. Cell lysates (34 µg of protein) were incubated with the probe (1 µM/5 min), and the reaction mixtures were resolved on SDS-PAGE before in-gel fluorescence analysis. CRTL, fibroblasts from a healthy individual. (B) AC activity of samples used in gel A, as determined with the fluorogenic assay. (C) Competition with unlabeled ligand. Lysates from FD1/AC cells were preincubated for 5 min with the specified concentrations of SOCLAC (competitor) followed by 5 min incubation with 1 µM probe.

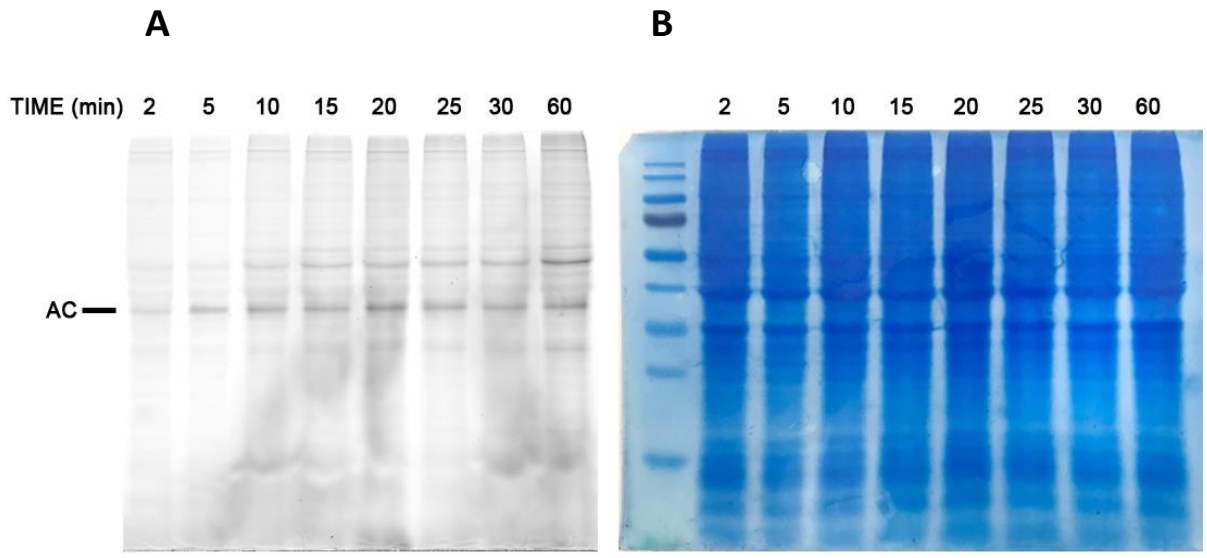

Figure 12: (A) Time course of in vitro labelling of acid ceramidase with Bodipy-SOCLAC. Lysates from control fibroblasts (25 µg of protein) were incubated with the probe (1 µM) for the specified times and the reaction mixtures were resolved on SDS-PAGE before in- gel fluorescence analysis. (B) the same gel stained with Coomassie blue to assess loading.

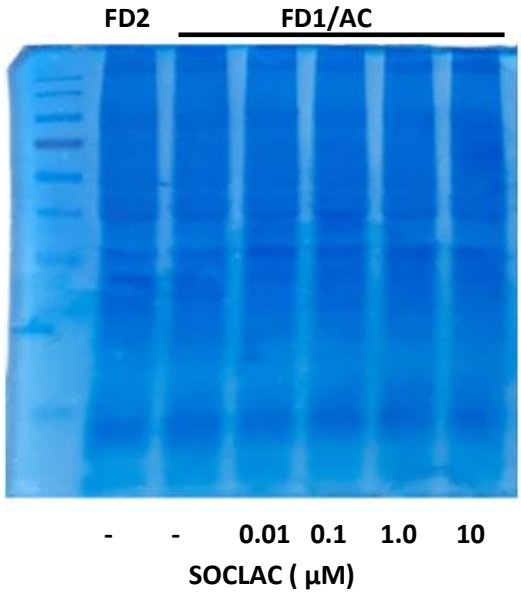

Figure 13: The same gel shown in figure 11C was stained with Coomassie blue to confirm that equal amounts of protein were loaded.

Because BODIPY-SOCLAC afforded an excellent labeling of AC in cell lysates, we next investigated whether labeling of AC in intact cells was also feasible. To this end, BODIPY- SOCLAC (1 µM/5 min) was added to culture medium of cell lines with different levels of AC expression, and labeling was analyzed by confocal scanning microscopy. Intracellular compartment staining was observed upon treatment of A549, fibroblasts, and FD1/AC cells with BODIPY-SOCLAC (Figure 14). Colocalization with LysoTracker indicated that BODIPY-SOCLAC was contained in the lysosomes, in agreement with the lysosomal location of AC, the probe target. In FD1 cells, BODIPY-SOCLAC did not afford a

vesicular pattern colocalizing with LysoTracker, in agreement with the absence of AC in this cell line. No lysosomal labeling was observed after BODIPY-SOCLAC treatment of three different homozygous Farber fibroblasts (FD2−FD4) producing mutant proteins. The impact of these mutations on AC activity was assessed using the fluorogenic assay (Figure 15). Interestingly, some lysosome labeling occurred with BODIPY- SOCLAC in FD4 cells, which are those retaining some AC activity. All in all, this part of the thesis has focused on the characterization of a novel ABP for AC based on the structure of the irreversible inhibitor SABRAC. The probe, bearing a chlorine moiety instead of a bromine, have proven useful in-gel AC detection and can be employed to stain endogenous levels of active, but not inactive, enzyme in intact cells. As a result, BODIPY-SOCLAC can be considered a valuable tool for the study of AC activity and may facilitate the screening of AC inhibitors or chaperones for the treatment of diseases characterized by an abnormal expression of AC.

AC is overexpressed in numerous human cancers and its inhibition can be beneficial for cancer treatment[212,213]. Therefore, and due to the important role of AC in cancer, several investigators have proposed the use of AC inhibitors in cancer therapy with the potential outcome of promoting apoptosis and/or lowering resistance to drugs[214,215]. The findings suggest that the inhibition of AC activity may act as a valuable target, whether used solely or combined with other anti-oncogenic treatments[215]. Although AC inhibition has been intensely investigated in the last decade, only very few inhibitors were useful in vivo[216]. Moreover, most of the reported inhibitors are structurally related to ceramide which has a negative impact on their selectivity, potency and drug-like properties. Thus, the discovery of ceramide-unrelated hits would be highly desirable. The main issue facing the investigators concerning the use of AC inhibitors is the specificity and potency of the discovered hits[214]. AC is among five other mammalian ceramidases, thus the development of highly specific inhibitors is important to avert off-targeting and toxicity effects[214]. Some potent and structurally unrelated inhibitors of AC have already been described. Representative examples of this class of compounds are carmofur, identified after the screening of a commercial library using a LC/MS-based assay[217] and the related dioxypyrimidine and benzoxazolone carboxamides[218–220]. Despite these relevant examples, there is still a great need for the identification of novel molecules that can expand the toolbox of AC inhibitors. One of the best methods to identify structurally diverse inhibitors is through the screening of large compound libraries. However, this approach requires a powerful, robust and cost-effective high-throughput screening (HTS) assay, allowing the rapid and reliable testing of a large number of compounds. In order to fulfill this demand, in the third section of this Ph.D. thesis a fluorescence-based AC assay has been optimized and adapted to a 384-well format. Once validated, it has been employed to evaluate a 4100-compound library leading to the identification of novel AC inhibitors.

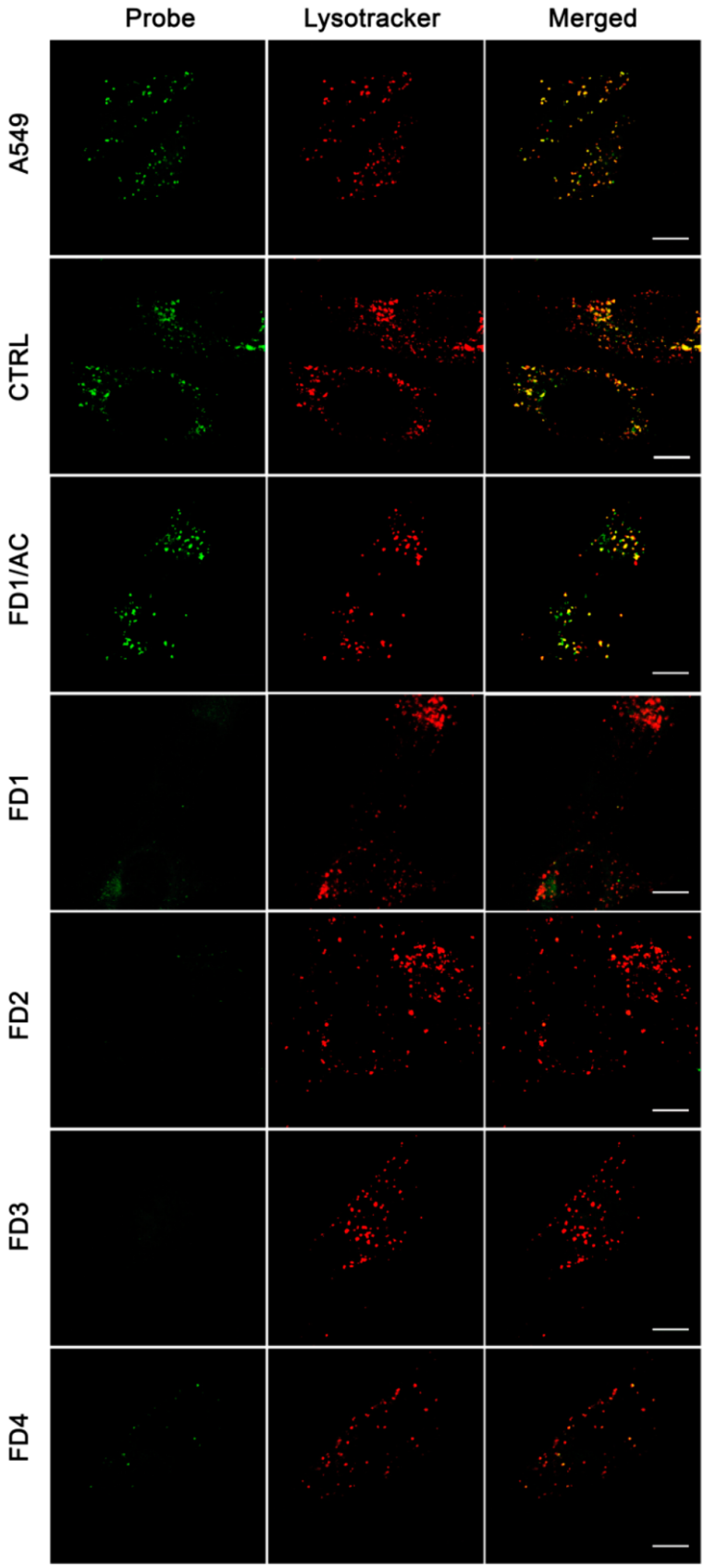

Figure 14: In situ AC labeling. Representative fluorescence micro- graphs of cells with different levels of AC, namely, lung adenocarcinoma A549, skin fibroblasts of a healthy individual (CTRL), FD1 cells transduced to overexpress AC (FD1/AC), and different Farber cells (FD1–FD4). Cells were treated with BODIPY- SOCLAC (1 μM/5 min). Then they were washed and placed back in the incubator, and images were taken after 2 (A549), 3.5 (CTRL), and 5 h (FD1–FD4 and FD1/AC). LysoTracker (75 nM/60 min) was added 1 h prior to visualization.

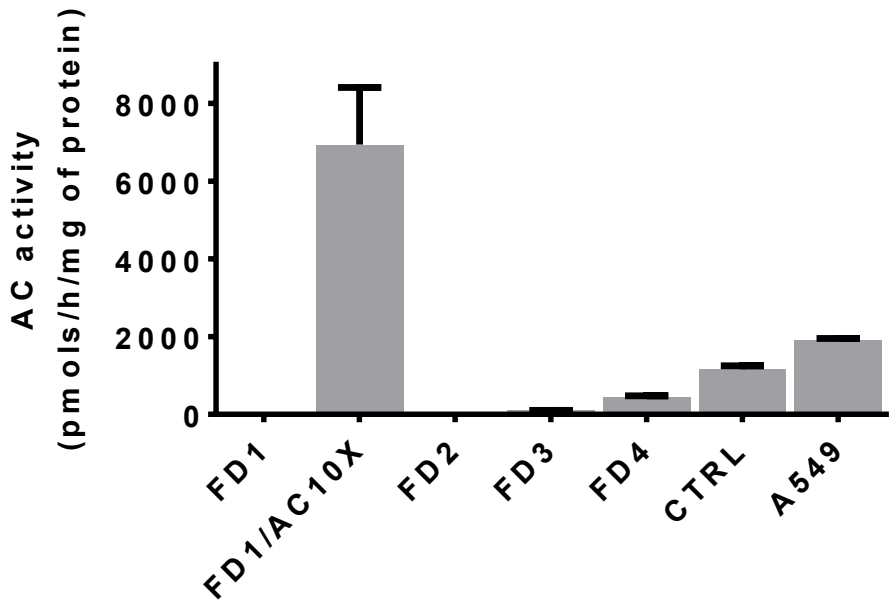

Figure 15: AC activity of cells imaged in Figure 14. Activity was determined in cell lysates at pH 4.5 following the standard fluorogenic protocol. FD refers to Farber cells and CTRL refers to skin fibroblasts of a healthy individual. Data (mean ± SD, n=4) were obtained from two experiments with triplicates.

As mentioned above, the screening for specific and potent AC inhibitors requires the availability of a HTS assay capable of examining relatively large number of compounds simultaneously. A fluorescent-based assay in a 96-well format was previously set up in our group and applied to measure AC activity using cell lysates and intact cells as sources of enzyme. The assay is based on the coumarinic substrate RBM14-C12, that shows a high affinity and specificity for AC over neutral and alkaline ceramidases. Briefly, the hydrolysis of the amide bond of RBM14-C12 by AC yields an aminodiol that can be then oxidized upon treatment with sodium periodate. The resulting aldehyde undergoes a β-elimination reaction to release the fluorescent product umbelliferone. The assay has been largely used by our group and others to identify novel ceramidase inhibitors[218,221]. However, increasing the capacity of assays is necessary to expedite drug discovery by conducting high-throughput screening (HTS) of massive chemical libraries. This will not only speed up the process but would cut down costs as well. Consequently, this thesis tackled this challenge by miniaturizing the existing 96-well AC assay and adapted it to a 384-well format. And to ensure the reliability and efficiency of this miniaturized assay, a 4100-compound library was screened, resulting in the discovery of novel AC inhibitors.

To start with, the final reaction volume was adapted from 100 µL (96-well-format) to 32 µL (384 well-format) with a final concentration of substrate of 20 µM. Similarly, the volumes of methanol and buffered solution added in 96-well assay were proportionally reduced by approximately threefold. Next, protein concentration was adjusted using cell lysates of AC-overexpressing A375 melanoma cells. Ideally, the optimal amount of protein is the one that ensures reaction linearity over a period of time together with less than 10% of substrate depletion, in order to assume that the enzyme operates at steady-state conditions. Thus, different amounts of cell lysates were mixed with the substrate and product formation was measured over 1 hour (Figure 16(A)). Finally, an amount of 0.4 µg of protein was chosen, as higher amounts of proteins were not in the linear portion whereas lower amounts would compromise the signal window. The optimal incubation time of the reaction mixture was next determined. A higher signal was witnessed at 2 hours reaction time. However, we chose a final reaction time of one hour since it exhibited an excellent signal window. As a first validation step, we performed a control run consisting of 60 wells representing AC activity and 60 wells representing the signal in absence of the enzyme. Excellent separation between high and low control wells resulting in a signal-to-background ratio >8 and a Z´factor of 0.72. The calculated coefficients of variation (CV) for both the high and low controls were 6.08% and 5.61% respectively. These data demonstrated that the assay was very robust, stable and possessed minimal well-to-well variability and therefore it is appropriate for HTS for AC inhibitors (Figure 16(B)).

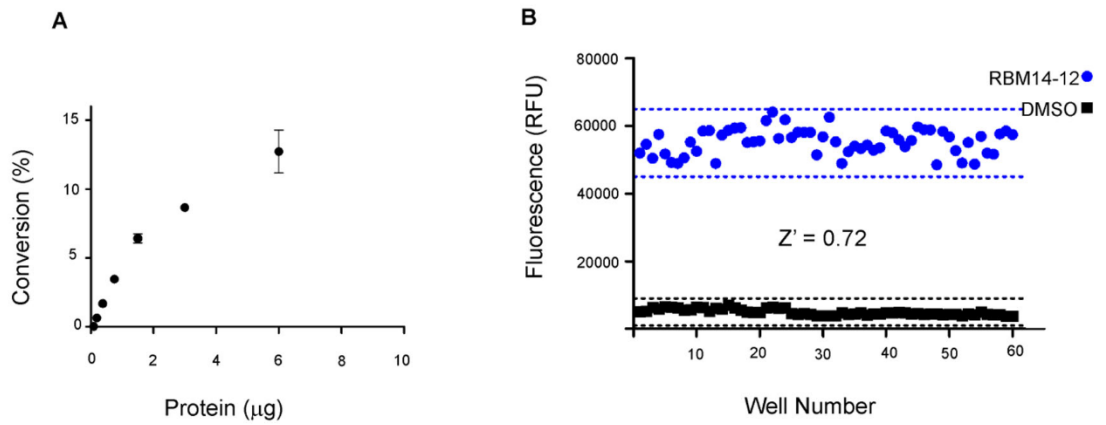

Figure 16: (A) Percentage of substrate conversion obtained using different amounts of AC (measured as µg of total protein). (B) Determination of the Z'-factor (Z') of the AC assay in the 384-well plate format. Solid black squares and solid blue circles represent negative (without protein) and positive reaction, respectively.

After having successfully established the optimal reaction conditions in a 384-well format, we employed this newly miniaturized AC assay in a pilot screen against a library of 4100 compounds. The screen was carried out at a single dose of 20 µM for each library compound in 6% DMSO (v/v) and in duplicate. The robustness of the screening assay was ensured by including six controls, six SOCLAC samples (AC potent inhibitor) and six blank samples. A total of 116 compounds of the 4100 screened at 20 µM met the active criterion, based on the hit cutoff at % inhibition >40, in the single-point primary screen, which resulted in a hit rate of 2.8%. The inhibitory activity of these hits was then confirmed in an alternative assay performed in triplicates at a single-point concentration.

To confirm the results from the primary screening, top hits were cherry-picked and tested in a concentration-dependent response assay with triplicates per sample. Thus, 101 compounds were then subjected to 7-points two-fold dilution series starting at a maximum concentration of 200 micromolar. Among them, nine exhibited a dose-dependent inhibition of AC with IC_{50} values under 50 µM (Table 2, Figure 17), whereas other compounds showed an IC_{50} > 50 µM or did not yield a concentration-dependent inhibition (structures not disclosed). The concentration-dependent inhibition of AC using these 9 compounds was repeated with triplicates for reassurance, and they persisted in giving an IC_{50} under 50 µM. The chemical structures of these 9 compounds were revealed by their provider (Eli Lilly and Company) (Figure 17).

Unique ID	% Inhibition	IC_{50} (μM)
W000113414_I13	67.39	6.6 (9.5–12.9)
W000113402_O07	53.75	7.9 (6.9–9.0)
W000113403_I18	63.38	10.6 (9.5–11.7)
W000113402_C12	75.46	10.6 (9.3–12.0)
W000113414_H19	61.39	11.1 (9.5–12.9)
W000113400_H06	41.71	15.8 (11.1–22.8)
W000113407_J11	59.17	23.9 (20.1–28.4)
W000113414_D15	60.38	36.7 (30.2–45.5)
W000113414_C16	58.95	48.9 (41.9–57.5)

Values shown are means of three replicates experiments.

Table 2: The hit molecules identified through the primary assay performed at a single-point concentration of 20 μM were dose-titrated to establish their IC_{50} values (95% confidence interval).

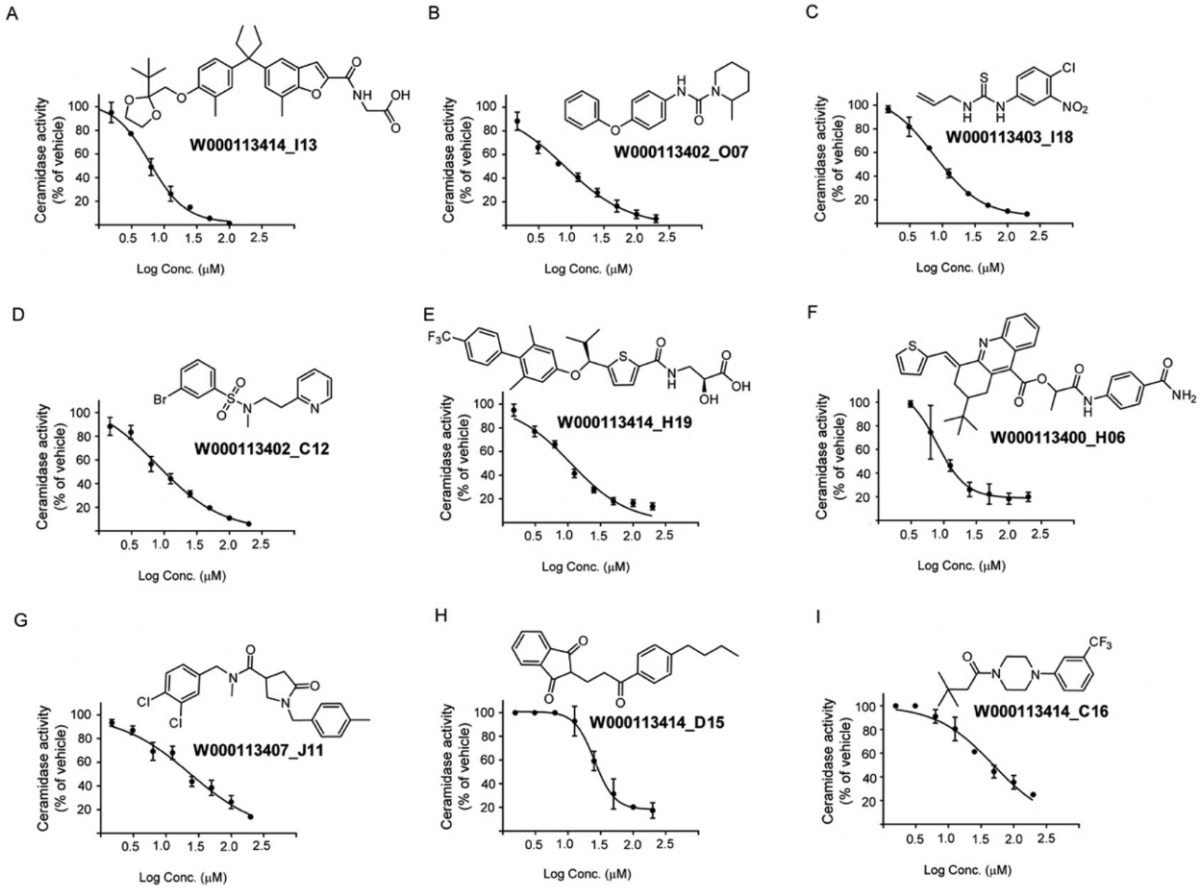

Figure 17: Structure of the identified inhibitors and their concentration-response curves. Active compounds were dose-titrated to establish the corresponding IC_{50} values (*N* = 3 well per replicate point, errors bars are shown).

As mentioned above, hydrolysis of ceramides occurs by the action of ceramidases which are encoded by five known genes and are distinguished by the pH required for their optimal activity. A common problem with AC inhibitors, especially those with a scaffold related to the structure of ceramide, is the lack of selectivity over other ceramidases. Thus, to discard the selectivity issue, the activity of the nine detected hits against neutral ceramidase was next explored. Activity over NC was tested using recombinant human NC (rhNC) and a specific NC substrate bearing a nervonic acid amide (RMB14-C24:1)[222]. Remarkably, none of the molecules elicited a significant inhibitory activity, thereby confirming the selective inhibition of AC over NC (Table 3).

Unique ID	% Inhibition Neutral Ceramidase
W000113414_I13	22.9
W000113402_O07	8.5
W000113403_I18	23.4
W000113402_C12	-5.9
W000113414_H19	-8.9
W000113400_H06	35.6
W000113407_J11	20.8
W000113414_D15	-1.3
W000113414_C16	-4.1

Table 3: The hit molecules in the AC assay were investigated in the NC assay performed at a single-point concentration of 50 µM. Values shown are means of three replicates.

On the basis of AC inhibition by the previously identified specific and potent 9 inhibitors in the cell-free system, their ability to inhibit endogenous AC in intact cells was subjected to investigation.
Cell-based assays allow the evaluation of biological activity in a more physiologically relevant system that also considers additional factors that might have a positive impact on inhibitory potencies such as permeabilization through cellular membranes, metabolization or concentration by intracellular compartmentalization. Thus, the activity of the nine selected hits was next examined in intact cells using AC-overexpressing A375 cells and the fluorogenic substrate RBM14-C12. First, compounds were tested in a primary screening assay. Measurements were performed in triplicate at a single-point concentration of 20 µM. The results showed that only two out of the 9 tested compounds exhibited significant inhibition of AC activity at this concentration: W000113402_C12 with a 53% inhibition and W000113414_H19 with a weaker 32% inhibition, whereas slight effects were observed for the other hits (Figure 18(A)). Dose-dependent inhibition could be also confirmed for: W000113402_C12 in the cell-based assay displaying an IC_{50} value of 32 µM (24.3-44.7) (Figure 18(B)).

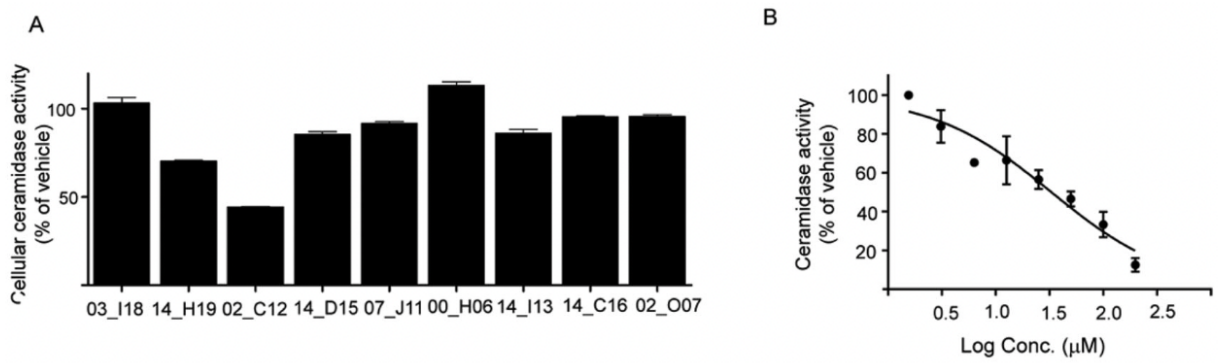

Figure 18: (A) Cellular validation of hit compounds on AC. The hit molecules identified during the primary validation were investigated using a cellular assay. Values shown are mean of three replicates and results are expressed as percentage of activity compared to vehicle control. Compounds are identified with the last 5 letters/numbers of their unique code (B) Concentration-response curve of the most potent hit molecule W000113402_C12 in a cellular assay.

The cytotoxicity of W000113402_C12 and W000113414_H19 compounds, which demonstrated decent AC inhibition both in vitro and in vivo, was studied in melanoma (A375), prostate cancer (PC3M) and colorectal cell lines (HT29). Both compounds were not toxic at concentrations under 100 μM in all three cell lines.

DISCUSSION

SLs are a structural and functional class of bioactive lipids[223,224]. They comprise of a wide range of biologically significant molecules, and are the second most found lipids in the membranes of eukaryotic cells[225]. Their defining feature is the amino-alcohol backbone of eighteen carbon atoms, also known as "spingoid base", which is synthesized in the endoplasmic reticulum (ER) from precursors of nonsphingolipid origins[225–227]. This basic structure, when it is modified, gives rise to several other SLs that play key roles in cell biology[226]. SLs are involved in the regulation of many essential biological processes such as cell signaling[228], growth[229], differentiation[230], proliferation[231,232], apoptosis[233], senescence[234] and cell death[235,236]. The proper regulation of their metabolism is fundamental to maintain cellular homeostasis. Conversely, the dysregulation of their metabolism is associated with key human diseases[224,237]. For instance, mutations in the central enzymes involved in SL metabolism cause lysosomal storage disorders[238] such as Gaucher and Farber's diseases, which are characterized by aberrant accumulation of SLs. In contrast, in numerous tumors, the high expression levels of theses enzymes increase sphingolipid metabolism, thus generating more SLs with pro-survival signaling[239]. Therefore, studies targeting these metabolic enzymes may present promising therapeutic approaches and aid in better understanding their roles and functions.

Among these enzymes, ceramidases (CDases) play a significant role in maintaining cellular homeostasis. And this is done by regulating the rheostat between the pro-apoptotic species of Cer[82] and the pro-survival and proliferative S1P[105] and, thus, contributing substantially to the cellular fate. CDases are a family of amidohydrolases that hydrolyses Cer to So and a fatty acid[121]. S1P can be generated only by the phosphorylation of So, therefore their levels are dependent on the activity of CDases. There are five human CDases, encoded by five different genes. According to their optimum pH, they are classified into acid ceramidase (AC), neutral ceramidase (NC) and three alkaline ceramidases (ACER1, ACER2 and ACER3). Each of these enzymes resides in different cellular compartment and displays distinct substrate specificities. AC is located in the lysosomes and to a lesser extent in the extracellular space[141,240]. It functions optimally at a pH value of 4.5[145] and prefers unsaturated ceramide substrates of medium chain size[144]. NC resides to the outer leaflet of the plasma membrane as an integral protein[125] and can be found secreted in the intestinal lumen[155]. NC has a pH optima that ranges from 7 to 9 and has a substrate preference for D-erythro-ceramide isomer over other ceramide isomers[124]. ACER1 is found in the ER and favors unsaturated ceramide substrates of very long chain[129,161]. ACER2 is localized to the Golgi apparatus and it utilizes ceramide of long or very long chain size as substrates[130,163]. Lastly, ACER3 is located both in the ER and Golgi apparatus and favors unsaturated ceramide of long chain, however not very long ones, as substrates[133,166].

There is growing evidence for the role that these CDases play in several cellular responses, specially by balancing the levels of Cer, So and S1P. As example, it has been reported that alkaline ceramidases (ACER1-3) are the only active ceramidases in erythrocytes and are responsible for generating the plasma S1P through regulation of So production[241]. ACER1 action has been also shown to mediate in the calcium-induced growth arrest and differentiation of epidermal keratinocytes by regulating So and S1P levels[128,129]. Similarly, ACER2 activity has been shown to regulate cell proliferation and survival by controlling the levels So and S1P[163]. In another study, ACER2 activity has also demonstrated a role in regulating the maturation of beta 1 integrin and

cell adhesion through the control of So generation[242]. Mao et al. demonstrated a role of ACER2 activity in mediating the cytotoxicity of an inhibitor of dihydroceramide desaturase in tumor cells, in this case through regulation of dhSo levels[143]. In the case of ACER3, it has been shown that its knockdown did not only inhibit cell proliferation but also inhibited serum-deprivation-induced apoptosis[166]. The role of NC in the regulation of Cer and S1P has been also extensively studied. Hence, numerous reports have shown that the activation of NC renders cells protection from cytokines-induced apoptosis by controlling Cer and S1P levels[243–246]. Tani et al. demonstrated that in CHOP cells this increase in So and S1P levels is caused by NC-mediated hydrolysis of ceramides specifically those located in the plasma membrane and the extracellular matrix[127]. In addition, Kono et al. have shown that the loss of NC activity decreases the degradation of intestinal ceramide, which therefore suggests a key role of this enzyme in the degradation of dietary SLs as well as in the regulation of Cer and So cellular levels in the gastrointestinal tract[158]. Moreover, Snider et al. demonstrated that a decrease in NC activity in inflammatory bowel diseases leads to an unanticipated increase in S1P and inflammatory responses, suggesting a possible protective role for NC in this disease[247]. In the case of AC, generally, its overexpression promotes the survival of cancerous cells through the excessive conversion of Cer into S1P. However, additional roles have been suggested for AC. Thus, Lucki et al. reported that the nuclear expression of AC in adrenocortical cells plays a role in regulating steroidogenic gene transcription by governing the levels of nuclear SLs[248,249]. Furthermore, AC expression has been found to play a critical role in the survival of newly formed embryos, as it has been shown that the knockout of AC in mice caused death in the early stages of embryos[154,250]. Conversely, death was delayed in embryos after treatment with exogenous S1P, indicating that the death occurred in embryos as a result of AC silencing was partly due to the inability to generate S1P. Additionally, AC activity has been identified to play a significant role in the development of ovaries and the survival of oocyte in theca cells, thus protecting them from death[251].

In part due to this involvement in the regulation of cell survival and proliferation, mutations or the aberrant expression of CDases are strongly connected to several diseases. For instance, genetic deficiency of ACER3 activity results in leukodystrophy in early childhood[174], a rare disease with no current treatment. Additionally, ACER3 activity has been shown to contribute to hepatocellular carcinoma[175] and acute myeloid leukemia pathogenesis[176]. On the other hand, the downregulation of ACER3 activity has been reported to not only inhibit cell proliferation through the upregulation of the cyclin-dependent kinase inhibitor p21 but also inhibit serum-deprivation-induced apoptosis[166]. There is an evidence that NC has also role in cancer supported by the findings that its downregulation has been involved in gemcitabine-induced growth suppression[252], and by recent studies demonstrating that NC participates in the regulation of cell survival in colon cancer[253,254]. Collectively, these studies have shown that NC inhibition in a xenograft model has delayed tumor growth and that mice lacking NC were protected from azoxymethane-induced tumor formation[253]. High expression of AC has been documented in various types of cancers[255], entailing head and neck cancer[256], colon adenocarcinoma[217], prostate cancer[149,150,257–261] and melanoma[151,262,263]. In fact, the overexpression of AC renders cancerous cells resistance against therapy (chemo-/radio-therapy), whereas its inhibition sensitizes them to the therapy, decreasing tumor growth and preventing cancer relapse[153,264–268]. On the other hand, genetic deficiency in genes encoding AC leads to substantial decrease in its activity causing a lysosomal storage

disorder, known as Farber disease (FD)[142]. All of the above explains the significance of CDases in diseases, the growing interest in their study and why they have been considered promising drug targets in the past few years[269]. Therefore, in this thesis, we have focused on the development of tools to study, characterize and modulate the activity of CDases. The work performed in this thesis and that will be discussed below include the development of three important tools facilitating the study of CDases: selective inhibitors, activity-based probes (ABPs) and a powerful high-throughput screening (HTS) assay.

A number of CDase inhibitors have been reported along the past two decades. The majority were identified as AC inhibitors, fewer were active on NC and almost none were potent on ACER. The problem with these identified inhibitors is that most of them were structurally related to ceramide. And this in turn has a negative impact on their selectivity, potency and drug-like properties[269]. A handful of these inhibitors, however, were not ceramide-related. For example, carmofur which is a potent AC ceramidase inhibitor identified through a screening of a commercial library[217]. Also, dioxypyrimidine and benzoxazolone carboxamides, which are structurally related to carmofur[218,220]. Despite these relevant examples, there is still a great need for the identification of novel molecules that can expand the toolbox for inhibitors of CDases.

As mentioned above, in contrast to the better-characterized AC or NC, selective inhibitors of ACER were still lacking at the time of performing this study. Here we have identified two highly selective inhibitors for ACER3, which is the most ubiquitous ACER[121]. To start with, a set of compounds belonging to the 1-deoxy (dihydro) Cer compound class was selected. These compounds are of interest because they lack the hydroxyl at the C1 position what prevents its further metabolization in complex sphingolipids thereby ensuring its metabolic stability. Initially, the screening of the compounds using a recombinant NC (rhNC) identified certain inhibitors. However, when the screening was performed with cell lysates as a source of NC, none of the inhibition could be confirmed. These results indicate that rhNC may not be an adequate source of enzyme for the identification of inhibitors. The reason behind these controversial results may lie on the structural differences existing between the commercially available rhNC and the natural enzyme. Thus, while the NC is bound to the plasma membrane with a transmembrane helix, the rhNC is a truncated enzyme soluble in water. Next, the set of compounds was tested on AC using cell lysates as a source of enzyme; however, no inhibition was observed. Finally, a screening assay to test them as ACER3 inhibitors enabled the identification of two potent inhibitors **20l** and **20m** (Figure 19). Interestingly, both compounds have a 2R,3R stereochemistry, differing from the natural 2S,3R, what suggests that they may bind an allosteric pocket and therefore they do not compete with the natural substrate for the binding site. In addition, another group member tested the inhibition effect of these inhibitors in cellular context and both compounds also inhibited ACER3 in this model system. This interesting result discloses a scaffold for further medicinal chemistry efforts aimed at improving the ACER3 inhibitory potency. Docking studies against the crystal structure of ACER3[270] should aid in the design of the best ligands for further use in the study or treatment of diseases linked to ACER3 alterations. These include enzyme blockers in the event of overexpression and chemical chaperones in case of genetic deficiencies.

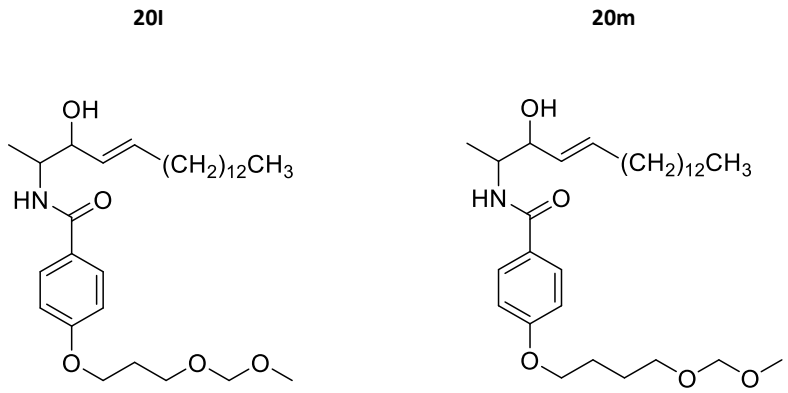

Figure 19: Chemical structures of 20l and 20m, which were found to be highly selective ACER3 inhibitors.

Another attractive enzyme target in the field of CDases is the lysosomal AC, found overexpressed in many types of cancer and responsible, when mutated, for a rare lysosomal storage disease. As a result, there is growing interest in the development of tools to characterize and study this enzyme. Our interest in this field of research was the development of novel activity-based Probes (ABPs) for AC relying on the structure SABRAC, a known AC inhibitor. SABRAC is an irreversible AC inhibitor reported previously by our group[271]. It is a ceramide analogue modified at the amide linkage with a 2-bromoacetyl moiety. SABRAC and its analogues form adducts with the catalytic Cys143 by displacement of the halogen atom by the Cys thiolate function. The presence of the sphingoid base scaffold is expected to provide selectivity toward enzymes of sphingolipid metabolism, of which only AC has been reported to be a cysteine amidase[181]. Moreover, the fact of being a covalent and an irreversible inhibitor made it a perfect candidate for the development of an ABP probe.

To start with, a fluorescent tag was attached to the probe, either directly (BODIPY-SOBRAC) or indirectly (via click chemistry reaction of an azide moiety (N_3C_{14}SOBRAC) with a strained alkyne (DBCO-$PEG_4$5/6-TAMRA)). Although labeling could be observed in all the cases, high background was always an issue. In the case of DBCO-$PEG_4$5/6-TAMRA, the high background could be caused by the reaction of the strained cyclooctyne with cellular thiols, that could be diminished with a pretreatment step with iodoacetamide. However, the high background observed with BODIPY-SOBRAC was solely caused by the inherent nature of the probe. As bromoacetyl moieties are highly reactive, we reasoned that the substitution of the bromo by a chlorine atom could modulate the reactivity of the probe. As a result, BODIPY-SOCLAC was prepared and its suitability as an ABP for AC was investigated. The probe proved useful for in-gel AC detection at submicromolar concentrations and short incubation times, and it successfully stained endogenous levels of active enzyme, without additional labeling of background proteins. Moreover, no AC labeling occurred after protein denaturation, showing that the correct protein folding is a labeling requirement (as it is for activity). A challenge for the development of ABPs is their potential use in intact cells using fluorescence microscopy approaches. Hence, the only ABP for AC reported so far was a fluorescent analogue of the AC inhibitor carmofur which was employed for AC detection in Gaucher tissue homogenates[211]. However, no ABP has been successfully applied for imaging AC in living cells. As

a result, our next goal was to explore the use of the BODIPY-SOCLAC for the labeling of AC in cells. To achieve this, we incubate culture medium of cell lines with different levels of AC expression with the probe and visualize the localization of the ABP probe using confocal microscopy together with lysosomal tracker to explore a potential colocalization of the probe. BODIPY- SOCLAC (1 μM/5 min) was added to culture medium of cells, and labeling was analyzed by confocal scanning microscopy. Intracellular compartment staining was observed upon treatment of A549, fibroblasts, and FD1/AC cells with BODIPY-SOCLAC. Colocalization with LysoTracker indicated that BODIPY-SOCLAC was contained in the lysosomes, in agreement with the lysosomal location of AC, the probe target. In FD1 cells, BODIPY-SOCLAC did not afford a vesicular pattern colocalizing with LysoTracker, in agreement with the absence of AC in this cell line. No lysosomal labeling was observed after BODIPY-SOCLAC treatment of three different homozygous Farber fibroblasts (FD2–FD4) producing mutant proteins. The impact of these mutations on AC activity was assessed using the fluorogenic assay. Interestingly, some lysosome labeling occurred with BODIPY- SOCLAC in FD4 cells, which are those retaining some AC activity. BODIPY-SOCLAC have proven useful in-gel AC detection and can be employed to stain endogenous levels of active enzyme in intact cells. Importantly, although an ABP for AC has been previously reported[272], BODIPY-SOCLAC represents a major advantage in that it allowed the unprecedented lysosomal staining of active, but not inactive, AC in intact cells. These overall results might be of biomedical relevance to visualize the location and monitor the trafficking of active AC, as well as for to facilitate the screening and identification of novel pharmacological chaperones for the treatment of diseases characterized by aberrant AC expression. Recently, the use of ABPs has been expanded form protein profiling to drug discovery[273]. High-throughput screening (HTS) of a large number of potential inhibitors against a protein target is one of the basis of drug discovery[274]. Most of the reported HTS assays are *in-vitro* methods[275] which may lack the ability to provide the real interaction between the target protein and a potential drug in the cellular enviroment[274]. This often leads to failure of the potential hit in clinical trials due to undesirable side effects[276]. Thus, it is highly recommended that preclinical trials are performed in native cellular environment so that the mechanism of action of the discovered hit can be explored[277]. To overcome this drawback, recent studies have proposed the use of ABPs for drug screening in cellular context[273,278,279]. When the ABP binds the target protein, the signal is strongly visualized by fluorescent scanning. However, this signal is decreased in the presence of a competitor (potential drug target). This strategy allows the screening of drug candidates in a natural environment[280], and the evaluation of their selectivity and potency simultaneously in a single experiment. As a result, BODIPY-SOCLAC may open the door in combination with a HTS screening, as an alternative and complementary approach to identify AC inhibitors *in-vivo*.

Due to the relevance of AC as a target involved in several diseases, there is also a growing interest in the identification of selective and potent inhibitors of this enzyme. The identification of selective AC inhibitors has been mainly hampered by the lack of formats suitable for the screening of large libraries. This approach requires a powerful, robust and cost-effective HTS assay, allowing the rapid and reliable testing of large number of compounds. Recently, our group reported a flow-cytometry-based assay that uses a deoxyceramide analog to monitor AC activity in intact cells. This assay could be potentially useful in the future for screening purposes, but it would require proper optimization and the use of high-throughput flow cytometry platforms[281]. A fluorescent-based

assay in a 96-well format was previously set up in our group and applied to measure AC activity using cell lysates and intact cells as a source of enzyme. The assay is based on the coumarinic substrate RBM14-C12[173], that shows a high affinity and specificity for AC over neutral and alkaline CDases. Briefly, hydrolysis of the amide bond of RBM14-C12 by AC yields an aminodiol that can be then oxidized upon treatment with sodium periodate. The resulting aldehyde undergoes a β-elimination reaction to release the fluorescent product umbelliferone. The assay has been largely used by our group and others to identify novel ceramidase inhibitors[221,282,283]. However, to be able to identify the most promising drugs from large chemical libraries quickly and accurately, assays with higher capacity are essential. This would not only speed up the drug discovery process but also reduce its overall costs.

Interestingly, remarkable advances have been recently reported in this area of research. Although covering other members of the CDase family. Thus, Spicer et al, established a HTS assay for the identification of NC inhibitors utilizing an analogous substrate RBM14-C16, developed in our group[284]. This is a 96-well format NC inhibitor fluorescence assay which has been miniaturized and optimized in a 1536-well plate format for HTS. The high-throughput screening of >650,000 small-molecules has resulted in several hits that are now being pursued in crystal docking studies and in vitro drug metabolism and pharmacokinetics (DMPK). Furthermore, Granier et al. has reported a novel suite of doubly fluorophore-modified ceramides as turn-on for probes for the direct FRET-based analysis of CDsae activity in real-time. Although ACER3 was able to hydrolyze one of the probes, no synthetic substrates were hydrolyzed by AC[285]. Therefore, although the Granier's method has the advantage of monitoring CDase activity in real-time, it cannot be applied to AC until suitable FRET ceramide substrates are discovered for this enzyme. This assay, however has identified specific ACER3 inhibitors in live cells. Despite these advances covering NC and ACER3, there was no a suitable platform enabling HTS screening of AC. As mentioned earlier, a well set 96-well fluorescent assay for the evaluation of AC activity has already been used extensively by our group and others. And encouraged by the aforementioned HTS discoveries for NC and ACER3, we hypothesized that the correct miniaturization of this AC assay into a 384-well plate format would continue to give robust results, thereby ensuring a cost-effective assay that enables the screening of larger loads of compounds with a good signal window and a high reproducibility. To start with, the final reaction volume was adapted from 100 mL (96-well-format) to 32mL (384 well-format) with a final concentration of substrate of 20 μM. Next, protein concentration was adjusted using cell lysates of AC-overexpressing A375 melanoma cells. Ideally, the optimal amount of protein is the one that ensures reaction linearity over a period of time together with less than 10% of substrate depletion, in order to assume that the enzyme operates at steady-state conditions. Thus, different amounts of cell lysates were mixed with the substrate and product formation was measured over 1 h. The reaction progress curve for the hydrolysis of RBM14-C12 by AC was obtained at a range of protein concentrations. Finally, an amount of 0.4 mg of protein was chosen, as higher amounts of proteins were not in the linear portion whereas lower amounts would compromise the signal window. The optimal incubation time of the reaction mixture was next explored. Although a higher signal was witnessed at 2 h reaction time, a final reaction time of 1 h was chosen since it exhibited an excellent signal window. As a first validation step, we performed a control run consisting of 60 wells representing AC activity and 60 wells representing the signal in absence of the enzyme. The results revealed excellent separation between high and low control

wells resulting in a signal-to-background ratio >8 and a Z' factor of 0.72. The calculated coefficients of variation (CV) for both the high and low controls were 6.08% and 17.1% respectively. These data demonstrated that the assay was very robust, stable and possessed minimal well-to-well variability and therefore it is appropriate for HTS to identify AC inhibitors.

After having successfully established the optimal reaction conditions in a 384-well format, we employed this newly miniaturized AC assay in a pilot screen against a library of 4100 compounds. The screen was carried out at a single dose of 20 μM for each library compound in 6% DMSO (v/v) and in duplicate. The AC inhibitor SOCLAC was used as a pharmacological control for the assay[283]. The Z'-factors per plate were consistent with those obtained during the initial validation. A total of 116 compounds of the 4100 screened at 20 μM met the active criterion, based on the hit cut-off at % inhibition >40, in the single-point primary screen, what resulted in a hit rate of 2.8%. An example hit map from one screening plate is shown. The inhibitory activity of these hits was then validated in an additional assay performed at a single-point concentration in triplicates.

To confirm the results from the primary screening, top hits were cherry-picked and tested in a concentration-dependent response assay with triplicates per sample. Thus, 101 compounds were then subjected to 8-points two-fold dilution series starting at a maximum concentration of 200 micromolar. Among them, nine exhibited a dose-dependent inhibition of AC with IC_{50} values in the range of 6 and 49 μM, whereas 92 compounds showed a higher IC_{50} value or did not yield a concentration-dependent inhibition.

As mentioned above, hydrolysis of ceramides occurs by the action of CDases which are encoded by five known genes and are distinguished by the pH required for optimal activity[134]. A common problem with AC inhibitors, especially those one with a scaffold related to the structure of ceramide, is the lack of selectivity over other CDases. Thus, to discard a selectivity issue, the activity of nine detected hits against NC was next explored at 50 mM. Activity over NC was tested using recombinant human NC (rhNC) and a specific NC substrate bearing a nervonic acid amide (RBM14-C24:1)[222]. Remarkably, none of the molecules elicited a significant inhibitory activity, thereby confirming the selective inhibition of AC over NC.

Cell-based assays allow evaluating biological activity in a more physiologically relevant system that also considers additional factors that might have a positive impact on inhibitory potency such as permeabilization through cellular membranes, metabolization or concentration by intracellular compartmentalization. Thus, the activity of the nine selected hits was next examined in intact cells using AC overexpressing A375 cells and the fluorogenic substrate RBM14-C12. First, compounds were tested in a primary screening assay. Measurements were performed in triplicated at a single-point concentration of 20 μM. The results showed that only two of the 9 tested compounds exhibited a significant inhibition of AC activity at this concentration: W000113402_C12 with a 53% inhibition and W000113414_H19 with a weaker 32% inhibition, whereas slight effects were observed for the other hits. Dose-dependent inhibition could be also confirmed for W000113402_C12 in the cell-based assay displaying an IC_{50} of value of 32 μM (24.3–44.7).

HTS is still the primary hit-finding strategy both in academia and industry. However, the identification of novel AC inhibitors has been hampered by the unavailability of appropriate screening platforms. Herein, we report a robust and cost-effective assay for the determination of AC activity that enables the rapid profile of large compound libraries. The screening platform has been employed to evaluate a 4100 compound library leading to the identification of 9 novel compound classes targeting AC activity with low micromolar IC_{50}. Dose-dependent inhibition was confirmed for the primary hits identified in the screening campaign and now they can serve as a basis for hit-to-lead optimization through chemical modifications, thereby opening new venues in the field of AC inhibition. Noteworthy, the identified hits are non-ceramide related and belong to different non-carmofur chemical classes (Figure 20). Moreover, the reported technique can be considered an attractive drug-screening platform with a great potential to identify novel AC modulators. To further validate hits obtained in HTS campaigns of large libraries, an orthogonal assay using a different detection method (e.g. C12-Ceramide Bodipy and HPLC-based detection of substrate and reaction product) could be applied to discard potential interference of compounds on the fluorescence-based assay[169]. As several diseases are linked to altered AC activity, novel compounds modulating its activity should allow progress in drug discovery and expand our knowledge in the essential role of this enzyme.

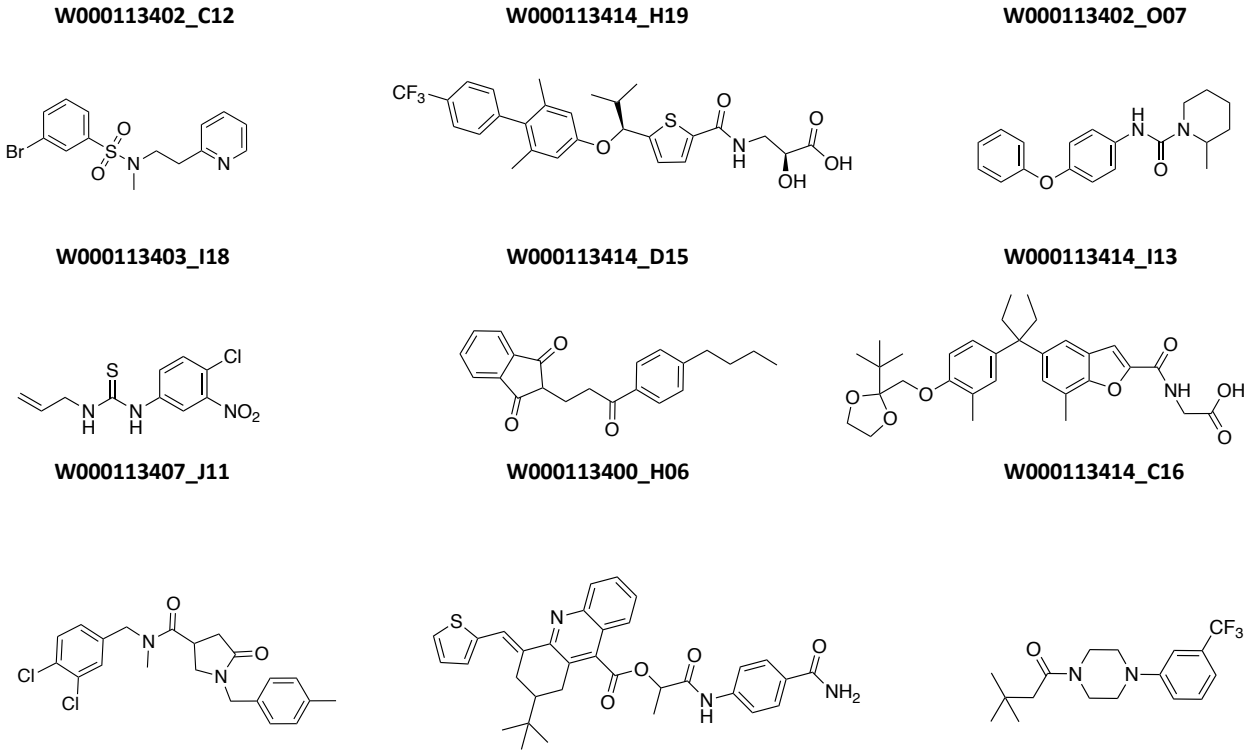

Figure 20: Chemical structures of the nine compounds which inhibited AC activity.

CONCLUSIONS

The following are the conclusions drawn from the studies presented in this thesis:

Discovery of deoxyceramide analogs as highly selective ACER3 inhibitors in live cells

- 1-deoxySLs are an interesting class of compounds to identify ACER3 inhibitors. Thus, the profiling of a set of 1-deoxySLs over different CDases has led to the identification of Compounds **20l** and **20m** as selective inhibitors of ACER3 activity.

Activity-Based Imaging of Acid Ceramidase in Living Cells

- We have proven that the irreversible AC inhibitor SOBRAC can be successfully employed as starting point for the development of an ABP for AC.
- The replacement of bromine by chlorine is a good approach to reduce the non-selective staining of the ABP, probably by diminishing its reactivity and side-target interactions.
- BODIPY-SOCLAC successfully stained endogenous levels of active AC in cell lysates and intact cells.
- BODIPY-SOCLAC can clearly detect the active form of AC and distinguish it from the inactive enzyme.
- BODIPY-SOCLAC represents a major advantage over a previously reported ABP, in that it allowed the unprecedented lysosomal staining of active, but not inactive, AC in intact cells.
- BODIPY-SOCLAC may be of biomedical relevance to visualize the location and monitor the trafficking of active AC, as well as for the analysis of novel pharmacological chaperones for the treatment of FD.
- BODIPY-SOCLAC may open the door for its use in combination with HTS assays as an alternative approach for the identification of AC inhibitors *in-vivo*.

High-throughput discovery of novel small-molecule inhibitors of acid Ceramidase

- The previously reported AC assay can be miniaturized and adapted to 384-well plate and it has been validated for the screening of AC inhibitors. The assay is a powerful platform for the identification of AC inhibitors in a cost-effective manner.
- The assay can be employed for the identification of novel inhibitors.
- Nine ceramide-unrelated compounds inhibited AC activity with $IC_{50} < 50$ µM.
- Two, out of nine, compounds **W000113402_C12** and **W000113414_H19** were AC inhibitors in intact cells. W000113402_C12 exhibited a 53% inhibition of AC activity in intact cells with an IC_{50} value of 32 µM, whereas W000113414_H19 showed a weaker 32% inhibition.
- Both compounds were not cytotoxic at concentrations under 100 µM in melanoma (A375), prostate cancer (PC3M) and colorectal cell lines (HT29).

REFERENCES

1. Harayama, T. & Riezman, H. Understanding the diversity of membrane lipid composition. *Nat. Rev. Mol. Cell Biol.* **19**, 281–296 (2018).
2. Casares, D., Escribá, P. V & Rosselló, C. A. Membrane Lipid Composition: Effect on Membrane and Organelle Structure, Function and Compartmentalization and Therapeutic Avenues. *Int. J. Mol. Sci.* **20**, (2019).
3. Bartke, N. & Hannun, Y. A. Bioactive sphingolipids: Metabolism and function. *J. Lipid Res.* **50**, 91–96 (2009).
4. Thudichum, J. L. W. A Treatise on the Chemical Constitution of the Brain. *Bailliere, Tindall Cox London* (1884).
5. Govindarajah, N. *et al.* Sphingolipids and acid ceramidase as therapeutic targets in cancer therapy. *Crit. Rev. Oncol. Hematol.* **138**, 104–111 (2019).
6. Hannun, Y. A. & Obeid, L. M. Principles of bioactive lipid signalling: Lessons from sphingolipids. *Nat. Rev. Mol. Cell Biol.* **9**, 139–150 (2008).
7. Leishman, E., Kunkler, P. E., Hurley, J. H., Miller, S. & Bradshaw, H. B. *Bioactive Lipids in Cancer, Inflammation and Related Diseases: Acute and Chronic Mild Traumatic Brain Injury Differentially Changes Levels of Bioactive Lipids in the CNS Associated with Headache*. *Advances in Experimental Medicine and Biology* vol. 1161 (2019).
8. Lingwood, D., Kaiser, H. J., Levental, I. & Simons, K. Lipid rafts as functional heterogeneity in cell membranes. *Biochem. Soc. Trans.* **37**, 955–960 (2009).
9. Zheng, L., Fleith, M., Giuffrida, F., O'Neill, B. V. & Schneider, N. Dietary Polar Lipids and Cognitive Development: A Narrative Review. *Adv. Nutr.* **10**, 1163–1176 (2019).
10. Lam, B. W. S. *et al.* The noncanonical chronicles: Emerging roles of sphingolipid structural variants. *Cell. Signal.* **79**, 109890 (2021).
11. Castillo, R. I. *et al.* From molecules to the clinic: Linking schizophrenia and metabolic syndrome through sphingolipids metabolism. *Front. Neurosci.* **10**, 1–15 (2016).
12. Menaldino, D. S. *et al.* Sphingoid bases and de novo ceramide synthesis: Enzymes involved, pharmacology and mechanisms of action. *Pharmacol. Res.* **47**, 373–381 (2003).
13. Carreira, A. C. *et al.* Mammalian sphingoid bases: Biophysical, physiological and pathological properties. *Prog. Lipid Res.* **75**, (2019).

14. Castro, B. M., Prieto, M. & Silva, L. C. Ceramide: A simple sphingolipid with unique biophysical properties. *Prog. Lipid Res.* **54**, 53–67 (2014).

15. Goñi, F. M. & Alonso, A. Biophysics of sphingolipids I. Membrane properties of sphingosine, ceramides and other simple sphingolipids. *Biochim. Biophys. Acta - Biomembr.* **1758**, 1902–1921 (2006).

16. Merrill, A. H., Wang, M. D., Park, M. & Sullards, M. C. (Glyco)sphingolipidology: an amazing challenge and opportunity for systems biology. *Trends Biochem. Sci.* **32**, 457–468 (2007).

17. Albrecht, S. *et al.* Comprehensive Profiling of Glycosphingolipid Glycans Using a Novel Broad Specificity Endoglycoceramidase in a High-Throughput Workflow. *Anal. Chem.* **88**, 4795–4802 (2016).

18. Van Meer, G., Wolthoorn, J. & Degroote, S. The fate and function of glycosphingolipid glucosylceramide. *Philos. Trans. R. Soc. B Biol. Sci.* **358**, 869–873 (2003).

19. Pruett, S. T. *et al.* Biodiversity of sphingoid bases ('sphingosines') and related amino alcohols. *J. Lipid Res.* **49**, 1621–1639 (2008).

20. Merrill, A. H. Sphingolipid and glycosphingolipid metabolic pathways in the era of sphingolipidomics. *Chem. Rev.* **111**, 6387–6422 (2011).

21. Pralhada Rao, R. *et al.* Sphingolipid Metabolic Pathway: An Overview of Major Roles Played in Human Diseases. *J. Lipids* **2013**, 1–12 (2013).

22. Sasset, L., Zhang, Y., Dunn, T. M. & Di Lorenzo, A. Sphingolipid De Novo Biosynthesis: A Rheostat of Cardiovascular Homeostasis. *Trends Endocrinol. Metab.* **27**, 807–819 (2016).

23. Wigger, D., Gulbins, E., Kleuser, B. & Schumacher, F. Monitoring the Sphingolipid de novo Synthesis by Stable-Isotope Labeling and Liquid Chromatography-Mass Spectrometry. *Front. Cell Dev. Biol.* **7**, (2019).

24. Merrill, A. H. De novo sphingolipid biosynthesis: A necessary, but dangerous, pathway. *J. Biol. Chem.* **277**, 25843–25846 (2002).

25. Ikushiro, H. & Hayashi, H. Mechanistic enzymology of serine palmitoyltransferase. *Biochim. Biophys. Acta - Proteins Proteomics* **1814**, 1474–1480 (2011).

26. Hanada, K. Serine palmitoyltransferase, a key enzyme of sphingolipid metabolism. *Biochim. Biophys. Acta - Mol. Cell Biol. Lipids* **1632**, 16–30 (2003).

27. Zhao, L. *et al.* Elevation of 20-carbon long chain bases due to a mutation in serine palmitoyltransferase small subunit b results in neurodegeneration. *Proc. Natl. Acad. Sci. U. S. A.* **112**, 12962–12967 (2015).

28. Lone, M. A., Santos, T., Alecu, I., Silva, L. C. & Hornemann, T. 1-Deoxysphingolipids. *Biochim. Biophys. Acta - Mol. Cell Biol. Lipids* **1864**, 512–521 (2019).

29. Lauterbach, M. A. *et al.* 1-Deoxysphingolipids cause autophagosome and lysosome accumulation and trigger NLRP3 inflammasome activation. *Autophagy* **00**, 1–15 (2020).

30. Muthusamy, T. *et al.* Serine restriction alters sphingolipid diversity to constrain tumour growth. *Nature* **586**, 790–795 (2020).

31. Pewzner-Jung, Y., Ben-Dor, S. & Futerman, A. H. When do Lasses (longevity assurance genes) become CerS (ceramide synthases)? Insights into the regulation of ceramide synthesis. *J. Biol. Chem.* **281**, 25001–25005 (2006).

32. Geeraert, L., Mannaerts, G. P. & Van Veldhoven, P. P. Conversion of dihydroceramide into ceramide: Involvement of a desaturase. *Biochem. J.* **327**, 125–132 (1997).

33. Yamaji, T., Kumagai, K., Tomishige, N. & Hanada, K. Two sphingolipid transfer proteins, CERT and FAPP2: Their roles in sphingolipid metabolism. *IUBMB Life* **60**, 511–518 (2008).

34. Tafesse, F. G., Ternes, P. & Holthuis, J. C. M. The multigenic sphingomyelin synthase family. *J. Biol. Chem.* **281**, 29421–29425 (2006).

35. Ichikawa, S. & Hirabayashi, Y. Glucosylceramide synthase and glycosphingolipid synthesis. *Trends Cell Biol.* **8**, 198–202 (1998).

36. Bornancin, F. Ceramide kinase: The first decade. *Cell. Signal.* **23**, 999–1008 (2011).

37. Hait, N. C., Oskeritzian, C. A., Paugh, S. W., Milstien, S. & Spiegel, S. Sphingosine kinases, sphingosine 1-phosphate, apoptosis and diseases. *Biochim. Biophys. Acta - Biomembr.* **1758**, 2016–2026 (2006).

38. Bandhuvula, P. & Saba, J. D. Sphingosine-1-phosphate lyase in immunity and cancer: silencing the siren. *Trends Mol. Med.* **13**, 210–217 (2007).

39. Marchesini, N. & Hannun, Y. A. Acid and neutral sphingomyelinases: Roles and mechanisms of regulation. *Biochem. Cell Biol.* **82**, 27–44 (2004).

40. Hill, C. H. *et al.* The mechanism of glycosphingolipid degradation revealed by a GALC-SapA

complex structure. *Nat. Commun.* **9**, 1–9 (2018).

41. Gómez-Muñoz, A. Ceramide 1-phosphate/ceramide, a switch between life and death. *Biochim. Biophys. Acta - Biomembr.* **1758**, 2049–2056 (2006).
42. Kitatani, K., Idkowiak-Baldys, J. & Hannun, Y. A. The sphingolipid salvage pathway in ceramide metabolism and signaling. *Cell. Signal.* **20**, 1010–1018 (2008).
43. Canals, D. & Clarke, C. J. Compartmentalization of Sphingolipid metabolism: Implications for signaling and therapy. *Pharmacol. Ther.* **232**, 108005 (2022).
44. Michel, C. & Van Echten-Deckert, G. Conversion of dihydroceramide to ceramide occurs at the cytosolic face of the endoplasmic reticulum. *FEBS Lett.* **416**, 153–155 (1997).
45. Stiban, J., Caputo, L. & Colombini, M. Ceramide synthesis in the endoplasmic reticulum can permeabilize mitochondria to proapoptotic proteins. *J. Lipid Res.* **49**, 625–634 (2008).
46. Körner, C. & Fröhlich, F. Compartmentation and functions of sphingolipids. *Curr. Opin. Cell Biol.* **74**, 104–111 (2022).
47. Fukasawa, M., Nishijima, M. & Hanada, K. Genetic evidence for ATP-dependent endoplasmic reticulum-to-Golgi apparatus trafficking of ceramide for sphingomyelin synthesis in Chinese hamster ovary cells. *J. Cell Biol.* **144**, 673–685 (1999).
48. Hanada, K. *et al.* Molecular machinery for non-vesicular trafficking of ceramide. *Nature* **426**, 803–809 (2003).
49. Hanada, K. Intracellular trafficking of ceramide by ceramide transfer protein. *Proc. Japan Acad. Ser. B Phys. Biol. Sci.* **86**, 426–437 (2010).
50. Kumagai, K. & Hanada, K. Structure, functions and regulation of CERT, a lipid-transfer protein for the delivery of ceramide at the ER–Golgi membrane contact sites. *FEBS Lett.* **593**, 2366–2377 (2019).
51. Jeckel, D., Karrenbauer, A., Burger, K. N. J., Van Meer, G. & Wieland, F. Glucosylceramide is synthesized at the cytosolic surface of various Golgi subfractions. *J. Cell Biol.* **117**, 259–267 (1992).
52. Perry, R. J. & Ridgway, N. D. Molecular mechanisms and regulation of ceramide transport. *Biochim. Biophys. Acta - Mol. Cell Biol. Lipids* **1734**, 220–234 (2005).
53. D'Angelo, G. *et al.* Glycosphingolipid synthesis requires FAPP2 transfer of glucosylceramide.

Nature **449**, 62–67 (2007).

54. Lannert, H., Gorgas, K., Meißner, I., Wieland, F. T. & Jeckel, D. Functional organization of the Golgi apparatus in glycosphingolipid biosynthesis. Lactosylceramide and subsequent glycospingolipids are formed in the lumen of the late Golgi. *J. Biol. Chem.* **273**, 2939–2946 (1998).
55. Halter, D. *et al.* Pre- and post-Golgi translocation of glucosylceramide in glycosphingolipid synthesis. *J. Cell Biol.* **179**, 101–115 (2007).
56. Eckford, P. D. W. & Sharom, F. J. The reconstituted P-glycoprotein multidrug transporter is a flippase for glucosylceramide and other simple glycosphingolipids. *Biochem. J.* **389**, 517–526 (2005).
57. Riboni, L., Giussani, P. & Viani, P. Sphingolipid transport. *Adv. Exp. Med. Biol.* **688**, 24–45 (2010).
58. Boath, A. *et al.* Regulation and traffic of ceramide 1-phosphate produced by ceramide kinase: Comparative analysis to glucosylceramide and sphingomyelin. *J. Biol. Chem.* **283**, 8517–8526 (2008).
59. Gómez-Munoz, A., Gangoiti, P., Granado, M. H., Arana, L. & Ouro, A. Ceramide-1-phosphate in cell survival and inflammatory signaling. *Adv. Exp. Med. Biol.* **688**, 118–130 (2010).
60. Sugiura, M. *et al.* Ceramide kinase, a novel lipid kinase: Molecular cloning and functional characterization. *J. Biol. Chem.* **277**, 23294–23300 (2002).
61. Zhang, Y., Zhang, X., Lu, M. & Zou, X. Ceramide-1-phosphate and its transfer proteins in eukaryotes. *Chem. Phys. Lipids* **240**, 105135 (2021).
62. Kolter, T. & Sandhoff, K. Lysosomal degradation of membrane lipids. *FEBS Lett.* **584**, 1700–1712 (2010).
63. Cocco, L., Maraldi, N. M., Manzoli, F. A., Stewart Gilmour, R. & Lang, A. Phospholipid interactions in rat liver nuclear matrix. *Top. Catal.* **96**, 890–898 (1980).
64. Cocco, L. *et al.* Phospholipids as components of the nuclear matrix: their possible biological significance. *Basic Appl. Histochem.* **31**, 413–419 (1987).
65. Lucki, N. C. & Sewer, M. B. Nuclear sphingolipid metabolism. *Annu. Rev. Physiol.* **74**, 131–151 (2012).

66. Hait, N. C. *et al.* Regulation of histone acetylation in the nucleus by sphingosine-1-phosphate. *Science (80-.).* **325**, 1254–1257 (2009).

67. Hernández-Corbacho, M. J., Salama, M. F., Canals, D., Senkal, C. E. & Obeid, L. M. Sphingolipids in mitochondria. *Biochim. Biophys. Acta - Mol. Cell Biol. Lipids* **1862**, 56–68 (2017).

68. Bionda, C., Portoukalian, J., Schmitt, D., Rodriguez-Lafrasse, C. & Ardail, D. Subcellular compartmentalization of ceramide metabolism: MAM (mitochondria-associated membrane) and/or mitochondria? *Biochem. J.* **382**, 527–533 (2004).

69. Meyer Zu Heringdorf, D., Van Koppen, C. J. & Jakobs, K. H. Molecular diversity of sphingolipid signalling. *FEBS Lett.* **410**, 34–38 (1997).

70. Rodriguez-Cuenca, S., Barbarroja, N. & Vidal-Puig, A. Dihydroceramide desaturase 1, the gatekeeper of ceramide induced lipotoxicity. *Biochim. Biophys. Acta - Mol. Cell Biol. Lipids* **1851**, 40–50 (2015).

71. Bielawska, A., Linardic, C. M. & Hannun, Y. A. Modulation of cell growth and differentiation by ceramide. *FEBS Lett.* **307**, 211–214 (1992).

72. G, W., SD, S. & E, B. Ceramide and S1P Signaling in Embryonic Stem Cell Differentiation. *Methods Mol. Biol.* **1697**, 153–171 (2018).

73. Obeid, L. M., Linardic, C. M., Karolak, L. A. & Hannun, Y. A. Programmed cell death induced by ceramide. *Science (80-.).* **259**, 1769–1771 (1993).

74. Pettus, B. J., Chalfant, C. E. & Hannun, Y. A. Ceramide in apoptosis: An overview and current perspectives. *Biochim. Biophys. Acta - Mol. Cell Biol. Lipids* **1585**, 114–125 (2002).

75. Thevissen, K., Francois, I., Winderickx, J., Pannecouque, C. & Cammue, B. Ceramide Involvement in Apoptosis and Apoptotic Diseases. *Mini-Reviews Med. Chem.* **6**, 699–709 (2006).

76. ME, V., JY, L., MJ, S., A, B. & LM, O. Role of ceramide in cellular senescence. *J. Biol. Chem.* **270**, 30701–30708 (1995).

77. S, J. *et al.* Role for ceramide in cell cycle arrest. *J. Biol. Chem.* **270**, 2047–2052 (1995).

78. Merrill, A. H., Sullards, M. C., Allegood, J. C., Kelly, S. & Wang, E. Sphingolipidomics: High-throughput, structure-specific, and quantitative analysis of sphingolipids by liquid

chromatography tandem mass spectrometry. *Methods* **36**, 207–224 (2005).

79. Hannun, Y. A. & Obeid, L. M. Many ceramides. *J. Biol. Chem.* **286**, 27855–27862 (2011).
80. Cingolani, F., Futerman, A. H. & Casas, J. Ceramide synthases in biomedical research. *Chem. Phys. Lipids* **197**, 25–32 (2016).
81. Grösch, S., Schiffmann, S. & Geisslinger, G. Chain length-specific properties of ceramides. *Prog. Lipid Res.* **51**, 50–62 (2012).
82. Saddoughi, S. A., Song, P. & Ogretmen, B. Roles of bioactive sphingolipids in cancer biology and therapeutics. *Subcell. Biochem.* **49**, 413–440 (2008).
83. Obeid, L. M. & Hannun, Y. A. Ceramide: A stress signal and mediator of growth suppression and apoptosis. *J. Cell. Biochem.* **58**, 191–198 (1995).
84. N, A.-A., V, G., R, S. & T, L. Ceramide in apoptosis signaling: relationship with oxidative stress. *Free Radic. Biol. Med.* **31**, 717–728 (2001).
85. Siskind, L. J. Mitochondrial ceramide and the induction of apoptosis. *J. Bioenerg. Biomembr.* **37**, 143–153 (2005).
86. Patwardhan, G. A., Beverly, L. J. & Siskind, L. J. Sphingolipids and mitochondrial apoptosis. *J. Bioenerg. Biomembr.* **48**, 153–168 (2016).
87. Colombini, M. Ceramide channels and mitochondrial outer membrane permeability. *J. Bioenerg. Biomembr.* **49**, 57–64 (2017).
88. Tsujimoto, Y. Role of Bcl-2 family proteins in apoptosis: Apoptosomes or mitochondria? *Genes to Cells* **3**, 697–707 (1998).
89. Colombini, M. Ceramide channels and their role in mitochondria-mediated apoptosis. *Biochim. Biophys. Acta - Bioenerg.* **1797**, 1239–1244 (2010).
90. Heinrich, M. *et al.* Cathepsin D targeted by acid sphingomyelinase-derived ceramide. *EMBO J.* **18**, 5252–5263 (1999).
91. Heinrich, M. *et al.* Ceramide as an activator lipid of cathepsin D. *Adv. Exp. Med. Biol.* **477**, 305–315 (2000).
92. Heinrich, M. *et al.* Cathepsin D links TNF-induced acid sphingomyelinase to Bid-mediated caspase-9 and -3 activation. *Cell Death Differ.* **11**, 550–563 (2004).
93. Ogretmen, B. & Hannun, Y. A. Biologically active sphingolipids in cancer pathogenesis and

treatment. *Nature Reviews Cancer* vol. 4 604–616 at https://doi.org/10.1038/nrc1411 (2004).

94. Ogretmen, B. *et al.* Role of Ceramide in Mediating the Inhibition of Telomerase Activity in A549 Human Lung Adenocarcinoma Cells. *J. Biol. Chem.* **276**, 24901–24910 (2001).
95. Ogretmen, B. *et al.* Molecular Mechanisms of Ceramide-mediated Telomerase Inhibition in the A549 Human Lung Adenocarcinoma Cell Line. *J. Biol. Chem.* **276**, 32506–32514 (2001).
96. Chalfant, C. E. *et al.* De novo ceramide regulates the alternative splicing of caspase 9 and Bcl-x in A549 lung adenocarcinoma cells. Dependence on protein phosphatase-1. *J. Biol. Chem.* **277**, 12587–12595 (2002).
97. Dbaibo, G. S. *et al.* Retinoblastoma gene product as a downstream target for a ceramide-dependent pathway of growth arrest. *Proc. Natl. Acad. Sci. U. S. A.* **92**, 1347–1351 (1995).
98. Connor, C. E. *et al.* Cell cycle arrest of hematopoietic cell lines after treatment with ceramide is commonly associated with retinoblastoma activation. *Cytometry* **43**, 164–169 (2001).
99. Lee, J. Y., Bielawska, A. E. & Obeid, L. M. Regulation of cyclin-dependent kinase 2 activity by ceramide. *Exp. Cell Res.* **261**, 303–311 (2000).
100. Okazaki, T., Bielawska, A., Bell, R. M. & Hannun, Y. A. Role of ceramide as a lipid mediator of 1α,25-dihydroxyvitamin D3-induced HL-60 cell differentiation. *J. Biol. Chem.* **265**, 15823–15831 (1990).
101. Pattingre, S., Bauvy, C., Levade, T., Levine, B. & Codogno, P. Ceramide-induced autophagy: To junk or to protect cells? *Autophagy* **5**, 558–560 (2009).
102. Morad, S. A. F. & Cabot, M. C. Ceramide-orchestrated signalling in cancer cells. *Nat. Rev. Cancer* **13**, 51–65 (2013).
103. Cartier, A. & Hla, T. Sphingosine 1-phosphate: Lipid signaling in pathology and therapy. *Science (80-.).* **366**, (2019).
104. Cirillo, F. *et al.* The antithetic role of ceramide and sphingosine-1-phosphate in cardiac dysfunction. *J. Cell. Physiol.* **236**, 4857–4873 (2021).
105. Takabe, K., Paugh, S. W., Milstien, S. & Spiegel, S. " Inside-Out " Signaling of Sphingosine-1-Phosphate : **60**, 181–195 (2008).
106. Liu, Y. *et al.* Edg-1, the G protein-coupled receptor for sphingosine-1-phosphate, is essential

for vascular maturation. *J. Clin. Invest.* **106**, 951–961 (2000).

107. Obinata, H. & Hla, T. Sphingosine 1-phosphate and inflammation. *Int. Immunol.* **31**, 617–625 (2019).
108. Lavieu, G. *et al.* Regulation of autophagy by sphingosine kinase 1 and its role in cell survival during nutrient starvation. *J. Biol. Chem.* **281**, 8518–8527 (2006).
109. Rosen, H. & Goetzl, E. J. Sphingosine 1-phosphate and its receptors: An autocrine and paracrine network. *Nat. Rev. Immunol.* **5**, 560–570 (2005).
110. Taha, T. A., Argraves, K. M. & Obeid, L. M. Sphingosine-1-phosphate receptors: Receptor specificity versus functional redundancy. *Biochim. Biophys. Acta - Mol. Cell Biol. Lipids* **1682**, 48–55 (2004).
111. Chun, J., Hla, T., Lynch, K. R., Spiegel, S. & Moolenaar, W. H. International Union of Basic and Clinical Pharmacology. LXXVIII. Lysophospholipid receptor nomenclature. *Pharmacol. Rev.* **62**, 579–587 (2010).
112. Rosen, H., Gonzalez-Cabrera, P. J., Sanna, M. G. & Brown, S. Sphingosine 1-phosphate receptor signaling. *Annu. Rev. Biochem.* **78**, 743–768 (2009).
113. Alvarez, S. E., Milstien, S. & Spiegel, S. Autocrine and paracrine roles of sphingosine-1-phosphate. *Trends Endocrinol. Metab.* **18**, 300–307 (2007).
114. Van Brocklyn, J. R. *et al.* Dual actions of sphingosine-1-phosphate: Extracellular through the G(i)- coupled receptor Edg-1 and intracellular to regulate proliferation and survival. *J. Cell Biol.* **142**, 229–240 (1998).
115. Cuvillier, O. & Levade, T. Enzymes of sphingosine metabolism as potential pharmacological targets for therapeutic intervention in cancer. *Pharmacol. Res.* **47**, 439–445 (2003).
116. Kolter, T. & Sandhoff, K. Sphingolipid metabolism diseases. *Biochim. Biophys. Acta - Biomembr.* **1758**, 2057–2079 (2006).
117. Gebert, R., Stadler, U. C., Orenstein, J. A. N. M. & Axel, R. Deficiency in Farber's Disease (Lipogranulomatosis). **178**, 4–6 (1971).
118. McGovern, M. M., Aron, A., Brodie, S. E., Desnick, R. J. & Wasserstein, M. P. Natural history of Type A Niemann-Pick disease: Possible endpoints for therapeutic trials. *Neurology* **66**, 228–232 (2006).

119. Grabowski, G. A. Gaucher disease and other storage disorders. *Hematology Am. Soc. Hematol. Educ. Program* **2012**, 13–18 (2012).

120. Kolter, T. A view on sphingolipids and disease. *Chem. Phys. Lipids* **164**, 590–606 (2011).

121. Coant, N., Sakamoto, W., Mao, C. & Hannun, Y. A. Ceramidases, roles in sphingolipid metabolism and in health and disease. *Adv. Biol. Regul.* **63**, 122–131 (2017).

122. F, P. *et al.* Role of Ceramidases in Sphingolipid Metabolism and Human Diseases. *Cells* **8**, (2019).

123. Duarte, C. *et al.* Elusive Roles of the Different Ceramidases in Human Health, Pathophysiology, and Tissue Regeneration. *Cells* **9**, 1–20 (2020).

124. El Bawab, S. *et al.* Molecular cloning and characterization of a human mitochondrial ceramidase. *J. Biol. Chem.* **275**, 21508–21513 (2000).

125. Hwang, Y. H., Tani, M., Nakagawa, T., Okino, N. & Ito, M. Subcellular localization of human neutral ceramidase expressed in HEK293 cells. *Biochem. Biophys. Res. Commun.* **331**, 37–42 (2005).

126. Sakamoto, W., Coant, N., Canals, D., Obeid, L. M. & Hannun, Y. A. Functions of neutral ceramidase in the Golgi apparatus. *J. Lipid Res.* **59**, 2116–2125 (2018).

127. Tani, M., Igarashi, Y. & Ito, M. Involvement of neutral ceramidase in ceramide metabolism at the plasma membrane and in extracellular milieu. *J. Biol. Chem.* **280**, 36592–36600 (2005).

128. Houben, E. *et al.* Differentiation-associated expression of ceramidase isoforms in cultured keratinocytes and epidermis. *J. Lipid Res.* **47**, 1063–1070 (2006).

129. Sun, W. *et al.* Upregulation of the human alkaline ceramidase 1 and acid ceramidase mediates calcium-induced differentiation of epidermal keratinocytes. *J. Invest. Dermatol.* **128**, 389–397 (2008).

130. Sun, W. *et al.* Substrate specificity, membrane topology, and activity regulation of human alkaline ceramidase 2 (ACER2). *J. Biol. Chem.* **285**, 8995–9007 (2010).

131. Ramachandra, N. & Conzelmann, A. Membrane topology of yeast alkaline ceramidase YPC1. *Biochem. J.* **452**, 585–594 (2013).

132. Vasiliauskaité-Brooks, I. *et al.* Structure of a human intramembrane ceramidase explains

enzymatic dysfunction found in leukodystrophy. *Nat. Commun.* **9**, 1–13 (2018).

133. Mao, C. *et al.* Cloning and characterization of a novel human alkaline ceramidase: A mammalian enzyme that hydrolyzes phytoceramide. *J. Biol. Chem.* **276**, 26577–26588 (2001).
134. Mao, C. & Obeid, L. M. Ceramidases: regulators of cellular responses mediated by ceramide, sphingosine, and sphingosine-1-phosphate. *Biochim. Biophys. Acta - Mol. Cell Biol. Lipids* **1781**, 424–434 (2008).
135. Li, F. *et al.* Maternal and fetal alkaline ceramidase 2 is required for placental vascular integrity in mice. *FASEB J.* **34**, 15252–15268 (2020).
136. Okino, N. *et al.* The reverse activity of human acid ceramidase. *J. Biol. Chem.* **278**, 29948–29953 (2003).
137. Tani, M. *et al.* Purification and characterization of a neutral ceramidase from mouse liver. A single protein catalyzes the reversible reaction in which ceramide is both hydrolyzed and synthesized. *J. Biol. Chem.* **275**, 3462–3468 (2000).
138. Kita, K., Okino, N. & Ito, M. Reverse hydrolysis reaction of a recombinant alkaline ceramidase of Pseudomonas aeruginosa. *Biochim. Biophys. Acta - Mol. Cell Biol. Lipids* **1485**, 111–120 (2000).
139. Mao, C., Xu, R., Bielawska, A. & Obeid, L. M. Cloning of an alkaline ceramidase from Saccharomyces cerevisiae. An enzyme with reverse (CoA-independent) ceramide synthase activity. *J. Biol. Chem.* **275**, 6876–6884 (2000).
140. El Bawab, S. *et al.* Biochemical characterization of the reverse activity of rat brain ceramidase. A CoA-independent and fumonisin B1-insensitive ceramide synthase. *J. Biol. Chem.* **276**, 16758–16766 (2001).
141. Bernardo, K. *et al.* Purification, characterization, and biosynthesis of human acid ceramidase. *J. Biol. Chem.* **270**, 11098–11102 (1995).
142. Koch, J. *et al.* Molecular cloning and characterization of a full-length complementary DNA encoding human acid ceramidase: Identification of the first molecular lesion causing farber disease. *J. Biol. Chem.* **271**, 33110–33115 (1996).
143. Mao, Z. *et al.* Alkaline ceramidase 2 (ACER2) and its product dihydrosphingosine mediate

the cytotoxicity of N-(4-Hydroxyphenyl)retinamide in tumor cells. *J. Biol. Chem.* **285**, 29078–29090 (2010).

144. Momol, T., Ben-Yoseph, Y. & Nadler, H. L. Substrate-specificities of acid and alkaline ceramidases in fibroblasts from patients with Farber disease and controls. *Biochem. J.* **205**, 419–425 (1982).
145. He, X. *et al.* Purification and characterization of recombinant, human acid ceramidase: Catalytic reactions and interactions with acid sphingomyelinase. *J. Biol. Chem.* **278**, 32978–32986 (2003).
146. Chavez, J. A., Holland, W. L., Bär, J., Sandhoff, K. & Summers, S. A. Acid ceramidase overexpression prevents the inhibitory effects of saturated fatty acids on insulin signaling. *J. Biol. Chem.* **280**, 20148–20153 (2005).
147. Huang, Y. *et al.* Elevation of the level and activity of acid ceramidase in Alzheimer's disease brain. *Eur. J. Neurosci.* **20**, 3489–3497 (2004).
148. He, X., Huang, Y., Li, B., Gong, C. X. & Schuchman, E. H. Deregulation of sphingolipid metabolism in Alzheimer's disease. *Neurobiol. Aging* **31**, 398–408 (2010).
149. Saad, A. F. *et al.* The functional effects of acid ceramidase overexpression in prostate cancer progression and resistance to chemotherapy. *Cancer Biol. Ther.* **6**, 1455–1460 (2007).
150. Liu, X. *et al.* Acid ceramidase upregulation in prostate cancer: Role in tumor development and implications for therapy. *Expert Opin. Ther. Targets* **13**, 1449–1458 (2009).
151. Musumarra, G., Barresi, V., Condorelli, D. F. & Scirè, S. A bioinformatic approach to the identification of candidate genes for the development of new cancer diagnostics. *Biol. Chem.* **384**, 321–327 (2003).
152. Realini, N. *et al.* Acid ceramidase in melanoma: Expression, localization, and effects of pharmacological inhibition. *J. Biol. Chem.* **291**, 2422–2434 (2016).
153. Elojeimy, S. *et al.* Role of acid ceramidase in resistance to fasL: Therapeutic approaches based on acid ceramidase inhibitors and fasL gene therapy. *Mol. Ther.* **15**, 1259–1263 (2007).
154. Eliyahu, E., Park, J.-H., Shtraizent, N., He, X. & Schuchman, E. H. Acid ceramidase is a novel factor required for early embryo survival. *FASEB J.* **21**, 1403–1409 (2007).

155. Tani, M., Iida, H. & Ito, M. O-glycosylation of mucin-like domain retains the neutral ceramidase on the plasma membranes as a type II integral membrane protein. *J. Biol. Chem.* **278**, 10523–10530 (2003).

156. El Bawab, S., Bielawska, A. & Hannun, Y. A. Purification and characterization of a membrane-bound nonlysosomal ceramidase from rat brain. *J. Biol. Chem.* **274**, 27948–27955 (1999).

157. Yoshimura, Y., Tani, M., Okino, N., Iida, H. & Ito, M. Molecular cloning and functional analysis of zebrafish neutral ceramidase. *J. Biol. Chem.* **279**, 44012–44022 (2004).

158. Kono, M. *et al.* Neutral ceramidase encoded by the Asah2 gene is essential for the intestinal degradation of sphingolipids. *J. Biol. Chem.* **281**, 7324–7331 (2006).

159. Choi, M. S. *et al.* Neutral ceramidase gene: Role in regulating ceramide-induced apoptosis. *Gene* **315**, 113–122 (2003).

160. Xu, R., Antwi Boasiako, P. & Mao, C. Alkaline ceramidase family: The first two decades. *Cell. Signal.* **78**, 109860 (2021).

161. Mao, C. *et al.* Cloning and characterization of a mouse endoplasmic reticulum alkaline ceramidase. An enzyme that preferentially regulates metabolism of very long chain ceramides. *J. Biol. Chem.* **278**, 31184–31191 (2003).

162. Liakath-Ali, K. *et al.* Alkaline ceramidase 1 is essential for mammalian skin homeostasis and regulating whole-body energy expenditure. *J. Pathol.* **239**, 374–383 (2016).

163. Xu, R. *et al.* Golgi alkaline ceramidase regulates cell proliferation and survival by controlling levels of sphingosine and S1P. *FASEB J.* **20**, 1813–1825 (2006).

164. Li, F. *et al.* Alkaline ceramidase 2 is essential for the homeostasis of plasma sphingoid bases and their phosphates. *FASEB J.* **32**, 3058–3069 (2018).

165. Hu, W. *et al.* Golgi fragmentation is associated with ceramide-induced cellular effects. *Mol. Biol. Cell* **16**, 1555–1567 (2005).

166. Hu, W. *et al.* Alkaline ceramidase 3 (ACER3) hydrolyzes unsaturated long-chain ceramides, and its down-regulation inhibits both cell proliferation and apoptosis. *J. Biol. Chem.* **285**, 7964–7976 (2010).

167. Nikolova-Karakashian, M. & Merrill, A. H. Ceramidases. *Methods Enzymol.* **311**, 194–201 (2000).

168. Tani, M., Okino, N., Mitsutake, S. & Ito, M. Specific and sensitive assay for alkaline and neutral ceramidases involving C12-NBD-ceramide. *J. Biochem.* **125**, 746–749 (1999).

169. He, X., Chen, F., Dagan, A., Gatt, S. & Schuchman, E. H. A fluorescence-based, high-performance liquid chromatographic assay to determine acid sphingomyelinase activity and diagnose types A and B Niemann-Pick disease. *Anal. Biochem.* **314**, 116–120 (2003).

170. He, X., Dagan, A., Gatt, S. & Schuchman, E. H. Simultaneous quantitative analysis of ceramide and sphingosine in mouse blood by naphthalene-2,3-dicarboxyaldehyde derivatization after hydrolysis with ceramidase. *Anal. Biochem.* **340**, 113–122 (2005).

171. Bhabak, K. P. *et al.* Development of a novel FRET probe for the real-time determination of ceramidase activity. *ChemBioChem* **14**, 1049–1052 (2013).

172. Bedia, C., Camacho, L., Abad, J. L., Fabriàs, G. & Levade, T. A simple fluorogenic method for determination of acid ceramidase activity and diagnosis of Farber disease. *J. Lipid Res.* **51**, 3542–3547 (2010).

173. Bedia, C., Casas, J., Garcia, V., Levade, T. & Fabriàs, G. Synthesis of a novel ceramide analogue and its use in a high-throughput fluorogenic assay for ceramidases. *ChemBioChem* (2007) doi:10.1002/cbic.200600533.

174. Edvardson, S. *et al.* Deficiency of the alkaline ceramidase ACER3 manifests in early childhood by progressive leukodystrophy. *J. Med. Genet.* **53**, 389–396 (2016).

175. Yin, Y., Xu, M., Gao, J. & Li, M. Alkaline ceramidase 3 promotes growth of hepatocellular carcinoma cells via regulating S1P/S1PR2/PI3K/AKT signaling. *Pathol. Res. Pract.* **214**, 1381–1387 (2018).

176. Chen, C. *et al.* ACER3 supports development of acute myeloid leukemia. *Biochem. Biophys. Res. Commun.* **478**, 33–38 (2016).

177. Bielawska, A. *et al.* (1S,2R)-D-erythro-2-(N-myristoylamino)-1-phenyl-1-propanol as an inhibitor of ceramidase. *J. Biol. Chem.* **271**, 12646–12654 (1996).

178. Thayyullathil, F. *et al.* Caspase-3 mediated release of SAC domain containing fragment from Par-4 is necessary for the sphingosine-induced apoptosis in Jurkat cells. *J. Mol. Signal.* **8**, 1–13 (2013).

179. Casasampere, M. *et al.* Activity of neutral and alkaline ceramidases on fluorogenic N -

acylated coumarin-containing aminodiols. *J. Lipid Res.* **56**, 2019–2028 (2015).

180. Gebai, A., Gorelik, A., Li, Z., Illes, K. & Nagar, B. Structural basis for the activation of acid ceramidase. *Nat. Commun.* **9**, (2018).
181. Shtraizent, N. *et al.* Autoproteolytic cleavage and activation of human acid ceramidase. *J. Biol. Chem.* **283**, 11253–11259 (2008).
182. Chen, W. W., Moser, A. B. & Moser, H. W. Role of lysosomal acid ceramidase in the metabolism of ceramide in human skin fibroblasts. *Arch. Biochem. Biophys.* **208**, 444–455 (1981).
183. Lai, M. *et al.* Complete Acid Ceramidase ablation prevents cancer-initiating cell formation in melanoma cells. *Sci. Rep.* **7**, 1–14 (2017).
184. Cho, S. M. & Kwon, H. J. Acid ceramidase, an emerging target for anti-cancer and anti-angiogenesis. *Arch. Pharm. Res.* **42**, 232–243 (2019).
185. Sugita, M., Dulaney, J. T. & Moser, H. W. Ceramidase deficiency in Farber's disease (Lipogranulomatosis). *Science (80-.).* **178**, 1100–1102 (1972).
186. Frohbergh, M., He, X. & Schuchman, E. H. The molecular medicine of acid ceramidase. *Biol. Chem.* **396**, 759–765 (2015).
187. Yu, F. P. S., Amintas, S., Levade, T. & Medin, J. A. Acid ceramidase deficiency: Farber disease and SMA-PME. *Orphanet J. Rare Dis.* **13**, 1–19 (2018).
188. Bao, X., Ma, M., Zhang, Z., Xu, Y. & Qiu, Z. Farber disease in a patient from China. *Am. J. Med. Genet. Part A* **182**, 2184–2186 (2020).
189. Devi, A. R. R. *et al.* Farber lipogranulomatosis: Clinical and molecular genetic analysis reveals a novel mutation in an Indian family. *J. Hum. Genet.* **51**, 811–814 (2006).
190. Cvitanovic-Sojat, L. *et al.* Farber lipogranulomatosis type 1 - Late presentation and early death in a Croatian boy with a novel homozygous ASAH1 mutation. *Eur. J. Paediatr. Neurol.* **15**, 171–173 (2011).
191. Chedrawi, A. K. *et al.* Novel V97G ASAH1 mutation found in Farber disease patients: Unique appearance of the disease with an intermediate severity, and marked early involvement of central and peripheral nervous system. *Brain Dev.* **34**, 400–404 (2012).
192. Al Jasmi, F. A novel mutation in an atypical presentation of the rare infantile Farber disease.

Brain Dev. **34**, 533–535 (2012).

193. Bashyam, M. D. *et al.* Molecular analyses of novel ASAH1 mutations causing Farber lipogranulomatosis: Analyses of exonic splicing enhancer inactivating mutation. *Clin. Genet.* **86**, 530–538 (2014).
194. Kim, S. Y. *et al.* Atypical presentation of infantile-onset farber disease with novel ASAH1 mutations. *Am. J. Med. Genet. Part A* **170**, 3023–3027 (2016).
195. Brooks, B. M. *et al.* Generation of an induced pluripotent stem cell line (TRNDi030-A) from a patient with Farber disease carrying a homozygous p. Y36C (c. 107 A>G) mutation in ASAH1. *Stem Cell Res.* **53**, 102387 (2021).
196. Ehlert, K. *et al.* Allogeneic hematopoietic cell transplantation in Farber disease. *J. Inherit. Metab. Dis.* **42**, 286–294 (2019).
197. Yeager, A. M. *et al.* Bone marrow transplantation for infantile ceramidase deficiency (Farber disease). *Bone Marrow Transplant.* **26**, 357–363 (2000).
198. Ramsubir, S. *et al.* In vivo delivery of human acid ceramidase via cord blood transplantation and direct injection of lentivirus as novel treatment approaches for Farber disease. *Mol. Genet. Metab.* **95**, 133–141 (2008).
199. Mena-Barragán, T. *et al.* PH-Responsive Pharmacological Chaperones for Rescuing Mutant Glycosidases. *Angew. Chemie - Int. Ed.* **54**, 11696–11700 (2015).
200. Parenti, G., Moracci, M., Fecarotta, S. & Andria, G. Pharmacological chaperone therapy for lysosomal storage diseases. *Future Med. Chem.* **6**, 1031–1045 (2014).
201. Parenti, G. Treating lysosomal storage diseases with pharmacological chaperones: From concept to clinics. *EMBO Mol. Med.* **1**, 268–279 (2009).
202. Parenti, G., Andria, G. & Valenzano, K. J. Pharmacological chaperone therapy: Preclinical development, clinical translation, and prospects for the treatment of lysosomal storage disorders. *Mol. Ther.* **23**, 1138–1148 (2015).
203. Benito, J. M., García Fernández, J. M. & Mellet, C. O. Pharmacological chaperone therapy for Gaucher disease: A patent review. *Expert Opin. Ther. Pat.* **21**, 885–903 (2011).
204. Trapero, A. & Llebaria, A. Glucocerebrosidase inhibitors for the treatment of Gaucher disease. *Future Med. Chem.* **5**, 573–590 (2013).

205. Suzuki, Y. Chaperone therapy update: Fabry disease, GM1-gangliosidosis and Gaucher disease. *Brain Dev.* **35**, 515–523 (2013).

206. Edgington, L. E., Verdoes, M. & Bogyo, M. Functional imaging of proteases: Recent advances in the design and application of substrate-based and activity-based probes. *Curr. Opin. Chem. Biol.* **15**, 798–805 (2011).

207. Willems, L. I. *et al.* Potent and selective activity-based probes for GH27 human retaining α-galactosidases. *J. Am. Chem. Soc.* **136**, 11622–11625 (2014).

208. Stoddard, E. G. *et al.* Activity-Based Probes for Isoenzyme- and Site-Specific Functional Characterization of Glutathione S-Transferases. *J. Am. Chem. Soc.* **139**, 16032–16035 (2017).

209. Witte, M. D. *et al.* Ultrasensitive in situ visualization of active glucocerebrosidase molecules. *Nat. Chem. Biol.* **6**, 907–913 (2010).

210. Lentz, C. S. What you see is what you get: Activity-based probes in single-cell analysis of enzymatic activities. *Biol. Chem.* **401**, 233–248 (2020).

211. Ouairy, C. M. J. *et al.* Development of an acid ceramidase activity-based probe. *Chem. Commun.* **51**, 6161–6163 (2015).

212. Ortega, J. A. *et al.* Pharmacophore Identification and Scaffold Exploration to Discover Novel, Potent, and Chemically Stable Inhibitors of Acid Ceramidase in Melanoma Cells. *J. Med. Chem.* **60**, 5800–5815 (2017).

213. Vijayan, Y., Lankadasari, M. B. & Harikumar, K. B. Acid Ceramidase: A Novel Therapeutic Target in Cancer. *Curr. Top. Med. Chem.* **19**, 1512–1520 (2019).

214. Frohbergh, M., He, X. & Schuchman, E. H. The molecular medicine of acid ceramidase. *Biol. Chem.* **396**, 759–765 (2015).

215. Clifford, R. E. *et al.* Targeting Acid Ceramidase to Improve the Radiosensitivity of Rectal Cancer. *Cells* **9**, 1–14 (2020).

216. Caputo, S. *et al.* Design, Synthesis, and Biological Evaluation of a Series of Oxazolone Carboxamides as a Novel Class of Acid Ceramidase Inhibitors. *J. Med. Chem.* **63**, 15821–15851 (2020).

217. Realini, N. *et al.* Discovery of highly potent acid ceramidase inhibitors with in vitro tumor

chemosensitizing activity. *Sci. Rep.* **3**, 1035 (2013).

218. Pizzirani, D. *et al.* Benzoxazolone Carboxamides: Potent and Systemically Active Inhibitors of Intracellular Acid Ceramidase. *Angew Chem Int Ed Engl* (2015) doi:10.1002/anie.201409042.
219. Bach, A. *et al.* Benzoxazolone Carboxamides as Potent Acid Ceramidase Inhibitors: Synthesis and Structure-Activity Relationship (SAR) Studies. *J. Med. Chem.* **58**, 9258–9272 (2015).
220. Di Martino, S. *et al.* Lead Optimization of Benzoxazolone Carboxamides as Orally Bioavailable and CNS Penetrant Acid Ceramidase Inhibitors. *J. Med. Chem.* **63**, 3634–3664 (2020).
221. Bielsa, N. *et al.* Discovery of deoxyceramide analogs as highly selective ACER3 inhibitors in live cells. *Eur. J. Med. Chem.* **216**, (2021).
222. Casasampere, M. *et al.* New fluorogenic probes for neutral and alkaline ceramidases. *J. Lipid Res.* **60**, 1174–1181 (2019).
223. Iqbal, J., Walsh, M. T., Hammad, S. M. & Hussain, M. M. Sphingolipids and Lipoproteins in Health and Metabolic Disorders. *Trends Endocrinol. Metab.* **28**, 506–518 (2017).
224. Hannun, Y. A. & Obeid, L. M. Sphingolipids and their metabolism in physiology and disease. *Nat. Rev. Mol. Cell Biol.* **19**, 175–191 (2018).
225. Padron, J. Sphingolipids in Anticancer Therapy. *Curr. Med. Chem.* **13**, 755–770 (2006).
226. Gault, C. R., Obeid, L. M. & Hannun, Y. A. An overview of sphingolipid metabolism: from synthesis to breakdown. *Adv. Exp. Med. Biol.* **688**, 1–23 (2010).
227. Sahu, S. K., Hannun, Y. A. & Yao, N. Emergence of membrane sphingolipids as a potential therapeutic target. *Biochimie* **158**, 257–264 (2019).
228. Ipatova, O. M., Torkhovskaya, T. I., Zakharova, T. S. & Khalilov, E. M. Sphingolipids and cell signaling: Involvement in apoptosis and atherogenesis. *Biochem.* **71**, 713–722 (2006).
229. Spiegel, S. & H.merrill, A. Sphingolipid metabolism and Cell Growth. *FASEB J.* 1388–1397 (2018).
230. Gomez-Larrauri, A. *et al.* Role of bioactive sphingolipids in physiology and pathology. *Essays Biochem.* **64**, 579–589 (2020).
231. Saddoughi, S. A. & Ogretmen, B. *Diverse Functions of Ceramide in Cancer Cell Death and*

Proliferation. *Advances in Cancer Research* vol. 117 (Elsevier Inc., 2013).

232. Cerbón, J., Baranda-Avila, N., Falcón-Muñoz, A., Camacho-Arroyo, I. & Cerbón, M. Sphingolipid synthesis and role in uterine epithelia proliferation. *Reproduction* **156**, 173–183 (2018).
233. Tirodkar, T. S. & Voelkel-Johnson, C. Sphingolipids in apoptosis. *Exp. Oncol.* **34**, 231–242 (2012).
234. Trayssac, M., Hannun, Y. A. & Obeid, L. M. Role of sphingolipids in senescence: implication in aging and age-related diseases. *J. Clin. Invest.* **128**, 2702–2712 (2018).
235. Morales, A., Lee, H., Goñi, F. M., Kolesnick, R. & Fernandez-Checa, J. C. Sphingolipids and cell death. *Apoptosis* **12**, 923–939 (2007).
236. Iessi, E. *et al. On the role of sphingolipids in cell survival and death*. *International Review of Cell and Molecular Biology* vol. 351 (Elsevier Inc., 2020).
237. Springer Nature, © & Switzerland, A. G. *Bioactive Ceramides in Health and Disease*. *Advances in Experimental Medicine and Biology* vol. 1159 (2019).
238. Abed Rabbo, M., Khodour, Y., Kaguni, L. S. & Stiban, J. Sphingolipid lysosomal storage diseases: from bench to bedside. *Lipids Health Dis.* **20**, 1–29 (2021).
239. Ogretmen, B. Sphingolipid metabolism in cancer signalling and therapy. *Nat. Rev. Cancer* **18**, 33–50 (2017).
240. Ferlinz, K. *et al.* Human acid ceramidase: Processing, glycosylation, and lysosomal targeting. *J. Biol. Chem.* **276**, 35352–35360 (2001).
241. Xu, R., Sun, W., Jin, J., Obeid, L. M. & Mao, C. Role of alkaline ceramidases in the generation of sphingosine and its phosphate in erythrocytes. *FASEB J.* **24**, 2507–2515 (2010).
242. Sun, W. *et al.* Alkaline ceramidase 2 regulates β1 integrin maturation and cell adhesion. *FASEB J.* **23**, 656–666 (2009).
243. Franzen, R. *et al.* Interleukin-1β Induces Chronic Activation and de Novo Synthesis of Neutral Ceramidase in Renal Mesangial Cells. *J. Biol. Chem.* **276**, 35382–35389 (2001).
244. Huwiler, A., Pfeilschifter, J. & Van Den Bosch, H. Nitric oxide donors induce stress signaling via ceramide formation in rat renal mesangial cells. *J. Biol. Chem.* **274**, 7190–7195 (1999).
245. Zhu, Q. *et al.* Chronic activation of neutral ceramidase protects β β β β-cells against

cytokine-induced apoptosis 1. *Acta Pharmacol Sin* **29**, 593–599 (2008).

246. Osawa, Y. *et al.* Roles for C16-ceramide and sphingosine 1-phosphate in regulating hepatocyte apoptosis in response to tumor necrosis factor-α. *J. Biol. Chem.* **280**, 27879–27887 (2005).
247. Snider, A. J. *et al.* Loss of neutral ceramidase increases inflammation in a mouse model of inflammatory bowel disease. *Prostaglandins Other Lipid Mediat.* **99**, 124–130 (2012).
248. Lucki, N. C., Bandyopadhyay, S., Wang, E., Merrill, A. H. & Sewer, M. B. Acid Ceramidase (ASAH1) Is a Global Regulator of Steroidogenic Capacity and Adrenocortical Gene Expression. (2012) doi:10.1210/me.2011-1150.
249. Lucki, N. C. *et al.* Acid Ceramidase (ASAH1) Represses Steroidogenic Factor 1-Dependent Gene Transcription in H295R Human Adrenocortical Cells by Binding to the Receptor. *Mol. Cell. Biol.* **32**, 4419–4431 (2012).
250. Li, C. M. *et al.* Insertional mutagenesis of the mouse acid ceramidase gene leads to early embryonic lethality in homozygotes and progressive lipid storage disease in heterozygotes. *Genomics* **79**, 218–224 (2002).
251. Eliyahu, E., Shtraizent, N., Shalgi, R. & Schuchman, E. H. Construction of conditional acid ceramidase knockout mice and in vivo effects on oocyte development and fertility. *Cell. Physiol. Biochem.* **30**, 735–748 (2012).
252. Wu, B. X., Zeidan, Y. H. & Hannun, Y. A. Downregulation of neutral ceramidase by gemcitabine: Implications for cell cycle regulation. *Biochim. Biophys. Acta - Mol. Cell Biol. Lipids* **1791**, 730–739 (2009).
253. García-Barros, M. *et al.* Role of neutral ceramidase in colon cancer. *FASEB J.* **30**, (2016).
254. Coant, N., Garciá-Barros, M., Zhang, Q., Obeid, L. M. & Hannun, Y. A. AKT as a key target for growth promoting functions of neutral ceramidase in colon cancer cells. *Oncogene* **37**, 3852–3863 (2018).
255. French, K. J. *et al.* Antitumor activity of sphingosine kinase inhibitors. *J. Pharmacol. Exp. Ther.* **318**, 596–603 (2006).
256. Mehta, S. *et al.* Combined cytotoxic action of paclitaxel and ceramide against the human Tu138 head and neck squamous carcinoma cell line. *Cancer Chemother. Pharmacol.* **46**,

(2000).

257. Norris, J. S. *et al.* Combined therapeutic use of AdGFPFasL and small molecule inhibitors of ceramide metabolism in prostate and head and neck cancers: A status report. *Cancer Gene Ther.* **13**, 1045–1051 (2006).

258. Seelan, R. S. *et al.* Human acid ceramidase is overexpressed but not mutated in prostate cancer. *Genes Chromosom. Cancer* **29**, 137–146 (2000).

259. Turner, L. S. *et al.* Autophagy is increased in prostate cancer cells overexpressing acid ceramidase and enhances resistance to C6 ceramide. *Prostate Cancer Prostatic Dis.* **14**, 30–37 (2011).

260. Morad, S. A. F. *et al.* Novel off-target effect of tamoxifen — Inhibition of acid ceramidase activity in cancer cells. *Biochim. Biophys. Acta - Mol. Cell Biol. Lipids* **1831**, 1657–1664 (2013).

261. Mahdy, A. E. M. *et al.* Acid ceramidase upregulation in prostate cancer cells confers resistance to radiation: AC inhibition, a potential radiosensitizer. *Mol. Ther.* **17**, (2009).

262. Liu, Y. *et al.* Serum autoantibody profiling using a natural glycoprotein microarray for the prognosis of early melanoma. *J. Proteome Res.* **9**, 6044–6051 (2010).

263. Bedia, C., Casas, J., Andrieu-Abadie, N., Fabriàs, G. & Levade, T. Acid ceramidase expression modulates the sensitivity of A375 melanoma cells to dacarbazine. *J. Biol. Chem.* **286**, (2011).

264. Gouazé-Andersson, V. *et al.* Inhibition of acid ceramidase by a 2-substituted aminoethanol amide synergistically sensitizes prostate cancer cells to N-(4-hydroxyphenyl) retinamide. *Prostate* **71**, (2011).

265. Szulc, Z. M. *et al.* Novel analogs of d-e-MAPP and B13. Part 1: Synthesis and evaluation as potential anticancer agents. *Bioorg. Med. Chem.* **16**, 1015–1031 (2008).

266. Bielawska, A. *et al.* Novel analogs of d-e-MAPP and B13. Part 2: Signature effects on bioactive sphingolipids. *Bioorg. Med. Chem.* **16**, 1032–1045 (2008).

267. Liu, X. *et al.* Modulation of Ceramide Metabolism Enhances Viral Protein Apoptin's Cytotoxicity in Prostate Cancer. *Mol. Ther.* **14**, 637–646 (2006).

268. Cheng, J. C. *et al.* Radiation-induced acid ceramidase confers prostate cancer resistance and tumor relapse. *J. Clin. Invest.* **123**, 4344–4358 (2013).

269. Saied, E. M. & Arenz, C. Inhibitors of Ceramidases. *Chem. Phys. Lipids* **197**, 60–68 (2016).

270. Vasiliauskaité-Brooks, I. *et al.* Structure of a human intramembrane ceramidase explains enzymatic dysfunction found in leukodystrophy. *Nat. Commun.* **9**, (2018).

271. Camacho, L. *et al.* Acid ceramidase as a therapeutic target in metastatic prostate cancer. *J. Lipid Res.* **54**, 1207–1220 (2013).

272. Ouairy, C. M. J. *et al.* Development of an acid ceramidase activity-based probe. *Chem. Commun. (Camb).* **51**, 6161–6163 (2015).

273. Wang, S. *et al.* Advanced activity-based protein profiling application strategies for drug development. *Front. Pharmacol.* **9**, 1–9 (2018).

274. Xu, J., Li, X., Ding, K. & Li, Z. Applications of Activity-Based Protein Profiling (ABPP) and Bioimaging in Drug Discovery. *Chem. - An Asian J.* **15**, 34–41 (2020).

275. Su, Y. *et al.* Target identification of biologically active small molecules via in situ methods. *Curr. Opin. Chem. Biol.* **17**, 768–775 (2013).

276. Wen, H., Jung, H. & Li, X. Drug Delivery Approaches in Addressing Clinical Pharmacology-Related Issues: Opportunities and Challenges. *AAPS J.* **17**, 1327–1340 (2015).

277. Filipp, F. V. Precision medicine driven by cancer systems biology. *Cancer Metastasis Rev.* **36**, 91–108 (2017).

278. Roberts, A. M., Ward, C. C. & Nomura, D. K. Activity-based protein profiling for mapping and pharmacologically interrogating proteome-wide ligandable hotspots. *Curr. Opin. Biotechnol.* **43**, 25–33 (2017).

279. Niphakis, M. J. & Cravatt, B. F. Enzyme inhibitor discovery by activity-based protein profiling. *Annu. Rev. Biochem.* **83**, 341–377 (2014).

280. Moellering, R. E. & Cravatt, B. F. How chemoproteomics can enable drug discovery and development. *Chem. Biol.* **19**, 11–22 (2012).

281. Casasampere, M. *et al.* Click and count: Specific detection of acid ceramidase activity in live cells. *Chem. Sci.* **11**, 13044–13051 (2020).

282. Pizzirani, D. *et al.* Benzoxazolone carboxamides: Potent and systemically active inhibitors of intracellular acid ceramidase. *Angew. Chemie - Int. Ed.* **54**, 485–489 (2015).

283. Ordóñez, Y. F. *et al.* Activity-Based Imaging of Acid Ceramidase in Living Cells. *J. Am. Chem.*

Soc. **141**, 7736–7742 (2019).

284. Otsuka, Y. *et al.* Identification of Small-Molecule Inhibitors of Neutral Ceramidase (nCDase) via Target-Based High-Throughput Screening. *SLAS Discov.* **26**, 113–121 (2021).

285. Healey, R. D. *et al.* Discovery and Mechanism of Action of Small Molecule Inhibitors of Ceramidases**. *Angew. Chemie - Int. Ed.* **61**, (2022).

MAZEN ALI ASEERI

2023